

Synthesis of Novel Heterocyclic Compounds for Red and Green Triplet Matrix Materials for OLED Application

Dissertation

Zur Erlangung des Doktorgrades der Naturwissenschaften

(Dr. rer. nat.)

an der Fakultät für Chemie und Pharmazie

der Universität Regensburg



vorgelegt von

Klaus Osazuwa Omoregbee

aus Bad-Neuenahr Ahrweiler

2023

The experimental work was performed between March 2020 and April 2023 in the laboratories of Product Research Chemistry, Display Solutions Merck Electronics KGaA Darmstadt and in the laboratories of AK König at the Universität Regensburg, Institute of Organic Chemistry under the supervision of Prof. Dr. Burkhard König and Dr. Amir Parham (Merck Electronics KGaA).

Board of examiners:

Chair: Prof. Dr. Frank-Michael Matysik

1st reviewer: Prof. Dr. Burkhard König

2nd reviewer: Prof. Dr. Matthias Bremer

Examiner: Prof. Dr. Robert Wolf

Date of submission: 12.05.2023

Date of colloquium: 11.07.2023

Parts of this work was published in:

- 1) A. Parham, C. Ehrenreich, **K. Omoregbee**, WO 2022/207678 A1, Organische Elektrolumineszierende Vorrichtung, Merck Patent GmbH, March 31st, **2021**.

- 2) A. Parham, **K. Omoregbee**, Materialien für organische Elektrolumineszenzvorrichtungen, international patent application, Merck Patent GmbH, filed Feb. 06, **2023**.

Scientific conferences:

- | | |
|---------|---|
| 09/2022 | ORCHEM , GDCh, poster presentation. |
| 07/2022 | Curious2022 – Future Insight conference , participation. |
| 05/2022 | 1st Merck Science Academy Conference , Merck Electronics KGaA, poster presentation. |
| 11/2021 | Merck Science Day , Merck Electronics KGaA, poster presentation and short talk. |
| 08/2021 | WiFo , GDCh, participation. |

Acknowledgements

Firstly, I would like to thank PROF. DR. BURKHARD KÖNIG for the opportunity to work in his group, the great advice, and helpful suggestions.

Secondly, I would like to thank PROF. DR. MATTHIAS BREMER for the second examination of this work. I sincerely thank PROF. DR. ROBERT WOLF for taking the role as the examiner and PROF. DR. FRANK-MICHAEL MATYSIK for taking the role as the chair of the examination board.

Furthermore, thanks to DR. AMIR PARHAM for his supervision. Thanks to DR. PHILIPP STOESEL, DR. CHRISTIAN EICKHOFF and DR. ROCCO FORTTE for carefully proofreading this thesis. I would also like to thank the physics team, especially DR. CHRISTIAN EICKHOFF and the analytics team of Merck Electronics. Many thanks go to the entire lab teams of Display Solutions.

Moreover, I thank the AK König for welcoming me during my short stay in Regensburg.

I would like to thank everyone, who brought light at dark days during my PhD and who smiled with me at days with successful experiments. I would like to thank my family (Mama, Louis, Louisa, Zoe, and Dorothee M.) and friends (Maximilian B., Maximilian S., Constanze D., and Jenny O.) for their great support during the past three years – particularly my wife Sabrina. Thank you for your encouragement not to give up when things did not go well at all. A PhD during Covid times in a new city and the long distance were hard, but we made it.

*„Auch aus Steinen, die einem in den Weg gelegt werden, kann man etwas Schönes bauen.“
– Johann Wolfgang von Goethe.*

Herewithin I certify that I have prepared and written my thesis independently and that I have not used any sources and aids other than those indicated by me.

Klaus Osazuwa Omoregbee

Table of Content

Acknowledgements	VII
1 Motivation and Background	1
1.1 OLED – Function and Requirements.....	1
1.1.1 Basics of Luminescence and Light Emission in Organic Semiconductors.....	2
1.1.2 Constitution and Working Principle.....	3
1.1.3 Emissive Layer and Triplet Matrix Material (TMM).....	6
1.1.4 OLED Characteristics.....	8
2 Research Objectives	11
3 Synthesis of Triplet Matrix Materials	12
3.1 Theoretical Considerations.....	13
3.2 Synthesis of Heteroaromatic TMM Building Blocks.....	18
3.2.1 Benzocarbazoles - Selective Formation.....	18
3.2.2 Benzofuopyrimidine.....	23
3.2.3 Naphthodibenzothiophene.....	24
3.2.4 Dibenzothiophensulfones.....	24
3.3 Synthesis of the targeted TMM's.....	25
3.3.1 Synthesis of green TMM's based on benzocarbazole 25 and derivatives.....	25
3.3.2 Synthesis of red TMM's based on benzocarbazole 18.....	35
3.3.3 Synthesis of further TMM's.....	38
3.3.4 Attempts for the Synthesis of Lactam TMM.....	40
4 Evaluation of Material Properties	46
4.1 General.....	47
4.2 Results of the red TMM's.....	47
4.2.1 Electrochemical Properties.....	47
4.2.2 Thermal Properties.....	49
4.2.3 Photophysical Properties.....	50
4.2.4 Device Results.....	52
4.3 Results of the green TMM's.....	56
4.3.1 Electrochemical Properties.....	56
4.3.2 Thermal Properties.....	57
4.3.3 Photophysical Properties.....	58
4.3.4 Device Results.....	60
4.4 Physical and Chemical Special Characteristics of [b]-annulated and [c]-annulated benzocarbazole based TMM's.....	64
5 Photoredoxcatalytic C-N Coupling for the Synthesis of TMM's	67
5.1 Introduction.....	68
5.2 Results.....	71
6 Conclusion and Outlook	77
7 Experimental Section	80
7.1 General Methods and Materials.....	80

7.2	Synthesis of compounds and analytical data	83
7.2.1	Synthesis of Heteroaromatic TMM Building Blocks (compounds of chapter 3.2)	83
7.2.2	Synthesis of green TMM's (compounds of chapter 3.3.1).....	94
7.2.3	Synthesis of red TMM's (compounds of chapter 3.3.2).....	108
7.2.4	Synthesis of further TMM's (compounds of chapter 3.3.3).....	115
7.2.5	Synthesis of Lactam TMM (compounds of chapter 3.3.4).....	119
7.2.6	Photoredoxcatalytic Reactions	124
7.3	Crystal structures.....	125
8	References	133
9	Appendix	140
9.1	GC-MS Spectra of the Photoredoxcatalytic Reactions with Product Formation	140
9.2	Curriculum Vitae	142
9.3	Eidesstattliche Erklärung	144

Abstract

In the past years, enormous progress has been achieved in the development of materials for OLED application. The development of more efficient, less energy consuming, and durable devices is of high importance for the progress and sustainability in electronics.

In this thesis, the synthesis of novel red and green triplet matrix materials (TMM's) is described, and structure-property relationships are investigated by the systematic exchange of electron and hole conducting and linking subunits. In this context, a variety of differently constituted heteroaromatic trisubstituted benzofuopyrimidine/triphenyltriazine and carbazole derivatives were designed, synthesized, and tested. The influence of the triplet and HOMO/LUMO energy level and structure were evaluated regarding the lifetime, efficiency, and driving voltage.

The first part of this work focuses on theoretical pre-evaluations by DFT, which led to the hypothesis, that benzofuopyrimidine is an attractive alternative to triphenyltriazine.

The second part of this work focuses on the synthesis of heteroaromatic building blocks based on benzofuopyrimidine/triphenyltriazine and benzocarbazoles. Here, the selective benzocarbazole formation was investigated. Furthermore, the synthesis of a trisubstituted benzofuopyrimidine building block was established. The third part of this thesis focuses on the coupling of the above-mentioned synthesized building blocks to give red and green TMM's respectively.

The fourth part of this thesis deals with the evaluation of the synthesized molecules by electrochemical, thermal and photophysical experiments (CV, DSC, UV/Vis and fluorescence spectroscopy) as well as their performance in OLED stacks (EQE, lifetime and driving voltage). Interestingly, [*c*]-annulated and [*b*]-annulated benzocarbazole regioisomeric materials showed significant differences in their properties. The studies for green TMM's showed, that benzofuopyrimidine in the electron accepting unit improves the lifetime compared to triazines, linking units improve voltage. Efficiency is good for all synthesized TMM's. For red TMM's, triazines provide better results in terms of efficiency and voltage.

In the last part of this work, a photo-redox catalytic cyanoarene-nickel system was tested for the synthesis of TMM precursors. The electrophiles were identified to be the main limiting factor as its electronics as well as sterics can influence the outcome of the C-N coupling. Steric hinderance of naphthyl electrophiles provided low yields, while phenyl electrophiles showed good coupling outcomes. Electron-poor electrophiles reacted better than electron-rich electrophiles.

The developed methodologies broaden the toolbox for the synthesis of TMM's or precursors. The investigated structure-property relationships will further help develop and optimize properties of TMM's.

Zusammenfassung

In den vergangenen Jahren wurden enorme Erfolge in der Entwicklung von OLED-Materialien erzielt. Die Entwicklung von effizienteren, energiesparenderen und beständigeren Geräten ist wichtig für den Fortschritt und die Nachhaltigkeit im Bereich der Elektronik.

In dieser Arbeit werden die Synthesen von roten und grünen Triplet-Matrix-Materialien (TMM's) beschrieben und Struktur-Eigenschaften-Beziehungen durch den systematischen Austausch von elektronen- und lochleitenden sowie Linkern untersucht. In diesem Zusammenhang wurden eine Auswahl an unterschiedlich konstituierten trisubstituierten Benzofuopyrimidin/Triphenyltriazin- und Benzocarbazol-enthaltenen Molekülen entworfen und synthetisiert. Der Einfluss der Triplett-Energie und der HOMO/LUMO-Energieniveaus und der Struktur in Bezug auf die Lebensdauer, Effizienz und Spannung wurde evaluiert.

Der erste Teil dieser Arbeit befasst sich mit DFT-Voruntersuchungen, welche zu der Hypothese führen, dass Benzofuopyrimidine attraktive Alternativen zu Triphenyltriazinen sind.

Der zweite Teil befasst sich mit der Synthese von heteroaromatischen Bausteinen, die auf Benzofuopyrimidinen/Triazinen und Benzocarbazolen basieren. Hier wurde die selektive Entstehung von Benzocarbazolen untersucht und eine Synthese zu Benzofuopyrimidin-Bausteinen eingeführt. Der dritte Teil fokussiert sich auf die Kopplung dieser Bausteine.

Der vierte Teil befasst sich mit der Evaluierung der synthetisierten Moleküle mithilfe von elektrochemischen, thermischen und photophysikalischen Experimenten (CV, DSC, UV/Vis und Fluoreszenz-Spektroskopie) und ihrer Performance in OLED-Geräten (EQE, Lebensdauer und Spannung). [c]- und [b]-annulierte regioisomere Benzocarbazol-Materialien zeigten interessanterweise unterschiedliche Eigenschaften. Die Studien für grüne TMM's zeigten, dass Benzofuopyrimidine als Elektronenakzeptor-Einheit die Lebensdauer verbessern, verglichen zu Triazinen, wobei Linker die Spannung verbessern. Die Effizienz aller synthetisierter Strukturen ist als gut zu bewerten. In roten TMM's zeigten Triazine die besten Ergebnisse bzgl. Effizienz und Spannung.

In dem letzten Teil dieser Arbeit wurde ein photoredox-katalytisches Cyanoaren-Nickel-System für die Synthese von TMM-Vorstufen getestet. Das Elektrophil stellte sich als der hauptlimitierende Faktor heraus, da dessen Elektronik und Sterik die Effizienz von C-N-Kopplungen beeinflusst. Sterische Hinderung in Naphthyl-Elektrophilen ergaben geringe Kopplungs-Ausbeuten, wohingegen Phenyl-Elektrophile hohe Kopplungs-Effizienzen zeigten. Elektronenarme Elektrophile mit elektronenziehenden Substituenten zeigten höhere Kopplungseffizienzen als elektronenreiche Elektrophile.

Die entwickelten Methoden erweitern die Werkzeugbox für die Synthese von OLED-Materialien oder Vorstufen und die erforschten Struktur-Eigenschaft-Beziehung werden dabei helfen Eigenschaften von TMM's zu optimieren.

Abbreviations

Abs.	Absolute
ACN	Acetonitrile
aq.	Aqueous
AQF	Automatic Quick Furnace Combustion Ion Chromatography
Ar	Aromatic
Boc	<i>tert</i> -Butyloxycarbonyl
BODIPY	Boron dipyrromethenes
BTB	4,4'-bis(4,6-diphenyl-1,3,5-triazin-2-yl)biphenyl
Bu	Butyl
CIE	Commission International de L'Éclairage
CIF	Crystallographic information files
COSY	Correlated spectroscopy
CV	Cyclovoltammetry
Cy	Cyclohexyl
CZIPN	1,2,3,5-Tetrakis(carbazol-9-yl)-4,6-dicyanobenzene,2,4,5,6-Tetrakis(9H-carbazol-9-yl)isophthalonitrile
Db	Dibenzylideneacetone
DFT	Density functional theory
DMAc	<i>N,N</i> -Dimethylacetamide
DMF	<i>N,N</i> -Dimethylformamide
Dmfc	Decamethylferrocene
DMSO	Dimethyl sulfoxide
DSC	Differential scanning calorimetry
EDG	Electron donating group
EIL	Electron injection layer
EML	Emissive layer
eq.	Equivalent
EQE	External Quantum Efficiency
ESI	Electrospray ionization
Et	Ethyl
ETL	Electron transport layer
e-TMM	Electron-Transport matrix material
EtOAc	Ethyl acetate
EWG	Electron withdrawing group
Fc	Ferrocene
Fmoc	Fluorenylmethyloxycarbonyl
FRET	Fluorescence resonance energy transfer
FWHM	Full width at half maximum
GC-MS	Gas chromatography-mass spectrometry
HIL	Hole injection layer
HMBC	Heteronuclear multiple bond correlation
HOMO	Highest Occupied Molecular Orbital
HPLC	High-performance liquid chromatography
HPLC-MS	High performance liquid chromatography Mass Spectrometry

Hpp	Hexahydropyrimidopyrimidine
HRMS	High-resolution mass spectrometry
HSQC	Heteronuclear Single Quantum Coherence
HTL	Hole transport layer
h-TMM	Hole-Transport matrix material
IC	Internal conversion
ICP-MS	Inductively coupled plasma mass spectrometry
ISC	Intersystem crossing
ITO	Indium tin oxide
IQE	Internal quantum efficiency
IZO	Indium zinc oxide
KGaA	Kommanditgesellschaft auf Aktien
LCD	Liquid crystal display
lit.	Literature
LT	Lifetime
LUMO	Lowest Occupied Molecular Orbital
Me	Methyl
MeCN	Acetonitrile
MS	Mass spectroscopy
MTBE	Methyl <i>t</i> -butyl ether
NBS	<i>N</i> -Bromosuccinimide
NIR	Near infrared
NMP	<i>N</i> -Methyl-2-pyrrolidone
NP	Normal phase
NMR	Nuclear magnetic resonance
NPD	<i>N,N'</i> -Bis(naphthalen-1-yl)- <i>N,N'</i> -bis(phenyl)-2,2'-dimethylbenzidine
o	Ortho
OAc	Acetoxy
OLED	Organic light-emitting diode
PEDOT	Poly(3,4-ethylenedioxythiophene)
Ph	Phenyl
Pin	Pinacolato
Piq	1-phenylisoquinoline
PL	Photoluminescence
ppm	Parts per million
Ppy	4-pyrrolidin-1-ylpyridine
R.t.	Room temperature
Rel.	Relative
R_f	Retention factor
RF	Reflux
RP	Reversed phase
RISC	Reversed intersystem crossing
Sat.	Saturated
S₀	Singlet ground state
S₁	Singlet excited state
TADF	Thermally activated delayed fluorescence

TBAHFP	Tetrabutylammonium hexafluorophosphate
TCTA	Tris-(4-carbazoyl-9-yl-phenyl)-amin
TD	Time dependent
TEA	Triethylamine
T₁	Triplet excited state
TLC	Thin layer chromatography
TGA	Thermogravimetric analysis
THF	Tetrahydrofurane
TMA	Tetramethylammonium
TMG	Tetramethylguanidine
TMM	Transport matrix material
TMS	Tetramethylsilane
TV	Television
UV-Vis	Ultraviolet-visible
VR	Vibrational
ZNO	Zinc oxide
XRD	X-ray diffraction
δ	Chemical shift in NMR spectra in ppm

1 Motivation and Background

1.1 OLED – Function and Requirements

Organic light-emitting diodes (OLED's) are light sources, which are used in displays of TV screens, laptops and smartphones. They are also used in panels for light applications.^[1]

The research and development of OLED device technology in academia and industry has significantly improved over the past 30 years and is still in progress. The fundamental research for the development of OLED's started back in the early 1960s, when the compound eosin was found to emit delayed fluorescence^[2] and the application of high voltage to anthracene crystals succeeded in electroluminescence.^[3] In 1987, at the company Eastman Kodak, Tang *et al.*^[4] reported the first low-voltage OLED device which was a multilayer device. This was the breakthrough of OLED technology.^{[5][4][1]}

OLED's offer features that grant them finer properties than conventional technologies like liquid crystal displays (LCDs). They offer a sustainable and new efficient method for lighting and display technologies. They for example do not have a backlight system in comparison to LCDs, which makes them energy efficient. They also enable "true black", thinner and lighter display panels.^{[6][7][8]} Besides that, OLED display panels exhibit enormous improvements in high contrast colors, image quality, broad viewing angles, and faster response time. They enable the feasibility to realize transparent, flexible, and rollable display panels. Therefore, they repudiate the previous technologies on the market.^[9]

Nowadays smartphones are barely inconceivable in our society. They require the development of compact, energy saving, light, colourful displays with high resolution. This was the main driving force for the rapid development of OLED technology. The focus here is a good energy efficiency to enable long battery durability. Moreover, the option for rollable display panels is very attractive for the application in smartphone screens. Within the last ten years, the smartphone business with OLED displays has rapidly grown. Leading smartphone manufacturers like Apple, Samsung, Huawei, HTC, Nokia, Microsoft, Google, LG, Samsung and other electronic producing companies use OLED touch screen displays. Samsung introduced the first foldable OLED display in 2019.^{[10][6][11]}

Besides mobile devices, OLED displays also dominate the TV screen market. Here, the motivation for the development focuses on energy efficiency due to new EU regulations such as the Energy Efficiency Index (EEI) for OLED TV's, which mandates the improvement of energy efficiency, the achievement of high contrast, colour space and a generally better movie experience.^[12] LG has commercialized ultra-high definition OLED displays, as well as transparent panels and the first rollable TV.^{[13][1]} Furthermore, the application of OLED's in lighting systems and automobiles is a growing market.^{[14][15]}

However, the technology of OLED's still faces key challenges with its material systems and device architecture. For example the device architecture of flexible OLED's is a challenge due to difficulties related to thermal and chemical instability of flexible substrates.^{[16][17]} Further innovation is necessary to increase the efficiency, lifetime, and light output of OLED devices. Additionally, the reduction of driving voltage is essential to improve power conversion efficiency.

1.1.1 Basics of Luminescence and Light Emission in Organic Semiconductors

Light is a form of energy and can be created upon the use of a different energy form. There are mainly two ways this can occur: incandescence and luminescence. Incandescence is simply light created by heat energy e.g., an electric stove heater or the sun and stars.^[18]

Luminescence is the spontaneous emission of light from a cool body. It is caused by the movements of electrons within a substance from high energetic states to low energetic states. There are various types of luminescence such as triboluminescence, chemiluminescence, bioluminescence, electrochemiluminescence and electroluminescence.^[19]

The working principle of OLED's is based on electroluminescence. Electroluminescence is an electrical and optical phenomenon, whereby the organic molecules in the OLED device emit light non-thermally upon passage of an electric field.^{[20][21]}

Semiconducting compounds based on organic molecules usually contain delocalized π - electrons. Since the π -bonds are the weakest bound electrons in the molecule, the lowest-energy electronic transitions are those between the highest occupied molecular orbital (HOMO, π -orbital) and lowest unoccupied molecular orbital (LUMO, π^* -orbital). The magnitude of the delocalized conjugated π -system determines the energy gap between HOMO and LUMO. This energy gap is typically between 1.5 - 3 eV for OLED compounds.^[22] This range covers the spectrum of visible light.

The Jablonski Energy diagram (Figure 1) illustrates various absorption and emission mechanisms. The first transition in the Jablonski Energy diagram is the absorption of a photon with a precise energy by an electron. Then the electron is excited from the ground state (S_0) into a higher energy excited state (S_1). However, the spin state of the electron does not change, which makes this a singlet-singlet transition ($S_1 \rightarrow S_0$). Based on the Franck-Condon principle, vertical conversions transit into higher vibration excited singlet states. As stated by Kasha's rule the spin state of the electron relaxes from the lowest excited state back into the ground state (radiative decay) and emission of a photon takes place.^[23]

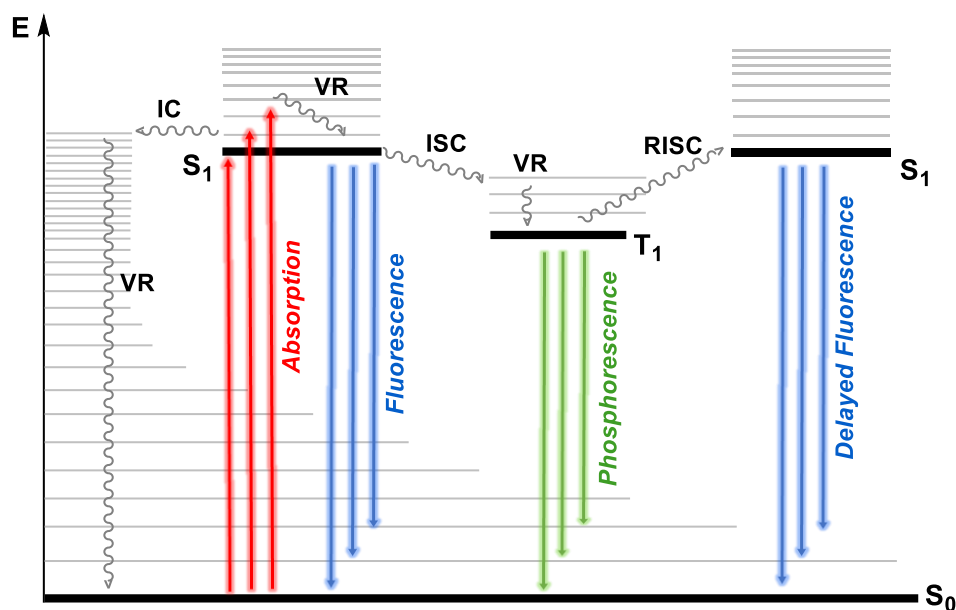


Figure 1: Jablonski energy diagram depicting the excitation of a molecule into the excited state ($S_0 \rightarrow S_1$) by absorption and follow-up transitions internal conversion (IC), intersystem crossing (ISC), reversed intersystem crossing (RISC), fluorescence, phosphorescence, and delayed fluorescence.

The emitted photon has a lower energy than the absorbed one. This leads to a shift in the fluorescence spectrum (Stokes shift). This process is known as fluorescence and involves radiationless internal conversion (IC). A further relaxation pathway is the conversion of energy into vibration (VR). Intersystem crossing (ISC) is a form of internal conversion. The electron changes its spin multiplicity from excited singlet state (S_1) into the excited triplet state (T_1). This transition is forbidden, but energetically favorable. The radiative transition from an excited triplet state into a singlet ground state is known as phosphorescence. Upon absorption of nearby thermal energy the excited triplet state is converted *via* reverse intersystem crossing (RISC) back into the first excited singlet, which then emits light by relaxation into the ground state. This process is known as thermal activated delayed fluorescence (TADF) or delayed fluorescence.^{[24][2]}

1.1.2 Constitution and Working Principle

OLED's are typically thin multilayer devices which consist of various semiconducting organic layers, that are sandwiched between two electrodes. The semiconducting organic layers have a thickness of approximately 300 nm.^[20] A multilayer OLED device consists of a cathode, an electron injection layer (EIL), an electron transport layer (ETL), emissive layer (EML), hole transport layer (HTL), hole injection layer (HIL) and an anode. A schematic device set-up of a multilayer OLED device is illustrated in Figure 2A.^[25]

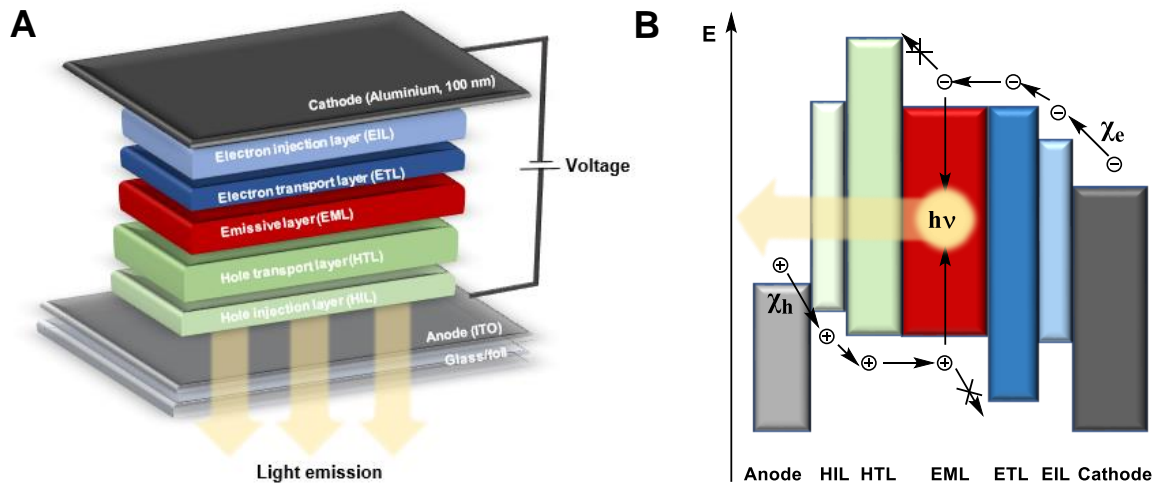


Figure 2: (A) Schematic device set-up of a multilayer OLED device, consisting of a cathode, an EIL, ETL, EML, HTL, HIL and an anode. (B) Illustration of energy levels, charge transport and light generation in a multilayer OLED setup.

There are mainly two types of OLED device architectures, which are the bottom and top emission stacks.^[26] In a bottom emission stack the light passes through the (semi-)transparent anode while in a top emission stack, the light passes through the (semi-)transparent cathode.^[27] Herein, only the bottom emission stack will be further elaborated.

The cathode is commonly a metallic layer with a low work function ($\phi_w \approx 2.9 - 4.0$ eV), which is made of reflective metal alloys like Mg:Ag, Al, Ca. These metal alloys allow low injection barriers. Meanwhile, the anode is a transparent conducting oxide like indium tin oxide (ITO), ZNO, IZO or PEDOT with a high work function ($\phi_w \approx 4.7 - 4.9$ eV) that allows light extraction. It should be treated with oxygen plasma to give a lowered injection barrier.^{[1][28][29]} The anode is deposited on a transparent substrate like flexible foil or glass. Literature-known examples for structures of HIL, HTL, EIL and ETL are shown in Figure 3.

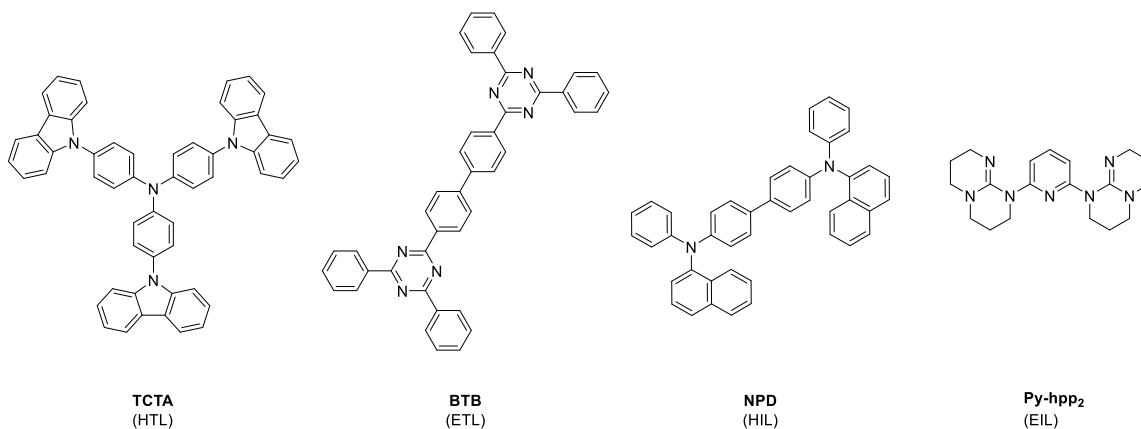


Figure 3: Literature-known structures of an HTL (TCTA)^[30], an ETL (BTB)^[31], a HIL (NPD)^[32] and EIL (Py-hpp₂)^[25]

Upon the application of voltage, electrons are transferred from the cathode into the lowest unoccupied molecular orbital (LUMO) of the EIL. This leads to the formation of a radical anion (Figure 2B). On the opposite side, the anode transfers a hole from the highest occupied molecular orbital (HOMO) into the HIL, which leads to the formation of a radical cation.

Amorphous organic semiconductors are usually disordered and therefore do not possess distinct valence bands like inorganic semiconductors, but they have assigned energy levels of the states involved. Thus, the charges travel across the hole transport layer (HTL) and electron transport layer (ETL) *via* multiple redox reactions also known as hopping processes into the emissive layer (EML) and recombine due to coulomb attraction to form a neutral excited state known as an exciton (hole-electron pair).^{[33][25]}

The emissive layer consists of an emitter that is embedded in a matrix (host). The host should be able to transport both charges. HTL and ETL usually have high HOMO and deep LUMO energy levels which can make them serve as electron and hole blocking layers and prevent charges from leaving the emissive layer.^{[21][34]}

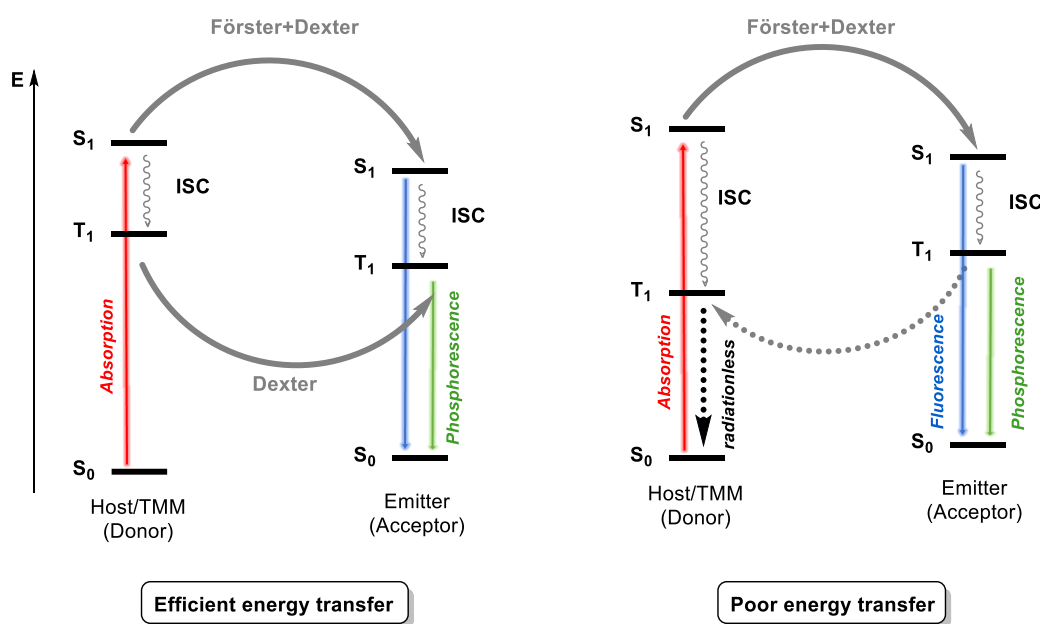


Figure 4: Illustration of Förster and Dexter energy transfer and visualization of a poor energy transfer ($T_1(\text{Host}) < T_1(\text{Emitter})$) and an efficient energy transfer ($T_1(\text{Host}) > T_1(\text{Emitter})$).

The excitons are transferred into the emitter either by Förster or Dexter transfer mechanism. Förster resonance energy transfer (FRET) is a non-radiative dipole-dipole coupling that transfers energy between excited singlet states of two chromophores (donor and acceptor molecule) over a long-range (4 - 10 nm). This requires the overlap between the emission spectrum of the donor (host) molecule and the absorption spectrum of the acceptor (emitter) molecule. Since the transition must be spin-allowed, solely singlet excitons are transferred. However, Dexter energy transfer involves the transfer of an excited electron of the host molecule into an emitter molecule *via* a non-radiative pathway. The overlap of both

wavefunctions from the host and emitter is necessary. Thus, the process can only occur in a short range (1 nm). The transfer is possible under spin-conservation and can allow both singlet and triplet exciton transfer (Figure 4).^{[35][36][37]}

According to the spin combinations of the electrons, there are four different states for the excited emitter to relax into the ground state and emit light. These are one singlet state and three triplet states. According to this, the singlet states can only give 25%, whereas the triplet states can reach up to 75% quantum efficiency. The relaxation of triplet excited states to the ground state is spin forbidden because it involves a spin conversion. To overcome this limitation, heavy metal atoms are embedded into the emissive layer, since they possess a strong spin-orbit coupling, that allows an efficient ISC to harvest the triplet excited states *via* phosphorescence. This makes triplet emitters very interesting for OLED's and superior in terms of efficient conversion of excitons to light.^{[38][39]}

1.1.3 Emissive Layer and Triplet Matrix Material (TMM)

The emissive layer requires not only the presence of an emitter, but also a host matrix material. The emitter is a molecule that either emits photons by phosphorescence, fluorescence or TADF (see Jablonski diagram Chapter 1.1.1, Figure 1). Phosphorescent emitters are superior to fluorescent emitters due to their ability to achieve high external quantum efficiencies at low current densities. With the introduction of heavy metal atoms like Iridium or Platinum into organic molecules, the development of phosphorescent emitters for the emissive layer of OLED devices enabled a significant increase in efficiency. The presence of these metals weakens the spin conservation law and allows the radiative transition of triplet excitons to the ground state.^[40]

When a phosphorescent emitter is used in the emissive layer, then the host compound in which it is encapsulated is called a triplet matrix material (TMM). The host is important to avoid triplet-triplet annihilation and concentration quenching, that initiates crucial efficiency roll-offs at higher current densities, due to exciton losses *via* radiative decay.^{[41][42]} Therefore, emitters are inserted into a TMM, that has appropriate optoelectronic characteristics. Especially, triplet excitons are strongly prone to quenching processes, because of their long lifetime.

A typical literature-known green emitter is Ir(ppy)₃ with a triplet energy level of 2.45 eV.^[43] A typical literature-known red emitter is Ir(piq)₃ with a triplet energy level of 2.0 eV.^[44] Both emitters are shown in Figure 5.

Various triplet energies can be achieved by variation of chemical units. A common motif for green and red TMM's is the combination of electron-rich compounds like carbazole-derivatives as a donor (hole conducting unit) and electron-poor compounds like quinazolines or triphenyltriazines as acceptors (electron conducting unit).^{[45][46][47][48]} A literature-known TMM

for green-emitting OLED's is for example **TMM-A**^{[45][46]}, while **TMM-B** is known to be a suitable TMM for red-emitting OLED's^[49] Figure 5.

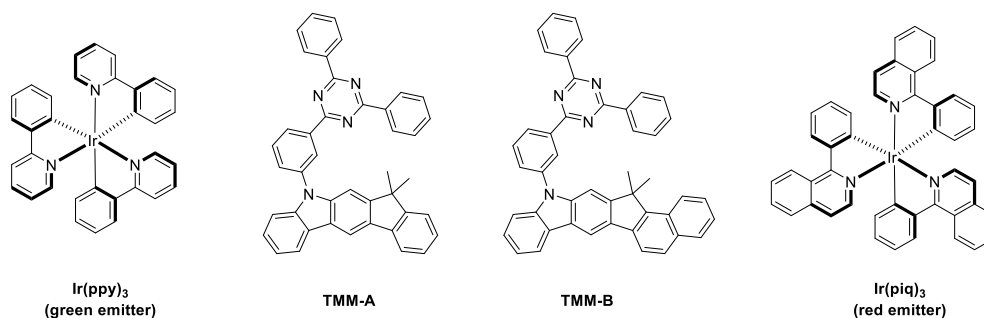


Figure 5: Literature-known TMM's for green- (**TMM-A**^[45]) and red-emitting (**TMM-B**^[49]) OLED's as well as literature-known emitter molecules.^[50]

The formation of excitons can take place either on the emitter or on TMM. If the formation of excitons is on the TMM, they are transferred directly to the emitter. For the inhibition of back transfer, it is necessary that the TMM has a large energy gap or high triplet energy for the exothermic host-emitter energy transfer. Therefore, this allows radiative decay to take place alternatively on the emitter.^{[51][52]}

The transfer of excitons within the organic layer is enabled by Dexter or Förster energy as already shown in Figure 4. The emitter molecule is the acceptor of excitons. It should possess a lower energy level than the TMM and a smaller energy gap between HOMO and LUMO.

Besides the emitter materials, TMM's are significant in an OLED and must fulfill a large variety of requirements. The host material can be a single TMM (single host concept) or a combination of different TMM's (mixed host concept). TMM's can transport holes (h-TMM) or electrons (e-TMM) into the emissive layer and participate in exciton formation. TMM's that can transfer both charges are known as bipolar TMM's. The formed exciton is transferred *via* Dexter energy, which is a short-range process (<1 nm). Thus, the TMM should possess a higher triplet energy than the emitter to limit exothermic reverse energy transfer (loss of efficiency) and ensure the retention of triplet excitons on the emitter. The HOMO and LUMO of the TMM should match those of adjacent layers to reduce charge injection barrier, thereby reducing the operating voltages. Furthermore, the HOMO and LUMO of the TMM should have a well-balanced charge carrier transport property within the EML. Moreover, TMM's must be chemically and thermally stable. A robust chemical stability is important to enable stable redox properties. Additionally, thermal stability is also essential for vapor application to avoid degradation during deposition of the molecule.

1.1.4 OLED Characteristics

To acquire a deeper understanding of OLED materials and improve them, they have to be fabricated into OLED devices and be tested. There are different parameters which are critical for the evaluation of OLED materials. Apart from voltage current (U/I) and voltage luminance (UIL)-curve, efficiency and lifetime are the most crucial parameters for evaluation of OLED devices.

1.1.4.1 Device Fabrication

An OLED device for testing the crucial parameters for the evaluation of OLED materials is depicted in Figure 6.

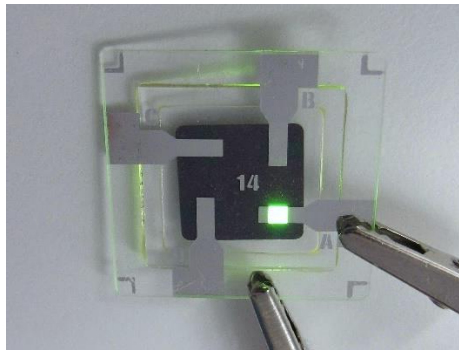


Figure 6: OLED device for evaluation of crucial parameters.¹

For the fabrication of such a device, an indium tin oxide (ITO) coated glass with a thickness of 50 nm and an area of 3x3 cm² is cleaned by oxygen-plasma and treated with UV light. Afterwards, it is transferred into a vacuum chamber with a base pressure of 10⁻⁷ mbar. Organic layers are then deposited by high vacuum thermal evaporation (VTE) with a rate of 1⁻¹⁰ Å/s. It is important to encapsulate the OLED device to avoid oxygen and moisture contact. This can detriment the performance of the device by formation of defect structures or quenching processes. Generally, impurities should be avoided, because they cause energetic traps and lead to reduction of lifetime of the device. Therefore, the device is encapsulated using cover glass and epoxy glue after deposition of an aluminum cathode.

1.1.4.2 Lifetime

Lifetime of OLED materials still needs further improvements - especially, in the commercialization of electronic devices.

¹ Picture was taken by the physics team of Merck Electronics KGaA. OLED devices in this thesis were fabricated and measured by the physics team of Merck Electronics KGaA.

The lifetime (LT) of an OLED device describes the decrease of luminance over time at a continuous current density. OLED devices are subjected to an aging process over time due to degradation of the used materials by thermal, photochemical, and electrical stress.

There are various reasons for the degradation and decrease of luminance density over time. The presence of trace impurities in ppm range like oxygen, halogens, water, and secondary amines can enormously reduce the lifetime of a device.^{[53][54]} The formations of radical ions within the organic layers can lead to reactions, whose products can serve as an energetic trap or even emit light at the range of the emitter. Structural changes within the organic layers can disturb the charge interfaces between the organic compounds and electrodes.^[55] This can as well lead to a change in the current flow. Unstable low work function cathodes and the generation of heat from internal energy losses within the device favors a low lifetime.^[56]

Generally, LT_{95} and/or LT_{90} are determined for OLED devices. This is simply the time, where 95% or 90% respectively of the initial luminance density remains at a constant current. To compare different materials regarding lifetime, the measured values are extrapolated according to its exponential decay function up to LT_{50} and the starting luminance is standardized to 100% to give a luminance-lifetime curve as exemplary shown in Figure 7.

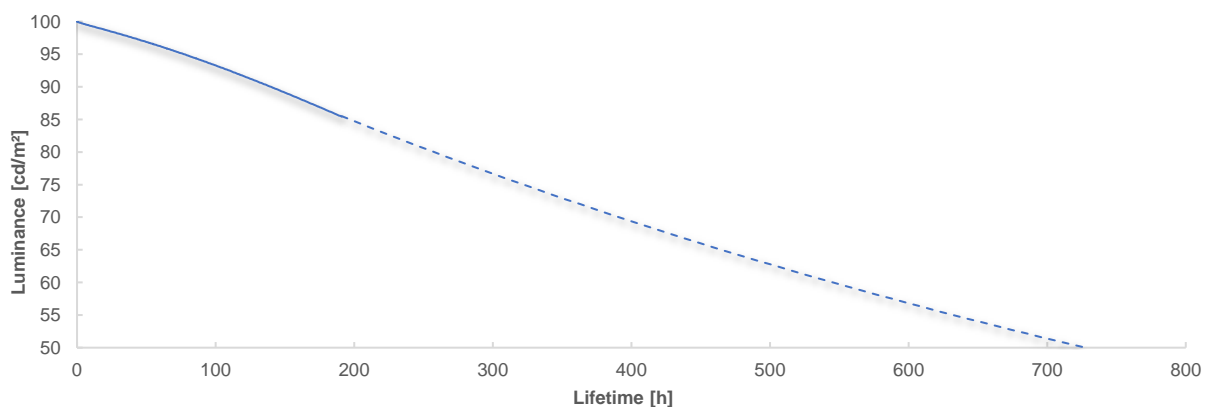


Figure 7: Example of raw data of relative lifetime of a reference stack.

1.1.4.3 Efficiency

The efficiency of OLED compounds is described by the external quantum efficiency (EQE). The EQE is important for the development and evaluation of novel OLED compounds. It is described by the ratio of emitted photons N_{photon} and injected electrons $N_{Electron}$ and is determined by using the voltage-luminescence-curve as exemplarily shown in Figure 8.^[57] The curve shows that the EQE decreases with increasing luminance. This phenomenon is called efficiency-roll-off and shows, that the energy consumption is over proportional at high luminance.^[58] It is caused by different non-radiative processes, such as high charge carrier

density in the emissive layer and triplet-triplet annihilation. The development of OLED materials aims a high EQE and flat efficiency-roll-off.

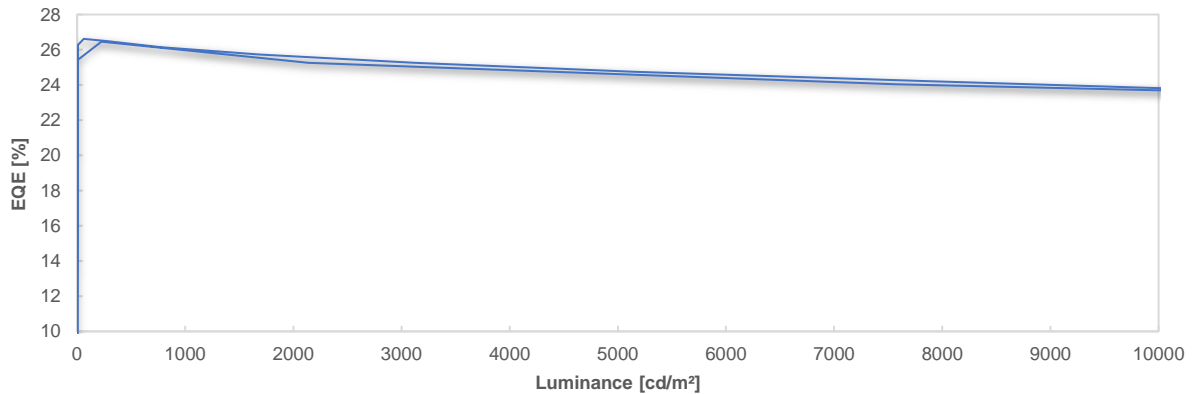


Figure 8: Example of raw data of EQE vs. luminance in a reference stack.

The calculation of the number of photons N_{Photon} takes all photons within the visible spectral range into account (380 to 780 nm). It also considers the high sensitivity of human eye to green light in the luminance (photometric unit) and can be calculated using the normalized emission intensity $I(\lambda)$ and a constant α (equation 1).^[59]

$$N_{Photon}(\lambda) = \int_{380}^{780} \left(\frac{\pi \cdot \alpha \cdot I(\lambda) \cdot \lambda}{683 \cdot hc} \right) d\lambda \quad (1)$$

$$EQE = \frac{N_{Photon}}{N_{Electron}} = IQE \cdot R_e = (\gamma \cdot \eta_{Exciton} \cdot \eta_{PL}) \cdot R_e \quad (2)$$

Equation (2) is the mathematical description of the EQE. The EQE is the ratio of emitted photons per injected electrons and equals the internal quantum efficiency (IQE) multiplied by the outcoupling photons R_e . The IQE is the product of the charge balance factor (γ , ideally 1.0, ratio of electrons and holes), the amount of radiatively relaxing excitons $\eta_{Exciton}$ (0.25 for fluorescent emitters, 0.75 for phosphorescent emitters) and the intrinsic quantum efficiency η_{PL} . The photon out-coupling efficiency η_{PL} mainly depends on the used substrate and is expected in the typical range of 15-20% in OLED devices. When assuming an internal quantum efficiency of 100%, the EQE can be around 20% for phosphorescent and 5% for fluorescent emitters.^{[60][61][62]}

2 Research Objectives

In the past years, enormous progress has been achieved in the development of materials for OLED application. However, especially the lifetime of OLED-screens has not yet reached the level of classical screens that are based on liquid crystals.^{[16][6]} The development of synthetic methods to access phosphorescent host materials for OLED devices and the development of more efficient, less energy consuming, and more stable OLED devices is of high importance for the progress of the field of electronics. Especially, long lifetime and low energy consumption are desired when talking about sustainability.

This thesis focuses on the synthesis and evaluations of novel red and green triplet matrix materials. For improving lifetime, efficiency and driving voltage of existing red and green TMM's, a deeper understanding of structure-property relationships of these molecules is required. This is achieved by the systematic exchange of electron conducting, hole conducting and linking subunits in the envisioned molecule. A typical electron conducting unit are substituted triazine and quinazoline cores. However, observations in Merck Electronic KGaA laboratories showed limited efficiency, lifetime and voltage in green and red host material applications. The search of an alternative for the triazine electron conducting unit lead to the material class of benzofuopyrimidines. Trisubstituted benzofuopyrimidine unit as a substitute for triazines have been poorly discussed in the context of red and green host material applications. Furthermore, the implementation or the removal of a linking unit as well as the variation of the hole conducting subunit are factors that give freedom to influence and optimize the structure and properties of a TMM. Since the purity standards for molecules in OLED application are high (minimum 99.9% HPLC purity and trace impurities such as for palladium, phosphor, and halogens below 3-4 ppm), synthetic methods with the highest possible conversion and lowest possible side-product formation are required.

In this context, a variety of differently constituted molecules were designed and synthesized and the influence of the triplet- and HOMO/LUMO energy level was evaluated on the lifetime, efficiency, and voltage.

Therefore, three specific aims are defined:

1. Identification and selection of structural motifs based on **DFT simulations**.
2. Development of **synthetic strategies** for the formation of heteroaromatic TMM building blocks based on benzofuopyrimidine/triazine and benzocarbazoles and its coupling. Additionally, a photo-redox catalytic system was tested to evaluate its applicability in the synthesis of precursors of TMM's and itself (Chapter 5).
3. Evaluation of the **material properties** to understand the structure-property relationship and judge their applicability in OLED devices.

3 Synthesis of Triplet Matrix Materials

Contribution: Klaus Osazuwa Omoregbee conducted and discussed the syntheses and purifications in this chapter. Compound **37** was scaled-up with the help of Christian Schreiber (Merck Electronics KGaA) up to 260 mmol. DFT calculations in the theoretical considerations were conducted and interpreted by Klaus Osazuwa Omoregbee using a script of Merck KGaA. Calculations based on DFT for the formation of compound **25** vs. **18** as well as compounds **5** and **6** were conducted by Jens Pfalzgraf. Compound characterization data (crystal structures, ¹H NMR spectra, ¹³C NMR spectra, ¹⁹F NMR spectra, HPLC-MS, HRMS) were measured by the analytic department of Merck KGaA.

3.1 Theoretical Considerations

Red, green, and blue TMM's have several common properties, such as bipolar charge transport (electron and hole conduction), triplet exciton confinement, and a good Dexter energy transfer. The design of new TMM's for phosphorescent organic light emitting diodes is challenging, as several physical property requirements need to be fulfilled. An important parameter in the design is the triplet energy of the TMM. They differentiate mainly in their triplet energy range, which is as low as 2.1-2.4 eV for red TMM's, 2.5-2.7 eV is preferred for green TMM's and high triplet energies > 2.7 eV are desired for blue TMM's.^{[63][64]} This is due to the fact, that the triplet energy level of the TMM needs to lie above the triplet energy level of the emitter. This ensures that exothermic reverse energy transfer of the emitter (loss of efficiency) is limited, and it also ensures the retention of triplet excitons on the emitter, as described in chapter 1.1.3. Furthermore, the HOMO level of a TMM needs to lie lower than the HOMO of the emitter to avoid quenching and to ensure a unidirectional charge flow towards the emitter. It is important to understand how a chemical structure influences the triplet energy level, lifetime, driving voltage and efficiency of the TMM. This would enable a structure-related design of a suitable TMM that rationalizes a balanced electron and hole transport within the emissive layer.

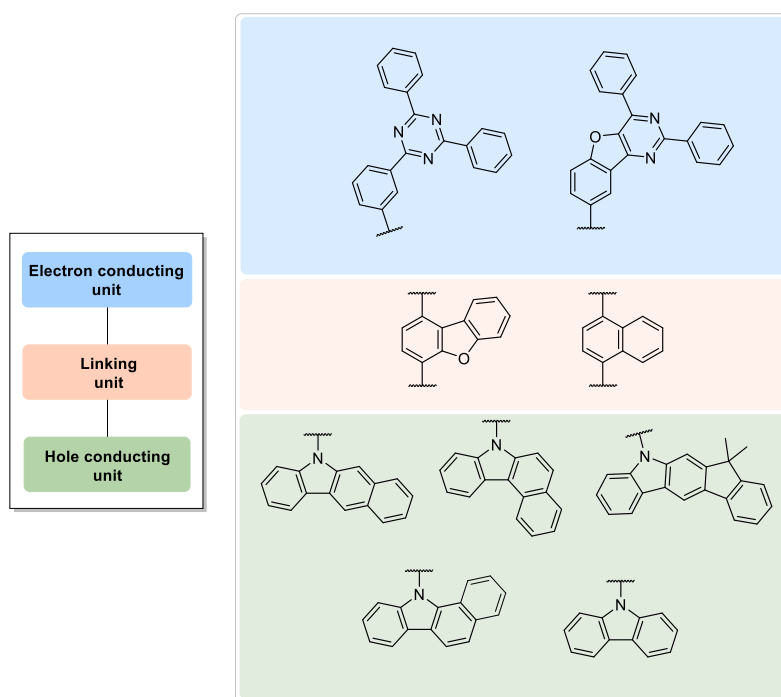


Figure 9: Overview on the variable units of TMM's and a selection of the here investigated building blocks for structure-property-relationships in this thesis.

Carbazole derivatives have a sufficiently high triplet energy level, which makes them suitable to host red and green triplet emitters. They are typical hole conducting units. Therefore,

benzocarbazoles, indenocarbazole, and carbazole were used in this thesis as a hole conducting unit. They show good hole properties and good stability due to their extended aromatic structure.^[65] They were combined with different linking units (naphthalene and dibenzofurane) and electron conducting units (benzofuopyrimidine and triphenyltriazine). These structures were then investigated for their application as red and green TMM's (Figure 9). The influence of a linking unit (naphthyl and benzofuranyl unit) will be further discussed.

As described above, diphenyltriazines and triphenyltriazines are common electron conducting units with good electron transport properties and stability under current.^[66] However, efficiency, lifetime and driving voltage are desired to be improved. Thus, the electron conducting unit was changed. Disubstituted benzofuopyrimidines have already been applied in OLED's.^{[67][68][69]} However, trisubstituted benzofuopyrimidines were not significantly applied in OLED's and have only been poorly discussed in the context of red and green TMM's. Theoretical calculations using DFT² (Figure 10) led to the hypothesis, that benzofuopyrimidine is an attractive alternative to triphenyltriazine or quinazolines (Figure 10), because the triplet energy level is higher than the triplet energy level of Merck Electronics KGaA emitters and the HOMO level is lower than that of the emitters.

This pre-evaluation was conducted for all suitable molecules by computational modeling using Gaussian 16 with the functional/basis set B3LYP/6-31G(d) in DFT.^[70] This gave an estimation for the energy levels of ground states (HOMO, LUMO in Hartree, 1 E_h = 27.211 eV) and excited states (S₁ and T₁). The HOMO and LUMO levels were also experimentally determined by cyclic voltammetry. The obtained theoretical HOMO and LUMO levels (Figure 10) were corrected by calibration with experimental cyclic voltammetry (CV) values which originated from a large internal data set of Merck Electronics KGaA using equation (3) and (4). The obtained T₁ levels are based on the difference to the lowest energy configuration S₀ of all electrons in the molecule.

$$E_{HOMO}[eV] = 0.831 \cdot (E_{calc} \cdot 27.211) eV - 1.118 \quad (3)$$

$$E_{LUMO}[eV] = 1.065 \cdot (E_{calc} \cdot 27.211) eV - 0.505 \quad (4)$$

All considered molecules and its energy levels of ground states (HOMO, LUMO) and T₁ levels are summarized and compared in Figure 10.

² DFT calculations were conducted using a script of Merck Electronics KGaA and were performed by Klaus Osazuwa Omoregbee.

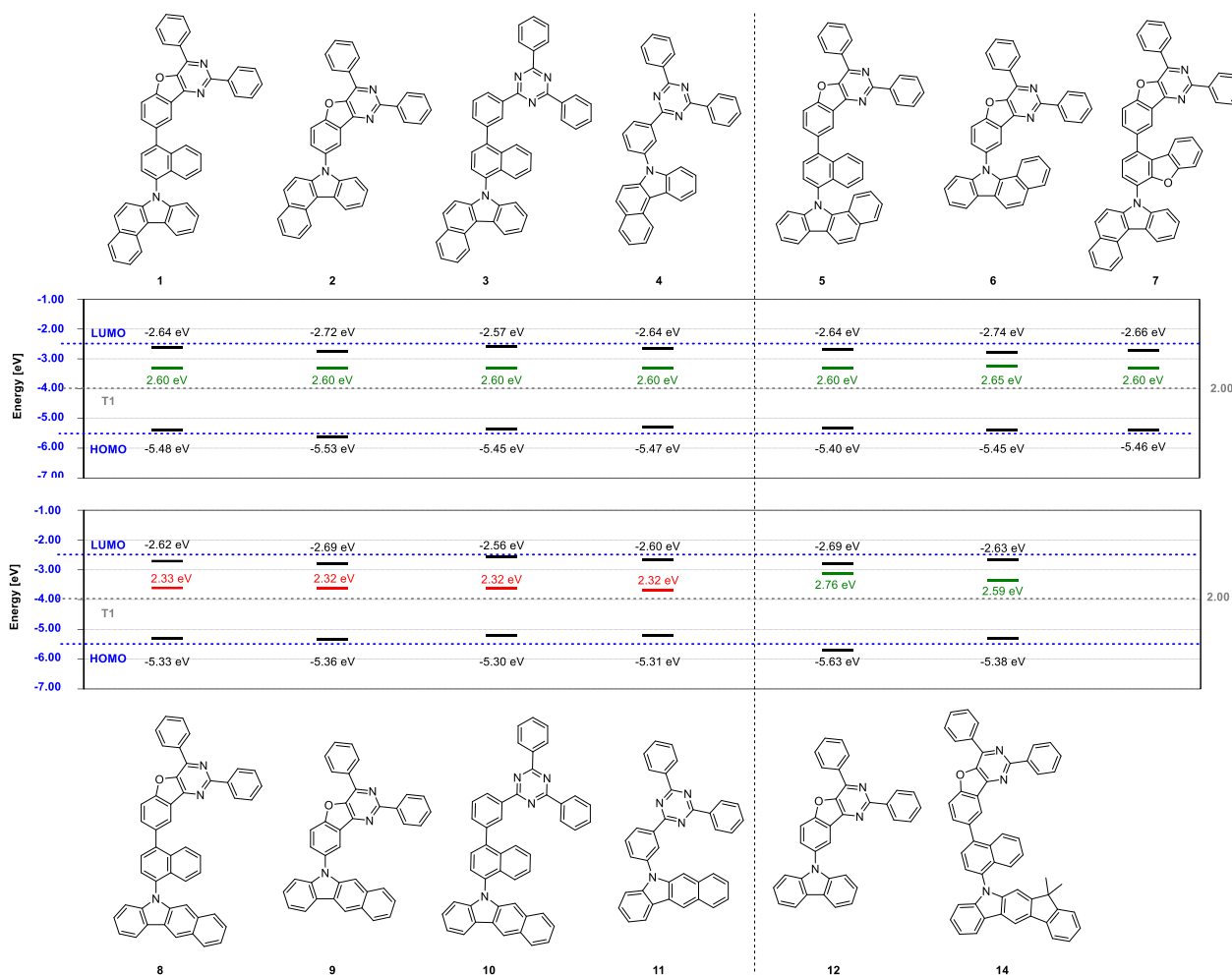


Figure 10: Overview on theoretically calculated compounds **1-14** and their HOMO, LUMO (blue) and T1 (red/green) energy levels. Energy levels of ground states (HOMO, LUMO) are corrected according to equation (1) and (2).

It is noticeable that linear [*b*]-annulated benzocarbazole units reduces the T₁ energy levels (~2.3 eV, compound **8-11**) compared to the angulated [*a*]- and [*c*]-annulated benzocarbazole units (~2.6 eV, compound **1-7**). In consequence linear [*b*]-annulated benzocarbazole units are expected to be suitable for the use as TMM for red OLED's, while [*a*]- and [*c*]-annulated benzocarbazole units are expected to be suitable for the use as TMM for green OLED's. Carbazole **12** and indenocarbazole **14** showed in different TMM's from Merck very interesting OLED properties. Therefore, they were selected for use in this thesis and are according to their triplet energy also suitable as TMM for green OLED's.

Generally, the linking unit seems to increase the HOMO level in all molecules. Noticeably, Carbazole **12** is not annulated and has a high T₁ level compared to all benzocarbazole TMM's. This could be beneficial for the application in green TMM's or even in blue TMM's.

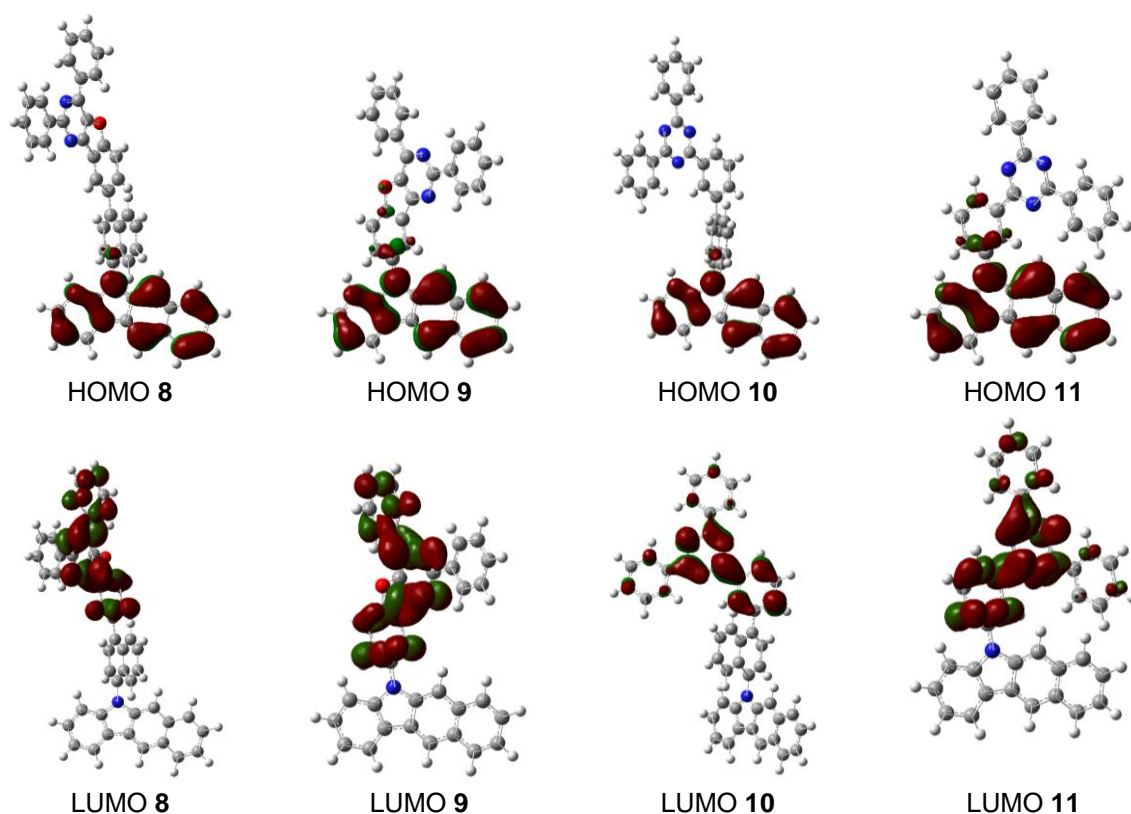


Figure 11: Frontier molecular orbital distribution (HOMO and LUMO) of red TMM's **8-11** optimized by density functional theory simulations (used functional/basis set B3LYP/6-31G(d), DFT).

Spatial distributions of the HOMO and LUMO energy levels of the molecules (Figure 11 for red TMM's and Figure 12 for green TMM's) show that the HOMO orbitals are mainly localized on the benzocarbazole units with contribution from the nitrogen heteroatom and proves it to be the hole conducting unit. The LUMO orbitals are localized on the benzofuopyrimidine or triphenyltriazine units proving it to be the electron conducting unit. Also, it can be estimated from the orbital calculation, that the hole related properties are regulated by the benzocarbazole unit and the electron related properties are governed by the benzofuopyrimidine/triphenyltriazine unit. However, there is a slight overlap between HOMO and LUMO in compound **9** and **11**. This overlap shows a weak electronic communication between benzocarbazole and benzofuopyrimidine/triphenyltriazine. In compound **8** and **10**, the HOMO is localized mainly on the benzocarbazole unit, while the LUMO is exclusively located on benzofuopyrimidine and triphenyltriazine. Nevertheless, the HOMO in **8** and **10** is slightly distributed on the linking unit.

In case of the green TMM's, the HOMO orbitals are localized mainly on the benzocarbazole, carbazole and indenocarbazole units with contribution from the nitrogen heteroatom and proves them to be the hole conducting unit. The LUMO orbitals are primarily distributed on the benzofuopyrimidine or triphenyltriazine units proving it to be the electron conducting unit. However, the HOMO and LUMO of compounds **2**, **4** and **12** have a marginal overlap. These compounds like **9** and **11** bear a linking group.

Despite that, the HOMO of compounds **1**, **3**, **7** and **14** with a linking group are distributed primarily on benzocarbazole, carbazole and indenocarbazole. The LUMO are exclusively localized on benzofuopyrimidine/triphenyltriazine.

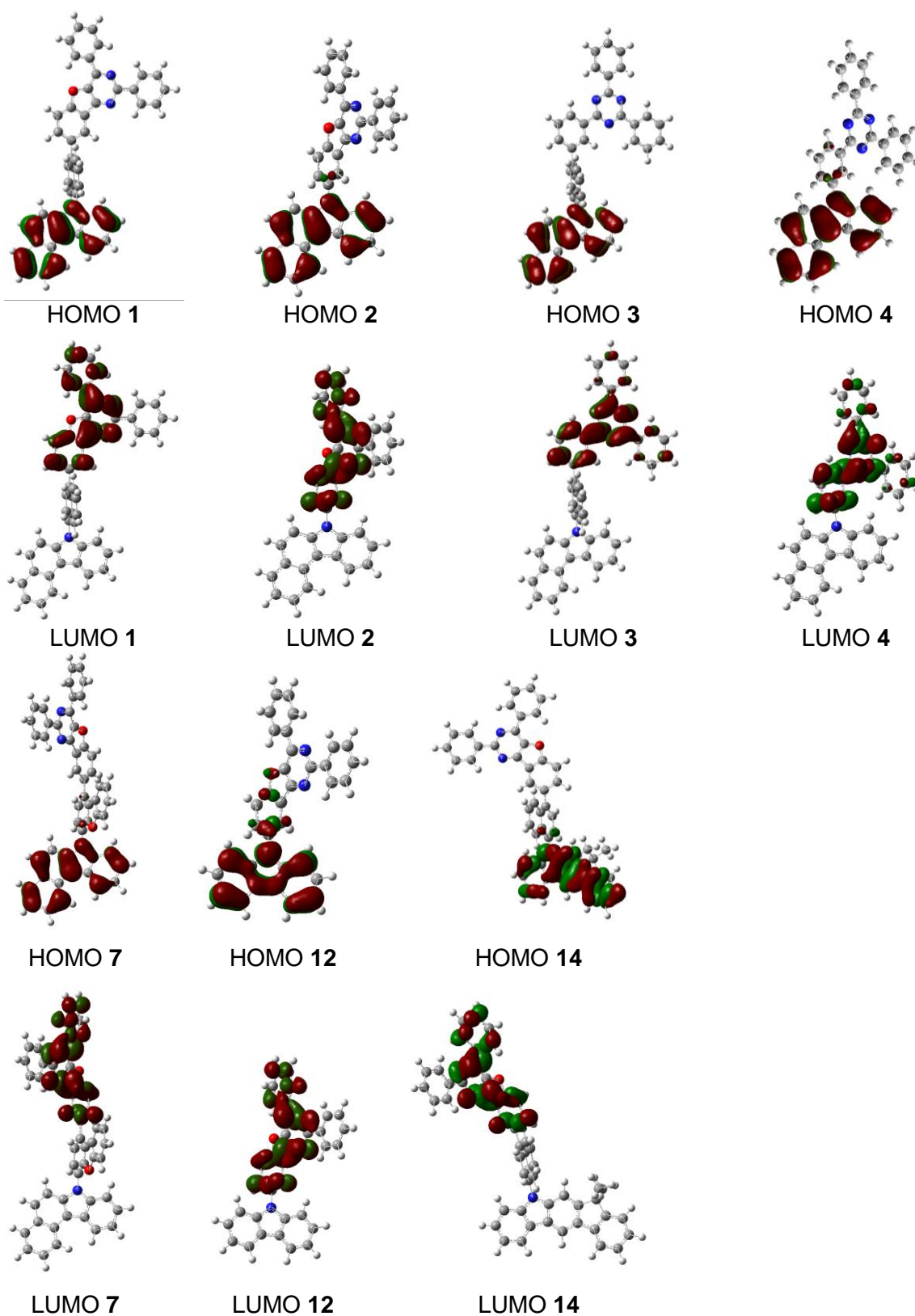
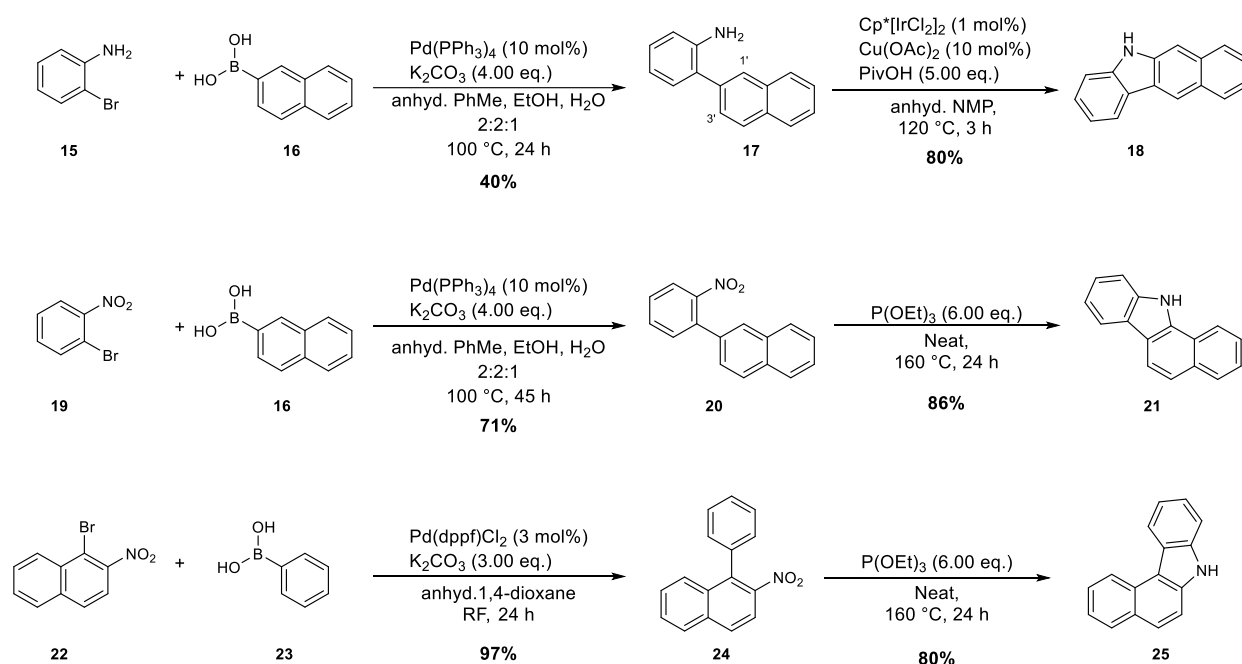


Figure 12: Frontier molecular orbital distribution (HOMO and LUMO) of green TMM's **1-4**, **7**, **12-14** optimized by density functional theory simulations (used functional/basis set B3LYP/6-31G(d), DFT).

3.2 Synthesis of Heteroaromatic TMM Building Blocks

3.2.1 Benzocarbazoles - Selective Formation

For the synthesis of target compounds **1-11** (Figure 10), the selective formation of benzocarbazole building blocks **18**, **21** and **25** is required (Scheme 1). While the red target compounds **8-11** contain the linear [*b*]-annulated benzocarbazole unit **18** (5*H*-benzo[*b*]carbazole), the green target compounds **1-4** and **7** contain an angulated [*c*]-annulated benzocarbazole unit **25** (7*H*-benzo[*c*]carbazole) and the green target compounds **5** and **6** contain the angulated [*a*]-annulated benzocarbazole unit **21** (11*H*-benzo[*a*]carbazole).



Scheme 1: Selective synthesis of various regioisomers of benzocarbazole (**18**, **21** and **25**).

Scheme 1 describes the successful and selective formations of each benzocarbazole isomer **18**, **21** and **25**. Angulated 11*H*-benzo[*a*]carbazole **21** was synthesized starting from the reaction of nitrobenzene **19** and naphthalen-2-ylboronic acid **16** to give **20** via Suzuki-Miyaura coupling.^[71] Compound **20** was then cyclized to **21** via a reductive amination, called Cadogan cyclization^[72] in this case with 100% regioselectivity.

For the synthesis of angulated 7*H*-benzo[*c*]carbazole **25**, bromide **22** was reacted with boronic acid **23** using Suzuki-Miyaura coupling to give **24**. The reductive amination can only give regioisomer **25** in the Cadogan cyclization.^[72] The mechanism of the Cadogan cyclization is depicted in Figure 13.

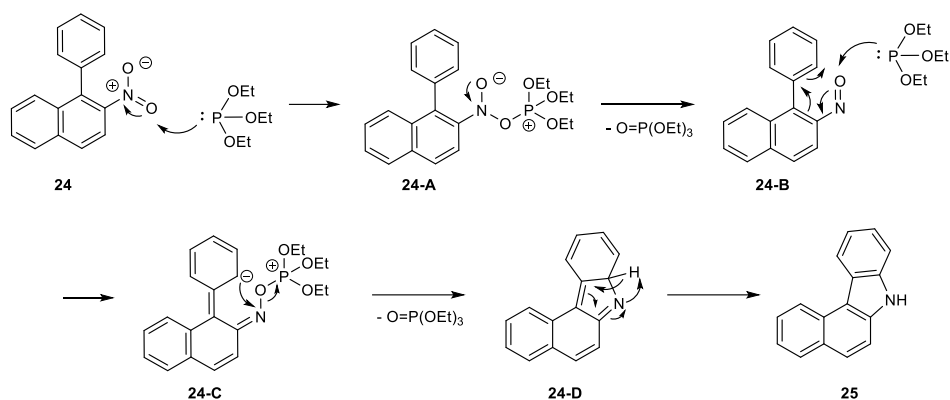


Figure 13: Proposed mechanism for the Cardogan cyclization of nitro-compound **24** to give *7H*-benzo[*c*]carbazole **25**.

Notably, the selective synthesis of linear *5H*-benzo[*b*]carbazole **18** was challenging. For the synthesis of linear *5H*-benzo[*b*]carbazole **18**, 2-bromoaniline **15** was reacted with naphthalen-2-ylboronic acid **16** *via* Suzuki-Miyaura coupling to give aniline **17** (Scheme 1). **17** was converted to **18** by an iridium(III)-catalyzed intramolecular C-H amination. Similar conditions were shown by Miura *et al.*^[73] The iridium(III)-catalyzed intramolecular C-H amination of **17** can give two regioisomeric products (desired [*b*]-annulated **18** and undesired [*c*]-annulated **21**), while the [*b*]-annulated linear benzocarbazole regioisomer **18** turned out to be favoured over the [*c*]-annulated carbazole **21** under the shown conditions. This can be explained by the mechanism for the iridium(III)-catalyzed intramolecular C-H amination proposed by Miura *et al.* (Figure 14).^[73]

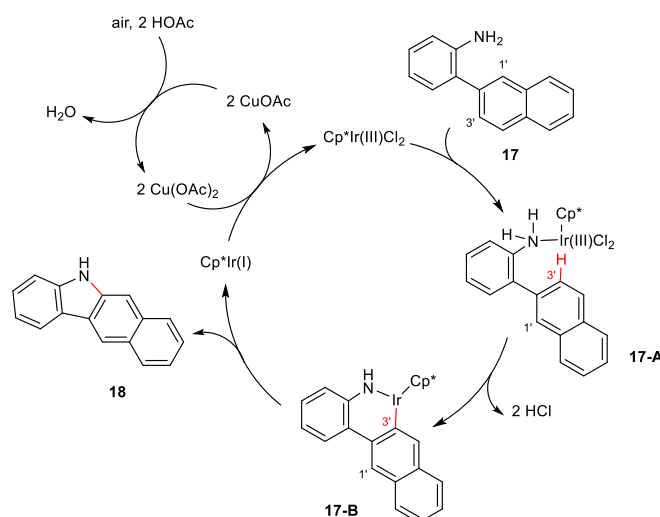
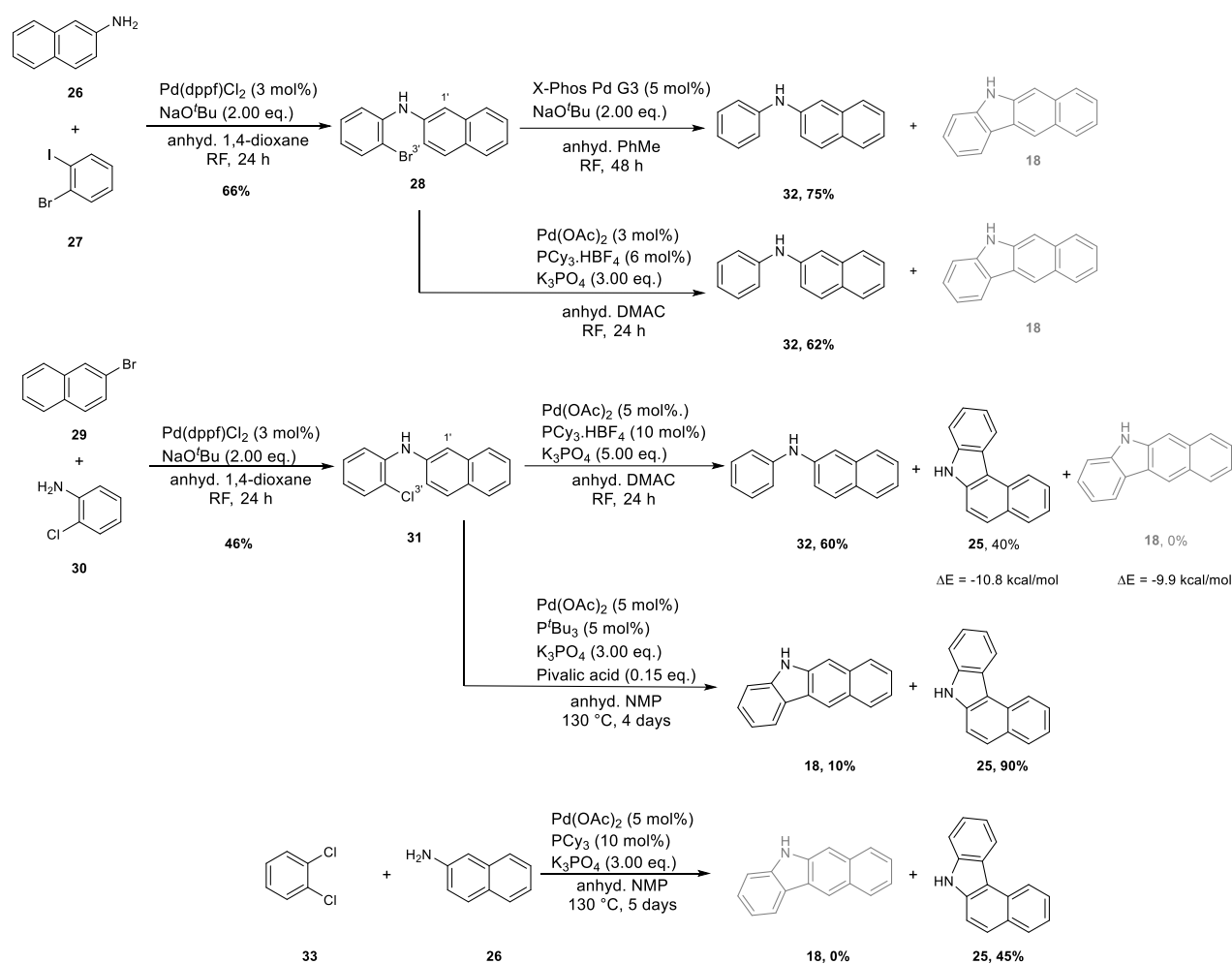


Figure 14: Mechanism of the Iridium(III)-catalyzed intramolecular C-H amination proposed by Miura *et al.*^[73]

Since the 3'-position is sterically less hindered than the 1'-position in aniline-derivative **17**, the C-H activation at 3'-position is favoured due to the sterically demanding nature of iridium-complex **17-A** and **17-B**. Coordination of the nitrogen atom of the amine group at **17** to a Cp*-iridium(III) species gives intermediate **17-A**, followed by the amino-directed C-H bond cleavage at sterically less hindered 3'-position (not at 1'-position). This forms an iridacycle intermediate

17-B, which undergoes C-N reductive elimination to afford the desired [*b*]-annulated linear benzocarbazole isomer **18**.

Further strategies were performed for the synthesis of [*b*]-annulated carbazole **18**, summarized in Scheme 2, that however showed less selectivity than the iridium(III)-catalyzed intramolecular C-H amination for the cyclization step, due to the preferred regioselectivity to **25**.



Scheme 2: Failed approaches on the selective synthesis of [*b*]-annulated linear benzocarbazole isomer **18**.

Apart from the successful iridium(III)-catalyzed intramolecular C-H amination strategy, the first imaginable strategy for the synthesis of [*b*]-annulated carbazole **18** is a Buchwald-Hartwig amination^{[74][75]} of the aniline-derivative **26** or **30** with the iodine or bromide species **27** or **29** to the secondary amine intermediate **28** or **31**. This intermolecular amination was successful for intermediate **28** as well as intermediate **31** using Pd(dppf)Cl₂ and sodium *tert*-butoxide with moderate yields. Then, an intramolecular ring closure *via* palladium catalyzed C-H activation was planned. Here, the C-H-activation at 1'-position and 3'-position are conceivable to give either desired [*b*]-annulated carbazole **18** or undesired [*c*]-annulated carbazole **25**. Using bromide **28** for the intramolecular ring closure only debrominated side product **32** was achieved under different palladium C-H activation conditions (X-Phos Pd G3 or Pd(OAc)₂). Therefore, it

was assumed, that bromide as an electrophile ($\Delta H(\text{C-Br}) = 285 \text{ kJ/mol}$) is too reactive and chloride-derivative **31** was used instead ($\Delta H(\text{C-Cl}) = 339 \text{ kJ/mol}$).^[76] Chlorides are often not reactive enough for palladium catalyzed C-H functionalizations, while it is known that the use of electron-rich tertiary phosphine ligands can allow the use of chlorides instead of bromides or iodides as electrophiles.^[77]

Upon the use of chloride **31**, dechlorinated species **32** was observed, but also undesired [c]-annulated carbazole **25**. This shows that the C-H-activation of chloride **31** is possible and leads to intramolecular ring closure. However, the ring closure results at the undesired 1'-position. This position is known to be more sterically hindered (directly neighbored aryl substituent), but on the other hand to be more C-H acidic than the 3'-position in case of naphthalene (quaternary carbon neighbored instead of C-H neighbored).^[78] Theoretical calculations³ support this phenomenon, as the free energy for formation of [c]-annulated carbazole **25** is -10.8 kcal/mol, while the free energy for formation of [b]-annulated carbazole **18** is -9.9 kcal/mol.

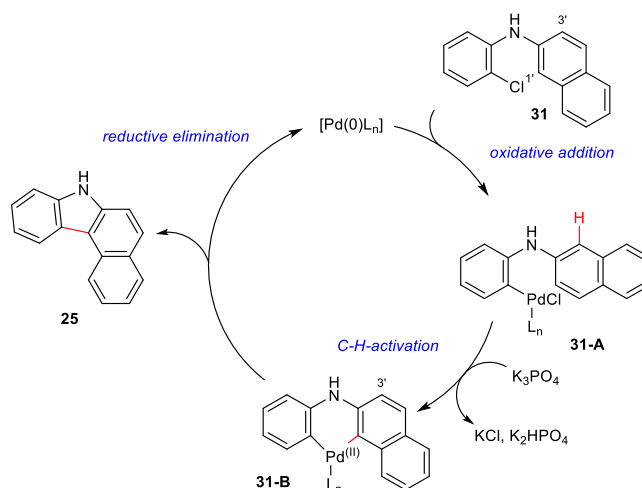


Figure 15: Proposed mechanism of the intramolecular ring closure by palladium-catalyzed C-H activation.

The proposed mechanism for aryl-aryl couplings for intramolecular ring closure *via* C-H activation is depicted in Figure 15. All synthesized benzocarbazoles building blocks are ready for further use for the synthesis of the TMM target compounds.

The overlaid ^1H NMR spectra of all three benzocarbazole regioisomers are shown in Figure 16 giving already an idea for the differences in the electron environment, shielding at the N-H-proton and the aromatic protons. The reactivity of all benzocarbazole building blocks in nucleophilic aromatic substitutions or Buchwald-Hartwig reactions are discussed in detail in chapter 3.3 for the synthesis of red and green TMM's.

³ Calculations based on DFT (b3lyp/631g*), conducted by Jens Pfalzgraf.

3 Synthesis of Triplet Matrix Materials

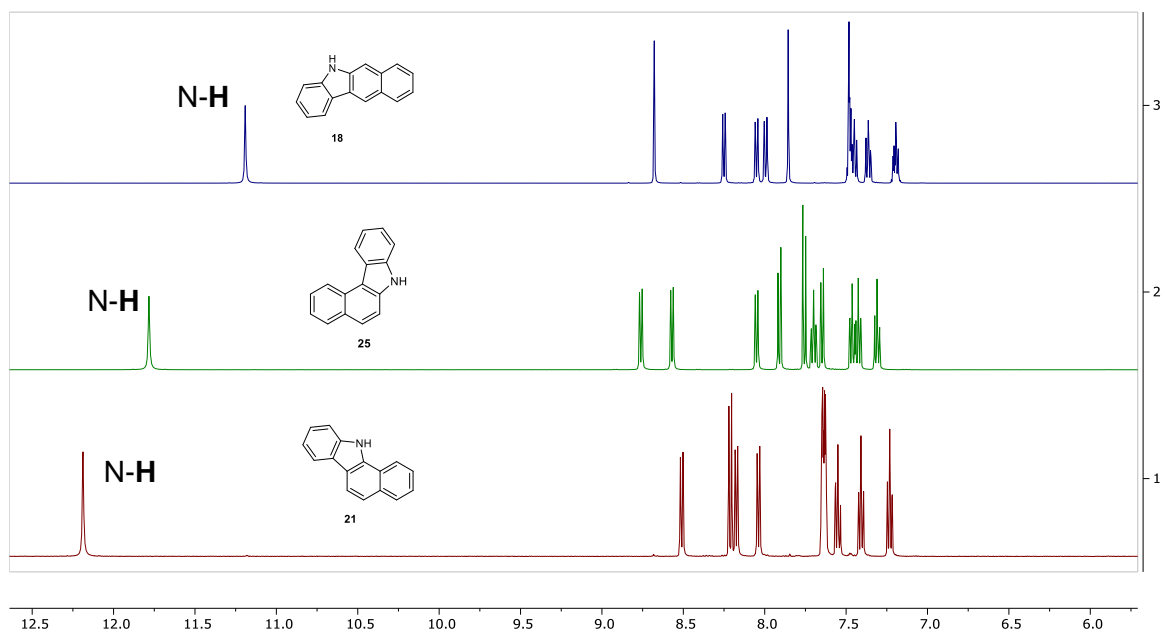
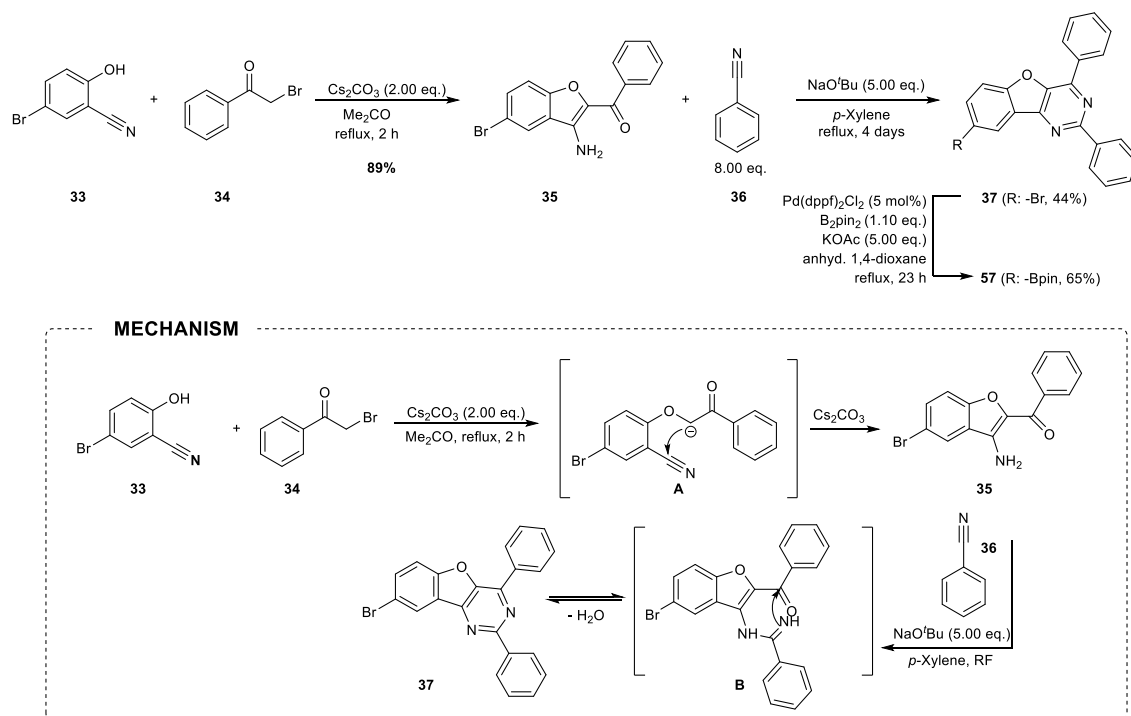


Figure 16: Comparison of chemical shifts of synthesized benzocarbazole regioisomers **18**, **25** and **21**, showing different electrical environment at the N-H-bond.

3.2.2 Benzofuopyrimidine

One of the key structural motifs in this work is the trisubstituted benzofuopyrimidine unit, which has only been poorly discussed for OLED application. Therefore, several target compounds (Figure 10) contain a benzofuopyrimidine unit.



Scheme 3: Synthesis of benzofuopyrimidine⁴ building block **37** and its proposed mechanism.

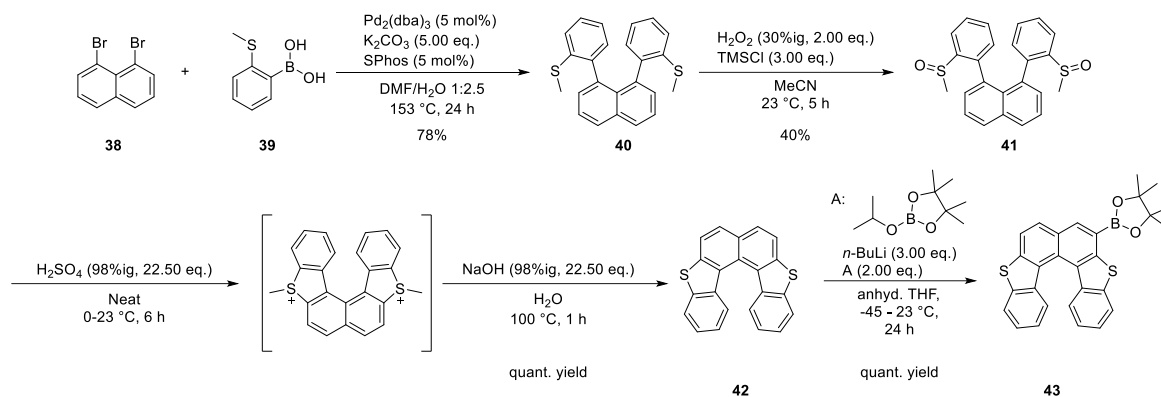
Scheme 3 shows the synthesis of benzofuopyrimidine building block **37**. Benzofuopyrimidine building block **37** is synthesized in a literature-known furan formation by S_N2 reaction of 2-hydroxybenzonitrile and 2-bromoacetophenone^[79] followed by a condensation reaction. 2-Hydroxybenzonitrile **33** is deprotonated by Cs₂CO₃ to generate an alcoholate, which as a nucleophile attacks 2-bromoacetophenone **34** in a S_N2 fashion to give 3-amino-2-aryl benzofuran **35** via intermediate **A**. This reaction is very fast, since the alcoholate is a strong nucleophile due to the +M-effect of the bromine at the para-position. Furthermore, **34** is a good electrophile and reactive, because bromine withdraws electron density out of the molecule (-M-effect) and because of enole formation. Both phenomena lead to an increase in C-H-acidity at the methylene group at **34**. The newly formed 3-amino-2-aryl benzofuran **35** then reacts with benzonitrile **36** via intermediate **B** in a nucleophilic addition. This reaction is very slow, because of the formation of water as a side product. This influences the equilibrium of the reaction and shifts it to the educts. The removal of water from the reaction system using a Dean-Stark trap gave benzofuopyrimidine building block **37** with a yield of 44%, which is ready

⁴ Scale-up of the described reaction was done with the help of Christian Schreiber (Merck Electronics KGaA) up to 260 mmol.

for further use for the synthesis of the TMM target compounds. For some further couplings, **37** was also converted to boronic ester **57** using Miyaura borylation conditions.

3.2.3 Naphthodibenzothiophene

For variation of the hole conducting benzocarbazole unit, the naphthodibenzothiophene building block **43** was synthesized according to literature procedure (Scheme 4).^[80]

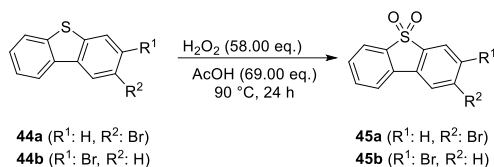


Scheme 4: Synthesis of compound naphthodibenzothiophene building block **43** according to literature procedure.^[80]

For the synthesis of naphthodibenzothiophene building block **43**, boronic ester **39** and bromide **38** were coupled in a Suzuki reaction. This resulted in the formation of sulfanyl compound **40**, which was then oxidized using hydrogen peroxide and TMSCl to give sulfinyl compound **41**.^[81] Electrophilic ring closure of the sulfinyl compound **41** was conducted using concentrated sulfuric acid to give naphthodibenzothiophene **42**. Lithiation with *n*-BuLi and reaction with **A** gave boronic ester **43** quantitatively. It is ready for further use for the synthesis of the TMM target compounds.

3.2.4 Dibenzothiophensulfones

Another structural motif for comparison is the dibenzothiophensulfone motif. Dibenzothiophensulfone building blocks **45a** and **45b** were synthesized in an oxidation of dibenzothiophenes **44a** and **44b** using hydrogen peroxide in acetic acid, as it has already been described for other substrates in literature.^[82]



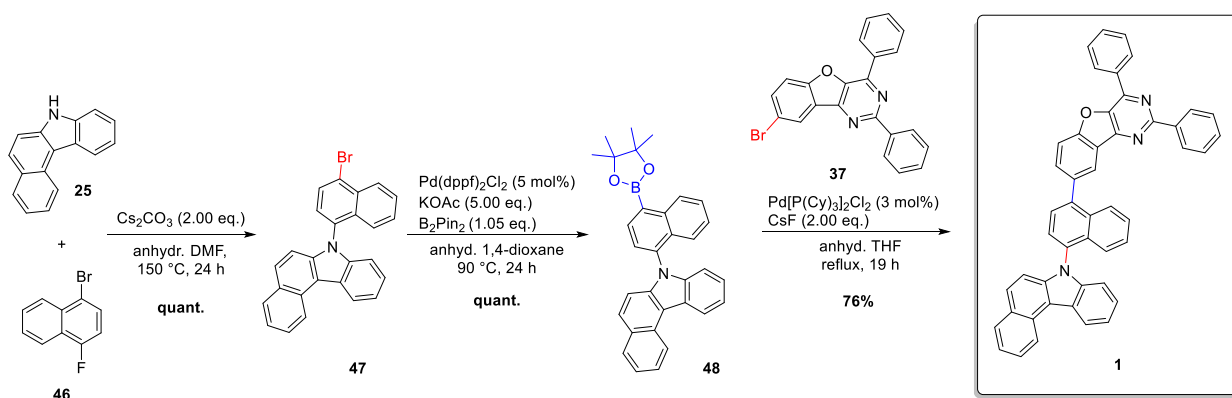
Scheme 5: Synthesis of dibenzothiophensulfone building blocks **45a** and **45b**.

3.3 Synthesis of the targeted TMM's

3.3.1 Synthesis of green TMM's based on benzocarbazole **25** and derivatives

For the synthesis of green target TMM's, mainly angulated [c]-annulated benzocarbazole unit **25** (7*H*-benzo[*c*]carbazole) was used as a hole conducting unit. Generally, the [c]-annulated benzocarbazole unit **25** was reliably coupled to the linker naphthyl-fluoride in a nucleophilic aromatic substitution with excellent yields. Here, the nitrogen of carbazole **25** is deprotonated by cesium carbonate. The free electron pair of the benzocarbazolate then acts as a nucleophile, which attacks the C-F bond on the aromatic naphthyl ring of compound **46** owing to the high nucleophilic substitution reactivity exhibited by the C-F bond. It is known that C-F bonds show much higher reactivity in nucleophilic substitution than C-Cl and C-Br bonds due to the extreme polarity of the C-F bond in arylfluorides caused by the strong electronegativity of fluor.^[83] The reaction is chemoselective and the nucleophilic aromatic substitution takes place at the fluoride of compound **46**.

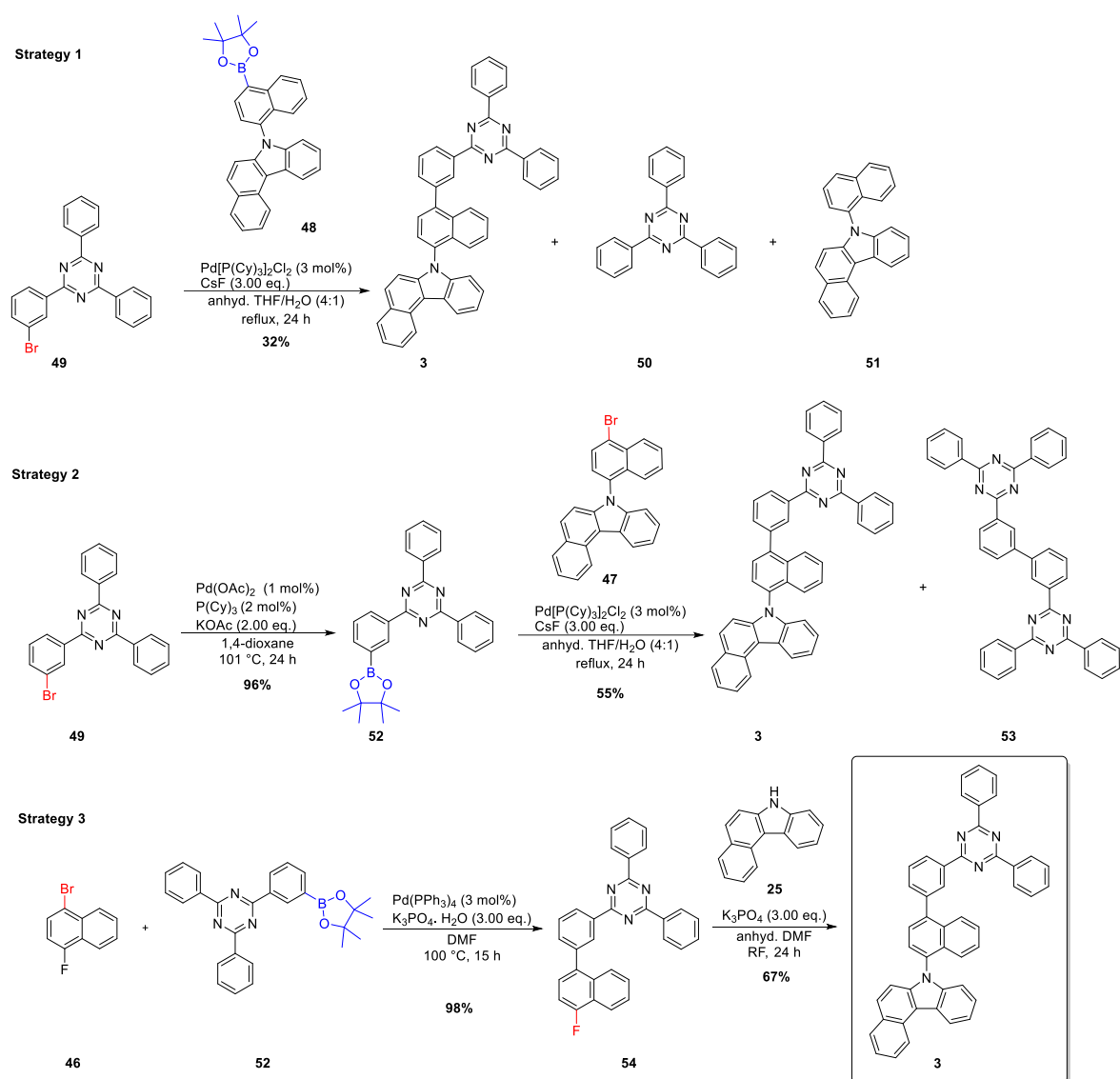
For the synthesis of target TMM **1**, [c]-annulated benzocarbazole unit **25** was coupled quantitatively to naphthyl-fluoride **46** to give compound **47**. Afterwards, bromide **47** was converted to a boronic ester *via* a Miyaura borylation under standard conditions to give boronic ester **48**. The boronic ester **48** was instantly used without further purification for the following Suzuki-Miyaura coupling with benzofuropyrimidine building block **37** to give target **1** with a yield of 76%.



Scheme 6: Synthesis of green target compound **1**.

For the synthesis of target TMM **3**, that contains a triazine unit, three different approaches were tested (Scheme 7) to obtain the optimal synthesis.

3 Synthesis of Triplet Matrix Materials



Scheme 7: Synthesis of green target compound **3** using strategy 1 and 2 with the formation of a significant amount of side products from homocoupling, debromination and deborylation or using efficient strategy 3 without significant side product formation.

Strategy 1 adapts the same procedure that was successful for the synthesis of target **1**. In the case of triazine bromide **49**, several side products were observed that were challenging to separate from target molecule **3**. The side products had similar solubility like the product itself. This made the separation *via* column chromatography or recrystallization tedious. This was not observed for the use of benzofuropyrimidine bromide **37**. The side products are attributed to debromination and deborylation of starting materials **49** and **48**.

In Strategy 2, triazine bromide **49** was converted in a Miyaura borylation to boronic ester **52**. However, this compound was prone to homocoupling in the following Suzuki-Miyaura reaction (Figure 17). The homocoupling product **53** was inseparable from target compound **3** and NMR quantification showed that 6.5% were present in the product mixture (93.5%). However, OLED purity standards require HPLC purity of 99.99%. Therefore, Strategy 2 was neglected, and Strategy 3 was evaluated.

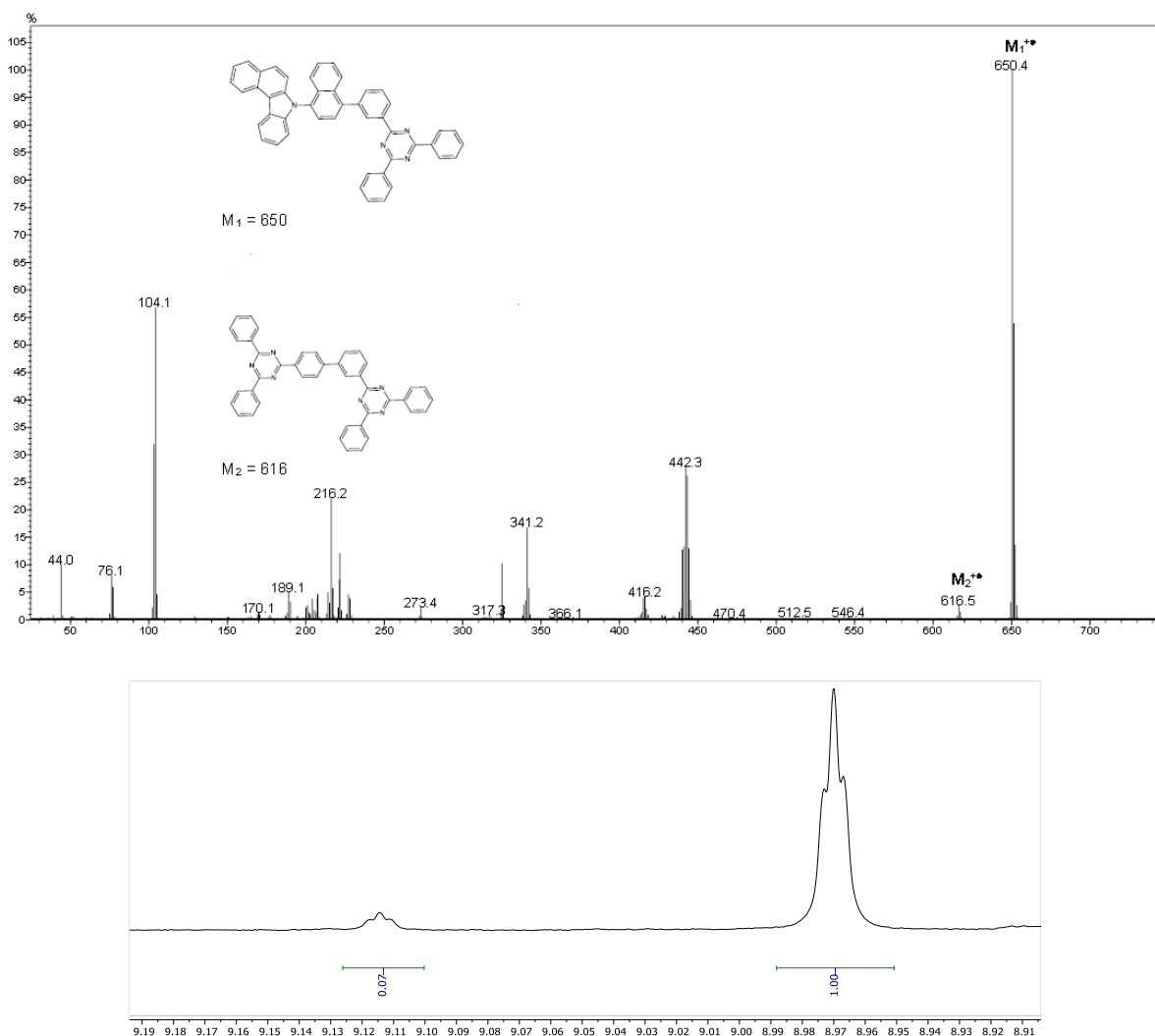
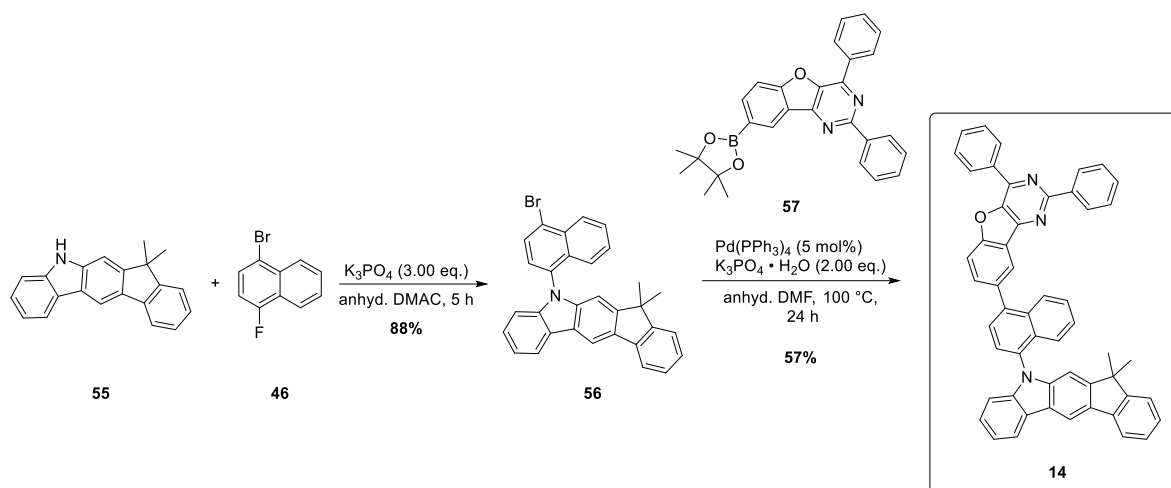


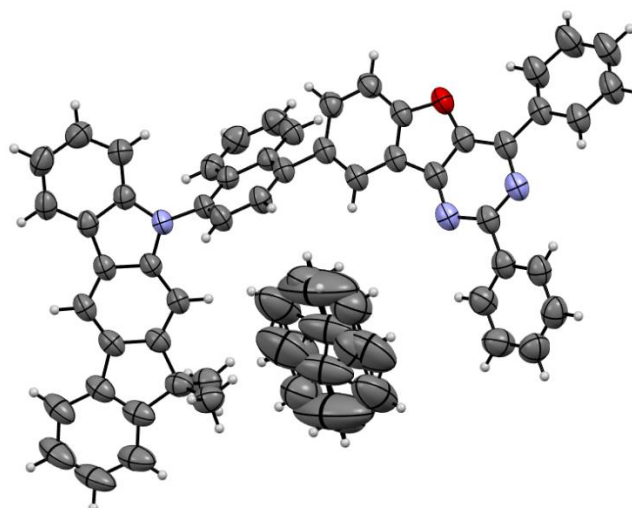
Figure 17: GC-MS of the product of strategy 2 (Scheme 7) showing the formation of homocoupling product **53** and extract from the ¹H NMR spectrum showing that the side product content of **53** is 6.5%.

For Strategy 3, boronic ester **52** was first coupled to the more reactive bromide **46** (compared to bromide **47** in Strategy 2). Bromide **46** is more reactive than bromide **47**, because the fluoride at bromide **46** has a strong -I-effect, which facilitates the reaction with boronic ester **52** and prevents homocoupling in this step. Fluoride **54** was then coupled to benzocarbazole **25** in a nucleophilic aromatic substitution to give target molecule **3** with a yield of 67% and without significant side product formations.

Scheme 8: Synthesis of target compound **14**.

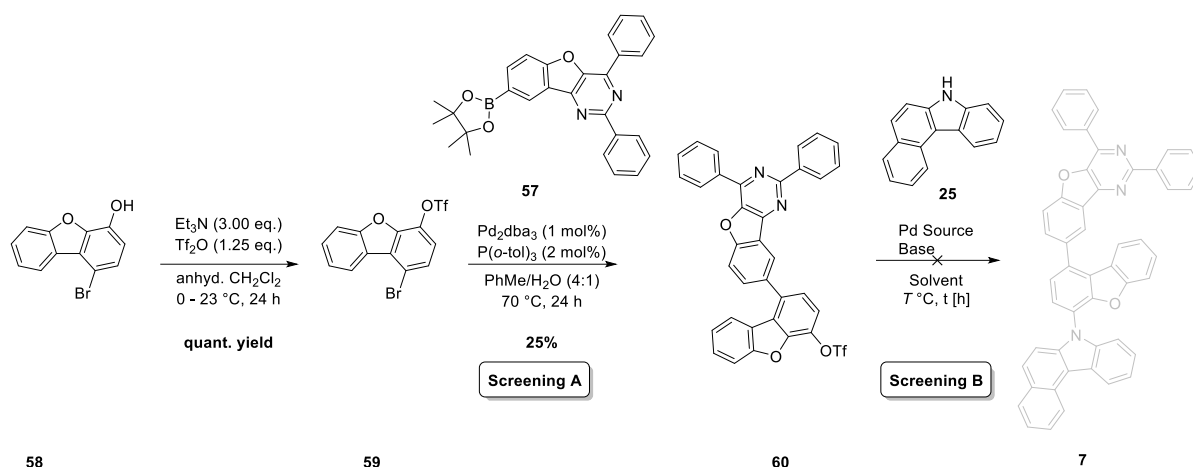
Indenocarbazole **55** was selected to substitute the benzocarbazoles, since it has been proven to have interesting properties in TMM's. For the synthesis of target TMM **14**, indenocarbazole **55** was reacted with fluoride **46** in a nucleophilic aromatic substitution to give bromide **56** with 88% yield. Afterwards, bromide **56** was coupled with boronic ester **57** via a Suzuki-Miyaura coupling to give compound **14** with a yield of 57%.

Compound **14** was crystallized from toluene to allow for single crystal structure analysis. For compound **14**, a crystal structure depicted in Figure 18 was obtained.

Figure 18: ORTEP plot of compound **14** with front view orthogonally at the indenocarbazole donor unit. A disordered toluene molecule is present in the single crystal.

To investigate the influence of the electronical and constitutional effect of the linker unit, the naphthyl motif was substituted by a dibenzofuran motif in target compound **7**. However, the synthesis of target **7** turned out to be more challenging than the equivalent target **1**. Two strategies and screenings were tested. The strategy described in Scheme 9 using a triflate

nucleophile was not successful, while the strategy described in Scheme 10 using a chloride nucleophile was successful.



Scheme 9: Synthesis of triflate **60** using Suzuki conditions and failed following Buchwald-Hartwig coupling to target **7**.

Commercially available phenol **58** was converted to triflate **59** with quantitative yield. Compound **60** was obtained *via* Suzuki-Miyaura coupling between triflate **59** and boronic ester **57** with a yield of 25%. Screening conditions (**Screening A**) for this conversion are summarized in Table 1. Here, different catalyst systems and bases with different pK_B values as well as different solvents were screened. Generally, triflates are known to be less reactive than bromides in Suzuki couplings.^[84] Selective Suzuki couplings at the C-Br bond on bromo-aryl triflates are reported for the use of tri-*tert*-butyl phosphine or triphenylphosphine or for the combination of $\text{Pd}(\text{OAc})_2$ and tri-ortho-tolylphosphine ($\text{P}(o\text{-tol})_3$) as a ligand.^{[85][86][87][88]}

It turned out, that the use of a weak base like potassium carbonate in combination with the catalytic system consisting of $\text{Pd}_2(\text{dba})_3$ and $\text{P}(o\text{-tol})_3$ gave the best results with a yield of 85%. The catalytic system is known to give good selectivity between bromide and triflate in a compound like **59**.

3 Synthesis of Triplet Matrix Materials

Table 1: Summary of screening conditions (**Screening A**, Scheme 9) for the coupling of bromide **59** with boronic ester **57** to triflate **60**. Best conditions are highlighted in blue.

Entry	Base	Catalyst-System (ratio)	T [°C]	Solvent ratio	t [h]	Yield [%]
1	K ₃ PO ₄ ·H ₂ O	Pd PePPSI-IPent	85	1,4-dioxane		-
2	K ₃ PO ₄ ·H ₂ O	Pd (P ^t Bu ₃) ₂	85	1,4-dioxane		10
3	K ₃ PO ₄ ·H ₂ O	Pd(dppf)Cl ₂	85	1,4-dioxane		-
4	K ₃ PO ₄ ·H ₂ O	Pd (PPh ₃) ₄	85	1,4-dioxane		<i>unselective</i>
5	K ₂ CO ₃	Pd ₂ (dba) ₃ /P(<i>o</i> -tol) ₃ 1:2	70	PhMe/H ₂ O 3:1		69
6	K ₂ CO ₃	Pd ₂ (dba) ₃ /dppb 1:3	70	PhMe/H ₂ O 3:1		54
7	K ₂ CO ₃	Pd(OAc) ₂ / P(<i>o</i> -tol) ₃ 1:2	70	PhMe/H ₂ O 3:1		50
8	K ₂ CO ₃	Pd ₂ (dba) ₃ /P(<i>o</i> -tol) ₃ 1:2	70	PhMe/H ₂ O 4:1		85

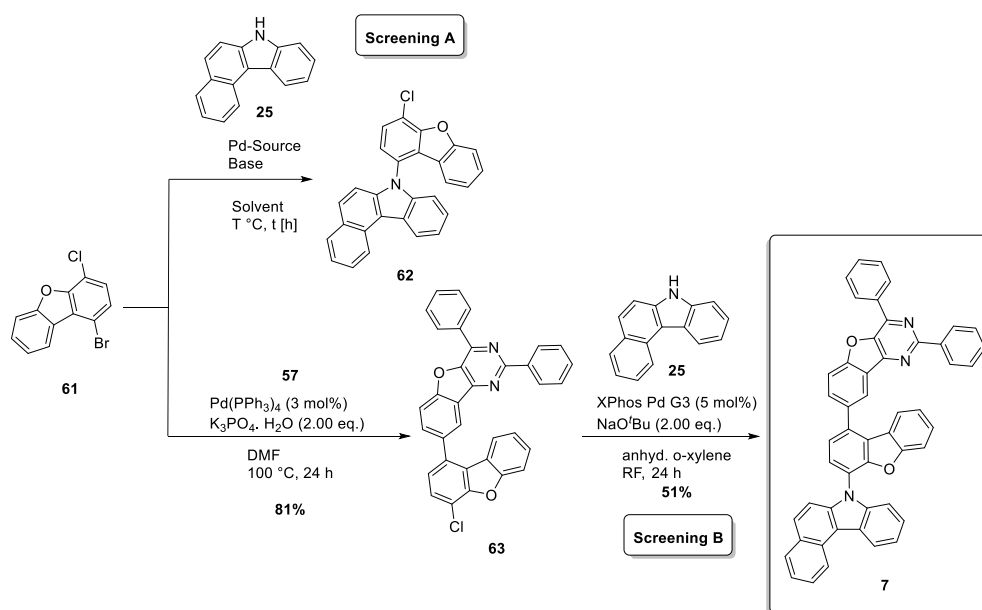
Afterwards, triflate **60** was approached to be coupled to benzocarbazole **25** in a Buchwald-Hartwig coupling. Screening conditions (**Screening B**) for this conversion are summarized in Table 2.

Nevertheless, target molecule **7** was not obtained from triflate **60**. There were no Buchwald-Hartwig conditions found, that worked with these substrates. Either no reaction took place, or the conditions were too harsh for the triflate so that only hydrolysis to give the phenol side product was observed. Buchwald-Hartwig conditions with benzocarbazole usually work with halides and is well researched, but the reaction of triflates in BHR is not well described in literature. Therefore, the strategy to synthesize target compound **7** was changed.

Table 2: Summary of screening conditions (**Screening B**, Scheme 9) for the failed coupling of triflate **60** with benzocarbazole **25** to target compound **7**.

Entry	Base	Catalyst-System (ratio)	T [°C]	Solvent ratio	t [h]	Yield [%]
1	NaO ^t Bu	Pd(P ^t Bu ₃) ₂	110	PhMe		<i>Only phenol</i>
2	LiO ^t Bu	Pd(OAc) ₂ /XPhos 1:2	80	PhMe		-
3	LiO ^t Bu	Pd(OAc) ₂ /XPhos 1:2	110	PhMe		<i>Only phenol</i>
4	LiO ^t Bu	Pd(OAc) ₂ /XPhos 1:2	50	PhMe		-
5	LiO ^t Bu	Pd(PPh ₃) ₄	80	PhMe		-
6	LiO ^t Bu	Pd(dppf)Cl ₂	80	PhMe		-
7	LiO ^t Bu	Pd(PCy) ₃ Cl ₂	80	PhMe		-

Since the above depicted method was unable to provide the desired compound **7**, a different approach was made starting from commercially available dibenzofuran **61** (Scheme 10). Two different ways of coupling dibenzofuran **61** were tested. First, bromide **61** was coupled to benzocarbazole **25**. Here, only yields up to 30% were achieved, as homocoupling and dehalogenation were significant side reactions, or the educts were fully recovered. Screenings for the Buchwald-Hartwig reaction to acquire compound **62** are summarized in Table 3. Also, Ullmann conditions failed. Originally, it was planned to couple compound **62** with boronic ester **57** to give target compound **7**.



Scheme 10: Synthesis of triflat **60** using Suzuki conditions and failed following Buchwald-Hartwig coupling to target **7**.

Table 3: Summary of screening conditions (**Screening A**, Scheme 10) for the coupling of bromide **61** with benzocarbazole **25** to compound **62**. Best conditions are highlighted in blue.

Entry	Base	Catalyst-System (ratio)	T [°C]	Solvent ratio	t [h]	Yield [%]
1	NaO ^t Bu	Pd(P ^t Bu ₃) ₂	110	PhMe	48	-
2	CS ₂ CO ₃	Pd(P ^t Bu ₃) ₂	110	PhMe	48	-
3	CS ₂ CO ₃	Pd ₂ (dba) ₃ /P ^t Bu ₃ 2:4	110	PhMe	24	-
4	CS ₂ CO ₃	Pd(OAc) ₂ /DPPF 1:2	110	PhMe	24	-
5	NaO ^t Bu	Pd(P ^t Bu ₃) ₂	140	o-xylene	48	10
6	NaO ^t Bu	Pd ₂ (dba) ₃ /DavePhos 1:3	140	o-xylene	24	30
7	NaO ^t Bu	Pd ₂ (dba) ₃ / ^t BuXPhos 1:2	140	o-xylene	24	10
8	NaO ^t Bu	Pd ₂ (dba) ₃ /DavePhos 1:3	140	DMF	24	-
9	K ₃ PO ₄	CuI/1,3-Di(2-pyridyl) -1,3-propanedione	140	o-xylene	24	-

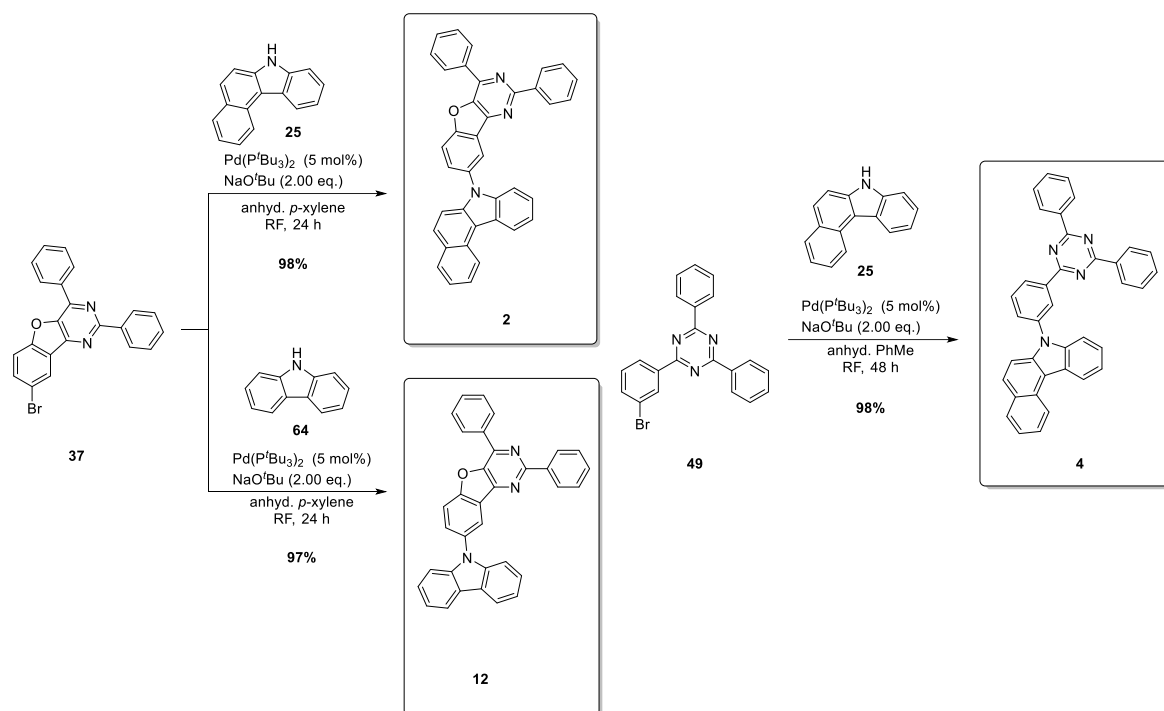
Since the yields were not satisfying and too low for an efficient synthesis as well as the poor separation of the side products from **62**, the strategy was switched and compound **61** was first coupled utilizing standard Suzuki-Miyaura conditions with boronic ester **57** to give chloride **63**. Chloride **63** was then cross coupled with benzocarbazole **25** using Buchwald-Hartwig conditions to give target compound **7** with a yield of 51%. Screening conditions (**Screening B**) for this conversion are summarized in Table 4. The conditions with the best yield of 51% were achieved for a 460 μ mol scale. When scaling up the reaction to a 20 mmol scale, the yield dropped to 20% with several side products. Therefore, the high purity standards for OLED application could not be reached as the huge amount of starting materials and side products was challenging to separate from the product **7**. This shows that the process of OLED material development not only includes the synthesis and identification of conditions that produce the molecule, but also the further purification is essential for succeeding in providing an OLED material that can be fabricated and evaluated.

Table 4: Summary of screening conditions (**Screening B**, Scheme 10) for the coupling of chloride **63** with benzocarbazole **25** to compound **7**. Best conditions are highlighted in blue.

Entry	Base	Catalyst-System (ratio)	T [°C]	Solvent ratio	t [h]	Yield ⁵ [%]
1	NaO ^t Bu	Pd ₂ (dba) ₃ /DavePhos 1:3	140	<i>o</i> -xylene	24	-
2	NaO ^t Bu	Pd(P ^t Bu ₃) ₂	140	<i>o</i> -xylene	24	-
3	NaO ^t Bu	XPhos Pd G3	140	<i>o</i> -xylene	24	51%
4	NaO ^t Bu	Pd(dppf)Cl ₂	140	<i>o</i> -xylene	24	-

Besides the synthesis of molecules that contain a linking unit, also molecules without linker were of interest to get an idea about the importance and effect of linking groups. Furthermore, carbazole derivatives were used to substitute the benzocarbazole unit. The synthesis of all green TMM compounds without linking unit are summarized in Scheme 11. Buchwald-Hartwig conditions were identified, that worked for all target compounds (**2**, **4**, and **12**) with good to excellent yields. Compound **4** is literature-known.^[48] The synthesis of compound **4** in this thesis showed better yields for the used system compared to literature (75% vs. 44%).

⁵ Only unreacted educt **25** and dehalogenated species of educt **63** was observed *via* TLC and GC-MS.

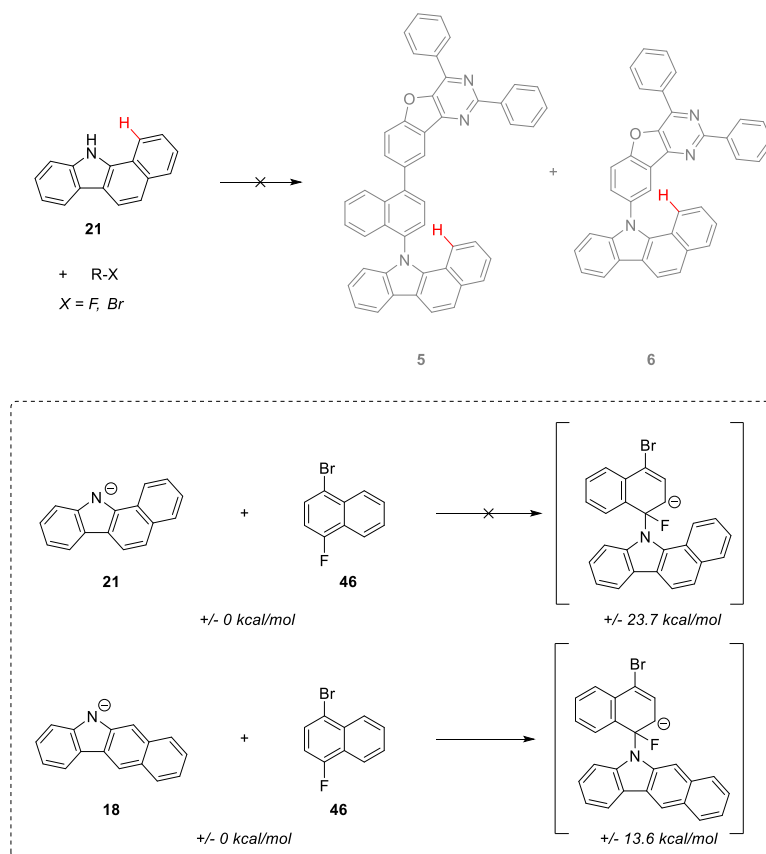


Scheme 11: Overview on the synthesis of target compounds without linking unit (**2**, **4**, and **12**) using Buchwald-Hartwig conditions.

Additionally, the coupling of [*c*]-annulated benzocarbazole unit **25** (7*H*-benzo[*c*]carbazole), also the angular [*a*]-annulated benzocarbazole unit **21** (11*H*-benzo[*a*]carbazole) is a promising building block to give green target molecules **5** and **6** (Scheme 12). Therefore, it was attempted for coupling with naphthyl fluoride **46** or bromide **37**. No product formation was observed when applying coupling conditions that were already described for the coupling of [*c*]-annulated benzocarbazole unit **25** above and for linear [*b*]-annulated benzocarbazole unit **18** (chapter 3.3.2).

It was found that there are energetic reasons for the failed coupling of **21**. Calculations were carried out in DMF as solvent (Scheme 12). Energy values given are with Zero Point correction (frequencies added). Since anions can only be described inadequately, there is naturally an intrinsic error in the calculation. Notably, all resulting products are energetically less favorable than the starting materials. If we assume that the reaction takes place *via* an anionic intermediate, their energies differ greatly from one another: the linear [*b*]-annulated benzocarbazole **18** intermediate is energetically more favorable by about 10 kcal/mol than the angular [*a*]-annulated benzocarbazole unit **21** intermediate. This is a possible explanation for the failed synthesis of **5**. Likewise, the cause of the phenomenon becomes visible when looking at the geometries and sterics: The anionic carbazole species needs to attack **46**. However, due to the steric hindrance of the [*a*]-annulated benzocarbazole species, this is sterically hindered and faces a high energy barrier.

3 Synthesis of Triplet Matrix Materials

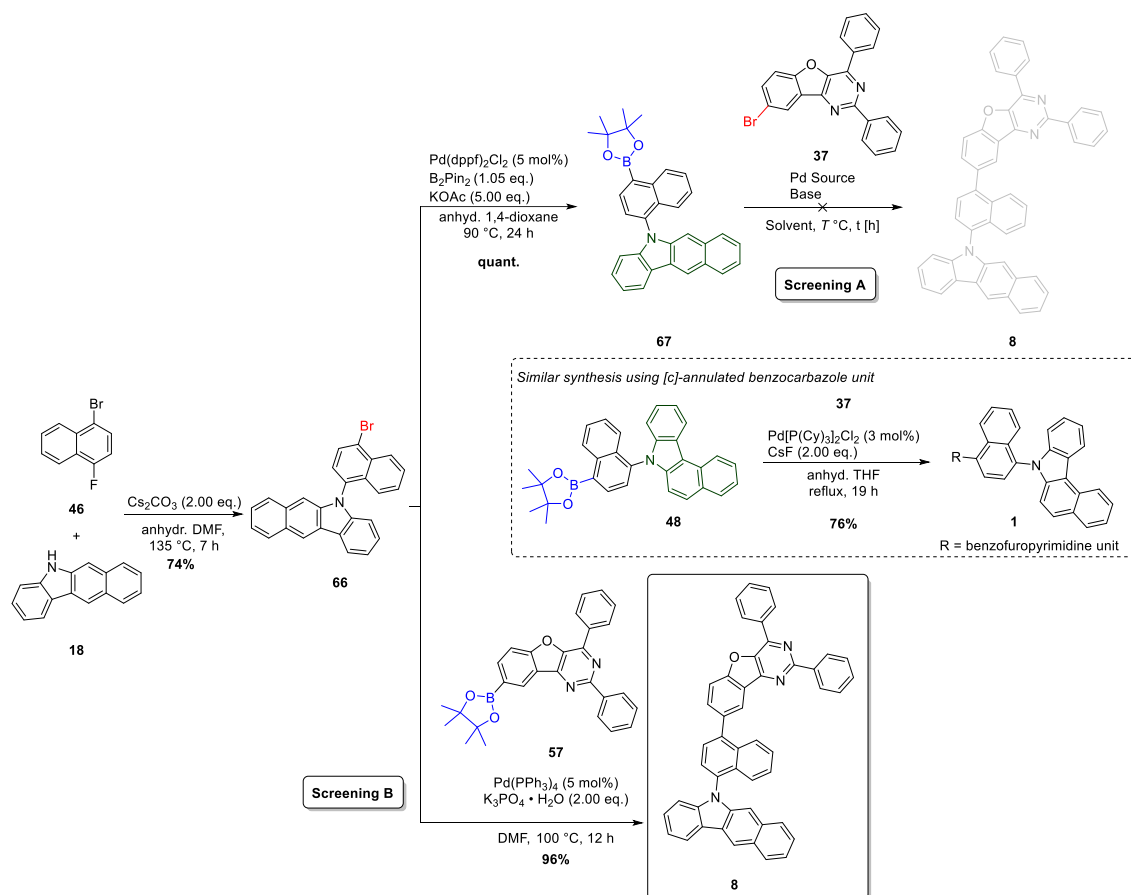


Scheme 12: Failed coupling of [a]-annulated benzocarbazole unit **21** and calculated energies⁶ compared to the coupling of linear [b]-annulated benzocarbazole unit **18** (DFT, b3lyp/631g*).

⁶ Calculations were carried out by Jens Pflanzgraf (Merck KGaA).

3.3.2 Synthesis of red TMM's based on benzocarbazole 18

For the synthesis of red target TMM's, linear [b]-annulated benzocarbazole unit **18** (5H-benzo[b]carbazole) was used as a hole conducting unit.



Scheme 13: Failed synthesis of red target compound **8** using the same strategy that was successful for target compound **1** containing [c]-annulated benzocarbazole unit; and successful synthesis of target compound **8** using a reversed approach. This overview highlights the difference in reactivity and chemical properties of isomeric target compounds **1** and **8**.

However, in contrast to the coupling of angular [c]-annulated benzocarbazole, reactivities changed and the synthetic strategy that was followed for the green TMM's was not applicable (Scheme 13). Generally, the [b]-annulated benzocarbazole unit **18** was coupled to the linker naphthyl-fluoride in a nucleophilic aromatic substitution with excellent yields to give **66** – like the angular [c]-annulated benzocarbazole. Afterwards, bromide **66** was converted to boronic ester **67** and then approached to couple with bromide **37** under Suzuki-Miyaura conditions. Those conditions were successful for the synthesis of green TMM's with the angular [c]-annulated benzocarbazole unit. Those conditions failed for the coupling of the linear benzocarbazole **18** and **8** was not formed, after screening various conditions (Table 5). The main undesired products of this reaction were the deborylated and debrominated intermediates.

3 Synthesis of Triplet Matrix Materials

Table 5: Summary of failed screening conditions (**Screening A**, Scheme 13) for the coupling of boronic ester **57** with benzofuropyrimidine **37** to compound **8**.

Entry	Base	Catalyst-System (ratio)	T [°C]	Solvent ratio	t [h]	Yield [%]
1	Na ₂ CO ₃	Pd(PPh ₃) ₄	70	THF/H ₂ O	24	-
2	K ₃ PO ₄	Pd ₂ (dba) ₃ /SPhos 3:5	90	1,4-dioxane/H ₂ O	18	-
3	KOAc	RuPhos Pd G3	90	1,4-dioxane	24	-
4	CsF	Pd(PCy ₃) ₂ Cl ₂	70	THF/H ₂ O	24	-
5	CsF	XPhos Pd G3	70	THF	18	-
6	CsF	Pd (P ^t Bu ₃) ₂	70	THF	25	-

Therefore, the strategy was reversed and instead of using bromide **37**, its boronic ester **57** was used and coupled to bromide **66**. This strategy enabled the formation of target compound **8** with a yield of 96% after screening several Suzuki-Miyaura conditions summarized in Table 6).

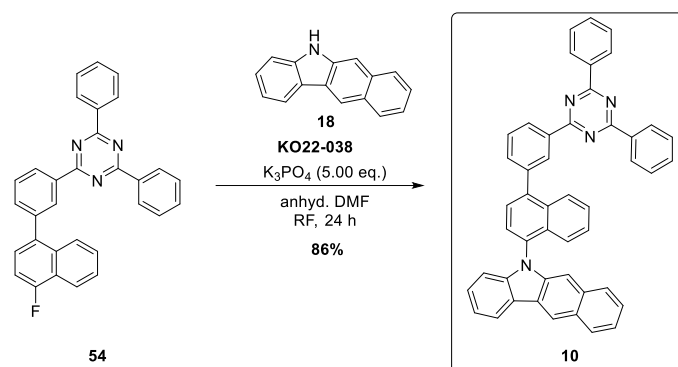
Table 6: Summary of failed screening conditions (**Screening B**, Scheme 13) for the coupling of boronic ester **67** with bromide **66** to compound **8**. Best conditions are highlighted in blue.

Entry	Base	Catalyst	T [°C]	Solvent ratio	t [h]	Yield [%]
1	CsF	Pd(PCy ₃) ₂ Cl ₂	70	THF/H ₂ O	24	-
2	CsF	Pd(PCy ₃) ₂ Cl ₂	162	Diglyme	24	- ⁷
3	CsF	Pd PePPSI-IPent	90	1,4-dioxane	24	-
4	KOAc	Pd PePPSI-IPent	70	THF	24	-
5	KOAc	Pd(amPhos)Cl ₂	70	THF	24	-
6	K ₃ PO ₄ .H ₂ O	Pd(PPh ₃) ₄	100	DMSO	24	20
7	K ₃ PO ₄ .H ₂ O	Pd(PPh ₃) ₄	100	1,4-dioxane	24	30
8	K ₃ PO ₄ .H ₂ O	Pd ₂ (dba) ₃	100	PhMe	24	-
9	K₃PO₄.H₂O	Pd(PPh₃)₄	100	DMF	24	96

The requirement of different strategies for the isomeric target compounds **1** and **8** highlight its differences in reactivity and chemical properties. It turned out to not only have different reactivities in Suzuki-Miyaura couplings, but also physical and chemical properties, which is later discussed (Figure 31, Chapter 4.3). This is an interesting observation which shows that

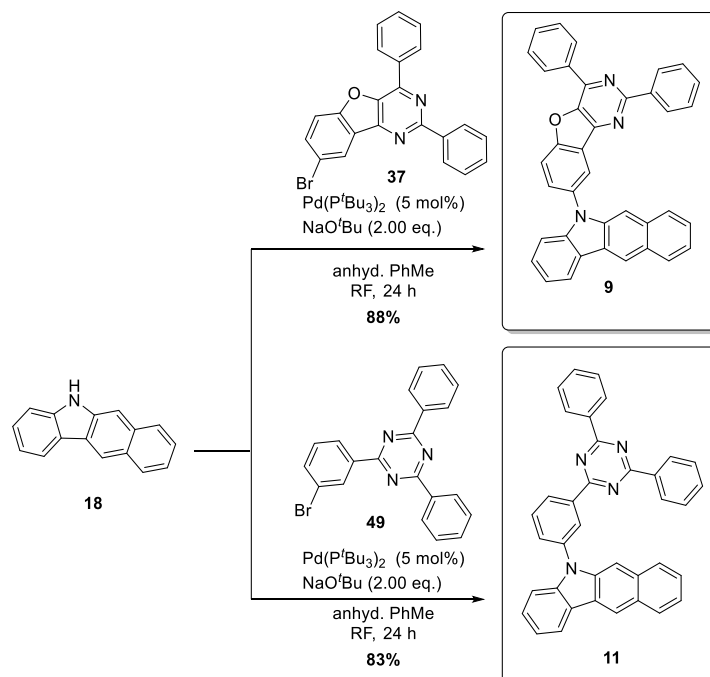
⁷ Only unreacted educt **66** and dehalogenated species of educt **67** were observed *via* TLC and TLC-MS.

reactivity, HOMO and LUMO levels as well as physical properties are strongly dependent on the structure and minimal changes can have huge effect. Interestingly, different regioisomers of benzocarbazole unit has an immense influence on the chemical and physical properties of respective TMM's. The variation of the electron accepting unit benzofuropyrimidine to triazine had only a smaller impact on the chemical and physical properties of the corresponding TMM's. For the synthesis of red triazine target compound **10**, fluoride **54** was coupled to benzocarbazole **18** via nucleophilic aromatic substitution with a yield of 86% (Scheme 14) – like the synthesis of target compound **3** avoiding the formation of homocoupling product **53**.



Scheme 14: Synthesis of target compound **10**.

Target compounds without linker (Scheme 15) were synthesized using standard Buchwald-Hartwig conditions from starting material **18** and **37** or **49** to give target compounds **9** and **11** with a yield of 88% and 83% respectively.



Scheme 15: Synthesis of compound **9** and **11**.

Compound **9** was crystallized from acetonitrile to allow for single crystal structure analysis. For compound **9**, a crystal structure depicted in Figure 18 was obtained.

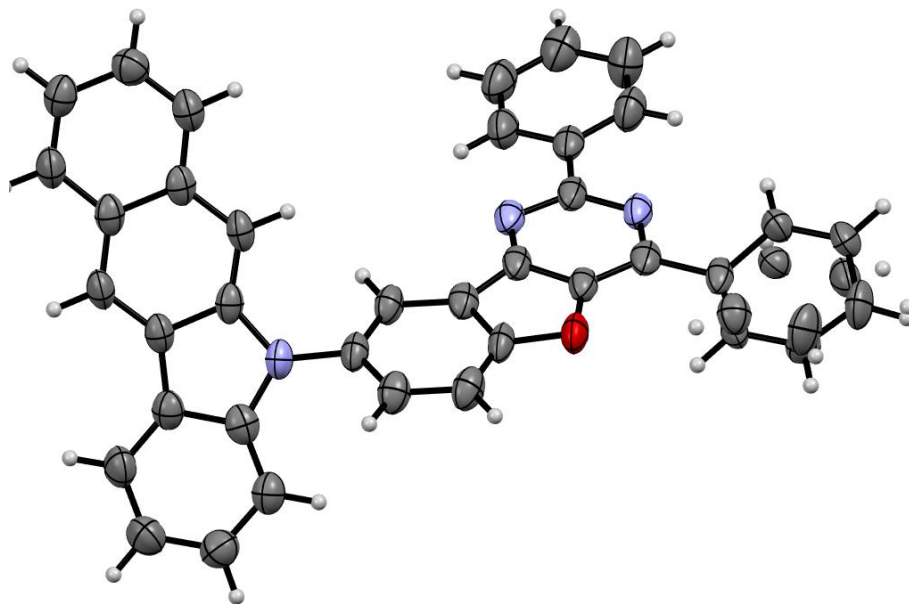
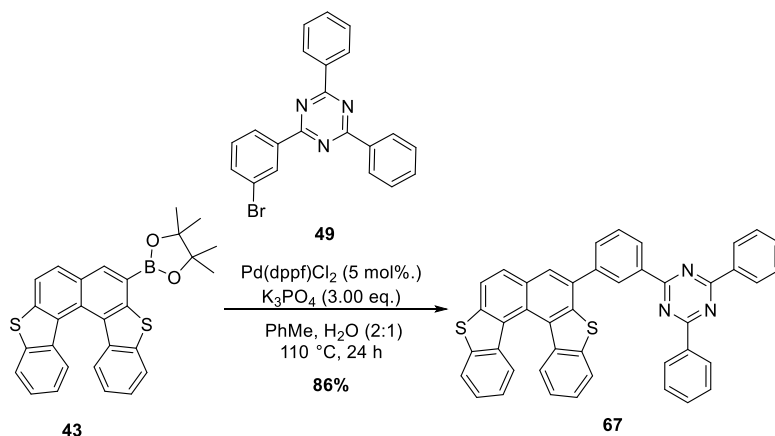


Figure 19: ORTEP plot of compound **9** with front view orthogonally at the indenocarbazole donor unit.

3.3.3 Synthesis of further TMM's

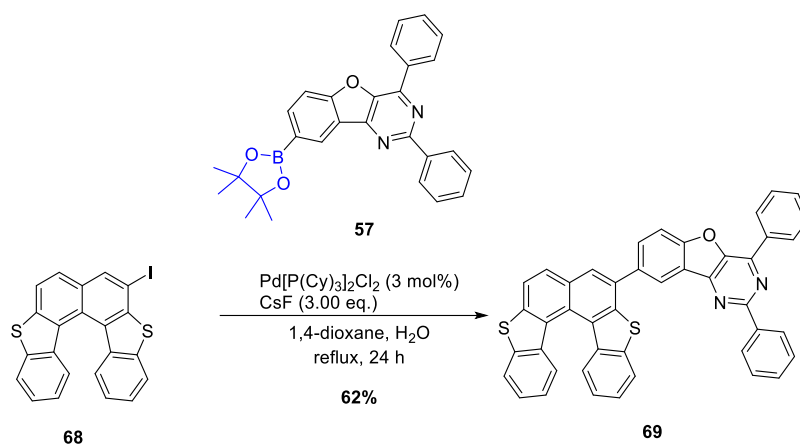
All compounds whose syntheses are discussed in this chapter are not further evaluated as capacity for overcoming either synthetic or purification challenges was limited within this thesis. Therefore, theoretical considerations as well as physical and device data are not further discussed. Some of the structural motifs in this chapter were planned to be synthesized for comparison to the described target molecules in Figure 10 in Chapter 3.1.

A naphthodibenzothiophene unit and a dibenzothiophenesulfone unit were coupled to a triazine unit to compare to benzocarbazole triazine structures **11** and **4**.



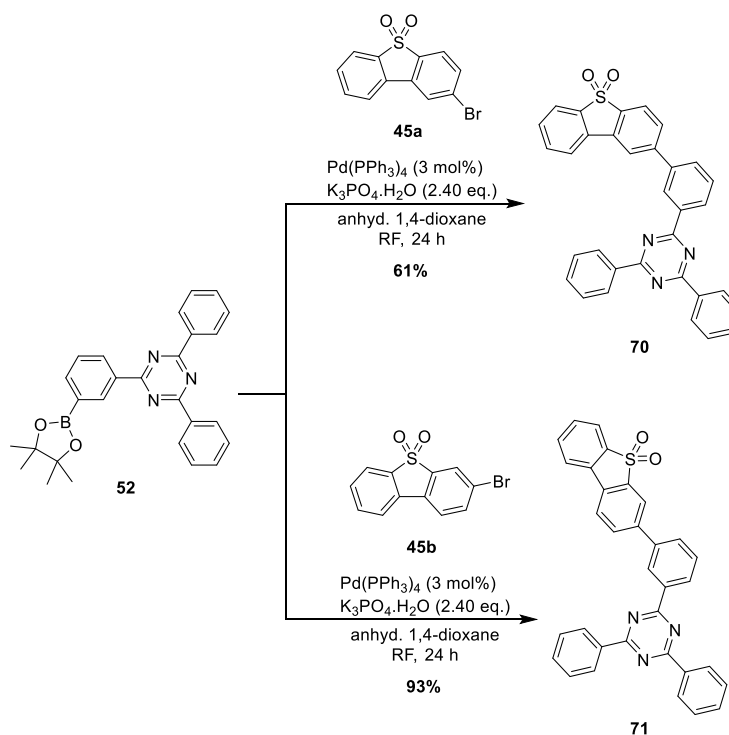
Scheme 16: Synthesis of compound **67** via Suzuki-Miyaura coupling of boronic ester **43** and bromide **49**.

Building block **43** was synthesized following a literature procedure^[80] as described in Scheme 4 (Chapter 3.2.3) and was then coupled to bromide **49** under Suzuki-Miyaura conditions to obtain target compound **67** (Scheme 16). The similar compound **69** that contains the benzofuroprimidine motif instead of the triazine motif was synthesized from iodide **68** and boronic ester **57** (Scheme 17). The use of boronic ester **43**, as it was used for the synthesis of **67**, failed and only deborylation was observed – probably due to the lower reactivity of bromide **37** compared to bromide **49**.



Scheme 17: Synthesis of compound **69** via Suzuki-Miyaura coupling of boronic ester **57** and iodide **68**.

Dibenzothiophensulfone building blocks **45a** and **45b** were synthesized using the strategy described in Scheme 5 (Chapter 3.2.4) and were then coupled to boronic ester **52** to give target compounds **70** and **71** (Scheme 18).



Scheme 18: Synthesis of dibenzothiophensulfone compounds **70** and **71**.

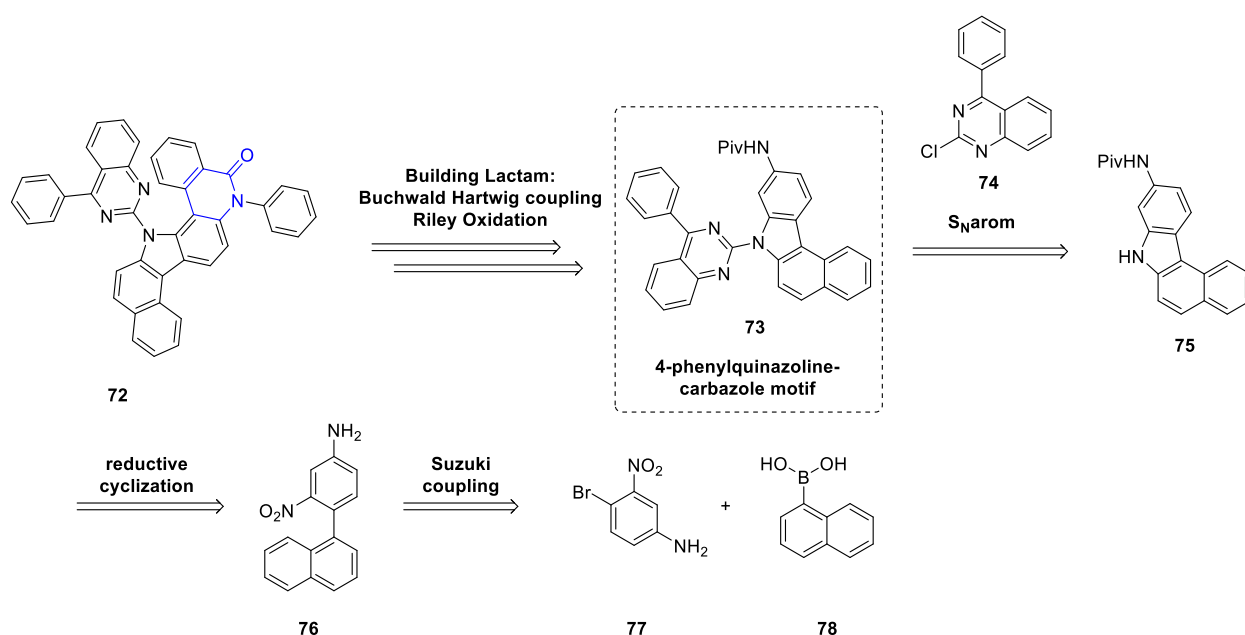
3.3.4 Attempts for the Synthesis of Lactam TMM

Synthetic plan

Another interesting structural motif that is not further discussed in this thesis, is a lactam motif (**72**, shown in Scheme 19). However, the synthesis showed several challenges and did not allow to proceed with the synthesis. Synthetic attempts to this motif are discussed in this chapter.

For the synthesis of lactam TMM **72** two different synthetic approaches were followed (Scheme 19 and Scheme 20) which differ in the order of the construction of the lactam scaffold.

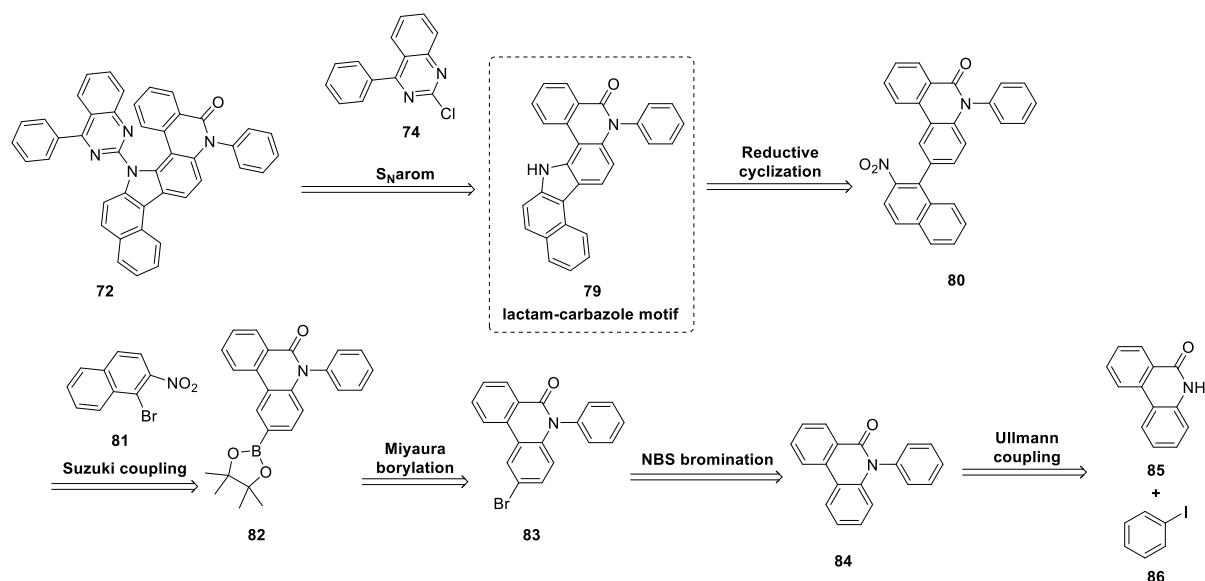
The first retrosynthetic plan (Scheme 19) is based on the construction of the 4-phenylquinazoline-benzocarbazole motif **73** first, followed by the construction of the lactam ring to provide **72**. The 4-phenylquinazoline-benzocarbazole motif **73** was planned to be synthesized starting from naphthylboronic acid **78** and aniline **77**. Compound **78** and **77** can be coupled *via* a Suzuki coupling to provide intermediate **76** followed by a reductive cyclization^[72] for the formation of the benzocarbazole scaffold **75**. The benzocarbazole **75** can be coupled to the 4-phenylquinazoline unit **74** to provide the 4-phenylquinazoline-benzocarbazole motif **73**.



Scheme 19: First retrosynthetic plan for the synthesis of **72** constructing first the 4-phenylquinazoline-benzocarbazole motif followed by the construction of the lactam ring.

The second retrosynthetic plan (Scheme 20) is based on the construction of the lactam-benzocarbazole motif **79** first, followed by the construction of the lactam ring to provide **72**. This plan was developed, because the reductive cyclization of **76** in the presence of an amine, that was required for the lactam construction, failed. Instead, lactam **85** can be used as a starting material, which can be phenylated using **86** in an Ullmann coupling followed by a NBS

bromination and Miyaura borylation to provide **82**. Boronic ester **82** can then be coupled with bromide **81** via a Suzuki coupling to provide nitronaphthalene **80** that is supposed to yield the lactam-benzocarbazole motif **79** via the reductive cyclization.^[72]

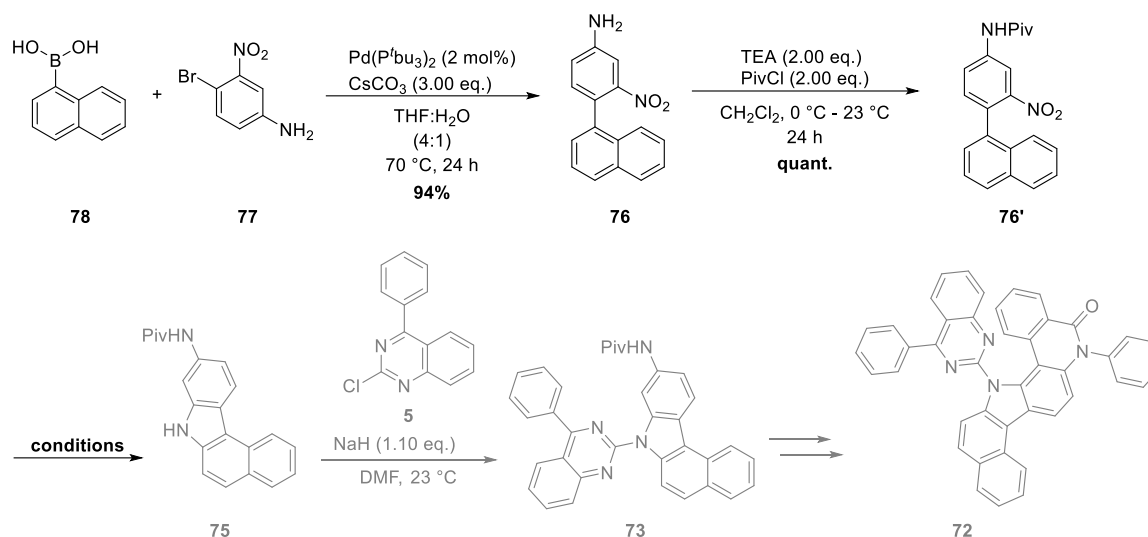


Scheme 20: Alternative retrosynthetic plan for the synthesis of **72** constructing first the lactam-benzocarbazole motif **79** followed by the installation of the 4-phenylquinazoline.

Synthesis of precursors of **72** following the first retrosynthetic plan

Nitronaphthalene **76** was synthesized starting from naphthylboronic acid **78** and aniline **77** in a Suzuki coupling with a yield of 94% (Scheme 21). As the reductive cyclization with the free amine **76** would lead to side products due to the basicity of the free amine, amine **76** was protected using the pivaloyl protecting group to give compound **76'** in quantitative yield using standard conditions.^[89] The pivaloyl protecting group – an amide protecting group – was chosen because of the high stability of the amide bond compared to other types of amine protecting groups such as carbamates (e.g. fmoc or boc). Also, the sterical hinderance of the *tert*-butyl residue is increasing the stability compared to simple amide protecting groups such as the acyl protecting group, which also decreases the basicity of the amine.

3 Synthesis of Triplet Matrix Materials

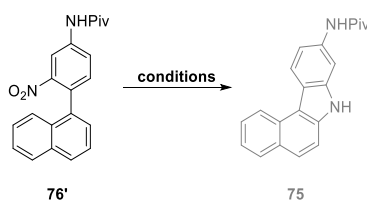


Scheme 21: Synthesis of nitronaphthalene **76'** and pending steps for the synthesis of **72** (highlighted in grey).

The conversion of nitronaphthalene **76'** to benzocarbazole **75** in a reductive cyclization was attempted using conditions summarized in Table 7. The reductive cyclization for a similar system was described by Freeman *et al.*^[72]

For the investigation of the reductive cyclization different organophosphorus reagents (PPh₃, P(OEt)₃ and DPPE) were tested with different stoichiometry at different temperatures (reaching from 23 to 170 °C) in various solvents. However, the product **75** was not observed.

Table 7: Summary of the reductive cyclization **conditions** for the synthesis of benzocarbazole **75** starting from **76'**. *Product conversion was followed by TLC, TLC-MS and crude ¹H NMR analysis. ^bFormation of several side products was observed which could not be identified.

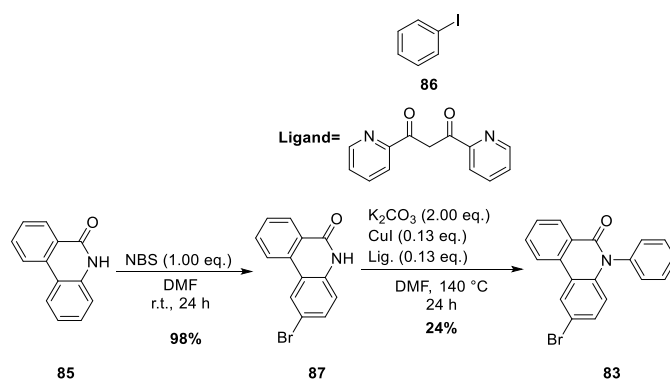


Entry	Organophosphorus reagent (eq.)	Temp. [°C]	Solvent	Yield
1	PPh ₃ (2.50)	150	DMA	-*
2	PPh ₃ (2.50)	130	<i>o</i> -DCB	-
3	P(OEt) ₃ (6.00)	170	neat	-
4	P(OEt) ₃ (3.30)	140	neat	-
5	P(OEt) ₃ (3.30)	40	neat	-
6	P(OEt) ₃ (2.00)	170	<i>o</i> -DCB	-
7	P(OEt) ₃ (2.00)	150	1,2-xylene	-
8	DPPE	150	<i>o</i> -DCB	^b

The use of DPPE resulted in a mixture of several side products, which could not be isolated and further identified. As the pivaloyl protected amine is the only functionality in **76'** besides the nitro group, the presence of the protected amine seems to influence the reaction and causes the formation of side products. Therefore, a new synthetic route was designed (Scheme 20) introducing the reductive cyclization in a later stage of the synthesis where no reactive functionality is present.

Synthesis of precursors of **72** following the second retrosynthetic plan

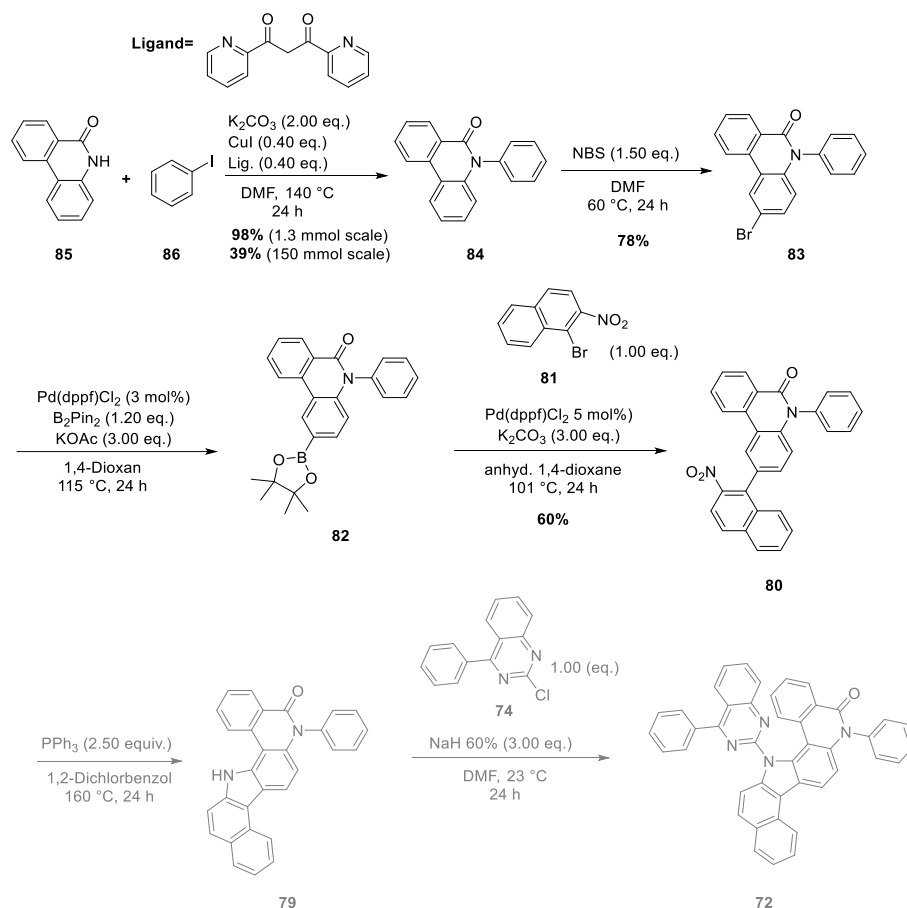
Before the synthetic approach for **83** described in the retrosynthetic plan (Scheme 20) was established, a different synthetic approach for compound **83** was tested, starting from the bromination of **85** (Scheme 22). However, the Ullmann coupling of **87** was not efficient because of side reactions, such as homo coupling, dehalogenation, and substitution of bromine by iodide and chloride.



Scheme 22: First approach for the synthesis of **83** starting from the bromination of **85**.

Alternatively, the approach described in Scheme 23 for the synthesis of bromide **83** was established *via* *N*-phenyllactam **84**. *N*-Phenyllactam **84** was synthesized using Ullmann coupling conditions (Scheme 23). However, the yield was not reproducible in the upscaling of the reaction (1.3 mmol (98%) up to 150 mmol scale (39%)). Different solvents and higher equivalents (0.1-0.4 eq.) of the ligand and copper iodide were tested to obtain compound **84** in a higher yield. However, 39% was the best result for the upscaling.

3 Synthesis of Triplet Matrix Materials



Scheme 23: Synthesis of nitronaphthalene **80** and pending steps for the synthesis of **72**, which failed due to difficulties in carbazole formation of compound **79**.

N-Phenylactam **84** was converted to bromide **83** via NBS bromination with a yield of 78% with 100% regioselectivity. The amide directs the bromination in para-position, which is energetically favored compared to the two ortho-positions (Figure 20). Additionally, the position of the bromide was determined via 2D-NMR spectroscopy (COSY, HSQC, HMBC).

Bromide **83** was then converted to the boronic ester **82** followed by Suzuki coupling to **81** providing nitronaphthalene **80** with a yield of 60% over two steps. The reductive cyclization to provide benzocarbazole **79** followed by the coupling to phenylquinazoline **5** are pending to obtain Target 1. When **72** is successfully synthesized with minimal 2 g with a purity of >99.4% (HPLC) will then be further photo-physically evaluated for OLED application.

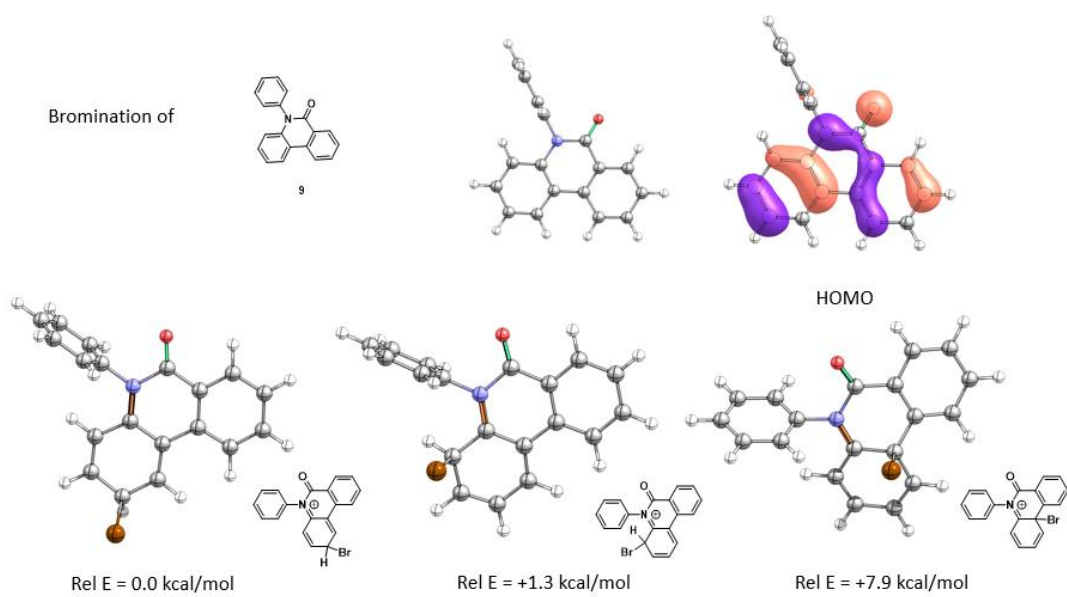


Figure 20: DFT-calculations of the relative energies (Rel E) for the bromination of **84** comparing the bromination in para- and ortho-position to the amide group.⁸

⁸ DFT-calculations conducted by Prof. Dr. Matthias Bremer, Merck KGaA (B3LYP/6-31G(d)).

4 Evaluation of Material Properties

Contribution: Device fabrication and all electrochemical, thermal and photophysical measurements (CV, DSC, Fluorescence, UV-Vis, determination of lifetime, EQE, luminance, driving voltage) were conducted by the physics department of Merck Electronics KGaA. Data evaluation, as well as scientific conclusions were done by Klaus Osazuwa Omoregbee.

4.1 General

In the following section, the target compounds that were synthesized in Chapter 3 were evaluated by electrochemical, thermal and photophysical experiments (CV, DSC, UV/Vis, and fluorescence spectroscopy). They were also tested for their performance in OLED-devices (EQE, lifetime and driving voltage).

It is very important that all target compounds maintain high purity standards that are state-of-the-art in organic semiconducting materials. This includes HPLC-purities of at least 99.9% and low trace amounts of halogens and active groups like alcohols and amines (< 3 ppm). This demands high requirements on the purification procedures of the synthesized materials. The compounds discussed in this chapter were sublimed at least twice after removal of halogens by end-capping and hot extraction according to Twisselmann (methods further described in the experimental section). The high purity is required because impurities, especially trace amounts of halogens drastically influence the performance of the OLED-device.^[90]

The evaluation is divided in two parts: the evaluation of red and green TMM's.

4.2 Results of the red TMM's

The red host materials evaluated in this thesis are again shown in Figure 21. All compounds (**8**, **9**, **10** and **11**) consist of the linear [*b*]-annulated benzocarbazole unit.

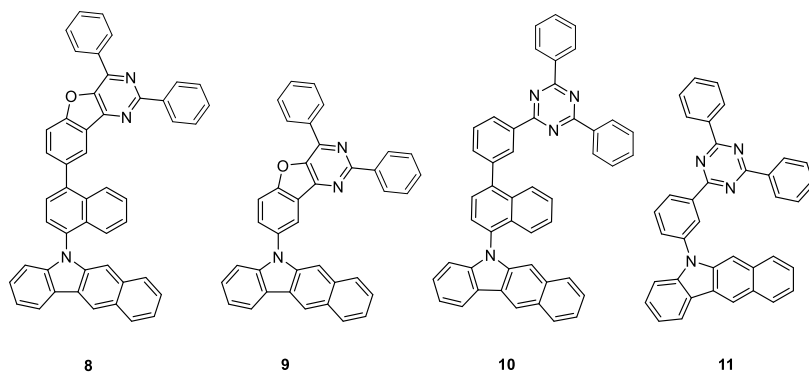


Figure 21: Overview of synthesized and evaluated red TMM's **8**, **9**, **10** and **11**.

4.2.1 Electrochemical Properties

The electrochemical properties of TMM's **8**, **9**, **10** and **11** were investigated by cyclic voltammetry (CV). The results are shown in Figure 22 and Table 8.

CV is a common technique to estimate HOMO and LUMO energies of TMM's, due to its easy practicability and low costs. It determines the relative molecular oxidation and reduction potentials, which are indirectly related to HOMO and LUMO energies. It also allows to correlate the measured potentials to the ionization energy and electron affinity. CV uses a three-

electrode arrangement for potential measurements in inert solvents, electrolytes as well as electrodes within the voltage range of the measurement. Therefore, dichloromethane (CH_2Cl_2) is the solvent of choice for the measurement of oxidation and tetrahydrofuran (THF) for reduction potentials. Furthermore, a reference compound as internal standard is used, which is ferrocene or decamethylferrocene due to its reversible redox potential and stability. The use of a reference enables the comparison of all measured compounds.^[91]

The CV measurements were performed using a *Metrohm* $\mu\text{AUTOLAB III}$ in anhydrous CH_2Cl_2 (oxidation) and THF (reduction) solutions of tetra (*n*-butyl) ammonium hexafluorophosphate (TBAHFP, 0.11 M) under an inert gas at a scan rate of 0.5 V/s. The working electrode was a gold electrode, and a platinum-wire was the counter electrode. Ag/AgCl 3 M KCl//0.025 M TEABr in ethylene glycol was used as reference electrode for the oxidation scans, while Ag/AgCl 3 M KCl//0.025 M TMAcI in ethylene glycol was used as reference electrode for reduction scans. The resulting curves were calibrated using ferrocene (Fc/Fc^+) or decamethylferrocene ($\text{dmfc}/\text{dmfc}^+$) redox pair as an internal standard.

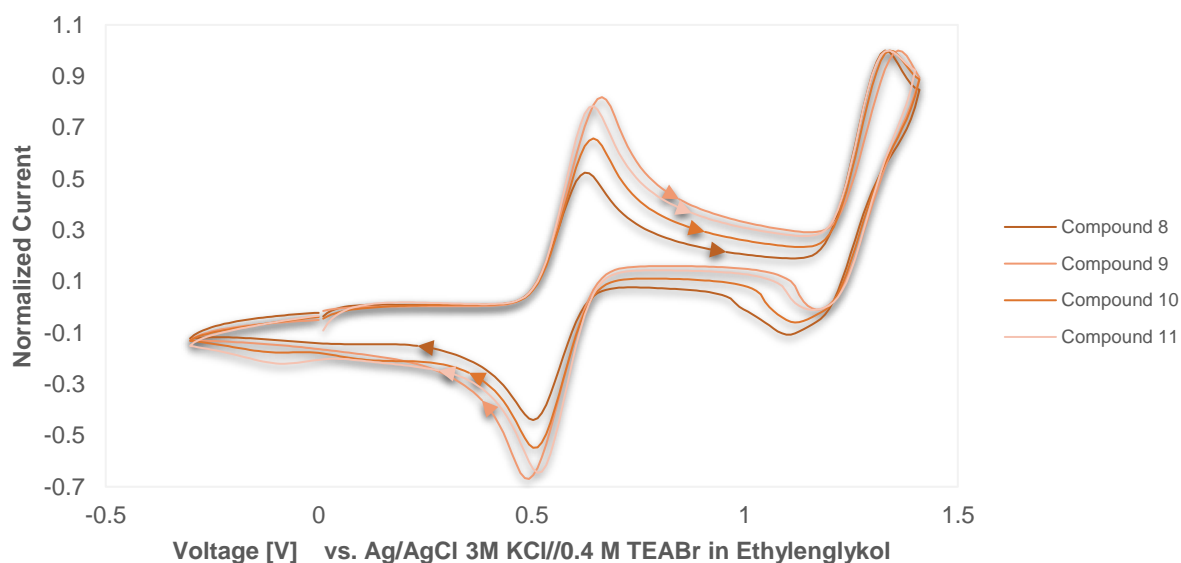


Figure 22: Cyclic voltammograms of red TMM's **8**, **9**, **10** and **11** with a scan rate of 0.5 V/s and the internal standard ferrocene.

The HOMO and LUMO energy levels were estimated from the first oxidation and reduction peak versus ferrocene/ferrocenium (Fc/Fc^+) or decamethylferrocene ($\text{dmfc}/\text{dmfc}^+$) with ferrocene (decamethylferrocene assumed to have an ionization energy of -4.80 eV (-4.25 eV for dmfc) below vacuum level. The estimation is based on equation (5) and (6):

$$E_{HOMO}[eV] = -4.80 - \left(E_{\frac{1}{2}}^{Ox,sample} - E_{\frac{1}{2}}^{Ox,Fc/Fc^+} \right) \quad (5)$$

$$E_{LUMO}[eV] = -4.80 - \left(E_{\frac{1}{2}}^{Red,sample} - E_{\frac{1}{2}}^{Red,Fc/Fc^+} \right) \quad (6)$$

Table 8: Comparison of the calculated and measured HOMO and LUMO levels for **red** TMM's **8**, **9**, **10** and **11**. Details on the calculation of theoretical HOMO and LUMO levels are described in the theoretical considerations (Chapter 3.1).

Compound	HOMO _{CV} [eV]	LUMO _{CV} [eV]	HOMO _{DFT} [eV]	LUMO _{DFT} [eV]
8	-5.48	-2.63	-5.33	-2.62
9	-5.49	-2.68	-5.36	-2.69
10	-5.48	-2.62	-5.30	-2.56
11	-5.48	-2.65	-5.31	-2.60

Calculated and experimental HOMO levels were in good agreement with a discrepancy of < 0.2 eV (Table 8). Experimental HOMO levels were always lower than calculated HOMO levels. Calculated and experimental LUMO levels were in very good agreement with a discrepancy of < 0.08 eV (Table 8). CV data of compounds **2**, **3**, **4** and **13** show electrochemical reversible oxidations in CH₂Cl₂ with similar potentials around 1.4 V. The CV experiment also suggests good electrochemical stability of the synthesized compounds.

4.2.2 Thermal Properties

It is important for host materials to be thermally stable due to their exposure to high temperatures during processing. Furthermore, the materials need to form stable amorphous films to facilitate homogeneous charge transport and to enable a proper emitter distribution in the OLED device.^[92] Therefore, the synthesized compounds were evaluated regarding their thermal properties using differential scanning calorimetry (DSC) and (vacuum) thermal gravimetric analysis ((vacuum)-TGA). DSC measures the heat flow in dependence on the applied temperature, whereas TGA (vacuum) provides the glass transition temperature (T_g), the melting temperature (T_m) and decomposition temperature (T_d).

The glass transition temperature (T_g) is the temperature, where movements of the molecular structure result from intramolecular rotations around bonds. The TMM's in OLED-devices require a high T_g value to avoid crystallization.^{[93][94]} Intramolecular interactions (e.g. hydrogen bonds or dipole interactions), high molecular weight and rigid or non-planar geometry can enhance the T_g value. A high T_g and T_d value are a proof of robust thermal stability, which is essential for the formation of amorphous thin films in OLED's and for the prevention of crystallization due to joule heating in the device. If vaporization is noticed before decomposition, a low T_d value can be observed even if the molecule is thermally stable.^{[93][92]}

The thermal properties of compound **8-11** are shown in Table 9. The melting temperatures of compound **8** and **10**, both consisting of a linking unit, could not be detected. This indicates that

the materials were already amorphous, which is beneficial for application in OLED-devices.^[92] Both compounds also provide a higher decomposition temperature T_d (of 466 °C and 449 °C) and T_g (180 °C and 157 °C). The corresponding compounds without linking unit (**9** and **11**) provide significantly lower decomposition temperatures than the compounds with linking unit (412 °C and 392 °C) and lower T_g (142 °C and 105 °C). This is an indication that the linking units increase thermal stability, which is desired for OLED application. Further studies on that will be elucidated in the device results in chapter 4.1.4.

Table 9: Thermal properties (measured T_g , T_m and T_d values) of red TMM's **8**, **9**, **10** and **11**.

Compound	T_g [°C] ⁹	T_m [°C] ¹⁰	T_d [°C] ¹¹
8	180	-	466
9	142	296	412
10	157	-	449
11	105	285	392

4.2.3 Photophysical Properties

For the photophysical characterization of the red TMM's **8-11**, ultraviolet-visible (UV-Vis) absorption and photoluminescence (PL) spectra were measured in solution (toluene, $\sim 10^{-6}$ M) and solid-state form (100% film, 50 nm). The normalized absorption and emission spectra are shown in Figure 23 and the characteristic photophysical numbers are summarized in Table 10.

The absorption is around 330 nm in solution for all compounds, while the film absorption is 30-60 nm higher. This could be because of π -electronic interaction between chromophores in the solid state. The absorption at this wavelength is caused by π - π^* absorption of the benzocarbazole moiety.^[95] The emission maxima show defined and broad emission bands between 460 and 486 nm. The form of the emission bands indicates the formation of an intramolecular charge-transfer between the benzocarbazole donor and the triazine/benzofuropyrimidine acceptor moiety in the excited state.^{[96][97]} The compounds with a larger π -system (**8** and **10**, containing linking unit) emit at lower wavelengths.

⁹ Measured by DSC in the second heating scan (heating rate: 20 °C/min).

¹⁰ Measured by DSC in the first heating scan (heating rate: 20 °C).

¹¹ Measured by TGA experiment with a heating rate of 10 °C/min in a nitrogen atmosphere or under vacuum. T_d is the temperature, where 5% weight loss is detected.

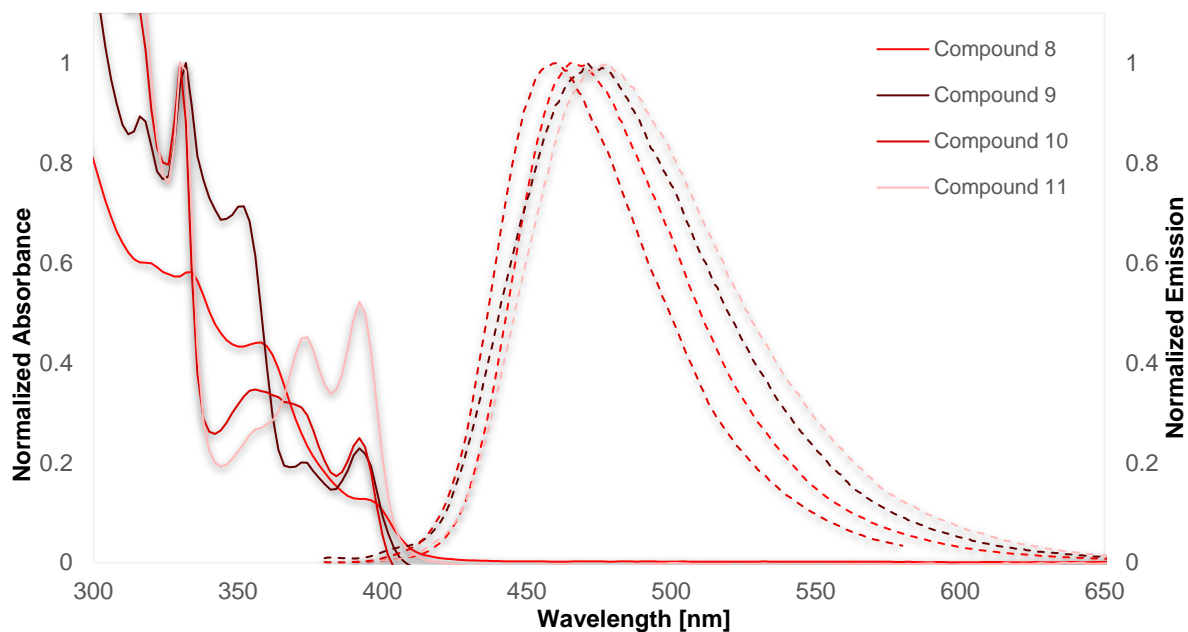


Figure 23: Normalized absorption (solid line) and emission (dashed line) of **red** TMM's **8-11** in solid-state form (100% film, 50 nm) at room temperature.

Table 10: Summary of the characteristic photophysical numbers of red TMM's **8-11**.

Comp.	Solution					Film				
	$\lambda_{em, max}$ [nm]	Stokes shift [nm]	CIEx	CIey	FWHM [nm]	$\lambda_{em, max}$ [nm]	Stokes shift [nm]	CIEx	CIey	FWHM [nm]
8	-	-	-	-	-	465	197	0.151	0.207	67
9	471	139	0.161	0.239	79	484	86	0.180	0.383	75
10	400	70	0.160	0.024	40	460	92	0.147	0.149	63
11	478	148	0.171	0.282	81	486	88	0.180	0.361	74

4.2.4 Device Results

For the evaluation of lifetime, efficiency and driving voltage, the red TMM's **8-11** were tested in a bottom emission OLED stack (internal Merck KGaA stack set-up, Figure 24). The focus of the investigations is on the relationship of chemical structure of the e-TMM on the device properties.

Each stack consists of an LiQ/Aluminium layer (100 nm), an electron injection layer with ETM1:LiQ (1:1, 30 nm), an electron transport layer with ETM2 (10 nm), the emissive layer containing the e-TMM and emitter (different ratios, 35 nm), the hole transport layers with HTM1 (10 nm) and HTM2 (90 nm), the injection layer with HTM2:PDM (5%, 20 nm) and the ITO (50 nm). The exact structure of the e-TMM, emitter, ETM1, ETM2, HTM1 and HTM2 are confidential. Exemplary materials can be found in Merck KGaA patents^[98] and literature-known emitters^[50]. OLED stack components are shown in Figure 3 in chapter 1.1.2 and Figure 5 in chapter 1.1.3.

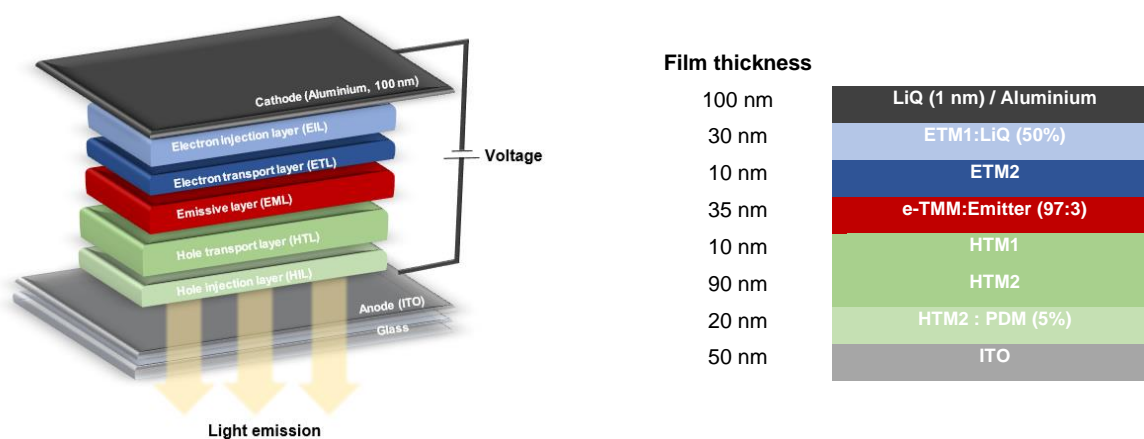


Figure 24: Schematic representation of the single-host OLED-stack for a red emitter, where the synthesized target e-TMM materials were built into the emissive layer.

Here, each e-TMM material **8-11** was built into the emissive layer (EML) of a single-host OLED-stack. Usually single-host devices are used to evaluate red TMM's, because acceptable lifetimes can be achieved, and the fabrication of mixed-host stacks are technically more complicated. However, for comparison, also a mixed-host stack was fabricated for TMM's **8-11**. In a mixed-host device an additional TMM (h-TMM) is added to the EML. This enables to regulate the charge balance, the hole transport and to adjust the recombination zone of electrons and holes. As a result of better results for the mixed-host device compared to the single-host device, a charge imbalance can be claimed.

For each material, four stacks were manufactured by high vacuum thermal evaporation. The fabrication of the stacks is described in section 1.1.4.1. The standard EML contains an e-TMM:emitter ratio of 97:3, but also stacks with e-TMM-emitter ratios of 94:6 and 91:9 as well as mixed hosts with a ratio of 57:40:3 (e-TMM:h-TMM:emitter) were fabricated.

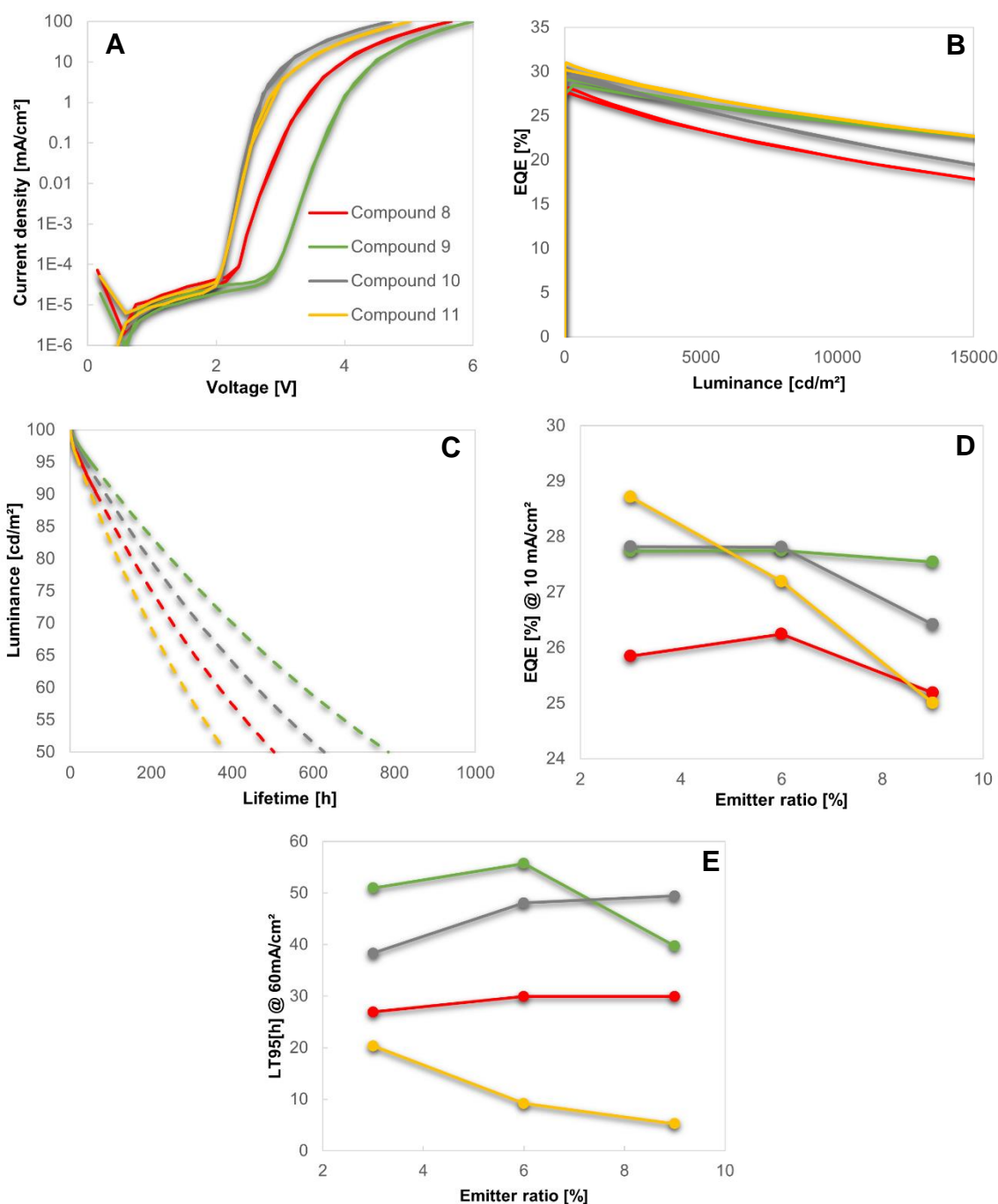


Figure 25: Device results of compound **8** (red), **9** (green), **10** (grey) and **11** (yellow) including (A) the current-density-voltage curve, (B) EQE vs. luminance, (C) luminance vs. lifetime (dashed line is extrapolated according to the exponential decay function up to LT₅₀), (D) EQE vs. emitter ratio and (E) lifetime vs. emitter ratio.

Current density-voltage curves, quantum efficiency-luminance curves, luminance-lifetime curves, EQE-emitter ratio dependencies and lifetime-emitter ratio dependencies are depicted in Figure 25. The electroluminescent properties (voltage and EQE) of the tested devices as well as lifetime results are summarized in Table 11. Relative values were obtained by dividing the measured values by triazine compound **10** (100%).

The current density-voltage correlation (Figure 25A) shows that benzofuopyrimidine TMM's **8** and **9** have a higher voltage than triazine TMM's **10** and **11** (129% for **8** and 147% for **9**

compared to **10** and 118% for **11**). The voltage of TMM **9** shows a significant higher voltage than all other compounds, which indicates an injection barrier into the EML or a lower charge mobility. Therefore, the emitter concentration was increased to enhance the hole mobility. Indeed, the driving voltage was significantly improved by increasing the emitter concentration for TMM's **8** and **9**. In opposite, the driving voltage was not significantly improved with a higher emitter concentration for TMM's **10** and **11**. This result shows, that the charge mobility is better in triazines than in benzofuropyrimidine TMM's. Triazine based compounds are known to reduce the driving voltage^[66], because they are very good electron withdrawing groups and thus provide good electron transport properties. Besides that, triphenyl triazines are planar (see Figure 11). This enables an effective overlap for a good charge transport.

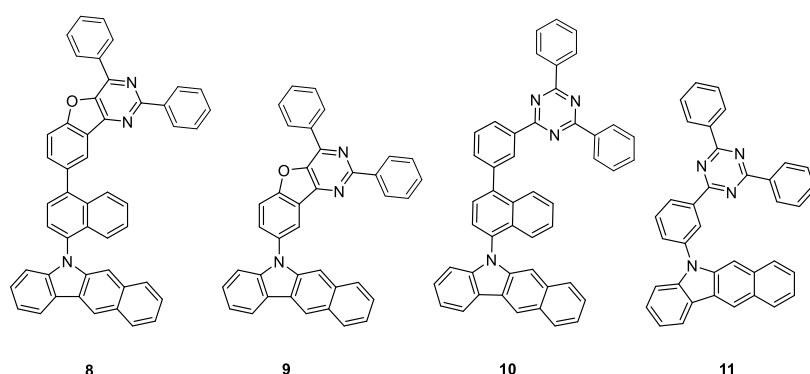


Table 11: Overview on the device results of compound **8-11** compared to a reference at different TMM-Emitter ratios. The absolute (Abs.) measured values are shown. Relative values were obtained by dividing the measured values by values of structure **10** for comparison.

Comp.	TMM:Emitter [%]	Voltage [V] ¹²		EQE [%] ¹³		LT95 [h] ¹⁴	
		Abs.	Rel.	Abs.	Rel.	Abs.	Rel.
8	97:3	3.68	1.29	25.85	0.93	27	0.69
	94:6	3.35	1.19	26.25	0.94	30	0.63
	91:9	3.15	1.12	25.19	0.95	31	0.63
8 (mixed host) ¹⁵	57:40:3	3.70	1.25	26.61	0.95	57	0.74
9	97:3	4.20	1.47	27.74	1.00	52	1.33
	94:6	3.94	1.40	27.75	1.00	56	1.17
	91:9	3.69	1.31	27.54	1.04	40	0.82
9 (mixed host) ¹⁶	57:40:3	3.67	1.24	26.72	0.96	87	1.13
10	97:3	2.86	1.00	27.82	1.00	39	1.00
	94:6	2.82	1.00	27.81	1.00	48	1.00
	91:9	2.81	1.00	26.42	1.00	49	1.00
10 (mixed host) ¹⁶	57:40:3	2.96	1.00	27.88	1.00	77	1.00
11	97:3	3.37	1.18	28.72	1.03	20	0.51
	94:6	3.29	1.17	27.20	0.98	9	0.19
	91:9	3.27	1.16	25.01	0.95	5	0.10
11 (mixed host) ¹⁶	57:40:3	3.12	1.05	28.05	1.01	75	0.97

¹² At a luminance of 1000 cd/m².

¹³ At a current density of 10 mA/cm².

¹⁴ At a current density of 60 mA/cm².

¹⁵ Mixed-host with a ratio 57:40:3 (e-TMM:h-TMM:emitter).

It is also observed that the compounds containing a linking unit (**8** and **10**) show advantages regarding the voltage compared to the compounds without linking unit (**9** and **11**). Therefore, the charge transport seems to be improved by a linking unit between the electron-accepting and electron-donating unit. The improved charge transport might be caused by the larger conjugated system in the compounds that contain a linking unit. Moreover, electrochemical investigations (CV, Table 8) also showed, that the LUMO energy is deeper than the LUMO of **9** and **11**, being closer to the LUMO of the emitter, which improves the electron transport. This could be another explanation for the better results for the current voltage of compounds with linking unit (**8** vs. **9** and **10** vs. **11**).

Figure 25B shows the results of the materials regarding the efficiency at a luminance of 10 mA/cm². Generally, all four compounds show similar efficiencies with low discrepancy. The linking unit does not show any significant influence on the EQE. The best efficiency is observed for the triazine compound **11** without linker (103% compared to **10**). However, the efficiency drops for compound **11**, when more emitter is built into the EML (Figure 25D), while the EQE is stable at different e-TMM-emitter ratios for compound **9**. At higher emitter concentrations, compound **11** runs out of charge balance and quenching seems to occur as also the lifetime drops with higher emitter concentration (Figure 25E). Low emitter concentrations are desirable to save rare and expensive transition metals and to avoid self-quenching of the emitter. Therefore, good EQE's at low emitter concentrations are beneficial for the development of OLED materials.

Lifetime experiments are shown in Figure 25C measured at 60 mA/cm². In general, there was no trend observed for factors that influence the lifetime – neither linker nor electron-accepting unit. Compound **9** shows by far the best lifetime, however, it also shows the worst results for the voltage. This shows the general challenges of the development of TMM's, as high lifetime often comes along with bad results for voltage and vice versa. Regarding all three parameters (efficiency, voltage, and lifetime), compound **10** is the best material for red TMM application, as a better efficiency and voltage were achieved with an acceptable lifetime.

4.3 Results of the green TMM's

The green TMM's evaluated in this thesis are again shown in Figure 26. Structures **1-4** contain an angulated [c]-annulated benzocarbazole unit, while compounds **12** and **14** contain carbazole-derivatives.

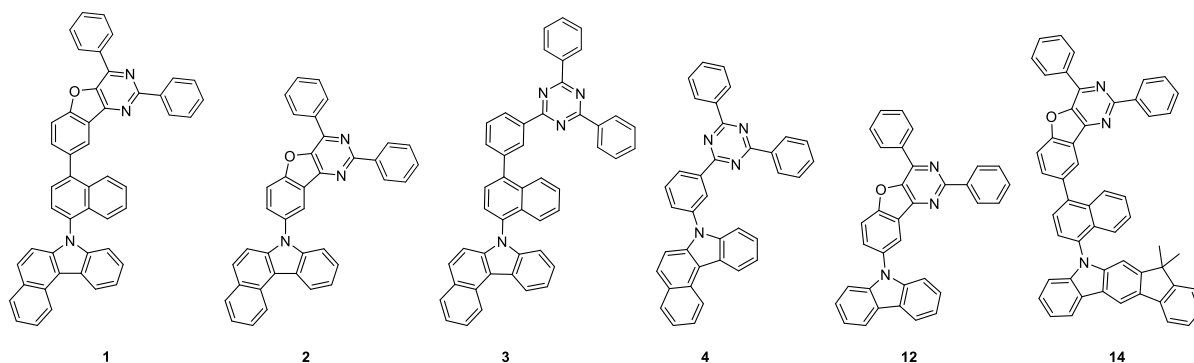


Figure 26: Overview of synthesized and evaluated **green TMM's 1-4 and 12, 14.**^[99]

4.3.1 Electrochemical Properties

As well as the red TMM's, the electrochemical properties of green TMM's **1-4** and **12-14** were investigated by CV. The results are shown in Figure 27 and Table 12. Experimental details were described in chapter 4.1.1 for red TMM's and were also used for the green TMM's in this chapter.

Calculated and experimental HOMO levels were in good agreement with a discrepancy of < 0.2 eV. Experimental HOMO levels were always lower than calculated HOMO levels. This is due to inaccuracy of DFT, where orbital energy values are based on interpreting the Kohn-Sham eigenvalues as quasiparticle energies and are only an auxiliary construct to approximate the electronic kinetic energy. This phenomenon was also observed for the red TMM's. Calculated and experimental LUMO levels were in very good agreement with a discrepancy of < 0.08 eV (Table 12).

CV data of compounds **2**, **3**, and **4** show electrochemical reversible oxidations in CH₂Cl₂ or DMF with similar potentials between 1.4 to 1.6 V. In contrast, compound **1** shows an irreversible oxidation at a potential of 1.7 V in opposite to compound **2**, **3** and **4**. This could be an indication for degradation in the redox process due to a side reaction, which can lead to a reduction of lifetime in OLED-devices, as the new species can serve as an energy trap.

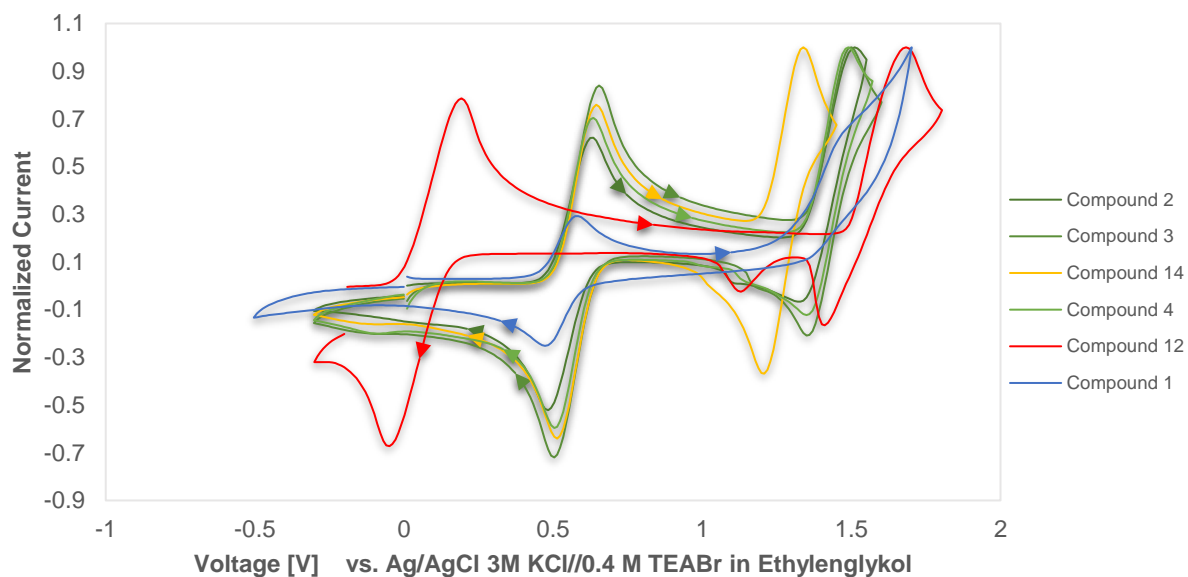


Figure 27: Cyclic voltammograms of **green** TMM's **1-4** and **12-14** with a scan rate of 0.5 V/s and the internal standard Ferrocene.

The internal standard for compound **12** was dmfc/dmfc⁺. Compound **12** shows clearly one oxidation peak at a potential of 1.7 V, but two reduction peaks at 1.1 V and 1.4 V respectively. This shows that compound **12** seems to gradually degrade after the first oxidation. It is also known that carbazole based compounds are prone to dimerization as shown by Browne *et al.*^[99] This might also correspond to the smaller aromatic system of the carbazole compared the benzocarbazole compounds, which influences the delocalization of the electron pair at the nitrogen that is oxidized in the first oxidation.

Table 12: Comparison of the calculated and measured HOMO and LUMO levels for **green** TMM's **1-4** and **12-14**. Details on the calculation of theoretical HOMO and LUMO levels are described in the theoretical considerations (Chapter 3.1).

Compound	HOMO _{CV} [eV]	LUMO _{CV} [eV]	HOMO _{DFT} [eV]	LUMO _{DFT} [eV]
1	-5.68	-2.77	-5.48	-2.64
2	-5.65	-2.69	-5.48	-2.64
3	-5.64	-2.61	-5.45	-2.57
4	-5.64	-2.67	-5.47	-2.64
12	-5.73	-2.66	-5.63	-2.69
14	-5.49	-2.66	-5.38	-2.63

4.3.2 Thermal Properties

The thermal properties of compounds **1-4**, **12** and **14** are shown in Table 13. All compounds with a linking unit (**1**, **3**, and **14**) show a higher decomposition temperature T_d (448-476 °C) and T_g (153-197 °C). The corresponding compounds without linking unit (**2**, **4** and **12**) provide

significantly lower decomposition temperatures than the compounds with linking unit and also lower T_g . This was already observed for the red TMM's and supports the indication that the linking unit increases thermal stability, which is desired for OLED application. Further studies on that will be elucidated in the device results in chapter 4.2.4.

Table 13: Thermal properties (measured T_g , T_m and T_d values) of **green** TMM's **1-4** and **12-14**.

Compound	T_g [°C] ¹⁶	T_m [°C] ¹⁷	T_d [°C] ¹⁸
1	177	361	476
2	137	-	417
3	153	-	448
4	104	260	415
12	114	236	379
14	197	-	472

4.3.3 Photophysical Properties

For the photophysical characterization of the green TMM's **1-4** and **14**, ultraviolet-visible (UV-Vis) absorption and photoluminescence (PL) spectra were measured in solid-state form (100% film, 50 nm). The normalized absorption and emission spectra are shown in Figure 28 and the characteristic photophysical data is summarized in Table 14.

The absorption of the green TMM's is < 330 nm for the film layer. The emission maxima show defined maxima and broad emission bands between 435 and 470 nm. The green host materials emission is at lower wavelength than for the red TMM's.

Again, it is observed, that the compounds with a larger π -system (**1**, **3** and **14**, containing linking unit) emit at lower wavelengths and are blue shifted. The form of the emission bands again suggests the formation of an intramolecular charge-transfer transition between the benzocarbazole donor and the triazine/benzofuropyrimidine acceptor moiety in the excited state. However, also intermolecular interactions could be responsible for it. It is noticeable, that compounds **2** and **4** show similar emission spectra (466/467 nm), as they possess similar a π -system.

¹⁶ Measured by DSC in the second heating scan (heating rate: 20 °C/min).

¹⁷ Measured by DSC in the first heating scan (heating rate: 20 °C).

¹⁸ Measured by TGA experiment with a heating rate of 20 °C/min in a nitrogen atmosphere or under vacuum. T_d is the temperature, where 5% weight loss is detected.

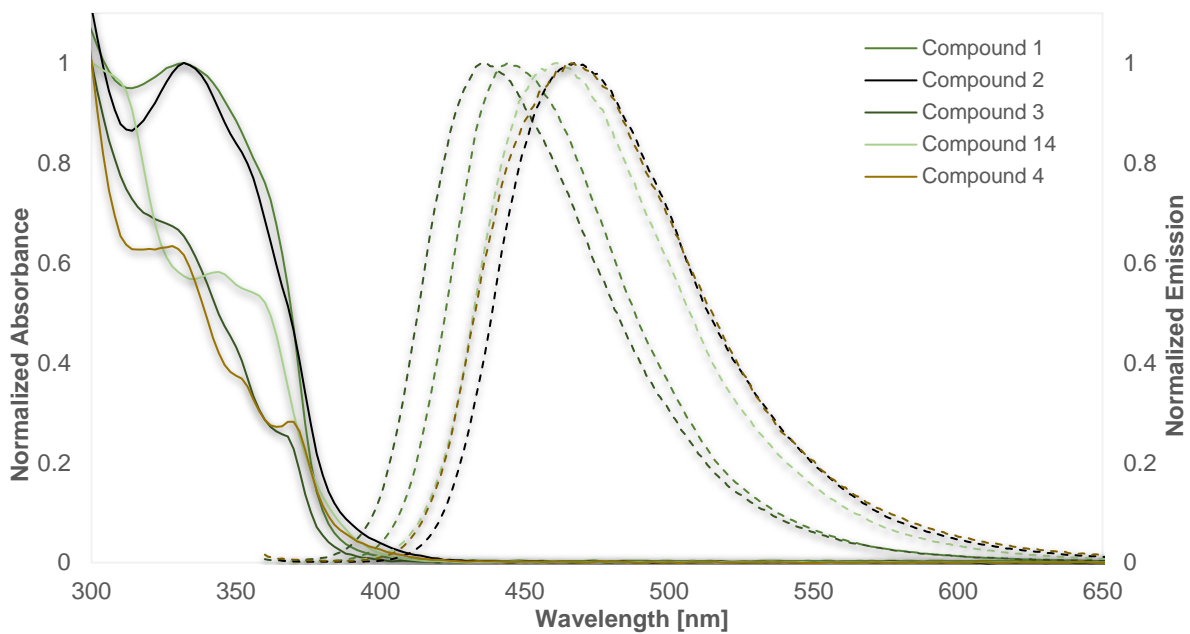


Figure 28: Normalized absorption (solid line) and emission (dashed line) of **green** TMM's **1-4** and **14** in solid-state form (100% film, 50 nm) at room temperature.

Table 14: Summary of the characteristic photophysical data of red TMM's **1-4** and **14**.

Comp.	$\lambda_{em, max}$ [nm]	Stokes shift [nm]	Film		
			CIE _x	CIE _y	FWHM [nm]
1	444	114	0.152	0.103	66
2	467	135	0.159	0.214	75
3	435	135	0.154	0.094	69
4	466	166	0.163	0.203	82
14	461	161	0.155	0.174	75

4.3.4 Device Results

For the evaluation of lifetime, efficiency and driving voltage, the green TMM's were tested in a bottom emission mixed-host OLED stack (internal Merck KGaA technology, Figure 29). The focus of the investigations is on the relationship of chemical structure of the e-TMM on the device properties. Usually, lifetime of green emitters is weak and, which is the main aspect to be improved by green TMM's.

Each stack consists of an LiQ/Aluminium layer (100 nm), an electron injection layer with ETM1:LiQ (1:1, 30 nm), an electron transport layer with ETM2 (5 nm), the emissive layer containing the e-TMM and emitter (different ratios, 40 nm), the hole transport layers with HTM1 (20 nm) and HTM2 (50 nm), the injection layer with HTM2:PDM (5%, 20 nm) and the ITO (50 nm). The exact structure of the e-TMM, emitter, ETM1, ETM2, HTM1 and HTM2 are confidential. Exemplary materials can be found in Merck KGaA patents^[98] and literature-known emitters^[50]. OLED stack components are shown in Figure 3 in chapter 1.1.2 and Figure 5 in chapter 1.1.3.

Here, each e-TMM material **1-4** and **14** was built into the emissive layer (EML) together with a h-TMM material to give a mixed-host OLED-stack. For each material, seven stacks were manufactured by high vacuum thermal evaporation. The standard EML contains an e-TMM:h-TMM:emitter ratio of 32:60:8, but also stacks with e-TMM:h-TMM:emitter ratios of 72:20:8, 62:30:8, 52:40:8 and 22:70:8 (e-TMM:h-TMM:emitter) were fabricated.

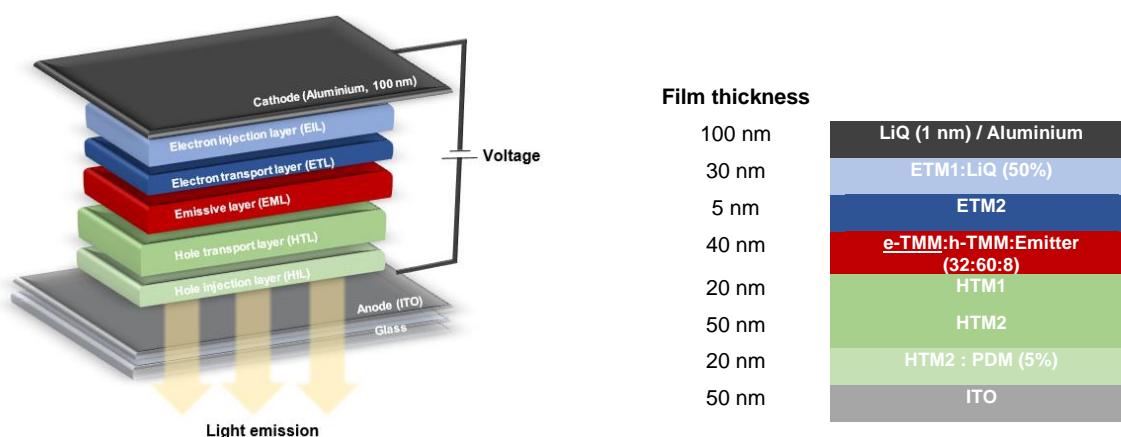


Figure 29: Schematic representation of the mixed-host OLED-stack for a green emitter, where the synthesized target e-TMM materials were built into the emissive layer.

Current density-voltage curves, quantum efficiency-luminance curves, luminance-lifetime curves, EQE-co-host ratio dependencies, and lifetime-co-host ratio dependencies of all green TMM's are depicted in Figure 30. The electroluminescent properties (voltage and EQE) of the tested devices as well as lifetime results are summarized in Table 15. Relative values were obtained by dividing the measured values by triazine compound **3** (100%).

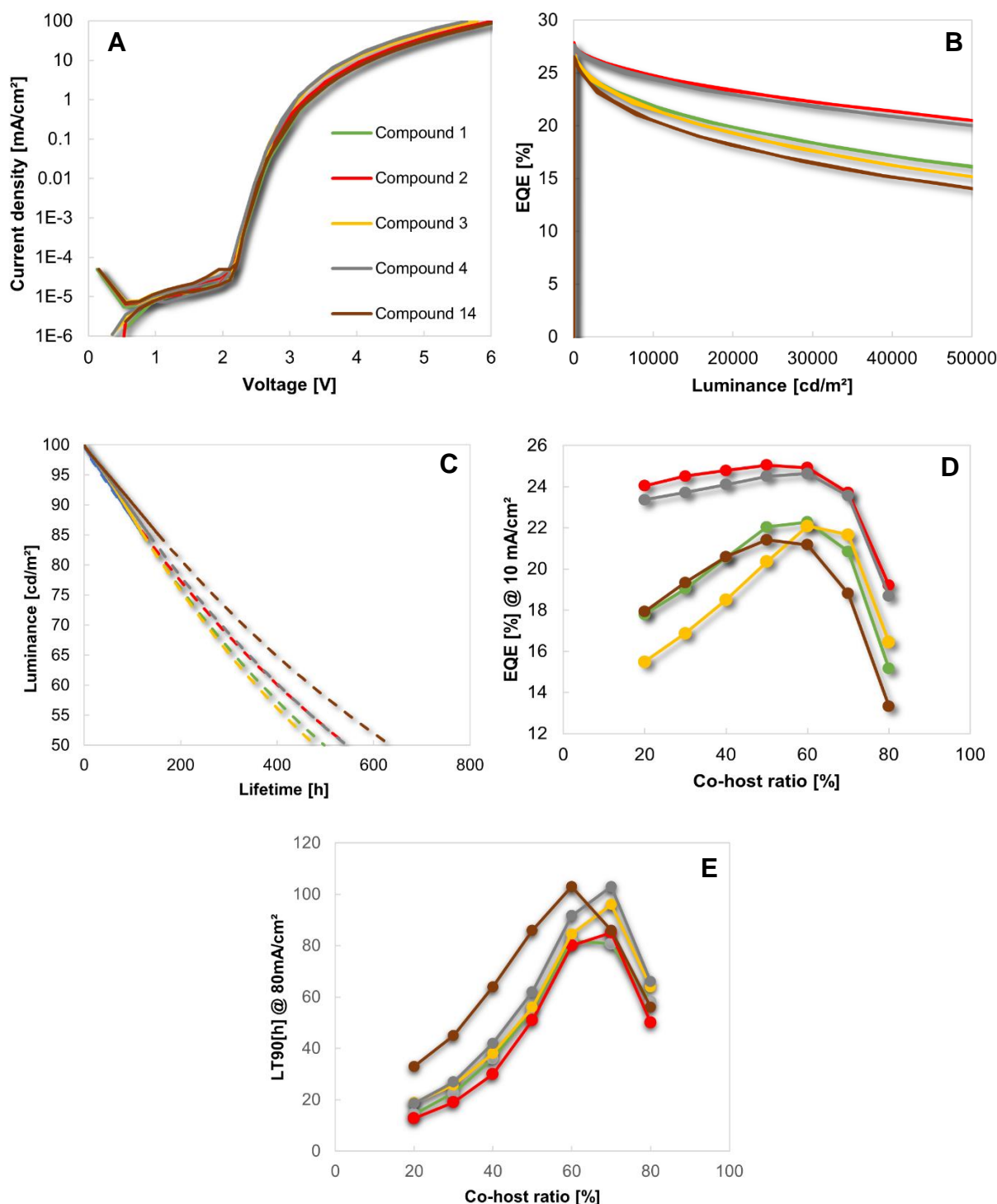


Figure 30: Device results of compound 1 (green), 2 (red), 3 (yellow), 4 (grey) and 14 (brown) including the (A) the current-density-voltage curve, (B) EQE vs. luminance, (C) luminance vs. lifetime (dashed line is extrapolated according to the exponential decay function up to LT₅₀) (D) EQE vs. co-host ratio and (E) lifetime vs. co-host ratio.

The current density-voltage correlation (Figure 30A) shows that compound 1 (containing a linker) shows the best results for voltage compared to compounds without a linking unit. This is the same trend that has already been observed for the red TMM's. Therefore, the general assumption is, that a linking unit increases the charge mobility and therefore decreases the voltage, which is beneficial for the application of TMM's in OLED application. Moreover, electrochemical investigations (CV, Table 12) again showed, that the compound with the

deepest LUMO (compound **1**), shows the best results for driving voltage. This is another evidence for the LUMO being closer to the LUMO of the emitter, which improves the electron transport and thus improves the driving voltage.

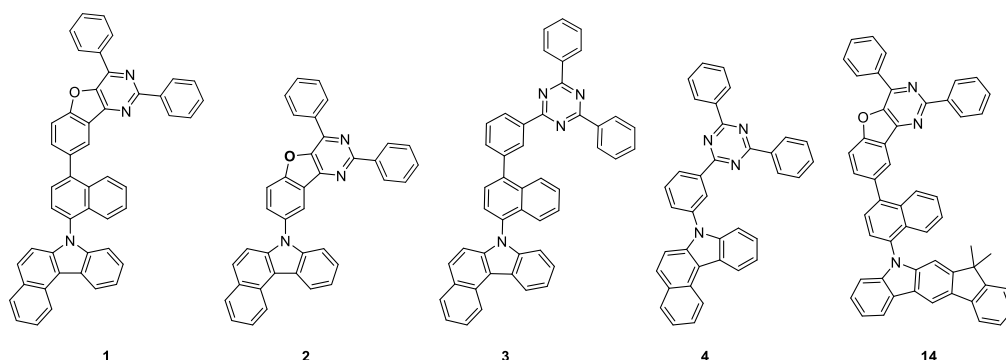


Table 15: Overview on the device results of compound **1-4** and **14** compared to a reference at different TMM-Emitter ratios. The absolute (Abs.) measured values as well as the values relative to the reference (Rel.) are shown.

Comp.	e-TMM:h-TMM:Emitter [%]	Voltage [V] ¹⁹		EQE [%] ²⁰		LT90 [h] ²¹	
		Abs.	Rel.	Abs.	Rel.	Abs.	Rel.
1	72:20:8	2.97	0.91	17.80	1.15	71	1.78
	62:30:8	3.02	0.90	19.04	1.13	94	1.77
	52:40:8	3.08	0.89	20.57	1.11	133	1.73
	42:50:8	3.16	0.86	22.04	1.08	177	1.61
	32:60:8	3.29	0.84	22.29	1.01	210	1.29
	22:70:8	3.45	0.82	20.85	0.96	173	0.95
	12:80:8	3.70	0.82	15.16	0.92	112	0.90
2	72:20:8	4.05	1.24	24.05	1.55	29	0.73
	62:30:8	3.99	1.19	24.52	1.45	44	0.83
	52:40:8	3.98	1.14	24.79	1.34	68	0.88
	42:50:8	4.01	1.10	25.05	1.23	113	1.03
	32:60:8	4.12	1.05	24.92	1.13	173	1.06
	22:70:8	4.30	1.02	23.71	1.09	180	0.99
	12:80:8	4.53	1.00	19.21	1.17	103	0.83
3	72:20:8	3.26	1.00	15.49	1.00	40	1.00
	62:30:8	3.36	1.00	16.87	1.00	53	1.00
	52:40:8	3.48	1.00	18.50	1.00	77	1.00
	42:50:8	3.66	1.00	20.36	1.00	110	1.00
	32:60:8	3.91	1.00	22.09	1.00	163	1.00
	22:70:8	4.20	1.00	21.67	1.00	182	1.00
	12:80:8	4.52	1.00	16.44	1.00	124	1.00
4	72:20:8	3.38	1.04	23.37	1.51	40	1.00
	62:30:8	3.43	1.02	23.72	1.41	59	1.11
	52:40:8	3.52	1.01	24.10	1.30	88	1.14
	42:50:8	3.66	1.00	24.51	1.20	128	1.16
	32:60:8	3.85	0.98	24.67	1.12	182	1.12
	22:70:8	4.11	0.98	23.56	1.09	200	1.10
	12:80:8	4.43	0.98	18.69	1.14	128	1.03
14	72:20:8	3.67	1.13	17.93	1.16	71	1.78
	62:30:8	3.76	1.12	19.34	1.15	94	1.77
	52:40:8	3.87	1.11	20.60	1.11	134	1.74
	42:50:8	4.02	1.10	21.42	1.05	177	1.61
	32:60:8	4.21	1.08	21.17	0.96	210	1.29
	22:70:8	4.41	1.05	18.81	0.87	173	0.95
	12:80:8	4.62	1.02	13.33	0.81	112	0.90

¹⁹ At a luminance of 1000 cd/m².

²⁰ At current density of 10 mA/cm².

²¹ At a current density of 60 mA/cm².

Figure 30B shows the results of the materials regarding the efficiency at a current density of 10 mA/cm². Generally, all three compounds with linker (**1**, **3** and **14**) show a similar efficiency (EQE error $\pm 5\%$). The best efficiency is observed for the compounds **2** and **4** without linker (150% relative to compound **3**).

Lifetime experiments are shown in Figure 30C. In general, compounds containing a benzofuopyrimidine electron accepting unit show longer lifetimes compared to triazine compounds. Compounds **1** and **14** provide the best lifetime results with 210 hours (LT₉₀). Compounds **1** and **14** are very similar in structure and only differentiate in the electron donor unit, which is the [*b*]-annulated benzocarbazole for compound **1** and the indenocarbazole unit for compound **14**. Electron accepting unit and linking unit are the same for both molecules. The lifetime and the efficiency results for both molecules are very similar, which shows that the electron donor carbazole unit does not have a significant influence on the lifetime and the efficiency. However, the driving voltage is different and the [*b*]-annulated benzocarbazole compound **1** performs significantly better than **14** in this regard. Therefore, the electron donor unit seems to have a larger influence on the voltage than on the efficiency and lifetime.

Regarding all three parameters (efficiency, voltage, and lifetime), compound **1** is the best material for green TMM application, as a better efficiency and voltage were achieved with a good lifetime. The studies showed, that benzofuopyrimidine in the electron accepting unit improves the lifetime compared to triazine, linking units improve the voltage and the efficiency is good for all synthesized TMM's. These results will contribute to further develop and optimize specific properties of TMM's.

4.4 Physical and Chemical Special Characteristics of [b]-annulated and [c]-annulated benzocarbazole based TMM's

TMM **8** and **1** are structurally similar regioisomers. They only differ at the benzocarbazole unit, bearing either a [b]-annulated or [c]-annulated benzocarbazole.

Nevertheless, theoretical considerations (chapter 3.1), synthetic attempts (3.3) as well as the material property evaluations (chapter 4) showed that both structures are extraordinarily different.

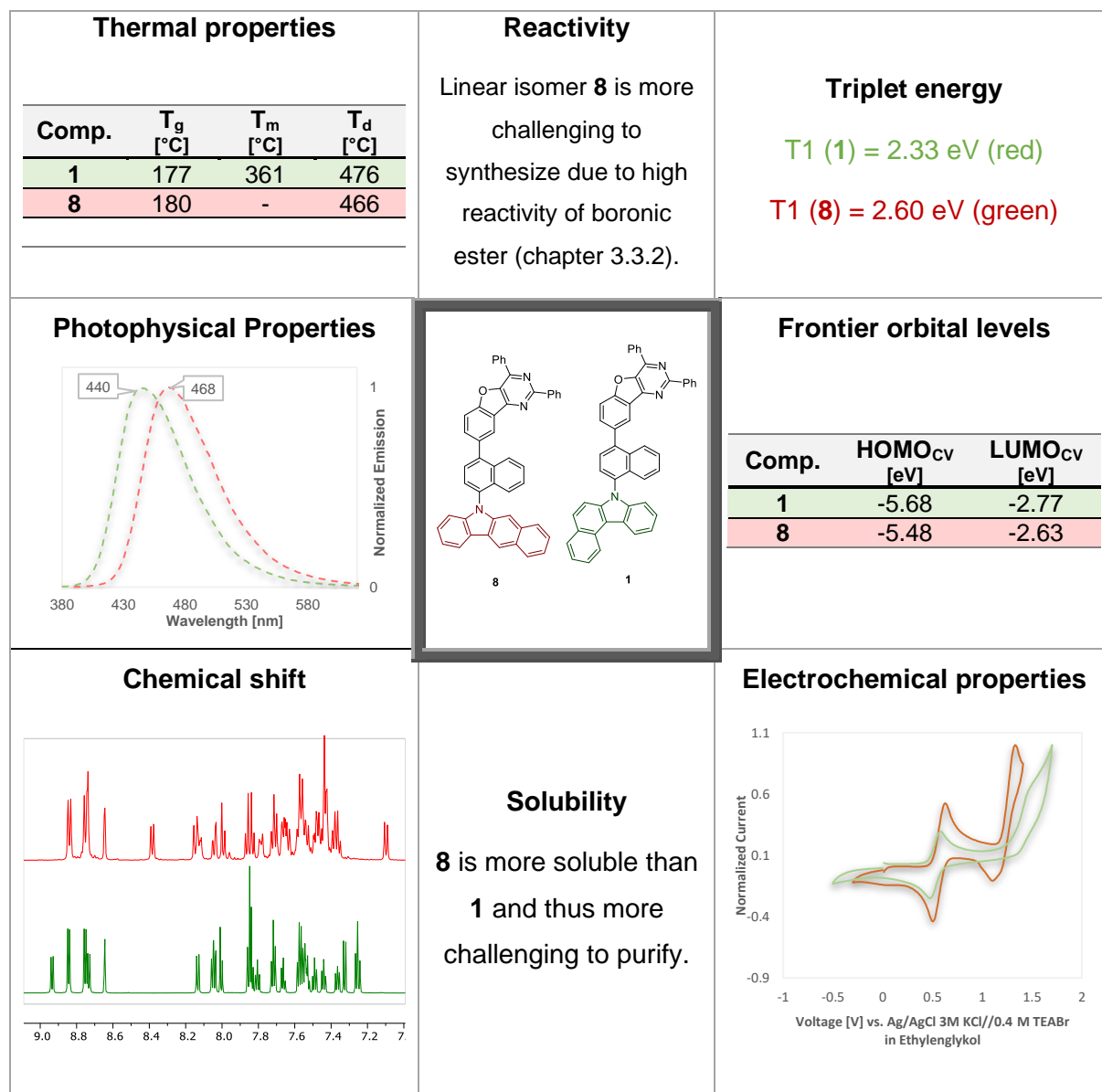


Figure 31: Comparison of physical and chemical properties of regioisomers **1** and **8**.

As shown in Figure 31, the small difference in structure at the benzocarbazole unit, has immense influence on electronic, physical, chemical, thermal, material and photophysical properties.

Theoretical considerations have already shown, that both structures will have different properties, since the calculated triplet energy levels (T1) was calculated to be different so that compound **1** would be suitable for green triplet host application, while compound **8** would be suitable for red triplet host application. The DFT calculations also showed a strong difference in spin density distribution (Figure 32A).

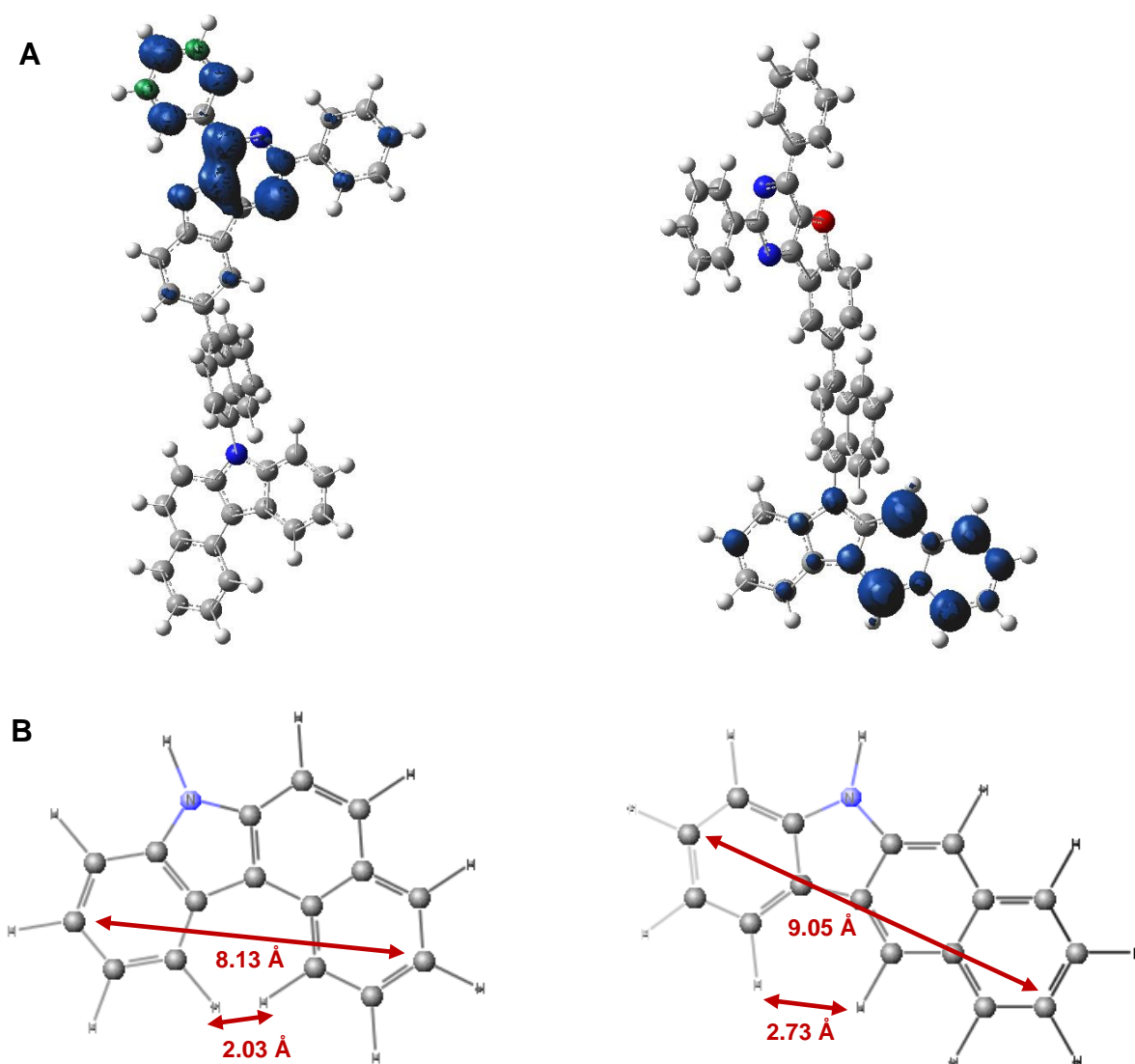


Figure 32: (A) Spin density distribution of compound **1** (left) and compound **8** (right), and (B) each benzocarbazole unit ([c]- and [b]-annulated) showing the maximum distance of C-atoms and the distance of protons.

When the syntheses of both structures were carried out, a strong difference in reactivity of the intermediate boronic ester was observed. Thus, linear isomer **8** was more challenging to synthesize (chapter 3.3.2). Boronic ester **48** was bench stable, while **67** decomposed already at room temperature after some hours. The observation of different properties of **1** and **8** continued in the purification since compound **8** was more soluble in common organic solvents than compound **1**. This increased challenges in purification since recrystallization and further

purification methods were not as efficient as for compound **1**. Furthermore, the fluorescence emission of compound **1** (440 nm) is at a wavelength 28 nm below compound **8** (468 nm).

TGA and DSC measurements also showed that the thermal properties of **1** and **8** differentiate. While compound **8** is amorphous and decomposes at 466 °C, a melting point of compound **1** was detectable and the decomposition took place 10 °C higher compared to compound **8**. CV measurement also showed significant differences in the HOMO (oxidation) and LUMO (reduction) energy levels. The oxidation of compound **1** takes place at a higher voltage (1.7 V) than compound **8** (1.3 V). All those results are also in accordance with the low lifetime of compound **8** that was observed in the device experiments.

Having a deeper look at the structures of both benzocarbazole units of **1** and **8** (Figure 32B), shows, that the maximum distance of C-atoms as well as some neighbored protons is different in both structures. The linear [*b*]-annulated benzocarbazole in **8** has a larger longitudinal skeleton size (9.05 Å^[100]) compared to the [*c*]-annulated benzocarbazole in **1** (8.13 Å^[100]). This also leads to a much shorter distance of the selected two neighbored protons in **8** (2.03 Å^[100]) compared to **1** (2.73 Å^[100]). The shorter distance increases the intramolecular interaction between the hydrogen atoms and is assumed to be directly connected to the reorganization energy for hole and electron transport.^[100] Therefore, the intramolecular hydrogen distances and interactions seem to be the main reason for both regioisomers to provide the various different chemical and physical properties.

5 Photoredoxcatalytic C-N Coupling for the Synthesis of TMM's

Contribution: The photoredoxcatalytic system used in this chapter was developed in the group of Prof. Dr. Burkhard König by Dr. Indrajit Ghosh (Universität Regensburg). The photoredoxcatalytic reactions were conducted by Klaus Osazuwa Omoregbee. GC spectra were recorded by Klaus Osazuwa Omoregbee. GC-MS spectra were recorded by Dr. Rudolf Vasold (Universität Regensburg).

5.1 Introduction

Transition metal-catalysed cross-coupling reactions are the fundamental method for the construction of TMM's for OLED application. C-N bonds, such as anilines or other aromatic C-N bonds, are not only a common structural motif in OLED materials, but also in active pharmaceutical ingredients, agrochemicals, natural products, and organic materials. As shown in chapter 3.3.1 and 3.3.2, Buchwald-Hartwig C-N cross-coupling, Ullmann coupling, Chan-Lam or nucleophilic aromatic substitution are powerful methods to access the carbazole-aromatic system motif in all TMM structures (**1-14**) in this thesis.

Over the past decades, many methods and systems have been developed for the coupling of amines with sp^2 aryl halides or pseudohalides. The main tool for the optimization of transition-metal catalyzed cross-couplings is the design of elaborate and specialized ligand frameworks to influence and optimize stereoelectronic properties of the active metal centre. A key feature in ligand design for C-N cross-couplings is the destabilization of the Pd(II) amido complex for the essential reductive elimination of the C-N bond.^{[101][102][102]}

Even though, palladium-catalyzed cross-coupling reactions^{[103][84][75]} are among the state-of-the-art for the construction of C-N bonds, replacing palladium with the more sustainable and more abundant nickel is desirable. Nickel is attractive as it exists in oxidation states that are necessary for cross-couplings. However, the oxidative addition of an aryl halide to Ni(0) and reaction with a nucleophile such as an amine or carbazole usually results in a thermodynamically stable Ni(II) species that does not allow for reductive elimination of the C-N bond.^[104]

Recent developments have shown, that this metal amido complex destabilization can be triggered through an electron transfer *via* photoredox catalysis. Systems were developed where the synergistic action of a photocycle and a nickel cross-coupling cycle can perform C-N and C-C cross couplings under mild conditions.^{[105][106][107][108][109][110][111][112]}

Depending on the substrate, different mechanisms invoked in photoredox Ni-catalyzed cross-coupling reactions have been proposed, including energy-transfer-mediated catalysis, oxidation-state modulation and a thermally sustained Ni(I/III) cycle.^{[113][106][114]} Activation of Ni(II) intermediates with energy transfer catalysis and photoredox catalysis for nickel oxidation state modulation is depicted in Figure 33.

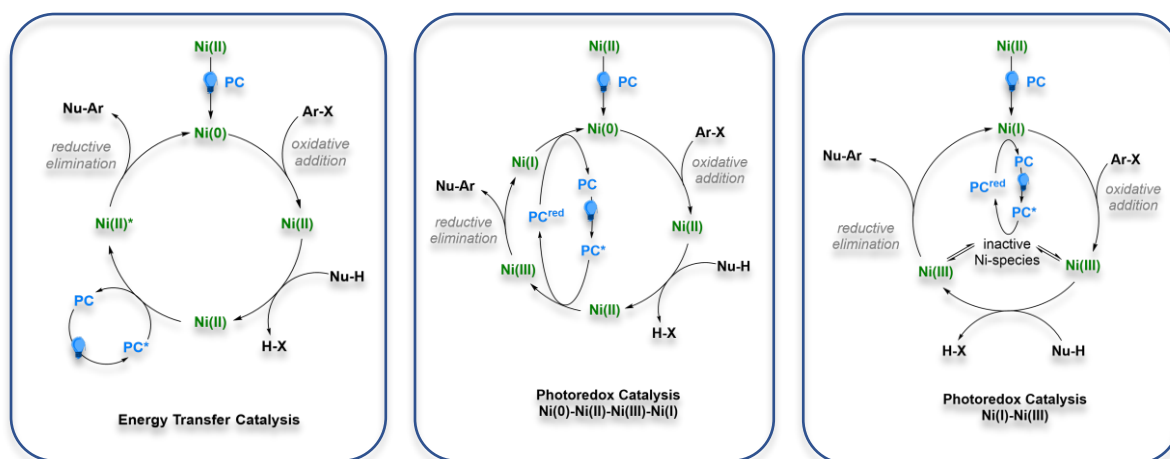


Figure 33: Activation of Ni(II) intermediates with energy transfer catalysis and photoredox catalysis for nickel oxidation state modulation.

The proposed mechanism for the photocatalytic C-N cross coupling is based on oxidative addition of the aryl halide or pseudohalide (Ar-X), followed by ligand exchange of the halide with the respective nucleophile (e.g. amine or carbazole in the case of C-N coupling) and reductive elimination of the desired C-N-product.^[113] Generally, a dynamic system of Ni(I)/Ni(II)/Ni(III) complexes is proposed to be part of the mechanism. The photocatalytic cycle is induced by a single electron transfer. The excited photocatalyst is quenched by accepting or donating a single electron to the co-catalyst, which enables oxidative or reductive quenching cycles. The reductive elimination is often described to be triggered by the oxidation of the Ni(II) species to Ni(III) by the photocatalyst. Mechanistic analysis by MacMillan *et al.* using stoichiometric organometallic studies along with a comprehensive kinetic study of metallaphotoredox C-N coupling unveiled the crucial role of photocatalysis in both initiating and sustaining a Ni(I)/Ni(III) cross-coupling mechanism.^[115] Here, the mechanism is proposed to proceed *via* the oxidative addition of the aryl halide at the Ni(I) species to give a Ni(III) species that releases the C-N product by reductive elimination and recovers the Ni(I) species to close the catalytic cycle.

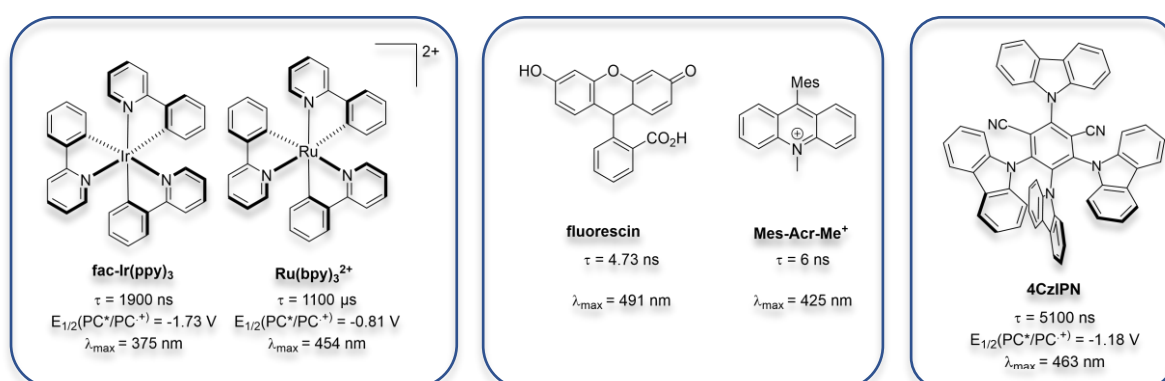


Figure 34: Structures and their photophysical and electrochemical properties^{[116][117][118][119]} of common photocatalysts including noble metal-based organometallic complexes and organic photocatalyst dyes.

Currently, most photocatalytic reactions are conducted using iridium or ruthenium polypyridyl complexes.^[116] These complexes can undergo metal-to-ligand charge transfer that enable them to form stable and long-life excited states. In contrast, organic dyes like cyanoarenes such as 4CzIPN, xanthenes and benzophenones as well as acridium salts and boron dipyrromethenes (BODIPY) are studied as metal-free alternatives to transition metal complexes (Figure 34).^{[116][117][118][119]}

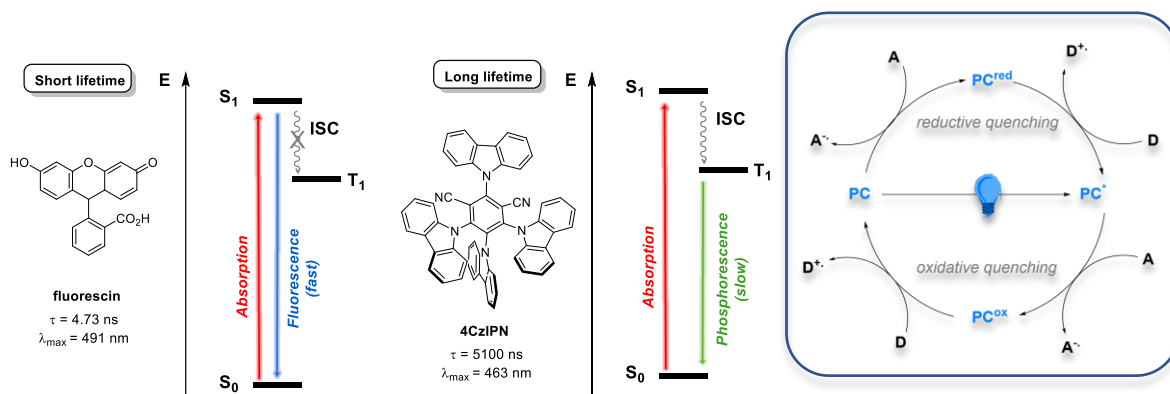


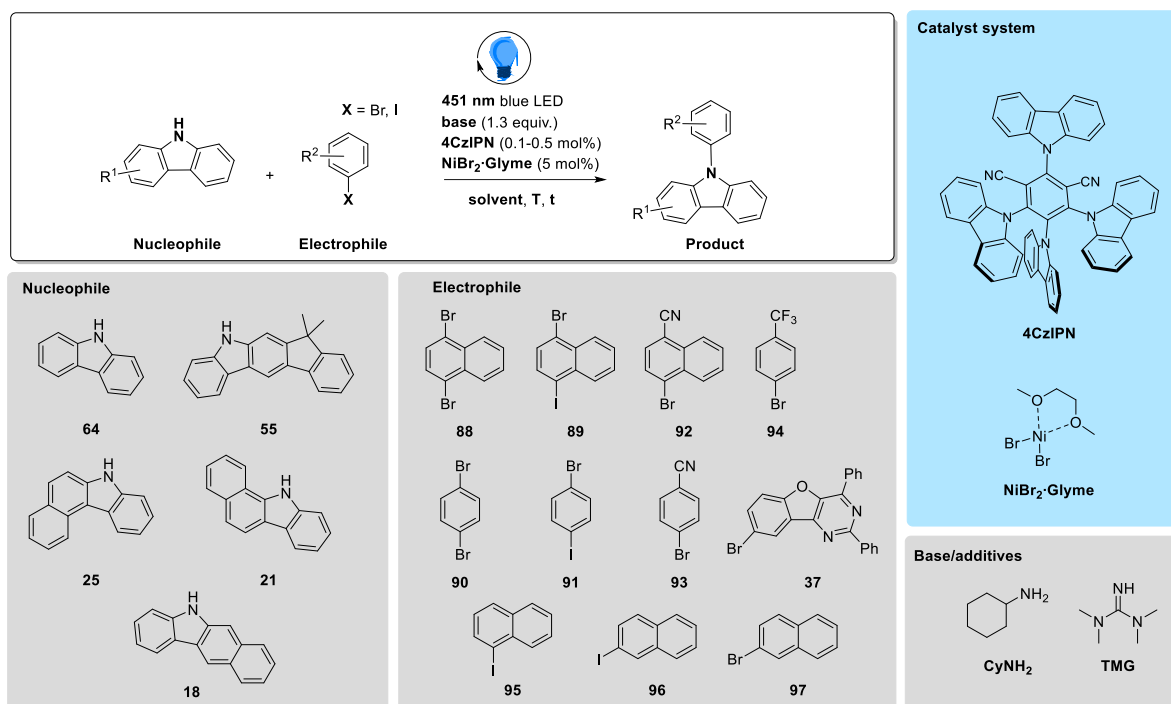
Figure 35: Unsuitable organic dye with short excited state lifetime (fluorescein) and suitable organic dye with long excited state lifetime for photocatalysis (4CzIPN) and reductive and oxidative quenching cycles in photoredox catalysis of the photocatalyst (PC) and acceptor (A) and donor (D).

Cyanoarenes, such as 4CzIPN, can reach long-lived triplet excited states through intersystem crossing, which makes them attractive for the use in photoredox catalysis (Figure 35).^{[120][121]}

Therefore, a cyanoarene-nickel system was developed by König *et al.* and was evaluated in this thesis for the suitability in the synthesis of precursors of TMM's for OLED application. Photoredox C-N coupling has been described mainly for primary and secondary amines^{[113][115]}, but has not been discussed for carbazoles. However, the investigated TMM's contain carbazole units. Therefore, the aim of this chapter is the evaluation of König *et al.*'s photocatalytic system for the C-N coupling of carbazole derivatives with aryl halides.

5.2 Results

For the evaluation of the suitability of the photoredox catalytic cyanoarene-nickel system (4CzIPN, NiBr₂-Glyme, Base, 451 nm blue LED light)²², a variety of carbazole derivative nucleophiles (**18**, **21**, **25**, **55** and **64**) were chosen for C-N coupling with different aryl-halides (**88-97** and **37**). An overview on the used substrates, catalyst, and additives in the photoredox catalytic C-N coupling reactions is shown in Scheme 24.



Scheme 24: Overview on the photoredox catalytic C-N coupling reactions. Selected nucleophiles are carbazole derivatives (**18**, **21**, **25**, **55**, **64**) based on the structural motifs of TMM's for OLED application. Aromatic halogens (electrophiles) are either linking units (**88-94**) with additional halogen substituent or EWG substituent or electron accepting unit **37**. The catalytic system and base/additives are based on research of König *et al.*

Photoredox catalytic C-N cross coupling of carbazole with naphthyl halides

The photoredox catalytic cyanoarene-nickel system was first tested on the C-N cross coupling of 9H-carbazole and naphthyl halides. 9H-carbazole was chosen to get an idea if the photoredox catalytic system works for the simplest carbazole nucleophile. Different naphthyl halides were tested, including the bromo-iodo-compound **89** that was also used for Buchwald-Hartwig couplings. Furthermore, the electron poor cyano-aryl-bromide **92** was tested to check if the increase in electrophilicity would enhance the photoredox catalytic C-N cross coupling. Furthermore, aryl-iodide **95** and **96** as well as aryl-bromide **97** were tested to check if the position of the halide at the aromatic system influences the outcome of the reaction and to avoid chemoselectivity problems due to the presence of two halides in compound **89**. Aryl-

²² This system was developed in the group of Prof. Dr. Burkhard König by Dr. Indrajit Ghosh.

iodide **95** and **96** as well as aryl-bromide **97** were also tested to get an idea, if the second halide in compounds **88** and **89** could increase or decrease reactivity due to its +M/-I effect.

Table 16: Overview on the photoredox-catalytic C-N cross coupling of carbazole with naphthyl halides and screened conditions. Reaction time was 24 hours. Reaction progress was monitored by TLC or GC analysis and a qualitative conclusion of the reaction outcome was made. Product formation is shown by GC-MS (Appendix 94). Products were not further characterized.

Nucleophile	Electrophile	Base	4CzIPN [mol%]	Solv.	T [°C]	Result
64	89	CyNH ₂	0.1/0.5	DMAc	60	Traces
64	89	TMG	0.1/0.5	DMAc	60	Traces
64	88	CyNH ₂	0.1	DMAc	60	Traces
64	88	TMG	0.1	DMAc	60	Traces
64	88	CyNH ₂	0.5	DMAc	25	No conversion
64	88	TMG	0.5	DMAc	25	No conversion
64	92	CyNH ₂	0.1	DMAc	60	Incomplete conversion
64	92	TMG	0.1	DMAc	60	Incomplete conversion
64	95	CyNH ₂	0.1	DMAc	25/60	Incomplete conversion, dehalogenation
64	95	TMG	0.1	DMAc	25/60	Incomplete conversion, dehalogenation.
64	96	CyNH ₂	0.1	DMAc	60	No conversion, dehalogenation
64	96	TMG	0.1	DMAc	60	Incomplete conversion
64	97	CyNH ₂	0.1	DMAc	60	No conversion, dehalogenation.
64	97	TMG	0.1	DMAc	60	Incomplete conversion

The results and tested conditions of the photoredox-catalytic C-N cross coupling of carbazole and naphthyl halides are summarized in Table 16.

The test-reactions of carbazole **64** and naphthyl halides **88** and **89** only provided traces of C-N coupling product **98**. Besides that, only starting materials were obtained. The variation of base (CyNH₂ and TMG) did not change the outcome of the reaction and also the use of more cyanoarene catalyst (0.5 instead of 0.1 mol%) did not improve the results. When lowering the temperature from 60 °C to 25 °C, no conversion was observed at all.

Since the C-N coupling to naphthyl halides **89** and **88** was not efficient, cyano-aryl-bromide **92** was tested. Cyano-aryl-bromide **92** contains the strongly electron-withdrawing cyano-group with an -M effect and therefore is expected to be a better electrophile than compound **89** and **88** (Figure 36). Therefore, the oxidative addition at Ni(0) or Ni(I) is expected to be more efficient and would thus enable the photoredoxcatalytic C-N cross coupling. Indeed, product formation was observed. The reaction was not completed, as starting materials were still detected. However, it was shown, that a stronger electrophile is beneficial for the photocatalytic C-N cross coupling of carbazoles and the carbazole nucleophile itself can be coupled with the existing system.

In the next step, aryl-iodide **95** and **96** as well as aryl-bromide **97** were tested. For electrophile **95**, more product formation than for corresponding iodide **89** was observed. Here, no halide substituent is exciting besides the iodide that reacts in the oxidative addition, and thus a decrease in electrophilicity due to the +M effect of bromide is not induced. This is an indication for the necessity of a certain level of electrophilicity of the aryl halide. This is also supported by the conversion observed when using electrophilic cyano-aryl-bromide **92**. Naphthyl halides **96** and **97** only provided dehalogenated starting material.

In a nutshell, it was shown, that electron-poor electrophiles enable the photoredoxcatalytic C-N cross coupling. However, no full conversion was observed. Another factor, that could inhibit or decrease reactivity for nickel-catalyzed C-N coupling is the steric hindrance by the neighbored H-5 proton close to the halide. This could inhibit the nucleophilic attack of the carbazole after oxidative addition as shown in Figure 36.

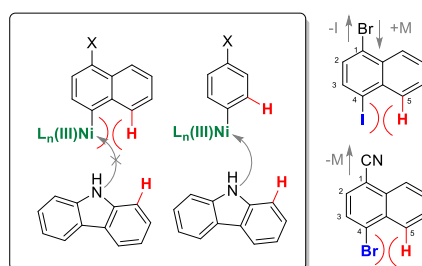


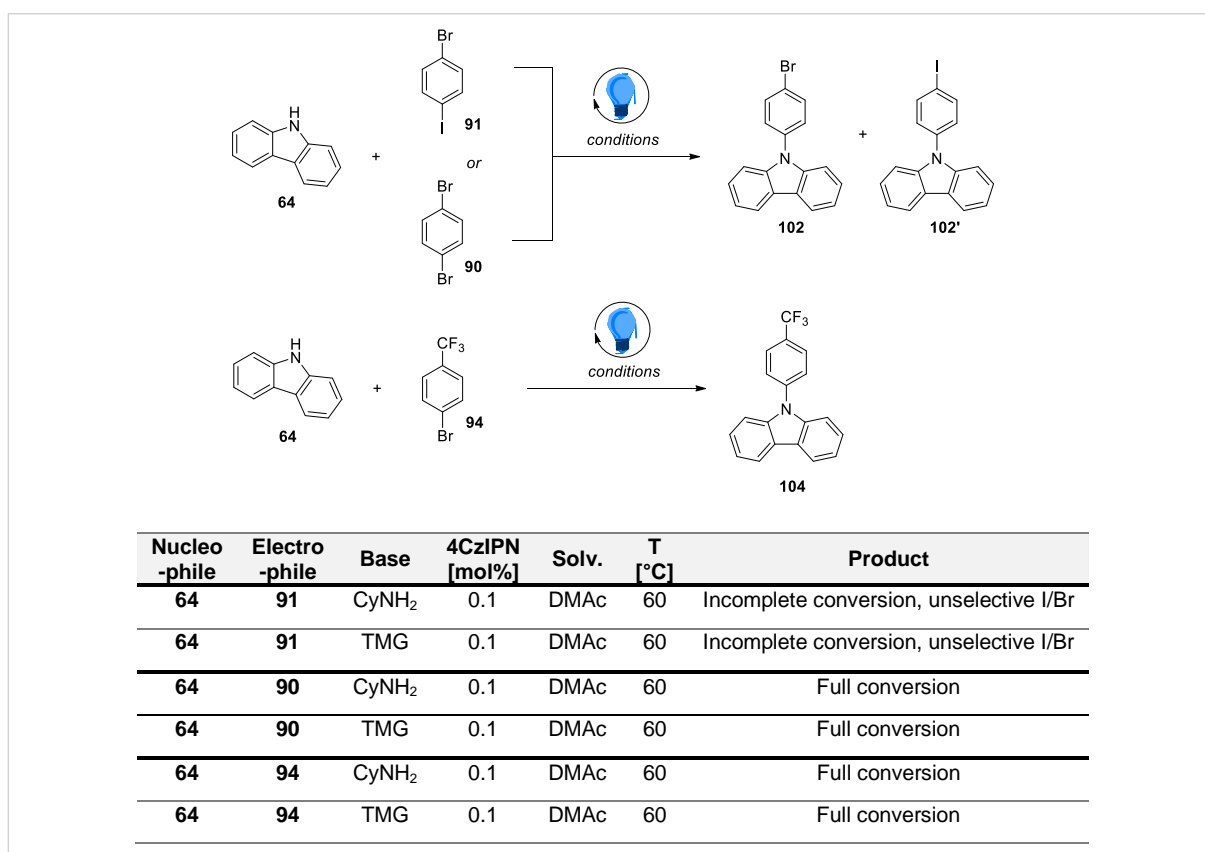
Figure 36: Proposed factors that could inhibit the coupling of carbazole with naphthyl halides including electronic effects (-I, -M, +M effects) and steric hindrance.

Photoredox-catalytic C-N cross coupling of carbazole with phenyl halides

The hypothesis of steric hindrance of the H-5 atom close to the halide in naphthyl electrophiles was supported by experiments using phenyl halides instead of naphthyl halides.

The results and tested conditions of the photoredox-catalytic C-N cross coupling of carbazole with phenyl halides are summarized in Table 17.

Table 17: Overview on the photoredox catalytic C-N cross coupling of carbazole with phenyl halides and screened condition. Reaction time was 24 hours. Reaction progress was monitored by TLC or GC analysis and a qualitative conclusion of the reaction outcome was made. Product formation is shown by GC-MS (Appendix 94). Products were not further characterized.



In the test-reactions of carbazole **64** with phenyl bromide **90** resulted in full conversion to C-N coupling product **102**. The coupling of carbazole **64** with phenyl iodide **91** was not selective for iodide and also bromide was coupled. As expected, due to the -I effect of the trifluoromethyl substituent at compound **94**, full conversion was also observed in the photoredox-catalytic C-N cross-coupling of **64** with **94** to give C-N coupling product **104**. However, those results show, that steric hindrance in naphthyl electrophiles seem to have a larger influence on efficiency of the photoredox-catalytic coupling of carbazoles than electron-donating substituents at the electrophile.

Photoredoxcatalytic C-N cross coupling of carbazole and phenyl halides

With the observed trends in hand, the more complex benzocarbazoles **25**, **21** and **18** as well as indenocarbazole **55** were tested for coupling using the approved cyanoarene-nickel photoredoxcatalytic system. The C-N couplings of the benzocarbazoles and indenocarbazole were tested with naphthyl-electrophiles **88** and **89** as well as more electrophilic and less sterically hindered cyano-phenyl electrophile **93** to give TMM precursors **47**, **107**, **66** and **56** as well as cyano compound **106**.

Table 18: Overview on the photoredox catalytic C-N cross coupling of carbazole with phenyl halides and screened condition. Reaction time was 24 hours. Reaction progress was monitored by TLC or GC analysis and a qualitative conclusion of the reaction outcome was made. Product formation is shown by GC-MS (Appendix 94). Products were not further characterized.

Nucleo-phile	Electro-phile	Base	4CzIPN [mol%]	Solv.	T [°C]	Product
25	89	CyNH ₂	0.1/0.5	DMAc	60	Traces
25	89	TMG	0.1/0.5	DMAc	60	Traces
25	93	CyNH ₂	0.1/0.5	DMAc	60	Incomplete conversion
25	93	TMG	0.1/0.5	DMAc	60	Incomplete conversion
21	88	CyNH ₂	0.1	DMAc	60	No conversion
21	88	TMG	0.1	DMAc	60	No conversion
18	88	CyNH ₂	0.1	DMAc	60	Traces
18	88	TMG	0.1	DMAc	60	Traces
55	88	CyNH ₂	0.1	DMAc	60	No conversion
55	88	TMG	0.1	DMAc	60	No conversion
64	37	CyNH ₂	0.1	DMAc	25/60	No conversion, dehalogenation
64	37	TMG	0.1	DMAc	25/60	No conversion, dehalogenation
64	37	CyNH ₂	0.1	DMAc/DMF (1:1)	25/60	No conversion, dehalogenation
64	37	TMG	0.1	DMAc/DMF (1:1)	25/60	No conversion, dehalogenation

The results in Table 16 and factors described in Figure 16 have already shown that the coupling of naphthyl electrophiles is less efficient than the coupling of phenyl electrophiles. These results are supported by the low efficiency of couplings summarized in Table 18. It was observed, that only in the C-N coupling reaction of **25** and **93**, significant product formation took place. For all other reactions, either no reaction or trace amounts of product were observed.

The results show that TMM's of this work cannot be efficiently coupled using the cyanoarene-nickel photoredoxcatalytic system as they all contain naphthyl linking units. However, naphthyl linking units proved to be difficult to couple using the cyanoarene-nickel photoredoxcatalytic system. On the other hand, the use of linkers with electron-withdrawing substituents would enable the synthesis of TMM precursors using the cyanoarene-nickel photoredoxcatalytic system. However, electron-withdrawing substituents such as trifluoromethyl and cyanide are not suitable in OLED materials since the harsh purification methods (sublimation at temperatures > 300 °C) would result in decomposition and potential formation of CN. Another reason for low efficiency of most of the coupling reactions could be the absorption of photons^[122] by the chromophore system of the substrates.

In a nutshell, the conducted qualitative studies have shown, that carbazoles and benzocarbazoles can be used with the cyanoarene-nickel photoredoxcatalytic system in C-N couplings. It was shown that the electrophile is the main limiting factor as its electronics as well as sterics can influence the efficiency of the C-N coupling. Sterical hinderance of naphthyl electrophiles provide low coupling yields, while phenyl electrophiles show high coupling efficiencies. On the other hand, electron-poor electrophiles with electron-withdrawing substituents show higher coupling efficiency than electron-rich electrophiles.

6 Conclusion and Outlook

In the past years, enormous progress has been achieved in the development of materials for OLED application. However, especially the lifetime of OLED-screens has not yet reached the level of classical screens that are based on liquid crystals. The development of more efficient, less energy consuming, and durable OLED devices is of high importance for the progress of the field of electronics. Especially, lifetime and energy consumption are important when talking about sustainability.

In this thesis the synthesis of novel red and green triplet matrix materials (TMM's) was described, and structure-property relationships were investigated by the systematic exchange of electron and hole conducting and linking subunits. In this context, a variety of differently constituted heteroaromatic trisubstituted benzofuopyrimidine/triphenyltriazine and carbazole derivatives were designed, synthesized, and tested. The influence of the triplet and HOMO/LUMO energy level and the structures of these compounds was evaluated regarding the lifetime, efficiency, and driving voltage.

The first part of this work focused on theoretical pre-evaluations of heteroaromatic TMM's based on trisubstituted benzofuopyrimidine, triphenyltriazine and carbazole derivatives (benzocarbazoles, indenocarbazole, carbazole). Triazines are common electron conducting units, while trisubstituted benzofuopyrimidines have only been poorly discussed in the context of red and green TMM's in combination with carbazole derivatives. Theoretical considerations using DFT led to the hypothesis, that trisubstituted benzofuopyrimidines are attractive alternatives to triphenyltriazines, because the triplet energy levels are higher than the triplet energy level of Merck Electronics KGaA emitters and the HOMO level is lower than those emitters.

The second part of this work focused on the synthesis of heteroaromatic TMM building blocks based on trisubstituted benzofuopyrimidine, triphenyltriazine and benzocarbazoles. Heteroaromatic compounds and intramolecular ring-closing reactions are often challenging and require sometimes control of selectivity. Here, the selective benzocarbazole formation was investigated. A series of strategies were applied for the challenging synthesis of [*b*]-annulated 5*H*-benzo[*b*]carbazole, while [*c*]-annulated and [*a*]-annulated benzocarbazoles were the favored products. Furthermore, the synthesis of a new electron accepting unit was established, consisting of a trisubstituted benzofuopyrimidine building block. A method *via* furan formation by an S_N2 reaction of 2-hydroxybenzocarbonitrile and 2-bromoacetophenone followed by a nucleophilic addition reaction proved to be a useful tool to synthesize the benzofuopyrimidine structural motif.

The third part of this thesis focused on the coupling of the synthesized building blocks to give a variety of final benzofuopyrimidine/triazine and benzocarbazoles based TMM's. Buchwald-Hartwig and Suzuki-Miyaura reactions were useful for the synthesis of all TMM's. Mostly palladium-based catalysts, base, solvent, and reaction temperature were adjusted depending on the used building blocks. Notably, [*c*]-annulated and [*b*]-annulated benzocarbazole units showed a difference in reactivity in cross coupling reactions. For several synthesized precursors or final TMM's, the high purity standards for OLED application could not be reached due to lack of capacity in this thesis. Homocoupling or dehalogenation species, methylated side product traces as well as halogen or metal traces in some cases prevented reaching desired HPLC (99.9%) and ICP-MS purity. Further investigation for purification remain a challenge and need to be properly addressed in future research. This shows that the process of TMM development does not only includes the synthesis of the desired molecules, but also the high purity is essential for succeeding in fabricating an OLED device that can be evaluated.

In the fourth part of this thesis, the synthesized TMM's were evaluated of their material properties to understand the structure-property relationship and judge the applicability in OLED devices. Regarding all three parameters (efficiency, voltage, and lifetime), compound **1** is the best material for green TMM application, as the best combination of efficiency, voltage and lifetime was achieved. The studies showed, that benzofuopyrimidine electron accepting units improve the lifetime of green TMM's compared to triazine electron accepting units, linking units improve the voltage and the efficiency gives good results for all structural motifs. These results will contribute to the design and optimization of TMM's.

Generally, in red TMM's it was shown that triazine structures give better voltage results compared to benzofuopyrimidine structures. Also, the incorporation of a linker leads to better results than structures without one. Moreover, for the efficiency, triazine structures show better results than benzofuopyrimidine structures and the linker does not have an observable influence. Compound **9** shows by far the best lifetime, however, it also shows the worst results for the voltage. This demonstrates a common challenge in the development of TMM's, as high lifetime often comes along with bad results for voltage and vice versa. With respect to efficiency, voltage, and lifetime, compound **10** is the best material for red TMM application, as a better efficiency and voltage were achieved with an acceptable lifetime.

Next steps in the development of red and green TMM's would be further improvement of lifetime, by modifying the synthesized structures. A possible next step could be the systematic introduction of electron-donating or electron-withdrawing groups on the benzocarbazole unit. Electron-donating substituents, such as phenyl groups (phenyl-benzocarbazoles) are promising tools to improve or further understand factors that influence lifetime of TMM's.

In the last part of this work, a photo-redox catalytic cyanoarene-nickel system was tested to evaluate its applicability in the synthesis of precursors of TMM's and itself. In a nutshell, the conducted qualitative studies showed, that carbazoles and benzocarbazoles can be used with the cyanoarene-nickel photoredoxcatalytic system in C-N couplings. It was shown that the electrophile is the main limiting factor as its electronics as well as sterics can influence the efficiency of the C-N coupling. Sterical hinderance of naphthyl electrophiles provided low coupling yields, while phenyl electrophiles showed high coupling efficiencies. On the other hand, electron-poor electrophiles with electron-withdrawing substituents showed higher coupling efficiency than electron-rich electrophiles.

The developed methodologies and synthetic routes in the thesis expand the toolbox for the synthesis of TMM's or precursors. The investigated structure-property relationships will further help to develop and optimize properties of TMM's.

7 Experimental Section

7.1 General Methods and Materials

Reagents and Solvents

Unless otherwise stated, all reactions and workups were performed without air exclusion. Reactions with air or moisture sensitive substances were performed under an argon atmosphere using the Schlenk technique and Schlenk flasks were dried *in vacuo* using a heat gun. All reagents and solvents were used as purchased from commercial suppliers unless otherwise stated.

NMR, HPLC, HPLC-MS, GC-MS, AQF, ICP-MS, UV/Vis, fluorescence, crystallography, CV, DSC, and TGA experiments/measurements were conducted by the analytical department of Merck Electronics KGaA Darmstadt.

All analytical data was acquired with the following equipment:

NMR spectroscopy

^1H , ^{13}C , ^{19}F and 2D spectra were obtained from Bruker Avance 400 (400 MHz with TXO probehead), Bruker Avance 400 (400 MHz with BBO-F probehead), Bruker Avance 500 (500 MHz with BBO-F probehead), Bruker Avance 500 (500 MHz with BBO-F CryoProbe) and a Bruker Avance 700 (700 MHz with TCI CryoProbe) in the reported deuterated solvents. Chemical shifts are reported in ppm (relative to the TMS signal) with reference to the residual solvent peaks. The multiplicities of the signals are reported using the following abbreviations: s=singlet, d=doublet, t=triplet, q=quartet, p=quintet. If no multiplicity was identified, the chemical range is given as m= multiplet.

HPLC and HPLC-MS

Merck's Purospher STAR RP-18e (250 x 4.6 mm x 4.6 μm) (short: RP-18) was used as column in combination with gradients of acetonitrile (ACN), THF and methanol (MeOH) on Agilent Infinity II with DAD for HPLC.

HPLC-MS measurements were carried on a Bruker Impact II 2022. The ion source was APCI with a positive ion mode. Merck's Purospher STAR RP-18e (250 x 4.6 mm x 4.6 μm) was used. The sample injection was done with of 1.0 ml/min, split rate of 1/3. The column temperature was at 30 °C.

GC-MS

GC-MS measurements (high resolution) were measured on a GC system Agilent Technologies 7890-A series/Mass selective detector, Agilent Technologies 5975 C, GCT-P CAB096

(HP6890 GC) with a VF-5ms 30 m x 0.25 mm ID DF= 0.25 μ m column. The mass detector was from waters GCT CA122. The separation of the masses was done by time of flight (TOF).

Automatic Quick Furnace Combustion Ion Chromatography (AQF)

AQF measurements were carried out on a Metrohm 930 Professional IC equipped with a Metrosep A Supp 5 150/4.0 column. With this method, trace impurities of F, Cl, Br and S were evaluated.

Inductively Coupled Plasma Mass Spectrometry (ICP-MS)

ICP-MS measurements were carried out on an Agilent 7700x G3281A (Plasma 1500 W). Helium was used as collision gas (flow rate 3.8 mL/min) with a sample concentration of 10 mg/mL in NMP was used (injection volume: 200 μ L, flow rate 50 μ L/min). With this method, trace impurities of B, P, Pd, Cu, Cl, Br, and I were evaluated.

Crystal Structure Evaluation

X-Ray diffraction measurements was done by Andreas Swoboda (Merck KGaA) using a SuperNova (Agilent) diffractometer with an Atlas CCD detector. Cu K α (1.5148 Å), x-ray mirrors were used for radiation. The cif files of the structures were visualized with Mercury CFC 3.10 and SHELX-97 was used for structure solution.^[123]

Cyclic Voltammetry (CV) and Square Wave Voltammetry (SWV)

CV and SWV measurements were conducted on a Metrohm μ AUTOLAB type 3 potentiostat. Voltammograms were recorded using a gold working electrode, a platinum counter electrode and an Ag/AgCl [3 M KCl/0.4 M TEABr (tetraethylammonium bromide) in ethylene glycol] and reference electrode for determination of the oxidation potentials in CH₂Cl₂. The reduction potentials were determined in THF, and an Ag/AgCl [3 M KCl/0.025 M TEACl (tetraethylammonium chloride) in ethylene glycol] reference electrode was used. Scan rates were 500 mV/s, sample concentrations were in the range of 1 · 10⁻³ mol/L. Tetrabutylammonium hexafluorophosphate (TBAHFP, c = 0.11 M) was employed as the supporting electrolyte. Ferrocene or decamethylferrocene was used as an internal reference.

Dynamic Differential Scanning Calorimetry (DSC)

DSC measurements were conducted on a DSC Q2000 V24.10 Build 122. Substrates were heated within a range of 0 - 500 °C (gradient of 5 °C/min), then cooled to 0 °C (ramp of 20 °C/min) and reheated to 500 °C (ramp of 20 °C/min). T_g was determined at onset, while T_m was evaluated at half step.

Column/Thin Layer Chromatography

Reaction progress was controlled *via* thin layer chromatography (silica gel 60 F 254, E. Merck) using UV light (λ = 254 nm) for visualization or the following staining agents: vanillin, KMnO₄

and anisaldehyde and heat as a developing agent and R_F values were determined with this method. Flash column chromatography was performed using silica gel M60 from Macherey & Nagel (particle size: 40-60 μm).

Thermogravimetry (TGA)

TGA measurements were conducted on a TGA Q5000 V3.15 Build 263 with a heating rate of 20 K/min (from 25 °C - 600 °C) under nitrogen atmosphere (flow rate at balance: 10 mL/min, sample area: 25 mL/min). Samples were placed in aluminum crucibles and measurements were aborted at a weight loss > 10 %.

UV/Vis and Fluorescence Spectroscopy

Measurements in solution were carried out in toluene (1 mg in 250 mL, Quartz cells, 10 mm). Films (50 nm, Quartz substrates SQ1, 3x3 cm², 1 mm) were prepared by evaporation. For absorption measurements, a Perkin Elmer Lambda 850 two channel spectrometer in combination with the Perkin Elmer PECSS software was used. For fluorescence measurements, a Hitachi F-4500 was used. The following parameters were used for measurements:

Absorption

- Start wave length: 250 nm
- End wave length: 800 nm
- Scan Speed: 240 nm/min
- Slit: 2.0 nm
- Smooth: 0 nm
- NIR Sensitivity: 3

Photoluminescence

- Ex-Slit: 5.0 nm
- Em-Slit: 5.0 nm
- PMT-Voltage: 700 V
- Response: Auto
- Shutter Control: Yes
- Corrected Spectra: Yes
- Scan Speed: 240 nm/min

Device fabrication and characterization

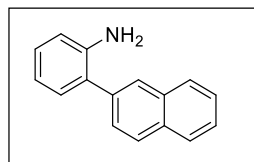
OLED devices in this thesis were fabricated and measured by the physics team of Merck Electronics KGaA OLED. The fabrication was conducted as already described in Chapter 1.1.4.1.

Current, voltage and luminance characteristics were investigated and measured with a Keithley 2400 source meter by setting a specific voltage and measure the current. Different pixel measurement was controlled using a Keithley 2700 multimeter/data acquisition system. Luminance of the OLED devices were recorded using a photodiode (calibrated) connected to a Keithley 6485 picoamperemeter. Electroluminescence spectra were recorded on an Ocean Optics USB4000 spectrometer. The external quantum efficiency (EQE) was calculated from the measured data. Operational lifetime measurements, that were applying constant current density of 40 mA/cm², were recorded using an Electronic Design & Engineering 8/16 Channel (Digital lifetime test unit LTU500/D).

7.2 Synthesis of compounds and analytical data

7.2.1 Synthesis of Heteroaromatic TMM Building Blocks (compounds of chapter 3.2)

2-(naphthalen-2-yl)aniline (**17**)



Under an argon atmosphere 2-bromoaniline **15** (0.50 g, 2.91 mmol, 1.00 eq.), boronic acid **16** (0.60 g, 3.49 mmol, 1.20 eq.) and K_2CO_3 (1.61 g, 11.63 mmol, 4.00 eq.) were charged into a 50 mL round bottom flask and dissolved in PhMe/EtOH/H₂O (2:2:1, 25 mL) at room temperature. The resulting two phasic solution was degassed for 30 Min. Catalyst **Pd(PPh₃)₄** (0.34 g, 0.29 mmol, 10 mol%) were added to the reaction mixture and heated by 100 °C for 24 h. The reaction mixture was cooled down to room temperature and volatiles were removed under reduced pressure. The crude was dissolved in EtOAc (50 mL). The organic phase was washed with H₂O (100 mL) and the aqueous phase was extracted with EtOAc (3 x 50 mL). The combined organic phases were washed with brine solution, dried (MgSO₄) and evaporated under reduced pressure. Purification by column chromatography (SiO₂, Hep/EtOAc 7:1 v/v) gave **17** (0.25 g, 1.14 mmol, **39%**) as a colorless solid.

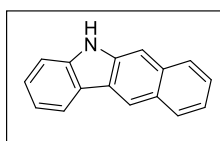
R_f (Heptane/EtOAc 4:1) = 0.48.

¹H NMR (500 MHz, CD₂Cl₂) δ 7.96 – 7.84 (m, 4H), 7.59 (dd, J = 8.4, 1.8 Hz, 1H), 7.56 – 7.47 (m, 2H), 7.24 – 7.13 (m, 2H), 6.88 – 6.78 (m, 2H), 4.00 (d, J = 77.8 Hz, 2H) ppm.

¹³C NMR (126 MHz, CD₂Cl₂) δ 144.68, 137.90, 135.44, 134.48, 133.26, 131.34, 129.35, 129.12, 128.69, 128.46, 128.39, 128.14, 127.05, 126.77, 119.33, 116.35 ppm.

APCI-MS: Calcd for C₁₆H₁₄N [M+H⁺] 220.11, found 220.00.

The acquired characteristic data is in accordance with literature.^{[124][73]}

5H-benzo[*b*]carbazole (18)

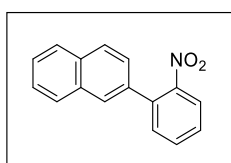
Under an argon atmosphere **17** (0.25 g, 1.14 mmol, 1.00 eq.), 2,2-dimethylpropanoic acid (0.23 g, 2.28 mmol, 2.00 eq.), (acetyloxy)cuprioacetate, (0.04 g, 0.23 mmol, 0.20 eq.) and bis[dichloro(pentamethylcyclopentadienyl)iridium] (0.01 g, 0.02 mmol, 0.02 eq.) were suspended in anhydrous NMP (10 mL). The reaction mixture was saturated with argon for 20 Min. The mixture was heated at 120 °C for 7 h. The mixture was cooled to room temperature. Subsequently, the solvent was removed *via* vacuum distillation and the residue was dissolved in PhMe (30 mL). The organic phase was washed with H₂O (3 x 50 mL). The organic phase was washed with brine solution (2 x 50 mL), dried (MgSO₄) and evaporated under reduced pressure. Purification by column chromatography (SiO₂, Hep/EtOAc 9:1 v/v) gave **18** (0.19 g, 0.87 mmol, **77%**) as a light grey powder.

R_f (Heptane/EtOAc 4:1) = 0.42.

¹H NMR (500 MHz, DMSO-*d*₆) δ 11.18 (s, 1H), 8.67 (s, 1H), 8.24 (d, *J* = 7.7 Hz, 1H), 8.07 – 7.96 (m, 2H), 7.85 (s, 1H), 7.51 – 7.32 (m, 4H), 7.21 – 7.17 (m, 1H) ppm.

¹³C NMR (126 MHz, DMSO-*d*₆) δ 142.4, 139.6, 132.2, 128.2, 127.5, 127.2, 126.9, 125.1, 124.7, 122.3, 122.1, 121.0, 118.5, 118.2, 110.5, 105.0 ppm.

The acquired characteristic data is in accordance with literature.^[73]

2-(2-nitrophenyl)naphthalene (20)

Under an argon atmosphere 1-bromo-2-nitrobenzene **19** (0.50 g, 2.48 mmol, 1.00 eq.), boronic acid **16** (0.51 g, 2.97 mmol, 1.20 eq.) and K₂CO₃ (1.37 g, 9.90 mmol, 4.00 eq.) were charged into a 50 mL round bottom flask and dissolved in PhMe/EtOH/H₂O (2:2:1, 25 mL) at room temperature. The resulting two phasic solution was degassed for 30 Min. Catalyst **Pd(PPh₃)₄** (0.29 g, 0.25 mmol, 1 mol%) were added to the reaction mixture and heated by 100 °C for 48 h. The reaction mixture was cooled to room temperature and the solvents were removed under reduced pressure. The crude was dissolved in EtOAc (50 mL). The organic phase was washed with H₂O (100 mL) and the aqueous phase was extracted with EtOAc (3 x 50 mL). The

combined organic phases were washed with brine solution, dried (MgSO₄) and evaporated under reduced pressure. Purification by column chromatography (SiO₂, Hep/EtOAc 4:1 v/v) gave **20** (0.44 g, 1.77 mmol, **71%**) as a yellow solid.

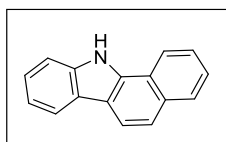
R_f (Heptane/EtOAc 9:1) = 0.41.

¹H NMR (500 MHz, CD₂Cl₂) δ 7.94 – 7.87 (m, 4H), 7.83 (d, J = 1.7 Hz, 1H), 7.69 (td, J = 7.5, 1.3 Hz, 1H), 7.56 (ddd, J = 13.1, 6.8, 2.4 Hz, 4H), 7.41 (dd, J = 8.5, 1.9 Hz, 1H) ppm.

¹³C NMR (126 MHz, CD₂Cl₂) δ 149.89, 136.87, 135.75, 133.86, 133.38, 133.13, 132.90, 128.95, 128.77, 128.65, 128.28, 127.47, 127.17, 126.38, 125.86, 124.79, 54.43, 54.22, 54.00, 53.78, 53.57, 32.46, 29.60, 23.27, 14.44 ppm.

The acquired characteristic data is in accordance with literature.^[125]

11H-benzo[a]carbazole (21)



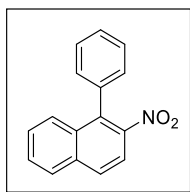
Under an argon atmosphere **20** (0.32 g, 1.28 mmol, 1.00 eq.) was charged into a 50 mL round bottom flask and dissolved in triethylphosphite (1.33 mL, 7.70 mmol, 6.00 eq.) at room temperature. The reaction mixture was heated by 160 °C for 24 h. Purification by column chromatography (SiO₂, Hep/EtOAc 7:1 v/v) gave **21** (0.24 g, 1.10 mmol, **86%**) as a colorless crystalline solid.

R_f (Heptane/EtOAc 9:1) = 0.29.

¹H NMR (500 MHz, DMSO-*d*₆) δ 12.18 (s, 1H), 8.51 (d, J = 8.1 Hz, 1H), 8.19 (dd, J = 19.0, 8.2 Hz, 2H), 8.07 – 8.01 (m, 1H), 7.63 (dd, J = 8.4, 2.5 Hz, 3H), 7.55 (dd, J = 8.2, 6.8 Hz, 1H), 7.41 (t, J = 7.0 Hz, 1H), 7.23 (t, J = 7.4 Hz, 1H) ppm.

¹³C NMR (126 MHz, DMSO-*d*₆) δ 138.73, 135.19, 131.90, 128.52, 125.42, 125.15, 124.50, 123.20, 121.82, 121.26, 119.71, 119.48, 119.11, 119.10, 117.27, 111.34 ppm.

The acquired characteristic data is in accordance with literature.^[126]

2-Nitro-1-phenylnaphthalene (24)

22 (5.00 g, 19.84 mmol, 1.00 eq.), phenylboronic acid **23** (2.54 g, 20.83 mmol, 1.05 eq.) and K_2CO_3 (8.22 g, 59.51 mmol, 3.00 eq.) were dissolved in anhyd. 1,4-dioxane (150 mL) at room temperature and degassed under an argon atmosphere for 30 Min. Catalyst **Pd(dppf) $_2$ Cl $_2$** (0.44 g, 0.60 mmol, 0.03 eq.) were added to the reaction mixture and refluxed at 101 °C for 24 h. Volatiles were removed under reduced pressure and the residue was redissolved in CH_2Cl_2 (200 mL). Subsequently, the reaction mixture was filtered over Celite. The organic phase was washed with H_2O (200 mL) and the aqueous phase was extracted with CH_2Cl_2 (3 x 150 mL). The combined organic phases were washed with brine and dried ($MgSO_4$). **24** (4.8 g, 19.26 mmol, **97%**) was obtained as a brown oil and used for the next reaction without further purification.

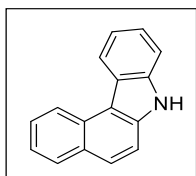
R_f (Heptane/EtOAc 4:1) = 0.63.

1H NMR (500 MHz, CD_2Cl_2) δ 8.00 (dd, $J = 11.2, 8.6$ Hz, 2H), 7.92 (d, $J = 8.8$ Hz, 1H), 7.70 – 7.63 (m, 1H), 7.60 (d, $J = 8.2$ Hz, 1H), 7.53 (td, $J = 4.2, 3.5, 1.7$ Hz, 4H), 7.34 (dd, $J = 5.0, 2.0$ Hz, 2H) ppm.

^{13}C NMR (126 MHz, CD_2Cl_2) δ 147.22, 135.57, 135.29, 135.08, 133.22, 133.08, 129.96, 129.70, 129.11, 129.01, 128.84, 128.71, 128.68, 128.38, 120.44 ppm.

The acquired characteristic data is in accordance with literature.^[127]

7H-benzo[c]carbazole (**25**)



Under an argon atmosphere **24** (0.50 g, 2.01 mmol, 1.00 eq.) was charged into a 50 mL round bottom flask and dissolved in triethylphosphite (2.08 mL, 12.04 mmol, 6.00 eq.) at room temperature. The reaction mixture was heated to 160 °C for 18 h. Column chromatography (SiO₂, Hep/EtOAc 7:1 v/v) gave **25** (0.35 g, 1.61 mmol, **80%**) as a colorless solid.

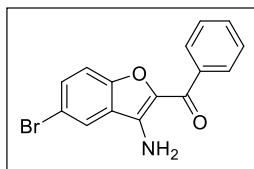
R_f (Heptane/EtOAc 4:1) = 0.40.

¹H NMR (500 MHz, CD₂Cl₂) δ 8.77 (d, J = 8.1, 1.1 Hz, 1H), 8.61 (s, 1H), 8.56 (d, 1H), 8.02 (d, J = 8.1, 1.3 Hz, 1H), 7.89 (d, J = 8.8 Hz, 1H), 7.76 – 7.67 (m, 2H), 7.63 (d, J = 8.1, 0.9 Hz, 1H), 7.53 – 7.44 (m, 2H), 7.42 – 7.37 (m, 1H) ppm.

¹³C NMR (126 MHz, CDCl₃) δ 138.46, 137.07, 129.95, 129.24, 129.21, 127.45, 126.89, 124.36, 124.05, 123.28, 123.02, 122.07, 120.27, 115.52, 112.57, 111.12, 77.28, 77.03, 76.77 ppm.

The acquired characteristic data is in accordance with literature.^[127]

2-benzoyl-5-bromo-1-benzofuran-3-amine (**35**)



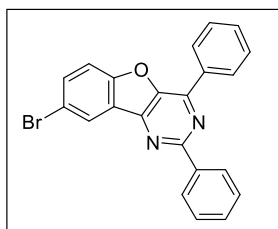
Under an argon atmosphere a 2 L 4 neck round bottom flask was charged with phenol **33** (43.00 g, 217.15 mmol, 1.00 eq.), 2-Bromoacetophenone **34** (43.22 g, 217.15 mmol, 1.00 eq.) and Cs₂CO₃ (141.51 g, 434.31 mmol, 2.00 eq.) and suspended in anhydrous Me₂CO (850 mL). The mixture was stirred vigorously and saturated with argon for 30 Min. After 1 h the reaction was controlled *via* TLC. The reaction mixture was stirred for another 1 h. A yellow-orange precipitate was formed. The mixture was cooled to room temperature and dissolved in EtOAc (1 L). The organic phase was washed with H₂O (3 x 300 mL) and brine solution (500 mL). The solvent was dried (MgSO₄) and evaporated under reduced pressure. The yellow-orange solid was recrystallized in acetone and dried in a vacuum drying cabinet at 50 °C for 5 h. **35** (68.70 g, 217.30 mmol, **quantitative**) was acquired as a light yellow solid. Further purification was not necessary.

¹H NMR (500 MHz, CDCl₃) δ 8.25 – 8.18 (m, 2H), 7.77 (d, *J* = 1.96 Hz, 1H), 7.65 – 7.50 (m, 5H), 7.35 (d, *J* = 8.80 Hz, 1H), 2.17 (d, *J* = 2.78 Hz, 1H) ppm.

¹³C NMR (126 MHz, CDCl₃) δ 183.5, 153.0, 140.6, 137.4, 135.9, 132.7, 132.1, 129.2, 128.3, 122.9, 122.8, 115.2, 114.4 ppm.

The acquired characteristic data is in accordance with literature.^[79]

12-bromo-4,6-diphenyl-8-oxa-3,5-diazatricyclo[7.4.0.0^{2,7}]trideca-1(9),2,4,6,10,12-hexaene (37)



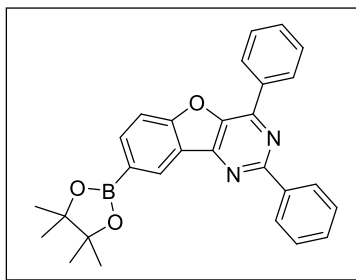
Compound **35** (66.80 g, 210 mmol, 1.00 eq.) was charged into a 2 L 4 neck round bottom flask and dissolved in *p*-xylene (1 L). The reaction mixture was heated at 80 °C. Then **36** (174.36 g, 1692.8 mmol, 8.00 eq.) and NaO^tBu (101.72 g, 1062.28 mmol, 5.00 eq.) were added portion wise. The reaction mixture was stirred and heated at 170 °C for 4 days. A water separator was installed to continuously remove H₂O from the reaction. The reaction was controlled *via* GC-MS and TLC and cooled to room temperature. Volatiles were removed under reduced pressure and the crude was diluted in PhMe (600 mL). The organic phase was washed with H₂O (500 mL). Subsequently, the aqueous phase was extracted with PhMe (4 x 150 mL). The combined organic phases were washed with brine solution, dried (MgSO₄) and evaporated *in vacuo*. Upon evaporation of the solvent a yellow precipitate was formed. The precipitate was washed with heptane (2 x 100 mL) and dried overnight in a vacuum cabinet at 60 °C. **37** (41.30 g, 92.63 mmol, **44%**) was obtained as a yellow solid.

¹H NMR (500 MHz, CDCl₃) δ 8.70 (ddt, *J* = 9.54, 6.10, 1.48 Hz, 4H), 8.49 (d, *J* = 1.97 Hz, 1H), 7.80 (dd, *J* = 8.78, 2.10 Hz, 1H), 7.73 – 7.45 (m, 8H) ppm.

¹³C NMR (126 MHz, CDCl₃) δ 160.0, 156.9, 150.9, 147.4, 144.8, 138.0, 134.3, 134.3, 131.4, 130.3, 129.3, 128.9, 128.6, 128.4, 125.4, 124.1, 117.2, 114.4 ppm.

HRMS (EI-MS): Calcd for C₂₂H₁₃BrN₂O [M] 400.02, found 400.01.

4,6-diphenyl-12-(4,4,5,5-tetramethyl-1,3,2-dioxaborolan-2-yl)-8-oxa-3,5-diazatricyclo[7.4.0.0^{2,7}]trideca-1(9),2,4,6,10,12-hexaene (57)



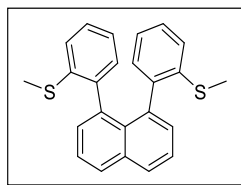
Under an argon atmosphere a 250 mL 4 neck round bottom flask was charged with bromide **37** (15.00 g, 37.38 mmol, 1.00 eq.), **B₂Pin₂** (10.44 g, 41.12 mmol, 1.10 eq.) and KOAc (18.34 g, 186.91 mmol, 5.00 eq.) and suspended in anhydrous 1,4-dioxan (150 mL). The mixture was saturated with argon for 30 Min. Catalyst **Pd(dppf)Cl₂** (1.37 g, 1.87 mmol, 0.05 eq.) were added to the reaction mixture and refluxed at 101 °C for 24 h. The reaction mixture was cooled to room temperature and the solvent was removed under reduced pressure. The crude was dissolved in EtOAc (300 mL). The organic phase was washed with H₂O (3 x 100 mL). A brown solid precipitated out of the solution. The precipitate was filtered and washed with EtOAc (3 x 100 mL) and brine solution (200 mL). The brown solid was dried in a vacuum drying cabinet at 50 °C for 3 h. **57** (10.92 g, 24.36 mmol, **65%**) was obtained as a brown solid. Further purification was not necessary.

R_f(Heptane/EtOAc 9:1) = 0.30.

¹H NMR (500 MHz, CD₂Cl₂) δ 8.81 (s, 1H), 8.78 – 8.70 (m, 4H), 8.14 (d, J = 8.2, 1.2 Hz, 1H), 7.77 (d, J = 8.4 Hz, 1H), 7.69 – 7.50 (m, 6H), 1.41 (s, 12H). ppm.

¹³C NMR (126 MHz, CD₂Cl₂) δ 160.93, 160.18, 152.70, 147.29, 144.98, 138.85, 138.39, 135.10, 131.72, 130.63, 130.06, 129.73, 129.41, 129.08, 128.84, 122.35, 112.79, 84.79, 67.63, 54.43, 54.22, 54.00, 53.78, 53.57, 25.32 ppm.

HRMS (EI-MS): Calcd for C₂₈H₂₅N₂O₃ [M] 448.20, found 448.19.

1,8-bis[2-(methylsulfanyl)phenyl]naphthalene (40)^[80]

Compound **38** (50.00 g, 174.85 mmol, 1.00 eq.), boronic acid **39** (65.95 g, 384.67 mmol, 2.20 eq.) and K_2CO_3 (120.83 g, 874.24 mmol, 5.00 eq.) were dissolved in DMF (550 mL) and H_2O (50 mL) at room temperature and degassed under an argon atmosphere for 30 minutes. Catalyst $Pd_2(dba)_3$ (8.01 g, 8.74 mmol, 0.05 eq.) and ligand **SPhos** (3.59 g, 8.74 mmol, 0.05 eq.) were added to the reaction mixture and refluxed for 5 h. The volume of the solvent was reduced to approx. 150 mL. The mixture was diluted with water (500 mL) and CH_2Cl_2 (200 mL). The aqueous phase was extracted with CH_2Cl_2 (4 x 300 mL). The combined organic phase was washed with brine solution (200 mL), dried ($MgSO_4$) and the solvent was evaporated under reduced pressure. **40** (48 g, 128.84 mmol, **74%**) was obtained as a colourless solid after purification *via* Soxhlet extraction (heptane, 5 d) and washing with ice-cold *n*-heptane.

R_f (Heptane/EtOAc 2:1) = 0.76.

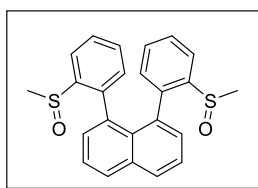
1H NMR (500 MHz, CD_2Cl_2) δ 7.98 (dd, $J = 8.3, 1.4$ Hz, 2H), 7.53 (dd, $J = 8.2, 7.0$ Hz, 2H), 7.24 (dd, $J = 7.5, 1.5$ Hz, 2H), 7.18 (dd, $J = 7.0, 1.4$ Hz, 2H), 6.92 (td, $J = 7.7, 1.5$ Hz, 2H), 6.78 (td, $J = 7.5, 1.2$ Hz, 2H), 6.72 (dd, $J = 8.0, 1.2$ Hz, 2H), 2.24 (s, 6H) ppm.

^{13}C NMR (126 MHz, CD_2Cl_2) δ 140.19, 138.03, 134.68, 130.61, 129.59, 129.24, 128.62, 127.52, 125.12, 122.78, 122.75, 14.72 ppm.

HRMS (EI-MS): Calcd for $C_{24}H_{20}S_2$ [M] 372.101, found 372.100.

The acquired characteristic data is in accordance with literature.^[80]

1,8-bis(2-methanesulfinylphenyl)naphthalene (**41**)^[80]



Thioether **40** (34.80 g, 93.41 mmol, 1.00 eq.) was dissolved in MeCN (150 mL). TMSCl (35.4 mL, 280.23 mmol, 3.00 eq.) was added at room temperature and the mixture was degassed for 15 Min. H₂O₂ (19.1 mL, 186.82 mL, 2.00 eq., 30% aqueous solution) was added dropwise over 1 h and the reaction mixture was stirred at room temperature overnight. The reaction was quenched using saturated aqueous Na₂SO₃ (150 mL). The aqueous phase was extracted with EtOAc (4 x 100 mL). The combined organic phase was dried (MgSO₄) and the solvents were evaporated under reduced pressure. The residue was washed with MeOH (150 mL) and filtrated. **40** (15.11 g, 37.36 mmol, **40%**) was obtained as a colorless solid and was used without further purification.

R_f(Heptane/EtOAc 1:1) = 0.12.

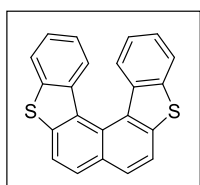
¹H NMR (500 MHz, CD₂Cl₂) δ 8.14 – 7.98 (m, 2H), 7.61 (t, *J* = 7.6 Hz, 2H), 7.41 (t, *J* = 8.1 Hz, 4H), 7.27 – 7.19 (m, 6H), 1.94 (s, 6H) ppm.

¹³C NMR (126 MHz, CD₂Cl₂) δ 145.19, 138.79, 136.03, 134.74, 132.41, 131.03, 130.59, 130.22, 128.89, 128.60, 126.09, 122.21, 41.77 ppm.

HRMS (EI-MS): Calcd for C₂₄H₂₀O₂S₂ [M] 404.090, found 404.091.

The acquired characteristic data is in accordance with literature.^[80]

Naphtho[2,1-*b*:7,8-*b'*]bis[1]benzothiophen (**42**)^[80]



H₂SO₄ (5.93 mL, 111.24 mmol, 22.50 eq.) was added dropwise to sulfoxide **19** (2.00 g, 4.94 mmol, 1.00 eq.) at 0 °C. The reaction mixture was warmed to room temperature and stirred overnight. Ice-water (30 mL) was added and after 15 min the reaction mixture was neutralized by aqueous NaOH (20%, 100 mL), which resulted in the precipitation of a yellow solid. The solid was filtered and washed with ice-cold *n*-heptane. The title compound **42** (1.0 g,

5.29 mmol, **quantitative**) was obtained as a yellow solid and was used without further purification.

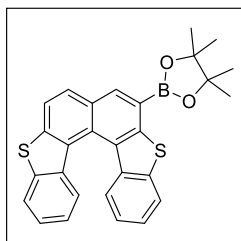
R_f (PhMe/EtOAc 4:1) = 0.82.

$^1\text{H NMR}$ (500 MHz, CD_2Cl_2) δ 6.28 – 6.20 (m, 6H), 5.71 (d, J = 8.2 Hz, 2H), 5.67 – 5.60 (m, 2H), 5.34 (ddd, J = 8.3, 7.0, 1.2 Hz, 2H) ppm.

$^{13}\text{C NMR}$ (75 MHz, THF- d_8) δ 142.1, 140.1, 137.7, 131.8, 130.1, 129.1, 129.0, 126.7, 125.8, 124.1, 123.7, 121.8 ppm.

The acquired characteristic data is in accordance with literature.^[80]

(Naphtho[2,1-*b*:7,8-*b'*]bis[1]benzothiophen-6-yl)boronsäurepinakolester (**43**)



Naphthodibenzothiophen **42** (3.00 g, 8.81 mmol, 1.00 eq.) was dissolved in anhyd. THF (25 mL). The solution was cooled to $-45\text{ }^\circ\text{C}$ (MeCN, dry ice). Then, *n*-BuLi (10.57 mL, 26.43 mmol, 3.00 eq., 2.5 M in hexanes) was added dropwise. The reaction mixture was stirred for 5 h at the same temperature. **A** (3.60 mL, 17.62 mmol, 2.00 eq.) was added and the solution was warmed up to room temperature and stirred overnight. Volatiles were removed *in vacuo*. The residue was redissolved in CH_2Cl_2 (20 mL). The solution was washed with H_2O (20 mL) and the aqueous phase was extracted with CH_2Cl_2 (4 x 20 mL). The combined organic phase was washed with brine solution (20 mL), dried (MgSO_4) and the solvent was evaporated under reduced pressure. The title compound **43** () was obtained as a colourless solid used without further purification for the Suzuki-Miyaura coupling.

R_f (Heptane/EtOAc 2:1) = 0.63.

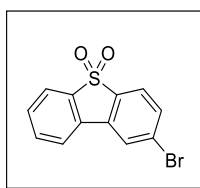
$^1\text{H NMR}$ (500 MHz, TCE- d_2) δ 8.46 (s, 1H), 8.10 – 7.81 (m, 4H), 7.54 – 7.26 (m, 4H), 7.05 (dddd, J = 11.91, 8.19, 7.03, 1.19 Hz, 2H), 1.41 (d, J = 1.98 Hz, 12H) ppm.

$^{13}\text{C NMR}$ (126 MHz, TCE- d_2) δ 145.8, 141.8, 139.5, 138.4, 136.5, 136.2, 135.8, 129.5, 128.8, 128.5, 128.1, 127.9, 127.6, 126.1, 125.7, 125.5, 123.2, 122.8, 122.6, 122.3, 120.7, 99.6, 84.8, 25.4, 25.0 ppm.

HRMS (EI-MS): Calcd for $\text{C}_{28}\text{H}_{23}\text{BO}_2\text{S}_2$ [M] 466.12, found 466.13.

The acquired characteristic data is in accordance with literature.^[80]

4-bromo-8λ⁶-thiatricyclo[7.4.0.0^{2,7}]trideca-1(9),2,4,6,10,12-hexaene-8,8-dione (45a)^[128]



Dibenzothiophene **44a** (20.00 g, 76.00 mmol, 1.00 eq.) was suspended in AcOH (300 mL, 5244 mmol, 69 eq.). Then H₂O₂ (30%, 450.27 mL, 4408 mmol, 58 eq.) was added dropwise for 1 h at room temperature. The reaction mixture was stirred vigorously for 24 h at 90 °C. A white precipitate was filtered and washed several times with H₂O (1 L) and Et₂O (800 mL). The white precipitate was dried in a vacuum cabinet at 80 °C for 6 h. **45a** (18.70 g, 63,36 mmol, **83%**) was obtained as a colourless solid.

R_f(Heptane/EtOAc 4:1) = 0.18.

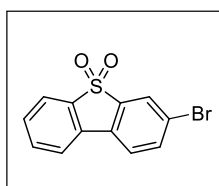
¹H NMR (500 MHz, CD₂Cl₂) δ 7.99 (d, *J* = 1.39 Hz, 1H), 7.81 (dd, *J* = 7.78, 6.19 Hz, 2H), 7.72 – 7.66 (m, 3H), 7.59 (t, *J* = 7.62 Hz, 1H) ppm.

¹³C NMR (126 MHz, CD₂Cl₂) δ 138.7, 137.2, 134.7, 134.2, 133.9, 131.7, 130.8, 129.1, 125.7, 123.8, 122.6, 122.6 ppm.

HRMS (EI-MS): Calcd for C₁₂H₇BrO₂S [M] 293.94, found 293.94.

The acquired characteristic data is in accordance with literature.^[128]

4-bromo-8λ⁶-thiatricyclo[7.4.0.0^{2,7}]trideca-1(9),2,4,6,10,12-hexaene-8,8-dione (45b)^[128]



Dibenzothiophene **44b** (1.60 g, 6.08 mmol, 1.00 eq.) was suspended in AcOH (24 mL, 419.64 mmol, 69.02 eq.). Then H₂O₂ (30%, 36.02 mL, 352.65 mmol, 58.00 eq.) was added dropwise for 1 h at room temperature. The reaction mixture was stirred vigorously for 24 h at 90 °C. A white precipitate was filtered and washed several times with H₂O (500 mL) and Et₂O (400mL). The white precipitate was dried in a vacuum cabinet at 80 °C for 6 h. **45b** (1.50 g, 5.08 mmol, **84%**) was obtained as a colourless solid.

R_f(Heptane/EtOAc 4:1) = 0.18.

¹H NMR (500 MHz, CD₂Cl₂) δ 7.94 (d, *J* = 1.83 Hz, 1H), 7.87 – 7.78 (m, 3H), 7.76 – 7.67 (m, 2H), 7.59 (td, *J* = 7.58, 1.07 Hz, 1H). 7.94 (d, *J* = 1.83 Hz, 1H), 7.87 – 7.78 (m, 3H), 7.76 – 7.67 (m, 2H), 7.59 (td, *J* = 7.58, 1.07 Hz, 1H) ppm.

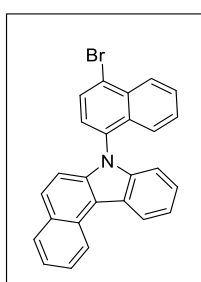
¹³C NMR (126 MHz, CD₂Cl₂) δ 139.8, 138.0, 137.5, 134.7, 131.3, 131.2, 131.1, 125.7, 124.6, 123.8, 122.6, 122.4 ppm.

HRMS (EI-MS): Calcd for C₁₂H₇BrO₂S [M] 293.94, found 293.93.

The acquired characteristic data is in accordance with literature.^[128]

7.2.2 Synthesis of green TMM's (compounds of chapter 3.3.1)

7-(4-bromonaphthalen-1-yl)-7H-benzo[*c*]carbazole (47)



Under an argon atmosphere a 250 mL 3 neck bottled flask was charged with **25** (2.00 g, 9.21 mmol, 1.00 eq.) and CsCO₃ (6.00 g, 18.41 mmol, 2.00 eq.) and dissolved in anhydrous DMF (150 mL). The reaction mixture was heated to 150 °C for 20 h. The volatiles were removed under reduced pressure and the residue was dissolved in PhMe and then H₂O was added (2:1). The mixture was stirred by 50 °C for 1 h. The organic phase was separated and washed with H₂O (4 x 150 mL). The organic phase was washed with brine solution (2 x 100 mL), dried (MgSO₄) and evaporated under reduced pressure. Column chromatography (SiO₂, Hep/EtOAc 7:1 v/v) gave the title compound **47** (3.30 g, 7.81 mmol, **85%**) as a yellow solid.

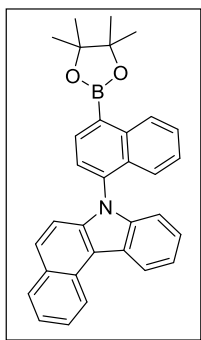
R_f(Heptane/EtOAc 9:1) = 0.35.

¹H NMR (500 MHz, CD₂Cl₂) δ 8.90 (d, *J* = 8.3 Hz, 1H), 8.70 (d, *J* = 8.1 Hz, 1H), 8.44 (d, *J* = 8.6 Hz, 1H), 8.06 (d, *J* = 7.8 Hz, 1H), 8.02 (d, *J* = 8.0 Hz, 1H), 7.82 – 7.76 (m, 2H), 7.72 – 7.65 (m, 1H), 7.59 (d, *J* = 7.8 Hz, 1H), 7.57 – 7.50 (m, 1H), 7.50 – 7.42 (m, 1H), 7.41 – 7.34 (m, 2H), 7.21 – 7.09 (m, 3H) ppm.

¹³C NMR (126 MHz, CD₂Cl₂) δ 140.11, 134.03, 133.58, 132.66, 130.42, 130.14, 129.87, 129.71, 129.65, 129.60, 128.73, 128.65, 128.35, 128.20, 127.98, 127.89, 127.49, 127.42, 127.40, 124.98, 124.19, 124.12, 123.64, 122.36, 121.15, 112.15 ppm.

HRMS (EI-MS): Calcd for C₂₆H₁₆BrN [M] 421.05, found 421.05.

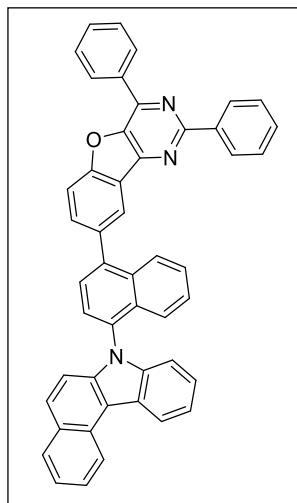
7-(4,4,5,5-tetramethyl-1,3,2-dioxaborolan-2-yl)-7H-benzo[c]carbazole (48)



Under an argon atmosphere a 250 mL 4 neck bottle flask was charged with **47** (0.42 g, 0.99 mmol, 1.00 eq.), **B₂Pin₂** (0.27 g, 1.04 mmol, 1.05 eq.) and KOAc (0.49 g, 4.97 mmol, 5.00 eq.). Anhydrous 1,4-dioxan was added to the mixture and degassed for 30 Min. Catalyst **Pd(dppf)₂Cl₂** (0.04 g, 0.05 mmol, 0.05 eq.) were added to the reaction mixture and refluxed at 101 °C for 25 h. The reaction mixture was cooled to room temperature and volatiles were removed under reduced pressure. The crude was dissolved in EtOAc (30 mL). The organic phase was washed with H₂O (100 mL) and the aqueous phase was extracted with EtOAc (3 x 50 mL). The combined organic phases were washed with brine solution and dried (MgSO₄). **48** is not stable and was used immediately in the next reaction without further purification.

$R_f(\text{Heptane/EtOAc } 9:1) = 0.37$.

¹H NMR (500 MHz, CD₂Cl₂) δ 8.95 (d, J = 8.6 Hz, 1H), 8.90 (d, J = 7.3 Hz, 1H), 8.29 (d, J = 7.2 Hz, 1H), 7.71 (d, J = 7.2 Hz, 1H), 7.63 – 7.49 (m, 5H), 7.40 – 7.34 (m, 1H), 7.33 – 7.26 (m, 1H), 7.20 – 7.08 (m, 4H), 1.49 (s, 12H) ppm.

12-(4-{7H-benzo[c]carbazol-7-yl}naphthalen-1-yl)-4,6-diphenyl-8-oxa-3,5-diazatricyclo[7.4.0.0^{2,7}]trideca-1(9),2,4,6,10,12-hexaene (1)

Under an argon atmosphere a 250 mL 4 neck bottle flask was charged with Bromide **37** (3.82 g, 9.52 mmol, 1.00 eq.), boronic ester **48** (6.70 g, 14.28 mmol, 1.50 eq.) dissolved in anhydrous THF and CsF (2.89 g, 19.04 mmol, 2.00 eq.) dissolved in H₂O (20 mL). The two-phasic solution was degassed for 30 Min. Catalyst **PdCl₂[P(cy)₃]₂** (0.21 g, 0.29 mmol, 0.03 eq.) were added to the reaction mixture and refluxed at 70 °C for 19 h. A white precipitate was formed. The white precipitate was filtered and recrystallized several times with anhydrous 1,4-dioxane. The title compound was purified by an endcapping reaction and hot extraction with *o*-xylene (200 mL). Subsequently, the product was further purified by sublimation *in vacuo* (1.4 x 10⁻⁵ mbar, 352 °C). 4.81 g (7.25 mmol, **76%**) of **1** was obtained as a colorless solid.

R_f(Heptane/NMP/THF 9:1:4) = 0.29.

¹H NMR (700 MHz, CD₂Cl₂) δ 8.93 (d, J = 8.2 Hz, 1H), 8.84 (d, J = 7.2 Hz, 1H), 8.74 (dd, J = 14.3, 7.6 Hz, 3H), 8.65 (d, J = 1.8 Hz, 1H), 8.13 (d, J = 8.6 Hz, 1H), 8.07 – 8.02 (m, 2H), 8.00 (d, J = 8.3 Hz, 1H), 7.87 – 7.78 (m, 4H), 7.74 – 7.64 (m, 3H), 7.59 – 7.51 (m, 5H), 7.51 – 7.43 (m, 2H), 7.36 (dd, J = 8.5, 7.1 Hz, 1H), 7.33 (d, J = 8.7 Hz, 1H), 7.28 – 7.23 (m, 2H) ppm.

¹³C NMR (176 MHz, NMP-d₉) δ 159.6, 158.3, 152.2, 147.1, 145.0, 141.5, 140.7, 139.9, 138.0, 136.8, 134.8, 134.4, 133.5, 133.1, 132.0, 131.6, 130.7, 129.9, 129.8, 129.6, 129.5, 129.3, 129.0, 128.3, 128.1, 127.9, 126.8, 125.1, 123.7, 123.6, 123.4, 122.4, 122.3, 121.1, 115.3, 113.9, 112.0, 110.7 ppm.

HRMS (LC-APCI-MS): Calcd for C₄₈H₃₀N₃O [M+H⁺] 664.2378, found 664.2387.

HPLC RP-18, ACN/THF 90:10, t_R = 17.5 Min, purity: **99.98%**

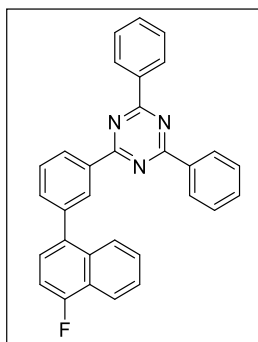
AQF [ppm]: F < 28, Cl < 5.2, Br < 14.6, S < 2

ICP-MS [ppm]: Cu < 0.04, B < 4.9, P < 1.2, Cl < 17, Br < 22.9, Pd < 0.01, I < 0.08.

DSC $T_m = 361\text{ }^\circ\text{C}$, $T_g = 177\text{ }^\circ\text{C}$

TGA 5% weight loss at $300\text{ }^\circ\text{C}$

2-[3-(4-fluoronaphthalen-1-yl)phenyl]-4,6-diphenyl-1,3,5-triazine (54)



Under an argon atmosphere a 500 mL 3 neck bottled flask was charged with bromide **46** (6.00 g, 26.66 mmol, 1.00 eq.), boronic ester **52** (11.61 g, 26.66 mmol, 1.00 eq.) and $\text{K}_3\text{PO}_4 \cdot \text{H}_2\text{O}$ (18.42 g 79.98 mmol). The reaction mixture was dissolved in anhydrous DMF (150 mL) and degassed for 30 Min. Afterwards $\text{Pd}(\text{PPh}_3)_4$ was added to the mixture and heated to $150\text{ }^\circ\text{C}$ for 24 h. The reaction was controlled *via* TLC. Upon cooling to room temperature, a grey precipitate was formed, filtered, and washed with DMF (2 X 50 mL) and H_2O (4 X 50 mL). The grey precipitate turned colourless after washing with DMF and was dried in a vacuum cabinet at $60\text{ }^\circ\text{C}$ for 10 h. **54** (11.90 g, 26.24 mmol, **98%**) was obtained as a colourless solid.

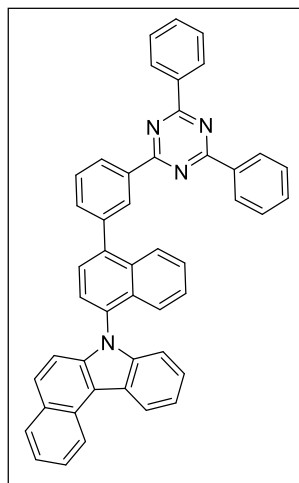
R_f (Heptane/EtOAc 9:1) = 0.31.

^1H NMR (500 MHz, CD_2Cl_2) δ 8.91 – 8.85 (m, $J = 1.66\text{ Hz}$, 2H), 8.80 – 8.75 (m, 4H), 8.23 (dd, $J = 8.41, 1.29\text{ Hz}$, 1H), 7.95 (ddt, $J = 8.59, 2.01, 0.90\text{ Hz}$, 1H), 7.76 – 7.72 (m, 2H), 7.66 – 7.48 (m, 9H), 7.30 (dd, $J = 10.48, 7.81\text{ Hz}$, 1H) ppm.

^{13}C NMR (126 MHz, CD_2Cl_2) δ 172.3, 172.2, 160.0, 158.0, 141.2, 137.1, 136.7, 136.5, 136.5, 134.9, 133.6, 133.6, 133.2, 131.0, 129.5, 129.3, 129.2, 128.5, 127.8, 127.5, 127.4, 126.9, 126.9, 126.5, 126.5, 124.4, 124.3, 121.2, 121.2, 109.6, 109.5 ppm.

^{19}F NMR (471 MHz, CD_2Cl_2) δ -124.31 ppm.

HRMS (TOF EI-MS): Calcd for $\text{C}_{31}\text{H}_{20}\text{FN}_3$ [M] 453.16, found 453.15.

2-[3-(4-{7H-benzo[c]carbazol-7-yl)naphthalen-1-yl}phenyl]-4,6-diphenyl-1,3,5-triazine (3)

Under an argon atmosphere a 50 mL round bottom flask was charged with **47** (0.22 g, 0.53 mmol, 1.00 eq.), boronic ester **52** (0.24 g, 0.89 mmol, 1.05 eq.) and CsF (0.24 g, 1.58 mmol, 3.00 eq.) dissolved in H₂O (5 mL). Anhydrous THF (20 mL) was added to the mixture and the two-phasic solution was saturated with argon for 30 Min. Catalyst **PdCl₂[P(cy)₃]₂** (0.01 g, 0.02 mmol, 0.03 eq.) were added to the reaction mixture and refluxed at 70 °C for 28 h. The solution was cooled to room temperature and the solvent was evaporated under reduced pressure. The crude was dissolved in CH₂Cl₂ (50 mL) and H₂O (20 mL) was added. The aqueous phase was separated and washed with CH₂Cl₂ (4 x 25 mL). Purification by column chromatography (SiO₂, Hep/EtOAc 95:5 v/v) gave **3** (0.19 g, 0.29 mmol, **56%**) as a colorless solid.

$R_f(\text{Heptane}/\text{CH}_2\text{Cl}_2\ 5:1) = 0.27$.

¹H NMR (500 MHz, CD₂Cl₂) δ 9.06 (t, J = 1.8 Hz, 1H), 8.95 (dd, J = 12.7, 8.0 Hz, 2H), 8.84 – 8.81 (m, 4H), 8.74 (d, J = 7.9 Hz, 1H), 8.13 (d, J = 8.6 Hz, 1H), 8.05 (d, J = 8.4, 1.4 Hz, 1H), 7.93 (dt, J = 7.5, 1.6 Hz, 1H), 7.87 – 7.80 (m, 5H), 7.68 – 7.57 (m, 7H), 7.58 – 7.41 (m, 5H), 7.26 (dd, J = 16.5, 8.0 Hz, 2H) ppm.

¹³C NMR (126 MHz, CD₂Cl₂) δ 172.4, 172.2, 142.0, 141.8, 141.3, 140.6, 138.5, 137.3, 136.8, 134.8, 134.0, 133.7, 133.2, 132.1, 131.0, 130.5, 130.1, 129.8, 129.5, 129.5, 129.5, 129.3, 128.9, 128.7, 128.0, 127.8, 127.7, 127.6, 127.4, 127.3, 125.8, 125.2, 124.3, 124.1, 123.9, 123.8, 122.6, 121.3, 115.9, 112.7, 111.4 ppm.

HRMS (LC-APCI-MS): Calcd for C₄₇H₃₁N₄ [M+H⁺] 651.2543, found 651.2545.

HPLC RP-18, ACN/THF 80:20, t_R = 10.7 Min, purity: **99.99%**

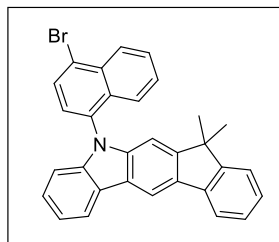
AQF [ppm]: F < 2.0, Cl < 3.0, Br < 0.5, S < 2.0

ICP-MS [ppm]: B < 4.0, P < 0.6, Cl < 32.0, Cu < 0.008, Br < 0.07, Pd < 0.003, I < 0.02.

DSC T_m = not available, T_g = 153 °C

TGA 5% weight loss at 448 °C

5-(4-bromonaphthalen-1-yl)-7,7-dimethyl-5H,7H-indeno[2,1-b]carbazole (56)



A 500 mL 4 neck round bottom flask was charged with **55** (12.00 g, 42.35 mmol, 1.00 eq.), fluoride **46** (9.53 g, 42.35 mmol, 1.00 eq.) and K_3PO_4 (26.97 g, 127.04 mmol, 3.00 eq.) and suspended in anhydrous DMAC (250 mL). The reaction mixture was refluxed at 165 °C for 5 h. The base was removed by filtration. The solvent was removed under reduced pressure and the residue was suspended in hot ethanol. A beige solid was obtained and washed several times with ethanol and dried in a vacuum dry oven at 80 °C overnight. **56** (18.21 g, 37.28 mmol, **88%**) was obtained as a beige solid. The product was used without further purification for the next reaction.

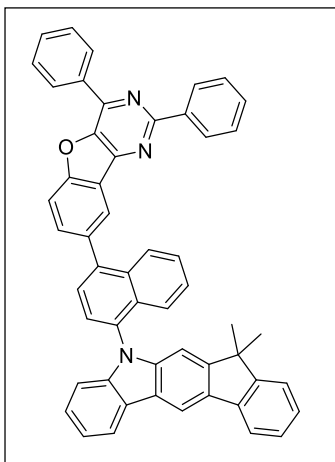
R_f (Heptane/ CH_2Cl_2 5:1) = 0.28.

1H NMR (500 MHz, CD_2Cl_2) δ 8.54 (d, J = 0.87 Hz, 1H), 8.47 – 8.42 (m, 1H), 8.31 – 8.25 (m, 1H), 8.06 (d, J = 7.75 Hz, 1H), 7.89 (dt, J = 7.52, 0.92 Hz, 1H), 7.70 (ddd, J = 8.31, 6.67, 1.26 Hz, 1H), 7.59 (d, J = 7.77 Hz, 1H), 7.44 – 7.26 (m, 7H), 7.04 (s, 1H), 6.98 – 6.94 (m, 1H), 1.43 (s, 3H), 1.37 (s, 3H) ppm.

^{13}C NMR ^{13}C NMR (126 MHz, CD_2Cl_2) δ 154.0, 143.1, 140.1, 134.7, 133.9, 133.0, 132.6, 130.8, 128.8, 128.4, 128.4, 128.0, 127.6, 126.9, 126.3, 124.6, 124.0, 124.0, 123.4, 123.1, 120.7, 120.6, 119.8, 111.8, 110.6, 104.9, 47.2, 28.2, 28.1 ppm.

HRMS (TOF-EI-MS): Calcd for $C_{31}H_{22}BrN$ [M] 488.22, found 488.21.

12-(4-{7,7-dimethyl-5H,7H-indeno[2,1-b]carbazol-5-yl}naphthalen-1-yl)-4,6-diphenyl-8-oxa-3,5-diazatricyclo[7.4.0.0^{2,7}]trideca-1(9),2,4,6,10,12-hexaene (14)



A 500 mL 4 neck round bottom flask was charged with bromide **56** (8.00 g, 16.38 mmol, 1.00 eq.), boronic ester **57** (7.34 g, 16.38 mmol, 1.00 eq.) and $K_3PO_4 \cdot H_2O$ (7.54 g, 32.76 mmol, 2.00 eq.). The reaction mixture was suspended in anhydrous DMF (250 mL) and saturated with argon for 30 Min. Catalyst $Pd(PPh_3)_4$ (0.95 g, 0.82 mmol, 0.05 eq.) were added to the reaction mixture and refluxed at 100 °C for 24 h. The mixture was cooled to room temperature and the solvent was evaporated *in vacuo*. The crude was dissolved in THF/EtOAc (1:2, 250 mL) and washed with brine solution (4 X 100 mL). The organic phase was dried ($MgSO_4$) and evaporated *in vacuo*. Recrystallization in heptan/toluene (1:1) gave **14** (8.57 g, 11.65 mmol, **57%**) as a colourless solid.

R_f (Heptane/ CH_2Cl_2 5:1) = 0.22.

1H NMR (500 MHz, $CDCl_3$) δ 8.98 – 8.92 (m, 2H), 8.90 – 8.84 (m, 2H), 8.80 (d, J = 1.81 Hz, 1H), 8.67 (s, 1H), 8.45 – 8.41 (m, 1H), 8.26 (d, J = 8.61 Hz, 1H), 8.14 (dd, J = 8.46, 1.86 Hz, 1H), 8.05 (dd, J = 10.56, 8.01 Hz, 2H), 7.91 (q, J = 7.36 Hz, 2H), 7.85 – 7.80 (m, 3H), 7.78 – 7.74 (m, 1H), 7.72 – 7.60 (m, 5H), 7.58 – 7.36 (m, 6H), 7.23 (dd, J = 7.16, 1.43 Hz, 1H), 1.63 (s, 3H), 1.57 (s, 3H) ppm.

^{13}C NMR (126 MHz, CD_2Cl_2) δ 160.2, 158.6, 154.0, 153.9, 152.7, 147.6, 145.5, 143.3, 141.0, 140.3, 138.8, 137.2, 135.1, 134.5, 134.4, 133.9, 132.8, 131.9, 131.8, 129.8, 129.1, 128.8, 128.3, 127.7, 127.5, 127.3, 127.1, 126.9, 126.3, 125.8, 124.4, 124.2, 124.0, 123.4, 123.1, 123.1, 120.7, 120.5, 119.8, 113.4, 111.8, 110.8, 105.1, 47.3, 28.3, 28.2 ppm.

HRMS (LC-APCI-MS): Calcd for $C_{53}H_{36}N_3O$ [$M+H^+$] 730.2853, found 730.2860.

HPLC RP-18, ACN/THF 90:10, t_R = 19.8 Min, purity: **99.92%**

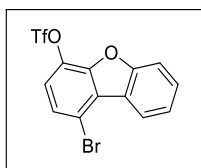
AQF [ppm]: F < 2.0, Cl < 3.0, Br < 0.5, S < 3.0

ICP-MS [ppm]: B < 4.9, P < 1.2, Cl < 29.3, Cu < 0.02, Br < 0.08, Pd < 0.0045, I < 0.013.

DSC T_m = not available, T_g = 197 °C

TGA 5% weight loss at 472 °C

3-bromo-8-oxatricyclo[7.4.0.0^{2,7}]trideca-1(13),2(7),3,5,9,11-hexaen-6-yl trifluoromethanesulfonate (59)



Phenol **58** (5.00 g, 18.82 mmol, 1.00 eq.) was dissolved in anhydrous DCM at room temperature. Et₃N (7.87 mL, 56.46 mmol, 3.00 eq.) was added dropwise and the colourless solution was cooled down to 0 °C with a cooling bath. Tf₂O (3.95 mL, 23.52 mmol, 1.25 eq.) was added dropwise to the reaction solution. Subsequently, the solution was allowed to warm up to room temperature and stirred for 20 h. The reaction mixture was acidified with 1M HCl (200 mL) and extracted with DCM (3 x 100 mL). The combined organic layers were washed with brine solution and dried (MgSO₄). The residual solvent was evaporated under reduced pressure to give the desired compound as a brown oil. **59** (7.00 g, 17.17 mmol, **94%**) was obtained as a brown oil and used without any further purification.

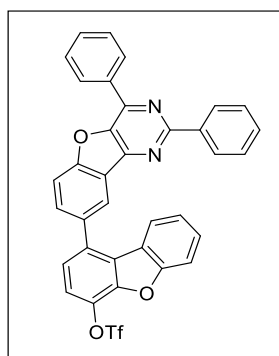
R_f(Heptane/EtOAc 9:1) = 0.19.

¹H NMR (500 MHz, DMSO-d₆) δ 8.47 (d, J = 7.85 Hz, 1H), 7.90 (d, J = 8.36 Hz, 1H), 7.80 – 7.68 (m, 3H), 7.59 (t, J = 7.61 Hz, 1H) ppm.

¹³C NMR (126 MHz, DMSO-d₆) δ 155.8, 146.2, 132.7, 129.7, 127.8, 126.1, 124.4, 122.2, 122.1, 121.6 ppm.

¹⁹F NMR (471 MHz, DMSO-d₆) δ -72.88 ppm.

HRMS (EI-MS): Calcd for C₁₃H₆BrF₃O₄S [M] 395.15, found 395.18.

3-{4,6-diphenyl-8-oxa-3,5-diazatricyclo[7.4.0.0^{2,7}]trideca-1(13),2,4,6,9,11-hexaen-12-yl}-8-oxatricyclo[7.4.0.0^{2,7}]trideca-1(13),2,4,6,9,11-hexaen-6-yl trifluoromethanesulfonate (60)

A 50 mL 4 neck round bottom flask was charged with **59** (4.40 g, 11.14 mmol, 1.00 eq.), boronic ester **57** (4.99 g, 11.14 mmol, 1.00 eq.) and K_2CO_3 (2.00 g, 22.27 mmol, 2.00 eq.). The reaction mixture was suspended in toluene/ H_2O (4:1) (150 mL) and saturated with argon for 30 Min. Precatalyst $Pd_2(dba)_3$ (0.01 g, 0.01 mmol, 0.01 eq.) and ligand **P(o-tol)** (0.01 g, 0.01 mmol, 0.02 eq.) were added to the reaction mixture and heated up to 70 °C for 24 h. The mixture was cooled to room temperature and the solvent was evaporated *in vacuo*. The crude was redissolved in CH_2Cl_2 (150 mL) and H_2O (100 mL) was added. The aqueous phase was separated and washed with CH_2Cl_2 (4 x 50 mL). Purification by column chromatography (SiO_2 , Hep/EtOAc 9:1 v/v) gave **60** (1.78 g, 2.80 mmol, **25%**) as a colorless solid.

R_f (Heptane/ CH_2Cl_2 5:1) = 0.22

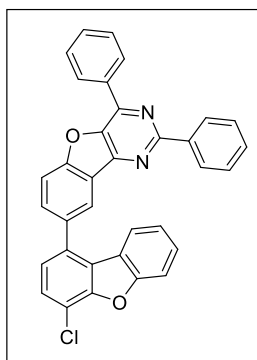
1H NMR (500 MHz, CD_2Cl_2) δ 8.81 – 8.79 (m, 2H), 8.71 – 8.68 (m, 2H), 8.57 (d, J = 1.81 Hz, 1H), 8.00 – 7.93 (m, 2H), 7.71 – 7.64 (m, 4H), 7.55 – 7.48 (m, 6H), 7.42 (d, J = 8.33 Hz, 1H), 7.21 – 7.16 (m, 1H) ppm.

^{13}C NMR (126 MHz, CD_2Cl_2) δ 160.3, 158.8, 157.4, 152.5, 147.7, 147.4, 145.5, 138.7, 137.7, 135.3, 135.0, 134.1, 133.1, 131.9, 130.7, 129.8, 129.5, 129.1, 128.8, 126.1, 125.5, 124.1, 123.6, 123.4, 123.2, 122.9, 120.7, 120.3, 118.2, 113.8, 112.7 ppm.

^{19}F NMR (471 MHz, CD_2Cl_2) δ -73.32 ppm.

HRMS (EI-MS): Calcd for $C_{35}H_{19}F_3N_2O_5S$ [M] 636.60, found 637.10.

12-{6-chloro-8-oxatricyclo[7.4.0.0^{2,7}]trideca-1(13),2(7),3,5,9,11-hexaen-3-yl}-4,6-diphenyl-8-oxa-3,5-diazatricyclo[7.4.0.0^{2,7}]trideca-1(9),2,4,6,10,12-hexaene (63)



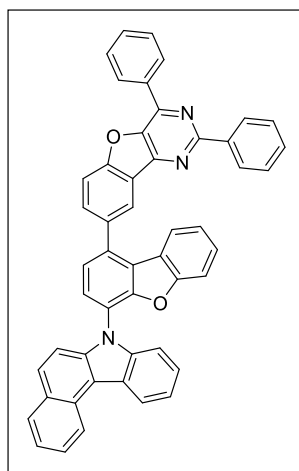
A 250 mL 4 neck round bottom flask was charged with bromide **61** (3.0 g, 11.19 mmol, 1.00 eq.), boronic ester **57** (5.02 g, 11.19 mmol, 1.05 eq.) and $K_3PO_4 \cdot H_2O$ (4.19 g, 21.31 mmol, 2.00 eq.). The reaction mixture was suspended in DMF (100 mL) and saturated with argon for 30 Minutes. $Pd(PPh_3)_4$ (0.62 g, 0.53 mmol, 0.05 eq.) was added to the reaction mixture and heated to 100 °C for 24 h. Upon cooling of the mixture to room temperature a colourless precipitate was formed and filtered. The precipitate was washed several times with H_2O (4 x 30 mL). Recrystallization in toluene gave **63** as a beige compound (4.50 g, 8.60 mmol, **81%**). **63** was dried at 100 °C in a vacuum drying oven for 24 h.

R_f (Heptane/ EtOAc 5:1) = 0.35.

¹H NMR (500 MHz, CD_2Cl_2) δ 8.81 (dd, $J = 7.31, 1.69$ Hz, 2H), 8.73 – 8.69 (m, 2H), 8.57 (d, $J = 1.85$ Hz, 1H), 8.01 – 7.93 (m, 2H), 7.73 – 7.64 (m, 4H), 7.60 (d, $J = 8.06$ Hz, 1H), 7.57 – 7.46 (m, 5H), 7.36 (d, $J = 8.04$ Hz, 1H), 7.15 (t, $J = 7.61$ Hz, 1H) ppm.

¹³C NMR (126 MHz, CD_2Cl_2) δ 160.3, 158.7, 157.0, 152.6, 147.7, 145.5, 138.7, 136.1, 135.9, 135.0, 133.3, 131.9, 130.7, 129.8, 129.5, 129.1, 128.8, 128.5, 127.7, 125.8, 124.2, 124.2, 123.6, 123.3, 123.1, 122.9, 117.0, 113.6, 112.6 ppm.

HRMS (EI-MS): Calcd for $C_{34}H_{19}N_2O_2Cl$ [M] 522.11, found 522.1088.

12-(6-(7H-benzo[c]carbazol-7-yl)-8-oxatricyclo[7.4.0.0^{2,7}]trideca-1(13),2(7),3,5,9,11-hexaen-3-yl)-4,6-diphenyl-8-oxa-3,5-diazatricyclo[7.4.0.0^{2,7}]trideca-1(9),2,4,6,10,12-hexaene (7)

A 50 mL 4 neck round bottom flask was charged with **25** (0.10g, 0.46 mmol, 1.00 eq.), chloride **63** (0.25 g, 0.48 mmol, 1.05 eq.) and NaO^tBu (0.09 g, 0.92 mmol, 2.00 eq.). The reaction mixture was suspended in anhydrous *o*-xylene (20 mL) and saturated with argon for 30 Min. Catalyst **XPhos Pd G3** (19.5 mg, 0.02 mmol, 0.05 eq.) were added to the reaction mixture and refluxed at 142 °C for 48 h. The mixture was cooled to room temperature and the formed grey precipitate was filtered. The grey precipitate was washed several times with PhMe (2 X 10 mL). Recrystallization in PhMe gave **7** (0.17 g, 0.23 mmol, **51%**) as a grey solid.

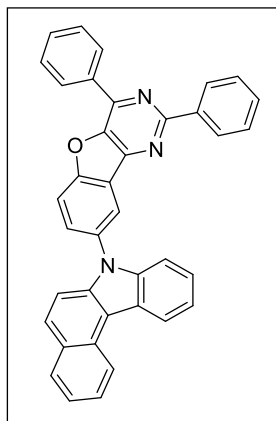
$R_f(\text{Heptane}/ \text{CH}_2\text{Cl}_2 \text{ 9:1}) = 0.21$

¹H NMR (500 MHz, CD₂Cl₂) δ 8.93 (d, J = 8.33 Hz, 1H), 8.87 – 8.83 (m, 2H), 8.78 – 8.71 (m, 4H), 8.18 (dd, J = 8.53, 1.87 Hz, 1H), 8.05 (dd, J = 15.01, 8.21 Hz, 2H), 7.91 (d, J = 8.91 Hz, 1H), 7.85 (d, J = 7.87 Hz, 1H), 7.80 (ddd, J = 8.44, 6.93, 1.33 Hz, 1H), 7.73 – 7.66 (m, 4H), 7.58 – 7.48 (m, 8H), 7.18 (ddd, J = 8.15, 6.86, 1.32 Hz, 1H), 7.13 – 7.05 (m, 3H) ppm.

¹³C NMR (126 MHz, CD₂Cl₂) δ 160.3, 158.9, 157.1, 152.7, 152.5, 147.7, 145.6, 140.8, 139.4, 138.8, 137.6, 136.2, 135.1, 133.4, 131.9, 130.7, 130.4, 130.2, 130.0, 129.8, 129.8, 129.5, 129.1, 128.9, 128.5, 128.1, 127.7, 127.4, 126.2, 126.0, 125.4, 125.2, 125.0, 124.7, 124.2, 123.9, 123.9, 123.6, 123.4, 123.3, 122.8, 122.6, 121.6, 116.3, 113.8, 112.6, 111.4 ppm.

HRMS (EI-MS): Calcd. for C₅₀H₂₉N₃O₂ [M] 703.23, found 703.40.

12-{7H-benzo[c]carbazol-7-yl}-4,6-diphenyl-8-oxa-3,5-diazatricyclo[7.4.0.0^{2,7}]trideca-1(9),2,4,6,10,12-hexaene (2)



A 250 mL 4 neck round bottom flask was charged with **25** (6.50 g, 29.92 mmol, 1.00 eq.), NaO^tBu (5.31 g, 55.23 mmol, 2.00 eq.) and bromide **37** (13.20 g, 32.91 mmol, 1.10 eq.). The reaction mixture was suspended in anhydrous *p*-Xylene (150 mL) and degassed for 30 Min. Then, Pd(P^tBu₃)₂ (0.76 g, 1.50 mmol, 0.05 eq.) was added to the reaction mixture and refluxed at 139 °C for 24 h. The reaction mixture was cooled to room temperature and a grey precipitate was obtained. The grey solid was washed several times with toluene and dried at 100 °C in a vacuum dry oven. Recrystallization in toluene gave **2** as a colourless solid (16.00 g, 24.18 mmol, **98%**).

R_f(Heptane/ EtOAc 9:1) = 0.28.

¹H NMR (500 MHz, CD₂Cl₂) δ 8.86 (d, J = 8.34 Hz, 1H), 8.82 – 8.76 (m, 2H), 8.71 – 8.63 (m, 3H), 8.57 (d, J = 2.06 Hz, 1H), 8.01 (dd, J = 19.50, 8.35 Hz, 2H), 7.94 – 7.85 (m, 2H), 7.77 (ddd, J = 8.25, 6.74, 1.33 Hz, 1H), 7.72 – 7.59 (m, 4H), 7.57 – 7.43 (m, 7H) ppm.

¹³C NMR 13C NMR (126 MHz, CD₂Cl₂) δ 160.3, 157.8, 152.1, 147.9, 145.8, 141.1, 139.5, 138.5, 134.9, 134.2, 132.0, 131.9, 130.8, 130.3, 130.1, 129.8, 129.8, 129.5, 129.1, 128.8, 128.1, 127.7, 125.2, 124.4, 124.2, 123.9, 123.8, 122.6, 122.3, 121.5, 116.0, 114.9, 112.0, 110.8 ppm.

HRMS (LC-APCI-MS): Calcd for C₃₈H₂₄N₃O [M+H⁺] 538.1908, found 538.1913.

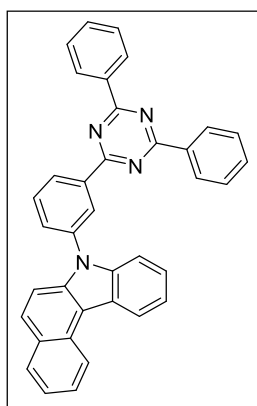
HPLC RP-18, MeOH/THF 90:10, t_R = 16.5 Min, purity: **99.96%**

AQF [ppm]: F < 1.0, Cl < 1.5, Br < 1.0, S < 1.0

ICP-MS [ppm]: B < 6.0, P < 0.6, Cl < 74.7.0, Br < 0.1, Pd < 0.005, I < 0.09.

DSC T_m = not detectable, T_g = 137 °C

TGA 5% weight loss at 417 °C

2-(3-(7H-benzo[c]carbazol-7-yl)phenyl)-4,6-diphenyl-1,3,5-triazine (4)

A 50 mL 4 neck round bottom flask was charged with **25** (6.50 g, 29.92 mmol, 1.00 eq.), NaO^tBu (0.18 g, 1.84 mmol, 2.00 eq.) and bromide **49** (12.20 g, 31.41 mmol, 1.05 eq.). The reaction mixture was suspended in anhydrous toluene (125 mL) and degassed for 30 Min. Afterwards, Pd(P^tBu₃)₂ (0.76 g, 1.50 mmol, 0.05 eq.) was added to the reaction mixture and refluxed at 110 °C for 24 h. The reaction mixture was cooled to room temperature and the yellow precipitate was filtered and washed several times with toluene. Recrystallization in toluene gave **4** as a pure yellow solid (15.43 g, 29.41 mmol, **98%**). **4** was dried at 100 °C in a vacuum dry oven.

R_f(Heptane/ EtOAc 9:1) = 0.21.

¹H NMR (500 MHz, CD₂Cl₂) δ 9.04 – 8.97 (m, 2H), 8.90 (d, J = 8.26 Hz, 1H), 8.79 – 8.75 (m, 4H), 8.71 – 8.68 (m, 1H), 8.06 (d, J = 7.92 Hz, 1H), 7.94 – 7.86 (m, 3H), 7.79 (ddd, J = 8.31, 6.92, 1.33 Hz, 1H), 7.67 (d, J = 8.95 Hz, 1H), 7.66 – 7.50 (m, 8H), 7.52 – 7.46 (m, 2H) ppm.

¹³C NMR (126 MHz, CD₂Cl₂) δ 172.5, 171.5, 136.6, 133.3, 132.4, 131.0, 129.8, 129.5, 129.3, 129.0, 128.8, 128.1, 127.7, 125.3, 123.9, 122.6, 121.4, 112.3, 111.0 ppm.

HRMS (LC-APCI-MS): Calcd for C₃₇H₂₅N₄ [M+H⁺] 525.2068, found 525.2077.

HPLC RP-18, MeOH/THF 85:15, t_R = 13.9 Min, purity: **99.99%**

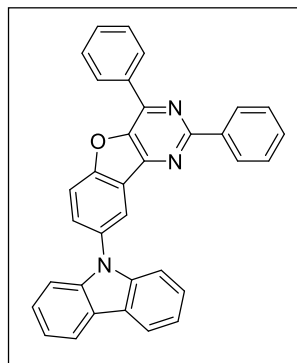
AQF [ppm]: F < 3.0, Cl < 3.0, Br < 0.5, S < 5.0

ICP-MS [ppm]: B < 3.1, P < 1.3, Cl < 9.7, Cu < 0.04, Br < 0.09, Pd < 0.004, I < 0.01.

DSC T_m = 260 °C, T_g = 104 °C

TGA 5% weight loss at 415 °C

12-(9H-carbazol-9-yl)-4,6-diphenyl-8-oxa-3,5-diazatricyclo[7.4.0.0^{2,7}]trideca-1(9),2,4,6,10,12-hexaene (12)



A 500 mL 4 neck round bottom flask was charged with carbazole **64** (6.50 g, 38.87 mmol, 1.00 eq.), NaO^tBu (7.47 g, 77.75 mmol, 2.00 eq.) and bromide **37** (17.16 g, 42.76 mmol, 1.10 eq.). The reaction mixture was suspended in anhydrous *p*-xylene (250 mL) and degassed for 30 Min. Afterwards, Pd(P^tBu₃)₂ (0.99 g, 1.94 mmol, 0.05 eq.) was added to the reaction mixture and stirred under reflux for 24 h. The reaction mixture was cooled to room temperature and a dark precipitate was obtained. The dark solid was washed with PhMe (4 X 150 mL) and recrystallization in toluene gave **12** as a colourless solid (18.40 g, 37.74 mmol, **97%**). **12** was dried at 100 °C for 8 h in a vacuum dry oven.

R_f(Heptane/ EtOAc 9:1) = 0.24.

¹H NMR (500 MHz, CD₂Cl₂) δ 8.84 – 8.76 (m, 2H), 8.74 – 8.67 (m, 2H), 8.54 (d, *J* = 2.14 Hz, 1H), 8.20 (d, *J* = 7.82 Hz, 2H), 7.98 (d, *J* = 8.67 Hz, 1H), 7.91 (dd, *J* = 8.69, 2.23 Hz, 1H), 7.74 – 7.61 (m, 3H), 7.59 – 7.40 (m, 7H), 7.34 (ddd, *J* = 7.92, 5.94, 2.08 Hz, 2H) ppm.

¹³C NMR (126 MHz, CD₂Cl₂) δ 160.3, 157.5, 152.2, 147.9, 145.8, 141.8, 138.6, 134.9, 134.6, 131.9, 131.4, 130.7, 129.8, 129.5, 129.1, 128.8, 126.7, 124.2, 124.0, 121.6, 120.9, 120.7, 114.9, 110.2 ppm.

HRMS (LC-APCI-MS): Calcd for C₃₄H₂₂N₃O [M+H⁺] 487.1757, found 487.1745.

HPLC RP-18, MeOH/THF 90:10, t_R = 12.5 Min, purity: **99.68%**

AQF [ppm]: F < 2.0, Cl < 3.0, Br < 0.5, S < 2.0

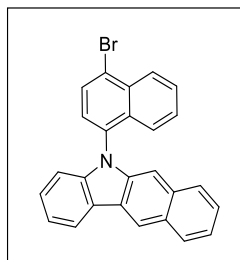
ICP-MS [ppm]: B < 0.17, P < 1.1, Cl < 5.7, Cu < 0.006, Br < 0.14, Pd < 0.003, I < 0.05.

DSC T_m = 236 °C, T_g = 114 °C

TGA 5% weight loss at 379 °C

7.2.3 Synthesis of red TMM's (compounds of chapter 3.3.2)

5-(4-bromonaphthalen-1-yl)-5H-benzo[b]carbazole (**66**)



Under an argon atmosphere a 500 mL 3 neck bottled flask was charged with carbazole **18** (10.00 g, 46.03 mmol, 1.00 eq.), fluoride **46** (11.39 g, 50.63 mmol, 1.10 eq.) and CsCO₃ (29.99 g, 92.05 mmol, 2.00 eq.) and dissolved in anhydrous DMF (250 mL). The reaction mixture was heated up to 135 °C for 7 h. The volatiles were removed under reduced pressure and the residue was dissolved in PhMe and then H₂O was added (2:1, 600 mL). The mixture was stirred by 50 °C for 1 h. The organic phase was separated and washed with H₂O (4 x 300 mL). The organic phase was washed with brine solution (2 x 300 mL), dried (MgSO₄) and evaporated under reduced pressure. Column chromatography (SiO₂, Hep/EtOAc 7:1 v/v) gave the title compound **66** (14.34 g, 33.96 mmol, **74%**) as a yellow solid.

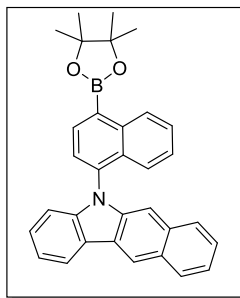
R_f(Heptane/EtOAc 9:1) = 0.33.

¹H NMR (500 MHz, CD₂Cl₂) δ 8.71 (s, 1H), 8.46 (d, J = 8.6 Hz, 1H), 8.36 (d, J = 7.7 Hz, 1H), 8.14 – 8.04 (m, 2H), 7.75 – 7.66 (m, 2H), 7.60 (d, J = 7.8 Hz, 1H), 7.45 – 7.30 (m, 7H), 6.97 (d, J = 8.1 Hz, 1H) ppm.

¹³C NMR (126 MHz, CD₂Cl₂) δ 145.12, 142.59, 134.81, 133.99, 133.29, 132.66, 130.87, 129.26, 128.96, 128.94, 128.83, 128.50, 128.41, 128.12, 128.10, 127.62, 125.90, 125.85, 124.52, 124.09, 123.67, 121.60, 120.64, 119.28, 110.21, 105.40, 54.43, 54.22, 54.00, 53.78, 53.57.ppm.

HRMS (EI-MS): Calcd for C₂₆H₁₆BrN [M] 421.05, found 421.05

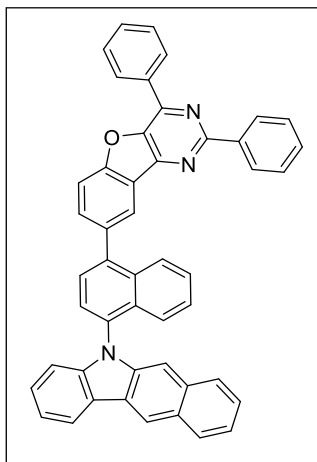
5-[4-(4,4,5,5-tetramethyl-1,3,2-dioxaborolan-2-yl)naphthalen-1-yl]-5H-benzo[b]carbazole (67)



Under an argon atmosphere a 100 mL 4 neck bottle flask was charged with bromide **66** (3.24 g, 7.67 mmol, 1.00 eq.), **B₂Pin₂** (2.05 g, 8.06 mmol, 1.05 eq.) and KOAc (3.76 g, 38.36 mmol, 5.00 eq.). Anhydrous 1,4-dioxan (60 mL) was added to the mixture and saturated with argon for 30 Min. Catalyst **Pd(dppf)₂Cl₂** (0.28 g, 0.38 mmol, 0.05 eq.) were added to the reaction mixture and refluxed at 101 °C for 23 h. The reaction mixture was cooled to room temperature and volatiles were removed under reduced pressure. The crude was dissolved in EtOAc (100 mL). The organic phase was washed with H₂O (100 mL). Subsequently, the aqueous phase was extracted with EtOAc (3 x 80 mL). The combined organic phases were washed with brine, dried (MgSO₄) and evaporated under reduced pressure. **67** (orange oil) was immediately used in the next reaction without further purification.

R_f(Heptane/EtOAc 9:1) = 0.34.

¹H NMR (500 MHz, CD₂Cl₂) δ 8.98 (d, J = 8.5 Hz, 1H), 8.70 (s, 1H), 8.37 – 8.30 (m, 2H), 7.75 – 7.70 (m, 2H), 7.64 – 7.54 (m, 2H), 7.43 – 7.29 (m, 8H), 6.96 (d, J = 8.1 Hz, 1H), 1.50 (s, 12H) ppm.

12-(4-methylnaphthalen-1-yl)-4,6-diphenyl-8-oxa-3,5-diazatricyclo[7.4.0.0^{2,7}]trideca-1(9),2,4,6,10,12-hexaene; 5H-benzo[b]carbazole (8)

Under an argon atmosphere a 500 mL 4 neck bottle flask was charged with bromide **66** (7.71 g, 18.26 mmol, 1.00 eq.), boronic ester **57** (8.18 g, 18.26 mmol, 1.00 eq.) and $K_3PO_4 \cdot H_2O$ (8.41 g, 36.51 mmol, 2.00 eq.). Subsequently, DMF (250 mL) was added to the mixture and saturated for 45 Min with argon. Catalyst $Pd(PPh_3)_4$ (1.05 g, 0.91 mmol, 0.05 eq.) were added to the reaction mixture and refluxed at 100 °C for 24 h. The suspension was cooled to room temperature and filtered. The precipitate was washed several times with H_2O (4 x 125 mL). Due to residue of DMF the precipitate was crystallized in 1,4-dioxane, washed with cold 1,4-dioxane. After recrystallization in 1,4-dioxane the color of the precipitate changed from white to grey. It was dried in a vacuum drying cabinet at 80 °C for 24 h. The title compound **8** (11.66 g, 17.57 mmol, **96%**) was obtained as a grey solid.

R_f (Heptane/EtOAc 9:1) = 0.35.

¹H NMR (500 MHz, THF-d₈) δ 8.85 (d, J = 8.16 Hz, 2H), 8.78 (d, J = 9.13 Hz, 3H), 8.65 (s, 1H), 8.39 (d, J = 7.65 Hz, 1H), 8.16 (d, J = 8.62 Hz, 1H), 8.12 – 8.03 (m, 3H), 7.90 (q, J = 7.35 Hz, 2H), 7.81 – 7.76 (m, 1H), 7.72 – 7.61 (m, 3H), 7.58 – 7.29 (m, 11H), 7.04 (d, J = 7.98 Hz, 1H) ppm.

¹³C NMR (126 MHz, THF-d₈) δ 160.6, 159.1, 153.1, 147.8, 145.9, 145.8, 143.1, 141.5, 139.2, 137.8, 134.8, 132.2, 131.0, 130.1, 129.8, 129.2, 129.2, 128.9, 128.3, 128.1, 128.0, 127.9, 127.7, 127.6, 125.9, 124.8, 124.6, 123.7, 121.9, 120.8, 119.6, 113.8, 110.6, 105.7 ppm.

HRMS (LC-APCI-MS): Calcd for $C_{48}H_{30}N_3O$ $[M+H]^+$ 664.2383, found 664.2387

HPLC RP-18, ACN/THF 90:10, t_R = 17.8 Min, purity: **99.98%**

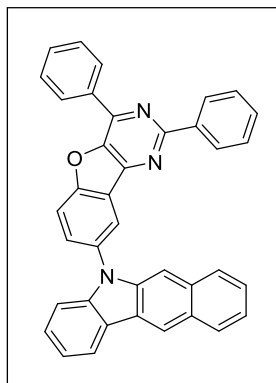
AQF [ppm]: F = 3.0, Cl < 3.5, Br < 3.5, S < 3.0

ICP-MS [ppm]: B < 3.54, P < 0.83, Cl < 23.8, Cu < 0.004, Br < 0.03, Pd < 0.003, I < 0.008.

DSC T_m = not detectable, T_g = 180 °C

TGA 5% weight loss at 466 °C

12-{5H-benzo[b]carbazol-5-yl}-4,6-diphenyl-8-oxa-3,5-diazatricyclo[7.4.0.0^{2,7}]trideca-1(9),2,4,6,10,12-hexaene (9)



A 250 mL 4 neck round bottom flask was charged with carbazole **18** (6.00 g, 27.62 mmol, 1.00 eq.), NaO^tBu (5.31 g, 55.23 mmol, 2.00 eq.) and bromide **37** (12.19 g, 30.38 mmol, 1.00 eq.). The reaction mixture was suspended in anhydrous toluene (150 mL) and degassed for 30 Min. Afterwards, Pd(P^tBu₃)₂ (0.71 g, 1.38 mmol, 0.05 eq.) was added to the reaction mixture and refluxed at 110 °C for 24 h. The reaction mixture was cooled to room temperature and the solvent was evaporated *in vacuo*. The crude was redissolved in toluene (100 mL) and upon addition of H₂O (200 mL) a yellow precipitate was obtained. The yellow solid was washed several times with H₂O. Recrystallization in toluene and drying at 100 °C in a vacuum dry oven gave **9** as a pure yellow solid (13.00 g, 24.18 mmol, **88%**)

R_f(Heptane/ EtOAc 9:1) = 0.32.

¹H NMR (500 MHz, CD₂Cl₂) δ 8.85 – 8.80 (m, 2H), 8.72 – 8.70 (m, 2H), 8.68 (s, 1H), 8.65 (d, J = 2.11 Hz, 1H), 8.33 (d, J = 7.70 Hz, 1H), 8.13 – 8.03 (m, 2H), 8.00 (dd, J = 8.65, 2.18 Hz, 1H), 7.88 (dd, J = 8.00, 1.57 Hz, 1H), 7.78 (s, 1H), 7.73 – 7.64 (m, 3H), 7.57 – 7.47 (m, 4H), 7.47 – 7.34 (m, 4H) ppm.

¹³C NMR (126 MHz, CD₂Cl₂) δ 160.4, 157.6, 152.3, 148.0, 145.8, 144.4, 141.8, 138.6, 135.0, 134.9, 133.3, 132.0, 131.6, 130.8, 129.8, 129.5, 129.4, 129.1, 128.9, 128.9, 128.1, 127.7, 126.0, 125.9, 124.4, 123.8, 123.7, 121.9, 121.6, 120.8, 119.3, 115.1, 109.8, 104.9 ppm.

HRMS (EI-MS): Calcd for C₃₈H₂₄N₃O [M+H⁺] 538.1914, found 538.1913.

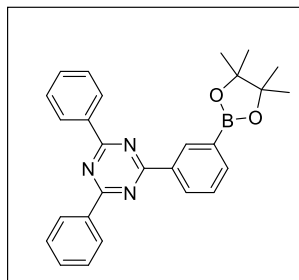
HPLC RP-18, ACN/THF 90:10, t_R = 11.5 Min, purity: **99.99%**

AQF [ppm]: F < 3.0, Cl < 3.0, Br < 0.5, S < 3.0

ICP-MS [ppm]: B < 3.34, P < 1.7, Cl < 37.5, Cu < 0.04, Br < 0.05, Pd < 0.002, I < 0.01.

DSC T_m = 296 °C, T_g = 142 °C

TGA 5% weight loss at 412 °C

2,4-diphenyl-6-[3-(4,4,5,5-tetramethyl-1,3,2-dioxaborolan-2-yl)phenyl]-1,3,5-triazine (52)

Under an argon atmosphere a 250 mL 4 neck bottle flask was charged with bromide **49** (5.00 g, 12.88 mmol, 1.00 eq.), **B₂Pin₂** (3.43 g, 13.52 mmol, 1.05 eq.) and KOAc (2.53 g, 25.76 mmol, 2.00 eq.) and suspended in anhydrous 1,4-dioxane (150 mL). The mixture was saturated with argon for 30 Min. Catalyst **Pd(OAc)₂** (0.03 g, 0.13 mmol, 0.01 eq.) and **ligand P(Cy)₃** (0.07 g, 0.26 mmol, 0.02 eq.) were added to the reaction mixture and refluxed at 101 °C for 24 h. The reaction mixture was cooled to room temperature and the solvent was removed under reduced pressure. The crude was dissolved in EtOH (100 mL) and H₂O (50 mL). The light grey precipitate was filtered and dried at 60 °C in a vacuum drying cabinet. **52** (5.40 g, 12.40 mmol, **96%**) was obtained as a light grey solid.

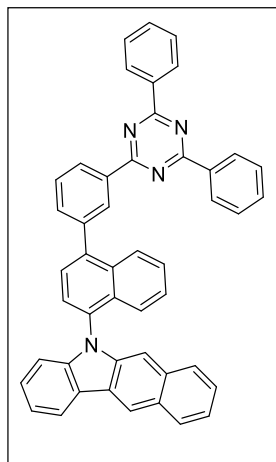
$R_f(\text{Heptane/EtOAc } 9:1) = 0.28$

¹H NMR (500 MHz, CD₂Cl₂) **¹H NMR** (500 MHz, Chloroform-d) δ 9.14 (s, 1H), 8.91 – 8.85 (m, 1H), 8.84 – 8.78 (m, 4H), 8.09 – 8.04 (m, 1H), 7.64 – 7.56 (m, 7H), 1.42 (s, 12H) ppm.

¹³C NMR (126 MHz, CDCl₃) δ 171.98, 171.78, 139.07, 136.40, 135.79, 135.27, 132.60, 132.02, 129.18, 128.75, 128.19, 84.20, 67.22, 26.79, 25.09 ppm.

HRMS (EI-MS): Calcd for C₂₇H₂₆BN₃O₂ [M] 435.21, found 435.19

**2-[3-(4-{5H-benzo[b]carbazol-5-yl)naphthalen-1-yl}phenyl]-4,6-diphenyl-1,3,5-triazine
(10)**



Under an argon atmosphere a 500 mL round bottom flask was charged with carbazole **18** (5.00 g, 23.01 mmol, 1.00 eq), fluoride **54** (10.44 g, 23.01 mmol, 1.00 eq) and K_3PO_4 (24.42 g, 115.07 mmol, 5.00 eq.) dissolved in H_2O (5 mL). DMF (150 mL) was added to the mixture and the two-phasic solution was saturated with argon for 30 Min. The reaction mixture was refluxed at 153 °C for 24 h. The solution was cooled to room temperature and the base was filtered. Then, the solvent was evaporated under reduced pressure. The crude was redissolved in CH_2Cl_2 (150 mL) and H_2O (200 mL) was added. The aqueous phase was separated and washed with CH_2Cl_2 (4 x 70 mL). Purification by column chromatography (SiO_2 , Hep/EtOAc 9:1 v/v) and recrystallization in 1,4-dioxane gave **10** (12.80 g, 19.67 mmol, **86%**) as a yellow solid.

R_f (Heptane/ CH_2Cl_2 2:1) = 0.36.

1H NMR (500 MHz, CD_2Cl_2) δ 9.06 (t, J = 1.8 Hz, 1H), 8.97 – 8.95 (m, 1H), 8.84 – 8.81 (m, 4H), 8.74 (s, 1H), 8.39 (dt, J = 7.7, 0.9 Hz, 1H), 8.13 (t, J = 8.6 Hz, 2H), 7.96 – 7.90 (m, 1H), 7.89 – 7.76 (m, 4H), 7.68 – 7.58 (m, 7H), 7.50 – 7.39 (m, 5H), 7.40 – 7.33 (m, 2H), 7.11 (d, J = 8.1 Hz, 1H) ppm.

^{13}C NMR (126 MHz, CD_2Cl_2) δ 172.38, 172.20, 145.37, 142.81, 141.59, 141.41, 137.27, 136.78, 134.83, 134.48, 133.24, 131.79, 131.01, 129.51, 129.28, 128.97, 128.11, 128.04, 127.66, 127.50, 127.41, 127.26, 125.80, 124.26, 123.57, 121.60, 120.48, 119.26, 110.38, 105.48, ppm.

HRMS (LC-APCI-MS): Calcd for $C_{47}H_{31}N_4$ $[M+H]^+$ 651.2543, found 651.2553.

HPLC RP-18, MeOH/THF 80:20, t_R = 10.8 Min, purity: **99.97%**

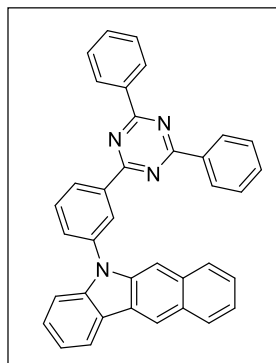
AQF [ppm]: F < 2.0, Cl < 2.0, Br < 1.5, S < 3.0

ICP-MS [ppm]: B < 4.17, P < 1.3, Cl < 28.4, Cu < 0.005, Br < 0.19, Pd < 0.006, I < 0.01.

DSC T_m = not detectable, T_g = 157 °C

TGA 5% weight loss at 449 °C

2-(3-(5H-benzo[b]carbazol-5-yl)phenyl)-4,6-diphenyl-1,3,5-triazine (11)



A 50 mL 4 neck round bottom flask was charged with carbazole **18** (0.20 g, 0.92 mmol, 1.00 eq.), NaO^tBu (0.18 g, 1.84 mmol, 2.00 eq.) and bromide **49** (0.38 g, 0.97 mmol, 1.05 eq.). The reaction mixture was suspended in anhydrous toluene (25 mL) and degassed for 30 Min. Afterwards, Pd(P^tBu₃)₂ (0.02 g, 0.05 mmol, 0.05 eq.) was added to the reaction mixture and refluxed at 110 °C for 24 h. The reaction mixture was cooled to room temperature and the yellow precipitate was filtered and washed several times with toluene. The yellow solid was dried at. After recrystallization in toluene and drying at 100 °C in a vacuum dry oven, **11** was obtained as a pure yellow solid (0.40 g, 0.76 mmol, **83%**).

R_f(Heptane/ EtOAc 9:1) = 0.22.

¹H NMR (700 MHz, NMP-d₉) δ 9.12 (t, J = 1.95 Hz, 1H), 9.02 (d, J = 7.82 Hz, 1H), 8.97 (s, 1H), 8.85 – 8.80 (m, 4H), 8.56 – 8.51 (m, 2H), 8.20 – 8.15 (m, 3H), 8.11 (t, J = 7.77 Hz, 2H), 8.04 (d, J = 8.16 Hz, 1H), 8.00 (s, 1H), 7.74 (t, J = 7.34 Hz, 2H), 7.68 (t, J = 7.56 Hz, 4H), 7.62 – 7.53 (m, 2H) ppm.

¹³C NMR (176 MHz, NMP-d₉) δ 172.0, 171.3, 143.4, 140.8, 138.7, 138.4, 135.9, 134.6, 133.5, 133.1, 132.0, 131.5, 129.3, 129.1, 128.5, 128.3, 128.1, 127.6, 127.4, 125.5, 123.4, 123.1, 121.6, 120.6, 119.3, 109.5, 104.8 ppm.

HRMS (LC-APCI-MS): Calcd. for C₃₇H₂₄N₄ [M+H⁺] 525.2074, found 525.2075.

HPLC RP-18, MeOH/THF 85:15, t_R = 13.9 Min, purity: **99.96%**

AQF [ppm]: F < 3.0, Cl < 3.0, Br < 3.7, S < 3.0

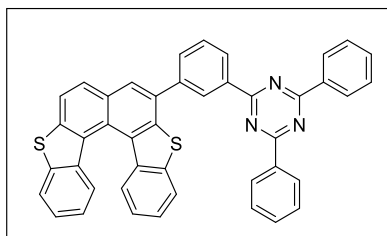
ICP-MS [ppm]: B < 3.7, P < 1.3, Cl < 29.9, Cu < 0.014, Br < 0.7, Pd < 0.012, I < 0.07.

DSC T_m = 285 °C, T_g = 105 °C

TGA 5% weight loss at 392 °C

7.2.4 Synthesis of further TMM's (compounds of chapter 3.3.3)

2-(3-(9,17-dithiahexacyclo[11.11.0.0²,¹⁰.0³,⁸.0¹⁶,²⁴.0¹⁸,²³]tetracos-1(24),2(10),3(8),4,6,11,13,15,18(23),19,21-undecaen-11-yl}phenyl)-4,6-diphenyl-1,3,5-triazine **67**



Boronic ester **43** (0.25 g, 0.54 mmol, 1.00 eq.), bromide **49** (0.21 g, 0.54 mmol, 1.00 eq.) in PhMe (20 mL) and K₃PO₄ (0.34 g, 1.61 mmol, 3.00 eq.) dissolved in H₂O (10 mL) were degassed under an argon atmosphere for 30 Min. Catalyst Pd(dppf)Cl₂ (0.02 g, 0.03 mmol, 0.05 eq.) was added to the reaction mixture and refluxed 110 °C for 24 h. Volatiles were removed under reduced pressure. The crude was redissolved in CH₂Cl₂ (50 mL) and filtered over celite. The solution was washed with H₂O (20 mL) and the aqueous phase was extracted with CH₂Cl₂ (4 x 20 mL). The combined organic phase was washed with brine solution (20 mL), dried (MgSO₄) and the solvent was evaporated under reduced pressure. The title compound **67** (0.3 g, 0.46 mmol, **86%**) was obtained as a yellow solid after recrystallization in MeOH.

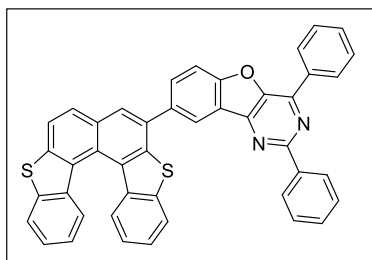
R_f(Heptane/EtOAc 2:1) = 0.66.

¹H NMR (500 MHz, CD₂Cl₂) δ 9.34 (t, *J* = 1.8 Hz, 1H), 8.95 (d, *J* = 7.8 Hz, 1H), 8.83 (d, *J* = 7.0 Hz, 4H), 8.79 (d, *J* = 6.8 Hz, 1H), 8.22 (s, 1H), 8.19 – 8.11 (m, 3H), 8.06 (d, *J* = 8.1 Hz, 1H), 8.00 (d, *J* = 8.0 Hz, 1H), 7.85 (t, *J* = 7.7 Hz, 1H), 7.65 – 7.57 (m, 7H), 7.44 (dt, *J* = 18.1, 7.5 Hz, 2H), 7.17 (dt, *J* = 18.4, 7.6 Hz, 2H) ppm.

¹³C NMR (126 MHz, CD₂Cl₂) δ 172.82, 171.33, 141.23, 140.43, 139.45, 138.34, 137.50, 137.08, 135.82, 133.05, 132.86, 131.13, 130.27, 129.84, 129.25, 129.10, 128.11, 127.13, 125.97, 124.18, 123.31, 122.92, 122.71, 121.37 ppm.

HRMS (EI-MS): Calcd for C₄₃H₂₅N₃S₂Na [M] 647.10, found 647.20.

12-{9,17-dithiahexacyclo[11.11.0.0²,¹⁰.0³,⁸.0¹⁶,²⁴.0¹⁸,²³]tetracos-1,3,5,7,10,12,14,16(24),18,20,22-undecaen-11-yl}-4,6-diphenyl-8-oxa-3,5-diazatricyclo[7.4.0.0²,⁷]trideca-1(9),2,4,6,10,12-hexaene (69)



Under an argon atmosphere a 50 mL 4 neck bottle flask was charged with **iodide 68** (0.25 g, 0.54 mmol, 1.00 eq.), boronic ester **57** (0.25 g, 0.55 mmol, 1.03 eq.) and CsF (0.24 g, 1.61 mmol, 3.00 eq.). The reactants were dissolved in 1,4-dioxane/H₂O (4:1, 15 mL). The two-phasic solution was degassed for 30 Min. Subsequently, Catalyst **PdCl₂[P(**cy**)₃]₂** (0.01 g, 0.02 mmol, 0.03 eq.) was added at room temperature to the reaction mixture and refluxed at 101 °C for 25 h. The reaction mixture was cooled to room temperature and the grey precipitate was filtered. The crude was stirred vigorously in hot 1,4-dioxane to remove further impurities. **69** (0.22 g, 0.33 mmol, **62%**) was obtained as a grey solid.

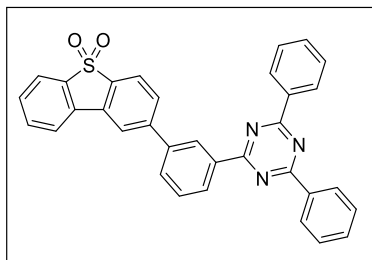
R_f (Heptane /EtOAc 4:1) = 0.4.

¹H NMR (500 MHz, DMSO-d₆) δ 8.76 (s, 1H), 8.63 (t, J = 7.79 Hz, 4H), 8.40 (s, 1H), 8.36 – 8.10 (m, 6H), 7.68 (dq, J = 13.77, 7.13 Hz, 3H), 7.60 – 7.36 (m, 7H), 7.18 (dt, J = 15.20, 7.69 Hz, 2H) ppm.

¹³C NMR: poor solubility.

HRMS (EI-MS): Calcd for C₄₄H₂₄N₂OS₂ [M] 660.13, found 660.10.

4-[3-(4,6-diphenyl-1,3,5-triazin-2-yl)phenyl]-8 λ ⁶-thiatricyclo[7.4.0.0^{2,7}]trideca-1(9),2,4,6,10,12-hexaene-8,8-dione (70)



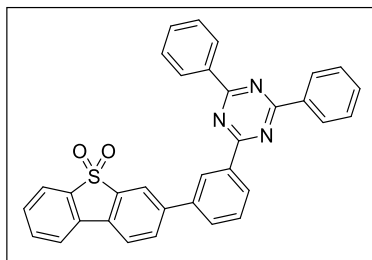
Under an argon atmosphere a 50 mL round bottom flask was charged with bromide **45a** (0.25 g, 0.85 mmol, 1.00 eq.), boronic ester **52** (0.39 g, 0.89 mmol, 1.05 eq.) and $K_3PO_4 \cdot H_2O$ (0.47 g, 2.03 mmol, 2.40 eq.) dissolved in H_2O (5 mL). Anhydrous 1,4-dioxane (20 mL) was added to the mixture and the two-phasic solution was saturated with argon for 30 Min. Catalyst **Pd(PPh₃)₄** (0.03 g, 0.03 mmol, 0.03 eq.) were added to the reaction mixture and refluxed at 101 °C for 26 h. The solution was cooled to room temperature. A colourless precipitate was filtered and washed with H_2O (4 x 20 mL). **70** (0.27 g, 0.52 mmol, **61%**) was obtained as a colorless solid without further purification.

R_f (Heptane/EtOAc 4:1) = 0.20.

¹H NMR (500 MHz, CD_2Cl_2) ¹H NMR (500 MHz, Methylene Chloride-d₂) δ 9.05 (t, J = 1.84 Hz, 1H), 8.87 (dt, J = 7.85, 1.42 Hz, 1H), 8.80 (dt, J = 6.93, 1.59 Hz, 4H), 8.15 (d, J = 1.54 Hz, 1H), 8.00 – 7.89 (m, 4H), 7.85 (d, J = 7.56 Hz, 1H), 7.78 – 7.69 (m, 2H), 7.67 – 7.56 (m, 7H) ppm.

¹³C NMR (126 MHz, CD_2Cl_2) δ 172.4, 171.8, 147.5, 140.5, 138.9, 137.8, 137.3, 136.6, 134.6, 133.3, 133.0, 132.0, 132.0, 131.2, 130.2, 130.1, 129.7, 129.5, 129.3, 128.3, 123.0, 122.5, 122.5, 121.2, 67.6 ppm.

HRMS (EI-MS): Calcd for $C_{33}H_{21}N_3O_2S$ [M] 523.14, found 523.30.

4-[3-(4,6-diphenyl-1,3,5-triazin-2-yl)phenyl]-8 λ ⁶-thiatricyclo[7.4.0.0²,⁷]trideca-1(9),2,4,6,10,12-hexaene-8,8-dione (71)

Under an argon atmosphere a 25 mL round bottom flask was charged with bromide **45b** (0.20 g, 0.68 mmol, 1.00 eq.), boronic ester **52** (0.31 g, 0.71 mmol, 1.05 eq.) and $K_3PO_4 \cdot H_2O$ (0.37 g, 1.63 mmol, 2.40 eq.) dissolved in H_2O (5 mL). Anhydrous 1,4-dioxane (20 mL) was added to the mixture and the two-phasic solution was saturated with argon for 30 Min. Catalyst **Pd(PPh₃)₄** (0.02 g, 0.02 mmol, 0.03 eq.) were added to the reaction mixture and refluxed at 101 °C for 5 h. The solution was cooled to room temperature. A colourless precipitate was filtered, washed with H_2O (4 x 20 mL) and dried in a vacuum oven at 100 °C for 2 h. **71** (0.33 g, 0.63 mmol, **93%**) was obtained as a colorless solid without further purification.

R_f (Heptane/EtOAc 4:1) = 0.10.

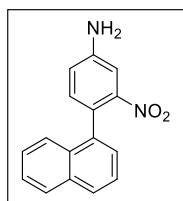
¹H NMR (500 MHz, $CDCl_3$) δ 9.00 (t, J = 1.83 Hz, 1H), 8.83 – 8.75 (m, 4H), 8.18 (d, J = 1.67 Hz, 1H), 8.02 (dd, J = 7.97, 1.75 Hz, 1H), 7.95 (d, J = 8.02 Hz, 1H), 7.87 (t, J = 7.26 Hz, 3H), 7.74 – 7.67 (m, 2H), 7.67 – 7.55 (m, 8H).

¹³C NMR (126 MHz, $CDCl_3$) δ 172.0, 171.4, 143.7, 139.6, 138.8, 138.2, 137.5, 136.2, 134.1, 133.0, 132.8, 131.2, 130.5, 129.7, 129.3, 129.2, 128.9, 127.5, 122.5, 122.3, 121.8, 121.1 ppm.

HRMS (EI-MS): Calcd for $C_{33}H_{21}N_3O_2S$ [M] 523.14, found 523.10.

7.2.5 Synthesis of Lactam TMM (compounds of chapter 3.3.4)

4-(Naphthalen-1-yl)-3-nitroaniline (**76**)



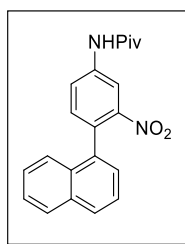
Compound **77** (0.50 g, 2.30 mmol, 1.00 eq.), boronic acid **78** (0.48 g, 2.76 mmol, 1.20 eq.) and Cs_2CO_3 (2.25 g, 6.91 mmol, 3.00 eq.) were dissolved in anhyd. THF (8 mL) and H_2O (2 mL) and degassed under an argon atmosphere for 45 Min. Catalyst $\text{Pd}(\text{P}^t\text{bu}_3)_2$ (0.02 g, 0.04 mmol, 0.02 eq.) were added to the reaction mixture and refluxed at 80 °C for 24 h. The reaction mixture was filtered over aluminium oxide (neutral), H_2O (50 mL) was added and the aqueous phase was extracted with EtOAc (4 x 50 mL). The combined organic phases were washed with brine solution, dried (MgSO_4) and the solvents were evaporated under reduced pressure. The title compound **76** (0.57 g, 2.16 mmol, **94%**) was obtained as a orange solid after purification *via* column chromatography (SiO_2 , heptane/EtOAc, 9:1 to 7:3).

$R_f(\text{PhMe}/\text{EtOAc } 9:1) = 0.53$.

$^1\text{H NMR}$ (500 MHz, CD_2Cl_2) δ 8.24 (d, $J = 2.0$ Hz, 1H), 7.93 (d, $J = 8.1$ Hz, 1H), 7.88 (dd, $J = 8.4, 4.1$ Hz, 2H), 7.57 – 7.39 (m, 5H), 6.98 (d, $J = 8.5$ Hz, 1H), 6.20 (s, 2H) ppm.

$^{13}\text{C NMR}$ (126 MHz, CD_2Cl_2) δ 144.40, 138.32, 137.95, 134.33, 132.55, 131.91, 129.96, 128.81, 128.31, 127.39, 127.17, 126.70, 126.33, 125.84, 125.74, 119.18 ppm.

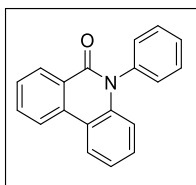
HRMS (EI-MS): Calcd for $\text{C}_{16}\text{H}_{12}\text{N}_2\text{O}_2$ [M] 264.089, found 264.089.

***N*-[4-(Naphthalene-1-yl)-3-nitrophenyl]pivalamide (**76'**)**

Compound **76** (2.00 g, 7.57 mmol, 1.00 eq.) was dissolved in anhyd. CH₂Cl₂ (30 mL). Then Et₃N (2.11 mL, 15.14 mmol, 2.00 eq.) was added dropwise. The reaction solution was stirred for 30 Min at room temperature. Afterwards, the reaction solution was cooled to 0 °C and pivaloyl chloride (1.85 mL, 15.14 mmol, 2.00 eq.) was added dropwise. The reaction mixture was warmed to room temperature and stirred vigorously for 24 h. Volatiles were removed under reduced pressure and the residue was redissolved in EtOAc (50 mL). H₂O (50 mL) was added and the aqueous phase was extracted with EtOAc (3 x 50 mL). The combined organic phase was washed with brine solution, dried (MgSO₄) and the solvent was evaporated under reduced pressure. The title compound **76'** (2.57 g, 7.38 mmol, **98%**) was obtained as a brown oil without further purification.

R_f(Heptane/EtOAc 4:1) = 0.35.

¹H NMR (500 MHz, CD₂Cl₂) δ 10.73 (s, 1H), 8.94 (d, *J* = 8.6 Hz, 1H), 8.37 (d, *J* = 2.2 Hz, 1H), 7.99 – 7.91 (m, 2H), 7.84 – 7.80 (m, 2H), 7.59 – 7.52 (m, 2H), 7.52 – 7.44 (m, 2H), 1.39 (s, 9H) ppm.

5-Phenylphenanthridin-6(5*H*)-one (84**)**

Lactam **85** (5.00 g, 25.10 mmol, 1.00 eq.), **86** (3.08 mL, 27.61 mmol, 1.10 eq.) and K₂CO₃ (6.94 g, 50.20 mmol, 2.00 eq.) were suspended in anhyd. DMF (150 mL) at room temperature. The suspension was degassed for 30 Min. Afterwards, CuI (0.96 g, 5.02 mmol, 0.20 eq.) and 1,3-di-pyridine-2-yl-prpane-1,3-dione (1.14 g, 5.02 mmol, 0.20 eq.) were added and was stirred at 140 °C for 24 h. The reaction mixture was diluted with MTBE (250 mL) and filtered over celite. Then, H₂O (150 mL) and NH₄Cl (250 mL) solution were added. The aqueous phase was extracted with MTBE (4 x 150 mL). The combined organic phase was filtered over Silica (SiO₂), washed with brine solution, dried (MgSO₄) and the solvent was evaporated under

reduced pressure. The title compound **84** (3.00 g, 11.06 mmol, **44%**) was obtained as a yellow-brown solid without further purification.

R_f (Heptane/EtOAc 2:1) = 0.43.

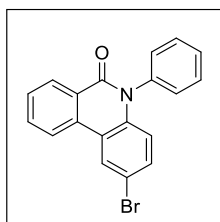
$^1\text{H NMR}$ (500 MHz, CD_2Cl_2) δ 8.50 (d, $J = 7.9$ Hz, 1H), 8.38 (d, $J = 8.2$ Hz, 1H), 8.36 – 8.30 (m, 1H), 7.84 (t, $J = 7.7$ Hz, 1H), 7.64 (t, $J = 7.4$ Hz, 3H), 7.56 (t, $J = 7.5$ Hz, 1H), 7.36 – 7.25 (m, 4H), 6.70 – 6.64 (m, 1H) ppm.

$^{13}\text{C NMR}$ (126 MHz, CD_2Cl_2) δ 161.82, 139.77, 139.04, 134.46, 133.18, 130.50, 129.65, 129.50, 129.09, 129.05, 128.49, 126.44, 123.41, 122.94, 122.33, 119.33, 117.32 ppm.

HRMS (EI-MS): Calcd for $\text{C}_{19}\text{H}_{13}\text{NO}$ [M] 271.100, found 271.098.

The acquired characteristic data is in accordance with literature.^[129]

2-Bromo-5-phenylphenanthridin-6(5H)-one (**83**)



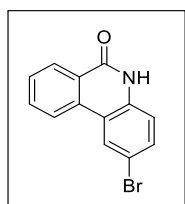
To a solution of compound **84** (2.70 g, 9.95 mmol, 1.00 eq.) in DMF (60 mL), a solution of NBS (2.66 g, 14.93 mmol, 1.50 eq.) in DMF (20 mL) was added dropwise at room temperature and was stirred for 24 h at 60 °C. Volatiles were removed under reduced pressure and the residue was redissolved in PhMe (100 mL). The organic phase was washed with H_2O (50 mL) and the aqueous phase was extracted with PhMe (4 x 50 mL). The combined organic phase was washed with brine solution (50 mL), dried (MgSO_4) and the solvent was evaporated under reduced pressure. The title compound **83** (2.73 g, 7.80 mmol, **78%**) was obtained as a brown solid and was used without further purification.

R_f (Heptane/EtOAc 2:1) = 0.46.

$^1\text{H NMR}$ (500 MHz, CD_2Cl_2) δ 8.49 (dd, $J = 8.0, 1.5$ Hz, 1H), 8.43 (d, $J = 2.2$ Hz, 1H), 8.30 (d, $J = 8.1$ Hz, 1H), 7.86 (ddd, $J = 8.3, 7.2, 1.4$ Hz, 1H), 7.70 – 7.61 (m, 3H), 7.57 (t, $J = 7.4$ Hz, 1H), 7.39 (dd, $J = 9.0, 2.2$ Hz, 1H), 7.31 (d, $J = 7.1$ Hz, 2H), 6.56 (d, $J = 8.9$ Hz, 1H) ppm.

$^{13}\text{C NMR}$ (126 MHz, CD_2Cl_2) δ 161.51, 138.79, 138.62, 133.43, 133.22, 132.14, 130.62, 129.51, 129.37, 129.31, 129.21, 129.18, 126.61, 126.18, 122.40, 121.12, 119.08, 116.00 ppm.

HRMS (EI-MS): Calcd for $\text{C}_{19}\text{H}_{12}\text{BrNO}$ [M] 349.010, found 349.010.

2-bromophenanthridin-6(5H)-one (87)

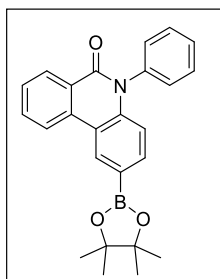
To a suspension of lactam **85** (7.00 g, 35.86 mmol, 1.00 eq.) in DMF (100 mL), a solution of NBS (6.38 g, 35.86 mmol, 1.00 eq.) in DMF (20 mL) was added dropwise at room temperature and was stirred for 48 h at room temperature. Volatiles were removed under reduced pressure. H₂O (100 mL) was added and the suspension was refluxed for 20 Min. A colourless precipitate was separated from the aqueous phase by filtration and the residue was washed with MeOH, H₂O and ice-cold *n*-pentane. The colourless solid was then dried for 24 h at 60 °C in a vacuum chamber. The title compound **87** (9.35 g, 34.11 mmol, **95%**) was obtained as a colourless solid.

R_f (Heptane/EtOAc 2:1) = 0.31.

¹H NMR (500 MHz, DMSO) δ 11.79 (s, 1H), 8.64 – 8.20 (m, 4H), 7.85 (t, J = 7.8 Hz, 1H), 7.71 – 7.61 (m, 2H) ppm.

HRMS (EI-MS): Calcd for C₁₃H₈BrNO [M] 272.98, found 272.98.

The acquired characteristic data is in accordance with literature.^[130]

5-phenyl-2-(4,4,5,5-tetramethyl-1,3,2-dioxaborolan-2-yl)-5,6-dihydrophenanthridin-6-one (82)

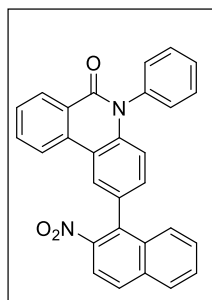
Bromide **83** (0.40 g, 1.14 mmol, 1.00 eq.), bis(pinacolato)diboron (0.32 g, 1.26 mmol, 1.10 eq.) and KOAc (0.34 g, 3.43 mmol, 3.00 eq.) were dissolved in anhyd. 1,4-dioxane (5 mL) and degassed under an argon atmosphere for 15 Min. Catalyst Pd(dppf)₂Cl₂ (0.05 g, 0.06 mmol, 0.05 eq.) was added to the reaction mixture and heated at 95 °C for 24 h. Volatiles were removed under reduced pressure. The residue was redissolved in CH₂Cl₂ (20 mL) and filtered over celite. The solution was washed with H₂O (30 mL) and the aqueous phase was extracted with CH₂Cl₂ (4 x 20 mL). The combined organic phase was washed with brine solution (50 mL),

dried (MgSO_4) and the solvent was evaporated under reduced pressure. The title compound **82** was used without further purification for the Suzuki-Miyaura coupling.

R_f (RP, MeCN/ H_2O 9:1) = 0.36.

HRMS (TOF-EI-MS): Calcd for $\text{C}_{25}\text{H}_{24}\text{BNO}_3$ [M] 397.18, found 397.18.

2-(2-nitronaphthalen-1-yl)-5-phenylphenanthridin-6(5H)-one (**80**)



Bromide **81** (0.15 g, 0.60 mmol, 1.00 eq.), boronic ester **82** (0.24 g, 0.60 mmol, 1.00 eq.) and K_2CO_3 (0.25 g, 1.79 mmol, 3.00 eq.) were dissolved in anhyd. 1,4-dioxane (5 mL) and degassed under an argon atmosphere for 15 Min. Catalyst $\text{Pd}(\text{dppf})_2\text{Cl}_2$ (0.02 g, 0.05 mmol, 0.02 eq.) were added to the reaction mixture and refluxed at 101 °C for 24 h. Volatiles were removed under reduced pressure. The residue was redissolved in EtOAc (20 mL) and filtered over celite. The solution was washed with H_2O (20 mL) and the aqueous phase was extracted with EtOAc (4 x 25 mL). The combined organic phase was washed with brine solution (20 mL), dried (MgSO_4) and the solvent was evaporated *in vacuo*. The title compound **80** (0.05 g, 0.11 mmol, 19%) was obtained as a white solid after purification *via* column chromatography (SiO_2 , heptane/EtOAc, 4:1 to 2:1).

R_f (Heptane/EtOAc 4:1) = 0.10.

^1H NMR (500 MHz, CD_2Cl_2) δ 8.53 (dd, J = 8.0, 1.5 Hz, 1H), 8.30 – 8.24 (m, 2H), 8.06 (d, J = 8.9 Hz, 1H), 8.02 (d, J = 8.2 Hz, 1H), 7.96 (d, J = 8.9 Hz, 1H), 7.80 (ddd, J = 8.4, 7.1, 1.5 Hz, 1H), 7.70 – 7.63 (m, 5H), 7.63 – 7.56 (m, 1H), 7.56 – 7.49 (m, 1H), 7.49 – 7.40 (m, 2H), 7.30 (s, 1H), 6.83 (d, J = 8.6 Hz, 1H) ppm.

HRMS (APCI positive): Calcd for $\text{C}_{29}\text{H}_{19}\text{N}_2\text{O}_3$ [M + H]⁺ 443.1390 found 443.1315.

7.2.6 Photoredoxcatalytic Reactions

All photoredoxcatalytic reactions were conducted according to the following general procedure. Stoichiometry of substrates, catalyst and additives are described in the results in chapter 5.2.

A 5 mL crimp-cap vial equipped with a stirring bar, was loaded with the corresponding carbazole nucleophile (302 μmol , 1.50 eq.) and aryl halide (201 μmol , 1.00 equiv.). A stock solution of $\text{NiBr}_2\cdot\text{Glyme}$ and 4CzIPN was prepared (3 mM 4CzIPN, 26 mM $\text{NiBr}_2\cdot\text{Glyme}$ in anhydrous DMAc). The stock solution (0.4 mL, 0.5 mol% 4CzIPN, 5.0 mol% $\text{NiBr}_2\cdot\text{Glyme}$) was added in the dark to the loaded crimp-cap vial (0.4 mL). The vial was sealed, evacuated, and back filled with N_2 (3x) before adding the additive (243 μmol , 1.20 eq.). The reaction mixture was subsequently purged with N_2 for 15 min and stirred under irradiation using a 2.2 W 451 nm (± 15 nm) LED set-up for 24 hours at the desired temperature (temperature controlled by a thermostat). Two stock solutions were prepared for either achieving either 0.1 or 0.5 mol% of 4CzIPN. For reactions with 0.1 mol% of 4CzIPN, another stock solution was prepared (0.6 mM 4CzIPN, 26 mM $\text{NiBr}_2\cdot\text{Glyme}$ in DMAc). For the reactions in MeCN, the stock solutions were prepared with the same concentrations as stated above dissolved in anhydrous MeCN.

Reaction progress was monitored by TLC or GC analysis and a qualitative conclusion of the reaction outcome was made. Product formation is shown by GC-MS (Appendix 1). Products were not further characterized.



Figure 37: Set-up of the photoredoxcatalytic reactions.

7.3 Crystal structures

Crystal structure of compound **9**:

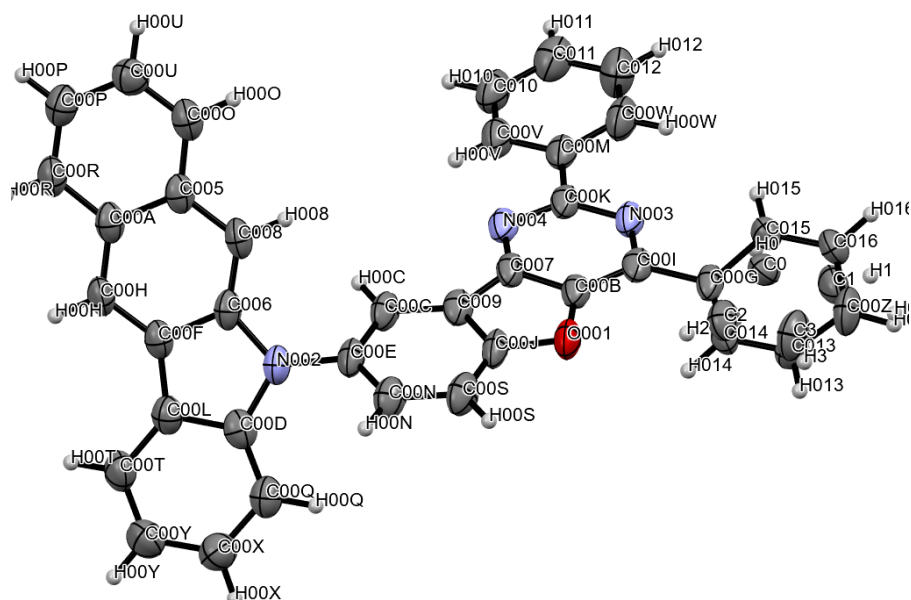


Table 19: Fractional atomic coordinates of compound **9**.

Number	Label	x	y	z
1	O001	0.67106(4)	0.5747(3)	0.59905(6)
2	N002	0.84488(5)	0.0912(4)	0.54454(7)
3	N003	0.62004(5)	1.0865(4)	0.47039(7)
4	N004	0.69314(5)	0.8556(4)	0.44379(7)
5	C005	0.84038(6)	-0.2915(4)	0.38301(8)
6	C006	0.85400(6)	-0.0537(4)	0.48706(9)
7	C007	0.69445(6)	0.7108(5)	0.50045(9)
8	C008	0.82336(6)	-0.1157(4)	0.43223(8)
9	H008	0.791325	-0.041354	0.427649
10	C009	0.72973(6)	0.5027(4)	0.53099(9)
11	C00A	0.88935(6)	-0.3956(4)	0.38944(9)
12	C00B	0.66011(6)	0.7476(5)	0.54353(9)
13	C00C	0.77300(6)	0.3864(4)	0.51444(9)
14	H00C	0.783779	0.431545	0.473705
15	C00D	0.88795(6)	0.1055(4)	0.58615(9)
16	C00E	0.79977(6)	0.2038(4)	0.55879(9)
17	C00F	0.90292(6)	-0.1490(4)	0.49360(8)
18	C00G	0.58233(6)	1.0055(4)	0.56854(9)
19	C00H	0.92007(6)	-0.3179(5)	0.44550(9)
20	H00H	0.952641	-0.382344	0.450021
21	C00I	0.62150(6)	0.9426(5)	0.52793(9)
22	C00J	0.71413(6)	0.4301(4)	0.59041(9)
23	C00K	0.65486(6)	1.0403(5)	0.43158(9)

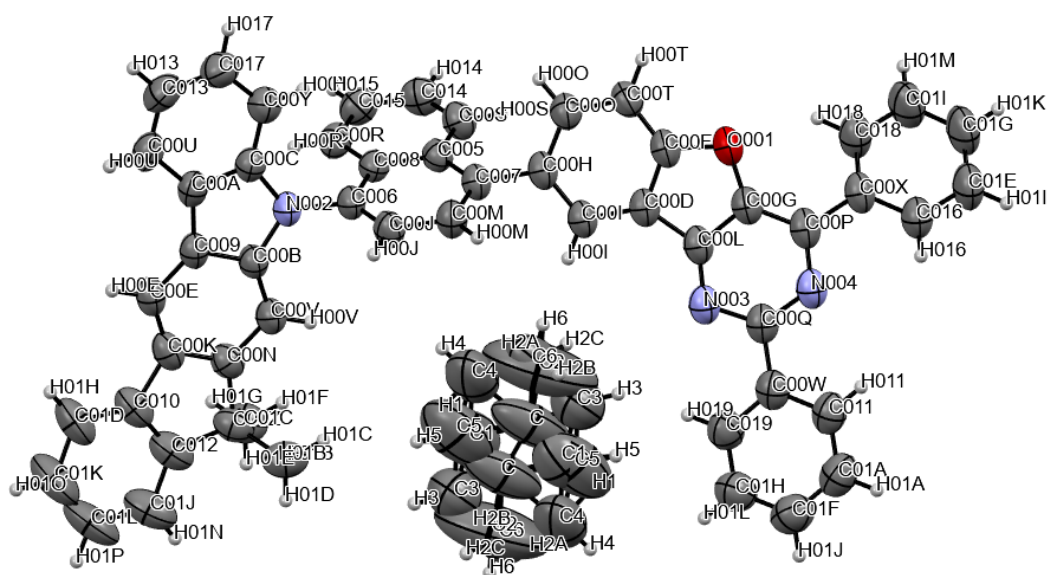
7 Experimental Section

24	C00L	0.92438(6)	-0.0401(4)	0.55618(9)
25	C00M	0.65080(6)	1.2098(5)	0.36972(9)
26	C00N	0.78276(6)	0.1288(5)	0.61807(9)
27	H00N	0.801411	-0.001577	0.647378
28	C00O	0.80987(6)	-0.3815(5)	0.32701(9)
29	H00O	0.777477	-0.313613	0.321629
30	C00P	0.87417(7)	-0.6649(5)	0.28707(9)
31	H00P	0.885168	-0.791249	0.254698
32	C00Q	0.89722(7)	0.2455(5)	0.64604(9)
33	H00Q	0.872434	0.345250	0.665576
34	C00R	0.90483(6)	-0.5810(5)	0.33986(9)
35	H00R	0.937247	-0.648129	0.343462
36	C00S	0.73935(6)	0.2405(5)	0.63493(9)
37	H00S	0.727734	0.189202	0.674818
38	C00T	0.97101(7)	-0.0479(5)	0.58779(9)
39	H00T	0.995963	-0.146389	0.568357
40	C00U	0.82593(7)	-0.5630(5)	0.28078(9)
41	H00U	0.804592	-0.621472	0.244077
42	C00V	0.68817(7)	1.2031(5)	0.33050(9)
43	H00V	0.716309	1.088.581	0.343650
44	C00W	0.60987(7)	1.3803(5)	0.34927(10)
45	H00W	0.584015	1.387.655	0.375233
46	C00X	0.94398(7)	0.2350(5)	0.67659(9)
47	H00X	0.951224	0.328572	0.717748
48	C00Y	0.98046(7)	0.0894(5)	0.64778(9)
49	H00Y	1.012.124	0.084623	0.669615
50	C00Z	0.50658(7)	1.1206(5)	0.64144(10)
51	H00Z	0.482393	1.169.078	0.668415
52	C010	0.68459(7)	1.3618(5)	0.27259(10)
53	H010	0.710157	1.353.731	0.246162
54	C011	0.64416(7)	1.5317(5)	0.25294(10)
55	H011	0.641986	1.642.704	0.213497
56	C012	0.60680(8)	1.5384(5)	0.29143(10)
57	H012	0.578743	1.653.010	0.277925
58	C013	0.5483(3)	0.9952(17)	0.6660(4)
59	H013	0.551940	0.935181	0.710256
60	C014	0.58623(19)	0.9493(15)	0.6300(2)
61	H014	0.615835	0.874891	0.650883
62	C015	0.53744(18)	1.1383(13)	0.5354(3)
63	H015	0.534822	1.192.579	0.490900
64	C016	0.49959(17)	1.1801(13)	0.5720(2)
65	H016	0.469271	1.246.974	0.551924
66	H00A	0.477712	1.147.754	0.660833
67	C0	0.55457(19)	1.2445(13)	0.5579(2)
68	H0	0.560465	1.378.015	0.523781
69	C1	0.51705(18)	1.3123(14)	0.5940(2)

70	H1	0.498823	1.492.383	0.585503
71	C2	0.5748(2)	0.8123(17)	0.6259(3)
72	H2	0.595089	0.643704	0.637327
73	C3	0.5374(3)	0.885(2)	0.6621(4)
74	H3	0.533092	0.775013	0.700387

Table 20: Structure Solution and refinement parameters of compound **9**.

Empirical formula	C ₃₈ H ₂₃ N ₃ O
Molecular weight	537.59 g/mol
Diffraction/Detector	Synergy (Rigaku), HyPix Arc 150 Detector
Radiation	Cu K α (1.5418 Å), X-ray mirrors
Crystal size	(0.21 x 0.1 x 0.03) mm ³
Temperature	100.00 (10) K
Diffraction Experiment ID	exp_104685_auto
Crystal system	monoclinic
Space group	P21/c
Lattice parameters:	
a, b, c	28.0058(5) Å, 4.40970(10) Å, 20.7566(4) Å
α, β, γ	90°, 96.387(2)°, 90°
Unit cell volume	2547.47(9) Å ³
Formula units per unit cell	4
F(000)	1120
Calculated density	1.402 g/cm ³
Linear absorption coeff.	0.668 mm ⁻¹
Scan	ω -scans
Measured reflections	18809
Index limits	-34 \leq h \leq 33; -5 \leq k \leq 2; -25 \leq l \leq 25
R_{int} (internal consistency of the dataset)	0.0381
Reflections used	5005
Refined parameters / restraints	416 / 96
R1 (I > 2σ)	0.0466
wR² (all data)	0.0466
Goof S	1.033
Max. shift in final cycle	\leq 0.001
Max./min. differential electron density	max: 0.166 / min: -0.237 e/Å ³
Structure Solution / Refinement	SHELX-97: G.M. Sheldrick, <i>Acta Cryst. A</i> , 64, 2008 , 112 G.M. Sheldrick, Univ. Göttingen, 1997 .
Automated Report	Olex2.1.2 2022.04.07 svn.rca3783a0 for OlexSys

Crystal structure of compound **14**:Table 21: Fractional atomic coordinates of compound **14**.

Number	Label	x	y	z
1	O001	0.36510(9)	0.50697(3)	0.20246(14)
2	N002	0.83584(10)	0.32962(4)	0.79184(17)
3	N003	0.61307(11)	0.53248(4)	0.16789(17)
4	N004	0.49612(11)	0.57413(4)	0.01465(18)
5	C005	0.61402(12)	0.36863(4)	0.49429(19)
6	C006	0.77033(12)	0.35488(4)	0.69620(19)
7	C007	0.63270(12)	0.40468(4)	0.53090(19)
8	C008	0.68390(12)	0.34333(4)	0.57824(19)
9	C009	0.97809(12)	0.30085(4)	0.9215(2)
10	C00A	0.89922(13)	0.29413(4)	1.0107(2)
11	C00B	0.93608(12)	0.32295(4)	0.7870(2)
12	C00C	0.81279(13)	0.31207(4)	0.9265(2)
13	C00D	0.52598(13)	0.48524(4)	0.29726(19)
14	C00E	1.07855(13)	0.28988(4)	0.9426(2)
15	H00E	1.108.130	0.275610	1.031.141
16	C00F	0.42349(13)	0.48097(4)	0.2943(2)
17	C00G	0.43348(13)	0.52819(4)	0.1466(2)
18	C00H	0.56017(13)	0.43211(4)	0.4514(2)
19	C00I	0.59567(13)	0.46045(4)	0.3767(2)
20	H00I	0.664557	0.462927	0.379429
21	C00J	0.78862(13)	0.38934(4)	0.7239(2)
22	H00J	0.847013	0.396545	0.798462
23	C00K	1.13246(13)	0.30084(5)	0.8282(2)
24	C00L	0.53281(13)	0.51658(4)	0.2034(2)
25	C00M	0.71958(13)	0.41416(4)	0.6404(2)
26	H00M	0.733431	0.437692	0.660251

27	C00N	1.08896(13)	0.32262(5)	0.6924(2)
28	C00O	0.45636(14)	0.42981(5)	0.4511(2)
29	H00O	0.433886	0.411306	0.506486
30	C00P	0.41447(14)	0.55709(4)	0.0442(2)
31	C00Q	0.58966(14)	0.56155(4)	0.0759(2)
32	C00R	0.66652(14)	0.30767(4)	0.5412(2)
33	H00R	0.711752	0.291127	0.596766
34	C00S	0.53081(14)	0.35640(5)	0.3720(2)
35	H00S	0.485216	0.372387	0.312586
36	C00T	0.38621(14)	0.45383(5)	0.3721(2)
37	H00T	0.317469	0.451766	0.371453
38	C00U	0.89299(15)	0.27466(5)	1.1516(2)
39	H00U	0.949243	0.262551	1.209.814
40	C00V	0.99013(13)	0.33404(5)	0.6712(2)
41	H00V	0.961029	0.348510	0.583197
42	C00W	0.67562(14)	0.58066(5)	0.0317(2)
43	C00X	0.31258(14)	0.56958(5)	-0.0421(2)
44	C00Y	0.72120(15)	0.31055(5)	0.9764(2)
45	H00Y	0.664151	0.322247	0.918124
46	C00Z	1.16506(14)	0.33057(6)	0.5860(2)
47	C010	1.23865(14)	0.29494(5)	0.8227(3)
48	C011	0.66499(17)	0.61503(5)	-0.0226(2)
49	H011	0.603942	0.626625	-0.027302
50	C012	1.25948(15)	0.31239(6)	0.6862(3)
51	C013	0.80316(17)	0.27364(5)	1.2029(3)
52	H013	0.799023	0.261075	1.297.710
53	C014	0.51595(16)	0.32190(5)	0.3395(2)
54	H014	0.459989	0.314589	0.259835
55	C015	0.58415(16)	0.29729(5)	0.4248(2)
56	H015	0.573177	0.273713	0.401963
57	C016	0.30166(16)	0.60250(5)	-0.1141(2)
58	H016	0.357913	0.617007	-0.102942
59	C017	0.71778(17)	0.29113(6)	1.1152(3)
60	H017	0.657230	0.289629	1.151.371
61	C018	0.22812(16)	0.54834(5)	-0.0612(3)
62	H018	0.234057	0.526264	-0.013577
63	C019	0.76781(17)	0.56435(6)	0.0412(3)
64	H019	0.776829	0.541560	0.079805
65	C01A	0.7445(2)	0.63204(6)	-0.0695(3)
66	H01A	0.736275	0.654934	-0.106922
67	C01B	1.18046(18)	0.36974(6)	0.5693(3)
68	H01B	1.199.640	0.379975	0.677998
69	H01C	1.118.381	0.380120	0.510110
70	H01D	1.233.025	0.373739	0.509405
71	C01C	1.13174(18)	0.31410(7)	0.4124(3)
72	H01E	1.182.633	0.318323	0.349363

7 Experimental Section

73	H01F	1.068.634	0.324241	0.355971
74	H01G	1.123.158	0.289458	0.423534
75	C01D	1.31449(16)	0.27687(7)	0.9323(3)
76	H01H	1.299.915	0.264987	1.022.794
77	C01E	0.20858(19)	0.61390(6)	-0.2018(3)
78	H01I	0.202014	0.636073	-0.248379
79	C01F	0.8348(2)	0.61564(7)	-0.0616(3)
80	H01J	0.888073	0.627280	-0.093237
81	C01G	0.12584(19)	0.59250(7)	-0.2202(3)
82	H01K	0.063134	0.600149	-0.280041
83	C01H	0.84697(19)	0.58164(7)	-0.0065(3)
84	H01L	0.908495	0.570318	-0.001240
85	C01I	0.13472(18)	0.55967(7)	-0.1507(3)
86	H01M	0.078269	0.545205	-0.163912
87	C01J	1.35678(18)	0.31204(8)	0.6571(3)
88	H01N	1.371.782	0.323471	0.565775
89	C01K	1.4106(2)	0.27694(9)	0.9042(4)
90	H01O	1.462.167	0.265331	0.977398
91	C01L	1.43185(18)	0.29394(10)	0.7694(4)
92	H01P	1.497.696	0.293435	0.752193
93	C5	0.9714(5)	0.5281(2)	0.3997(14)
94	H5	0.925814	0.546303	0.369080
95	C	0.9560(6)	0.5040(3)	0.5176(15)
96	C1	1.0242(8)	0.4767(3)	0.5633(12)
97	H1	1.013.852	0.460582	0.642211
98	C3	1.1078(7)	0.4736(2)	0.4911(13)
99	H3	1.153.454	0.455402	0.521681
100	C6	1.1233(6)	0.4977(3)	0.3732(13)
101	H6	1.179.237	0.495673	0.324851
102	C4	1.0551(7)	0.5250(2)	0.3275(12)
103	H4	1.065.419	0.541123	0.248549
104	C2	0.8776(17)	0.5055(8)	0.603(4)
105	H2A	0.882714	0.486049	0.677914
106	H2B	0.882789	0.526794	0.665897
107	H2C	0.813492	0.504781	0.525503
108	C5	1.0286(5)	0.4719(2)	0.6003(14)
109	H5	1.074.186	0.453697	0.630920
110	C	1.0440(6)	0.4960(3)	0.4824(15)
111	C1	0.9758(8)	0.5233(3)	0.4367(12)
112	H1	0.986148	0.539418	0.357789
113	C3	0.8922(7)	0.5264(2)	0.5089(13)
114	H3	0.846546	0.544598	0.478319
115	C6	0.8767(6)	0.5023(3)	0.6268(13)
116	H6	0.820763	0.504327	0.675149
117	C4	0.9449(7)	0.4750(2)	0.6725(12)
118	H4	0.934581	0.458877	0.751451

119	C2	1.1224(17)	0.4945(8)	0.397(4)
120	H2A	1.117.286	0.513951	0.322086
121	H2B	1.117.211	0.473206	0.334103
122	H2C	1.186.508	0.495219	0.474497

Table 22: Structure Solution and refinement parameters of compound **14**.

Empirical formula	C ₅₃ H ₃₅ N ₃ O
Molecular weight	729.84 g/mol
Diffractometer/Detector	SuperNova (Agilent), Atlas CCD Detector
Radiation	Cu K α (1.5418 Å), X-ray mirrors
Crystal size	(0.181 x 0.097 x 0.054) mm ³
Temperature	303.7(5) K
Diffraction Experiment ID	exp_5067_auto
Crystal system	monoclinic
Space group	P21/c
Lattice parameters:	
a, b, c	13.4952(3) Å, 38.3982(7) Å, 8.23335(16) Å
α, β, γ	90°, 102.491(2)°, 90°
Unit cell volume	4165.49(15) Å ³
Formula units per unit cell	4
F(000)	1528
Calculated density	1.164 g/cm ³
Linear absorption coeff.	0.539 mm ⁻¹
Scan	ω -scans
Measured reflections	32111
Index limits	-16 \leq h \leq 17; -42 \leq k \leq 47; -10 \leq l \leq 7
R_{int} (internal consistency of the dataset)	0.0312
Reflections used	8425
Refined parameters / restraints	567 / 43
R1 (I > 2σ)	0.0491
wR² (all data)	0.1439
Goof S	1.034
Max. shift in final cycle	\leq 0.002
Max./min. differential electron density	max: 0.177 / min: -0.198 e ⁻ /Å ³
Structure Solution / Refinement	SHELX-97: G.M. Sheldrick, <i>Acta Cryst. A</i> , 64, 2008 , 112 G.M. Sheldrick, Univ. Göttingen, 1997 .
Automated Report	Olex2.1.2 2022.04.07 svn.rca3783a0 for OlexSys

8 References

- [1] N. T. Kalyani, S. J. Dhoble, *Renew. Sustain. Energy Rev.* **2012**, *16*, 2696–2723.
- [2] C. A. Parker, C. G. Hatchard, *Trans. Faraday Soc.* **1961**, *57*, 1894–1904.
- [3] M. Pope, H. P. Kallmann, P. Magnante, *J. Chem. Phys.* **1963**, *38*, 2042–2043.
- [4] C. W. Tang, S. A. VanSlyke, *Appl. Phys. Lett.* **1987**, *51*, 913–915.
- [5] H. Kaur, S. Sundriyal, V. Pachauri, S. Ingebrandt, K.-H. Kim, A. L. Sharma, A. Deep, *Coord. Chem. Rev.* **2019**, *401*, 213077.
- [6] H. Chen, G. Tan, S.-T. Wu, *Opt. Express* **2017**, *25*, 33643–33656.
- [7] B. C. Kim, Y. J. Lim, J. H. Song, J. H. Lee, K.-U. Jeong, J. H. Lee, G.-D. Lee, S. H. Lee, *Opt. Express* **2014**, *22*, A1725–A1730.
- [8] J. Park, J.-H. Lee, *Appl. Opt.* **2019**, *58*, 3671–3675.
- [9] M. Y. Wong, E. Zysman-Colman, *Adv. Mater.* **2017**, *29*, 1605444.
- [10] J. Jang, *Mater. Today* **2006**, *9*, 46–52.
- [11] X. Liu, Y. Ma, W. Zhang, B. Song, L. Ding, M. Fung, J. Fan, *Chem. Eur. J.* **2018**, *24*, 11755–11762.
- [12] European Commission, *Commission Regulation (EC) No 1275/2008: Laying down Ecodesign Requirements for Electronic Displays Pursuant to Directive 2009/125/EC of the European Parliament and of the Council*, **2019**.
- [13] I. E. Serdiuk, C. H. Ryoo, K. Kozakiewicz, M. Mońka, B. Liberek, S. Y. Park, *J. Mater. Chem. C* **2020**, *8*, 6052–6062.
- [14] J. Hatfield, Y. Kobayashi, A. Nonaka, *Inf. Disp. (1975)*. **2015**, *31*, 28–31.
- [15] K. Diekmann, *ATZ-Automobiltechnische Zeitschrift* **2013**, *115*, 286–289.
- [16] G. L. Ingram, Y.-B. Zhao, Z.-H. Lu, *Org. Electron.* **2019**, *69*, 160–163.
- [17] M. Aleksandrova, N. Kurtev, V. Videkov, S. Tzanova, S. Schintke, *Microelectron. Eng.* **2015**, *145*, 112–116.
- [18] C. R. Ronda, *Luminescence: From Theory to Applications*, John Wiley & Sons, **2007**.
- [19] D. R. Vij, *Luminescence of Solids*, Springer Science & Business Media, **2012**.
- [20] Y. A. Ono, **1993**.
- [21] N. T. Kalyani, S. J. Dhoble, *Renew. Sustain. Energy Rev.* **2012**, *16*, 2696–2723.
- [22] S. L. M. Van Mensfoort, V. Shabro, R. J. De Vries, R. A. J. Janssen, R. Coehoorn, *J.*

- Appl. Phys.* **2010**, *107*, 113710.
- [23] M. Kasha, *Discuss. Faraday Soc.* **1950**, *9*, 14–19.
- [24] H. Jeong, H. Shin, J. Lee, B. Kim, Y.-I. Park, K. S. Yook, B.-K. An, J. Park, *J. Photonics Energy* **2015**, *5*, 57608.
- [25] T. Sasaki, M. Hasegawa, K. Inagaki, H. Ito, K. Suzuki, T. Oono, K. Morii, T. Shimizu, H. Fukagawa, *Nat. Commun.* **2021**, *12*, 2706.
- [26] T.-Y. Chu, J.-F. Chen, S.-Y. Chen, C.-J. Chen, C. H. Chen, *Appl. Phys. Lett.* **2006**, *89*, 53503.
- [27] M.-K. Wei, C.-W. Lin, C.-C. Yang, Y.-W. Kiang, J.-H. Lee, H.-Y. Lin, *Int. J. Mol. Sci.* **2010**, *11*, 1527–1545.
- [28] H. Aziz, Z. D. Popovic, *Chem. Mater.* **2004**, *16*, 4522–4532.
- [29] D. J. Milliron, I. G. Hill, C. Shen, A. Kahn, J. Schwartz, *J. Appl. Phys.* **2000**, *87*, 572–576.
- [30] Y. Kuwabara, H. Ogawa, H. Inada, N. Noma, Y. Shirota, *Adv. Mater.* **1994**, *6*, 677–679.
- [31] R. A. Klenkler, H. Aziz, A. Tran, Z. D. Popovic, G. Xu, *Org. Electron.* **2008**, *9*, 285–290.
- [32] D.-H. Lee, Y.-P. Liu, K.-H. Lee, H. Chae, S. M. Cho, *Org. Electron.* **2010**, *11*, 427–433.
- [33] O. Nuyken, S. Jungermann, V. Wiederhirn, E. Bacher, K. Meerholz, *Monatshefte für Chemie/Chemical Mon.* **2006**, *137*, 811–824.
- [34] C. W. Lee, O. Y. Kim, J. Y. Lee, *J. Ind. Eng. Chem.* **2014**, *20*, 1198–1208.
- [35] T. Förster, *Ann. Phys.* **1948**, *437*, 55–75.
- [36] D. L. Dexter, *J. Chem. Phys.* **1953**, *21*, 836–850.
- [37] H. Xu, R. Chen, Q. Sun, W. Lai, Q. Su, W. Huang, X. Liu, *Chem. Soc. Rev.* **2014**, *43*, 3259–3302.
- [38] H. Yersin, A. F. Rausch, R. Czerwieniec, T. Hofbeck, T. Fischer, *Coord. Chem. Rev.* **2011**, *255*, 2622–2652.
- [39] M. Godumala, S. Choi, M. J. Cho, D. H. Choi, *J. Mater. Chem. C* **2016**, *4*, 11355–11381.
- [40] M. A. Baldo, D. F. O'Brien, Y. You, A. Shoustikov, S. Sibley, M. E. Thompson, S. R. Forrest, *Nature* **1998**, *395*, 151–154.
- [41] J. Kalinowski, W. Stampor, J. Mezyk, M. Cocchi, D. Virgili, V. Fattori, P. Di Marco, *Phys. Rev. B* **2002**, *66*, 235321.
- [42] S. Reineke, K. Walzer, K. Leo, *Phys. Rev. B* **2007**, *75*, 125328.

-
- [43] T. Hofbeck, H. Yersin, *Inorg. Chem.* **2010**, *49*, 9290–9299.
- [44] W. S. Jeon, T. J. Park, J. H. Kwon, *J. Inf. Disp.* **2009**, *10*, 87–91.
- [45] D. Zhang, C. Zhao, Y. Zhang, X. Song, P. Wei, M. Cai, L. Duan, *ACS Appl. Mater. Interfaces* **2017**, *9*, 4769–4777.
- [46] P. S. C. Pflumm, A. Buesing, A. H. Parham, T. Mujica-Fernaund, H. Heil, *Materialien Für Organische Elektroluminiszenzvorrichtungen*, **2010**, WO2010136109.
- [47] H. J. Jang, J. Y. Lee, J. Kim, J. Kwak, J.-H. Park, *J. Inf. Disp.* **2020**, *21*, 1–9.
- [48] Y. H. Park, K. H. Lee, J. Y. Lee, *Dye. Pigment.* **2019**, *170*, 107551.
- [49] J. Kaiser, Host-Materialien Für Rote Organische Leuchtdioden, University of Regensburg, **2019**.
- [50] K. Goushi, Y. Kawamura, H. Sasabe, C. Adachi, *Jpn. J. Appl. Phys.* **2004**, *43*, L937.
- [51] M. Zhu, C. Yang, *Chem. Soc. Rev.* **2013**, *42*, 4963–4976.
- [52] H. Uoyama, K. Goushi, K. Shizu, H. Nomura, C. Adachi, *Nature* **2012**, *492*, 234–238.
- [53] M. M. Azrain, M. R. Mansor, S. Fadzullah, G. Omar, D. Sivakumar, L. M. Lim, M. N. A. Nordin, *Synth. Met.* **2018**, *235*, 160–175.
- [54] H. Fujimoto, T. Suekane, K. Imanishi, S. Yukiwaki, H. Wei, K. Nagayoshi, M. Yahiro, C. Adachi, *Sci. Rep.* **2016**, *6*, 1–9.
- [55] M. M. Azrain, M. R. Mansor, G. Omar, S. Fadzullah, S. R. Esa, L. M. Lim, D. Sivakumar, M. N. A. Nordin, *Synth. Met.* **2019**, *247*, 191–201.
- [56] P. Tyagi, R. Srivastava, L. I. Giri, S. Tuli, C. Lee, *Synth. Met.* **2016**, *216*, 40–50.
- [57] T. D. Schmidt, T. Lampe, M. R. Sylvinson, *Phys. Rev. Appl* **2017**, *8*, 37001.
- [58] C. Murawski, K. Leo, M. C. Gather, *Adv. Mater.* **2013**, *25*, 6801–6827.
- [59] M. Shukla, N. Brahme, *J. Int. Acad. Phys. Sci* **2011**, *15*, 231–238.
- [60] M. Shukla, N. Brahme, R. S. Kher, M. S. K. Khokhar, **2011**.
- [61] C. Mayr, T. D. Schmidt, W. Brütting, *Appl. Phys. Lett.* **2014**, *105*, 168_1.
- [62] C. Adachi, M. A. Baldo, M. E. Thompson, S. R. Forrest, *J. Appl. Phys.* **2001**, *90*, 5048–5051.
- [63] T. Tsuzuki, S. Tokito, *Adv. Mater.* **2007**, *19*, 276–280.
- [64] A. Y. Freidzon, A. A. Safonov, A. A. Bagaturyants, D. N. Krasikov, B. V Potapkin, A. A. Osipov, A. V Yakubovich, O. Kwon, *J. Phys. Chem. C* **2017**, *121*, 22422–22433.
- [65] S. M. Kim, J. H. Yun, S. H. Han, J. Y. Lee, *J. Mater. Chem. C* **2017**, *5*, 9072–9079.

- [66] D. R. Lee, S. H. Han, C. W. Lee, J. Y. Lee, *Dye. Pigment.* **2018**, *151*, 75–80.
- [67] S. W. Park, Jonggwang; Eom, Ka Young; Park, Hyoung Keun; Cho, Hyemin; Lee, Dae Won; Park, Jung Hwan; Choi, Yeon Hee; Yeo, *Preparation of Substituted Benzothieno- and Benzofuopyrimidine Derivatives for Organic Electronic Elements and Electronic Devices*, **2015**, WO2015182872.
- [68] K. Y. Kim, Hyung-Sun; Kim, Byung-Ku; Kim, Young-Kwon; Kim, Chang-Woo; Seo, Joo-Hee; Shin, Chang-Ju; Lee, Seung-Jae; Hwang, *Preparation of Fused Ring Compounds as Organic Electroluminescence Device Materials*, **2015**, WO2015108301A1.
- [69] J. Kim, Wonsam; Kim, Yuri; Hahn, Seunghoon; Song, Hyunju; Park, Junghwan; Lee, Sunhee; Lee, *Preparation of Benzothienopyrimidines and Related Compounds for Organic Electric Element and Electronic Device*, **2016**, WO2016013817.
- [70] D. J. Frisch, M.J., Trucks, G.W., Schlegel, H.B., Scuseria, G.E., Robb, M.A., Cheeseman, J.R., Scalmani, G., Barone, V., Mennucci, B., Petersson, G.A., Nakatsuji, H., Caricato, M., Li, X., Hratchian, H.P., Izmaylov, A.F., Bloino, J., Zheng, G., Sonnenberg, J.L., **2010**.
- [71] N. Miyaura, K. Yamada, A. Suzuki, *Tetrahedron Lett.* **1979**, *20*, 3437–3440.
- [72] A. W. Freeman, M. Urvoy, M. E. Criswell, *J. Org. Chem.* **2005**, *70*, 5014–5019.
- [73] C. Suzuki, K. Hirano, T. Satoh, M. Miura, *Org. Lett.* **2015**, *17*, 1597–1600.
- [74] F. Paul, J. Patt, J. F. Hartwig, *J. Am. Chem. Soc.* **1994**, *116*, 5969–5970.
- [75] J. P. Wolfe, S. Wagaw, S. L. Buchwald, *J. Am. Chem. Soc.* **1996**, *118*, 7215–7216.
- [76] F. Neufingerl, *Chemie. 1. Allgemeine Und Anorganische Chemie*, Jugend Und Volk, **2009**.
- [77] L. Ackermann, A. Althammer, P. Mayer, *Synthesis (Stuttg)*. **2009**, *2009*, 3493–3503.
- [78] M. E. Budén, V. A. Vaillard, S. E. Martin, R. A. Rossi, *J. Org. Chem.* **2009**, *74*, 4490–4498.
- [79] A. K. Panday, D. Ali, L. H. Choudhury, *ACS Omega* **2020**, *5*, 3646–3660.
- [80] J. Kaiser, A. Mekic, A. H. Parham, H. Buchholz, B. König, *European J. Org. Chem.* **2020**, *2020*, 66–69.
- [81] K. Bahrami, M. M. Khodaei, B. H. Yousefi, M. S. Arabi, *Tetrahedron Lett.* **2010**, *51*, 6939–6941.
- [82] H. Golchoubian, F. Hosseinpoor, *Molecules* **2007**, *12*, 304–311.
- [83] M. A. Iqbal, H. Mehmood, J. Lv, R. Hua, *Molecules* **2019**, *24*, 1145.

-
- [84] T. Ohe, N. Miyaura, A. Suzuki, *J. Org. Chem.* **1993**, *58*, 2201–2208.
- [85] T. Oh-e, N. Miyaura, A. Suzuki, *Synlett* **1990**, *1990*, 221–223.
- [86] G. Espino, A. Kurbangalieva, J. M. Brown, *Chem. Commun.* **2007**, 1742–1744.
- [87] A. F. Littke, C. Dai, G. C. Fu, *J. Am. Chem. Soc.* **2000**, *122*, 4020–4028.
- [88] Y. Ku, T. Grieme, Y. Pu, A. V Bhatia, *Adv. Synth. Catal.* **2009**, *351*, 2024–2030.
- [89] J. Park, J. Lee, S. Chang, *Angew. Chemie* **2017**, *129*, 4320–4324.
- [90] H. Becker, I. Bach, M. Holbach, J. Schwaiger, H. Spreitzer, *SID Symp. Dig. Tech. Pap.* **2010**, *41*, 39–42.
- [91] B. W. D'Andrade, S. Datta, S. R. Forrest, P. Djurovich, E. Polikarpov, M. E. Thompson, *Org. Electron.* **2005**, *6*, 11–20.
- [92] J. V Grazulevicius, P. Strohrriegl, *Adv. Mater* **2002**, *14*, 1439–1452.
- [93] Y. Shirota, *J. Mater. Chem.* **2000**, *10*, 1–25.
- [94] H. Huang, Y. Wang, B. Wang, S. Zhuang, B. Pan, X. Yang, L. Wang, C. Yang, *J. Mater. Chem. C* **2013**, *1*, 5899–5908.
- [95] M. Leung, Y.-H. Hsieh, T.-Y. Kuo, P.-T. Chou, J.-H. Lee, T.-L. Chiu, H.-J. Chen, *Org. Lett.* **2013**, *15*, 4694–4697.
- [96] A. P. Kulkarni, X. Kong, S. A. Jenekhe, *Adv. Funct. Mater.* **2006**, *16*, 1057–1066.
- [97] S. A. Jenekhe, L. Lu, M. M. Alam, *Macromolecules* **2001**, *34*, 7315–7324.
- [98] J. V. K. Amir Hossain Parham, Thomas Eberle, Anja Jatsch, Christof Pflumm, *Materialien Für Organische Elektrolumineszenzvorrichtungen*, **2014**, WO 2014/015931 A1.
- [99] L. Kortekaas, F. Lancia, J. D. Steen, W. R. Browne, *J. Phys. Chem. C* **2017**, *121*, 14688–14702.
- [100] S. Kania, B. Kościelniak-Mucha, J. Kuliński, P. Słoma, K. Wojciechowski, *Sci. Bull. Physics/Lodz Univ. Technol.* **2020**, *41*.
- [101] B. P. Fors, D. A. Watson, M. R. Biscoe, S. L. Buchwald, *J. Am. Chem. Soc.* **2008**, *130*, 13552–13554.
- [102] J. F. Hartwig, *Synlett* **1997**, *1997*, 329–340.
- [103] C. C. C. Johansson Seechurn, M. O. Kitching, T. J. Colacot, V. Snieckus, *Angew. Chemie Int. Ed.* **2012**, *51*, 5062–5085.
- [104] R. Han, G. L. Hillhouse, *J. Am. Chem. Soc.* **1997**, *119*, 8135–8136.

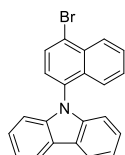
- [105] L. Marzo, S. K. Pagire, O. Reiser, B. König, *Angew. Chemie* **2018**, *130*, 10188–10228.
- [106] E. B. Corcoran, M. T. Pirnot, S. Lin, S. D. Dreher, D. A. DiRocco, I. W. Davies, S. L. Buchwald, D. W. C. MacMillan, *Science (80-.)*. **2016**, *353*, 279–283.
- [107] J. Twilton, C. Le, P. Zhang, M. H. Shaw, R. W. Evans, D. W. C. MacMillan, *Nat. Rev. Chem.* **2017**, *1*, 52.
- [108] K. L. Skubi, T. R. Blum, T. P. Yoon, *Chem. Rev.* **2016**, *116*, 10035–10074.
- [109] M. N. Hopkinson, B. Sahoo, J. Li, F. Glorius, *Chem. Eur. J.* **2014**, *20*, 3874–3886.
- [110] J. A. Milligan, J. P. Phelan, S. O. Badir, G. A. Molander, *Angew. Chemie Int. Ed.* **2019**, *58*, 6152–6163.
- [111] C. Zhu, H. Yue, J. Jia, M. Rueping, *Angew. Chemie* **2021**, *133*, 17954–17975.
- [112] C. Zhu, H. Yue, L. Chu, M. Rueping, *Chem. Sci.* **2020**, *11*, 4051–4064.
- [113] R. Sun, Y. Qin, D. G. Nocera, *Angew. Chemie* **2020**, *132*, 9614–9620.
- [114] M. Kudisch, C.-H. Lim, P. Thordarson, G. M. Miyake, *J. Am. Chem. Soc.* **2019**, *141*, 19479–19486.
- [115] N. A. Till, L. Tian, Z. Dong, G. D. Scholes, D. W. C. MacMillan, *J. Am. Chem. Soc.* **2020**, *142*, 15830–15841.
- [116] C. K. Prier, D. A. Rankic, D. W. C. MacMillan, *Chem. Rev.* **2013**, *113*, 5322–5363.
- [117] T.-Y. Shang, L.-H. Lu, Z. Cao, Y. Liu, W.-M. He, B. Yu, *Chem. Commun.* **2019**, *55*, 5408–5419.
- [118] E. Speckmeier, T. G. Fischer, K. Zeitler, *J. Am. Chem. Soc.* **2018**, *140*, 15353–15365.
- [119] N. A. Romero, D. A. Nicewicz, *Chem. Rev.* **2016**, *116*, 10075–10166.
- [120] J. Zhao, W. Wu, J. Sun, S. Guo, *Chem. Soc. Rev.* **2013**, *42*, 5323–5351.
- [121] J. Lu, B. Pattengale, Q. Liu, S. Yang, W. Shi, S. Li, J. Huang, J. Zhang, *J. Am. Chem. Soc.* **2018**, *140*, 13719–13725.
- [122] X. Zhang, C. Qian, Z. Ma, X. Fu, Z. Li, H. Jin, M. Chen, Z. Ma, *Chem. Mater.* **2023**, DOI 10.1021/acs.chemmater.3c00193.
- [123] G. M. Sheldrick, *Acta Crystallogr. Sect. A Found. Crystallogr.* **2008**, *64*, 112–122.
- [124] I. T. Alt, B. Plietker, *Angew. Chemie Int. Ed.* **2016**, *55*, 1519–1522.
- [125] X. Guan, H. Zhu, Y. Zhao, T. G. Driver, *European J. Org. Chem.* **2020**, *2020*, 57–60.
- [126] Z. Qu, P. Wang, X. Chen, G.-J. Deng, H. Huang, *Chinese Chem. Lett.* **2021**, *32*, 2582–2586.

-
- [127] Y. Chen, W. Liang, W. H. Choi, J. Huang, Q. Dong, F. Zhu, J. Su, *Dye. Pigment.* **2015**, 123, 196–203.
- [128] M. Bhanuchandra, H. Yorimitsu, A. Osuka, *Org. Lett.* **2016**, 18, 384–387.
- [129] H. Liu, W. Han, C. Li, Z. Ma, R. Li, X. Zheng, H. Fu, H. Chen, *European J. Org. Chem.* **2016**, 2016, 389–393.
- [130] C. Tian, X. Yao, W. Ji, Q. Wang, G. An, G. Li, *European J. Org. Chem.* **2018**, 2018, 5972–5979.

9 Appendix

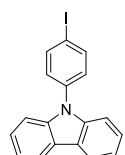
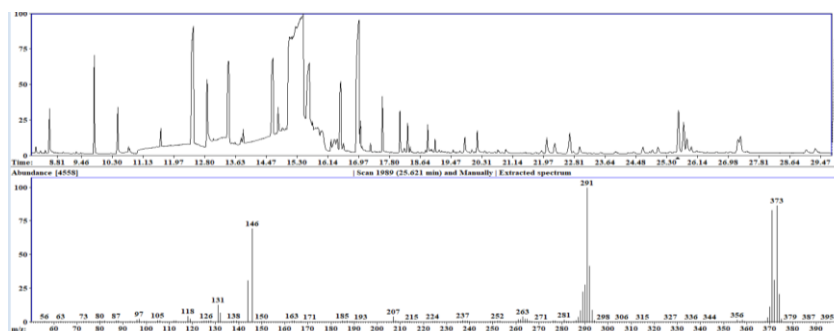
9.1 GC-MS Spectra of the Photoredox catalytic Reactions with Product Formation

GC-MS



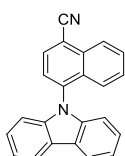
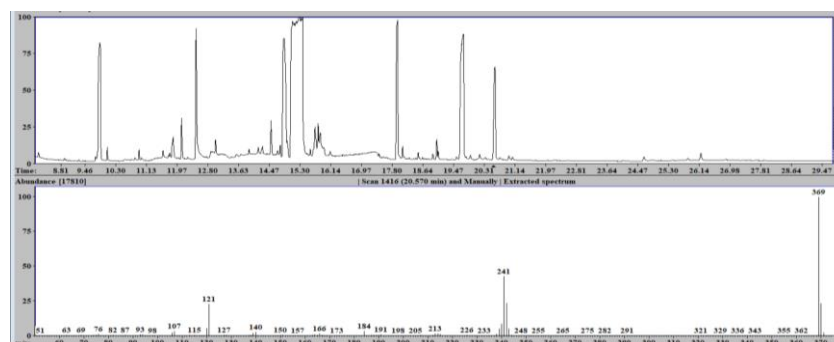
98

Exact Mass: 371,03



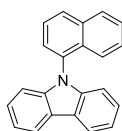
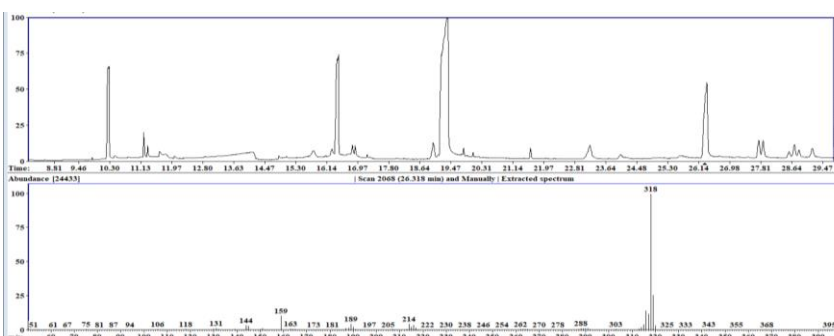
102'

Exact Mass: 369,00



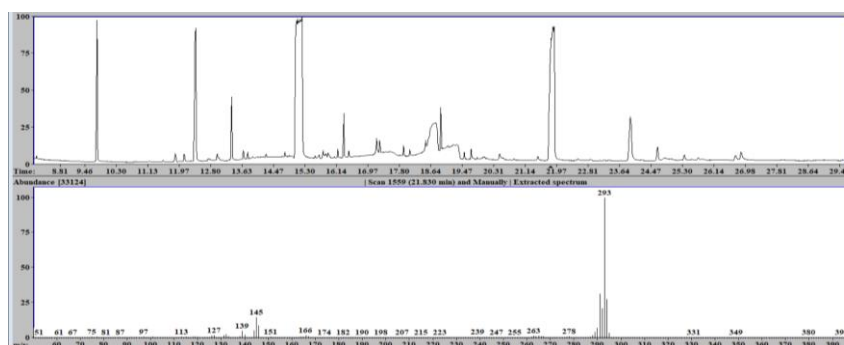
99

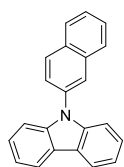
Exact Mass: 318,12



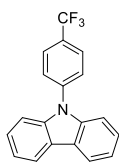
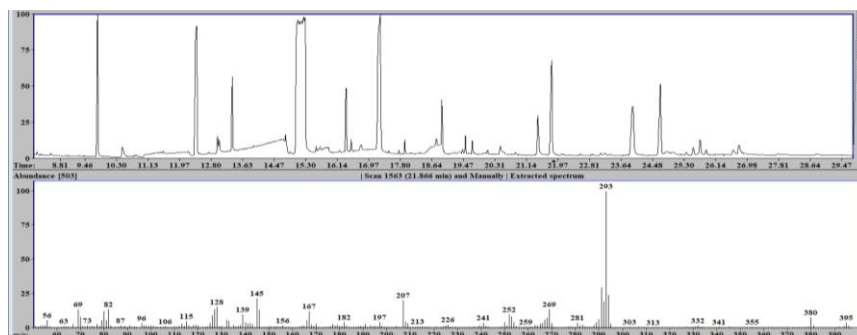
100

Exact Mass: 293,12

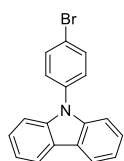
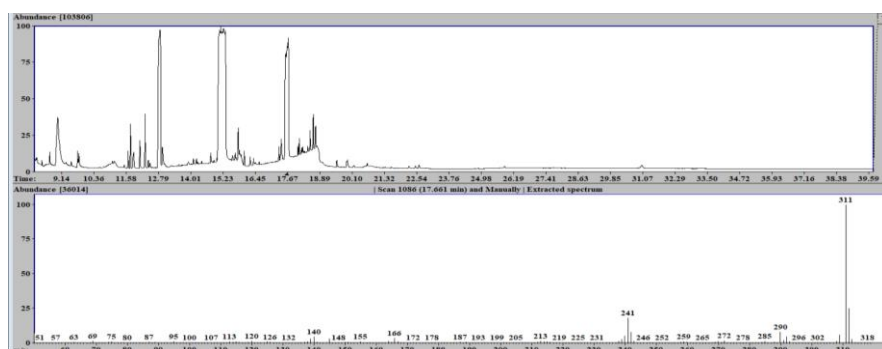




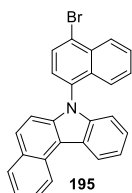
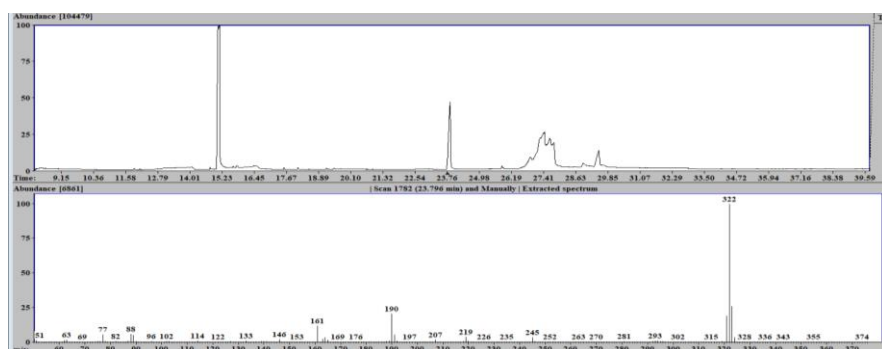
101
Exact Mass: 293,12



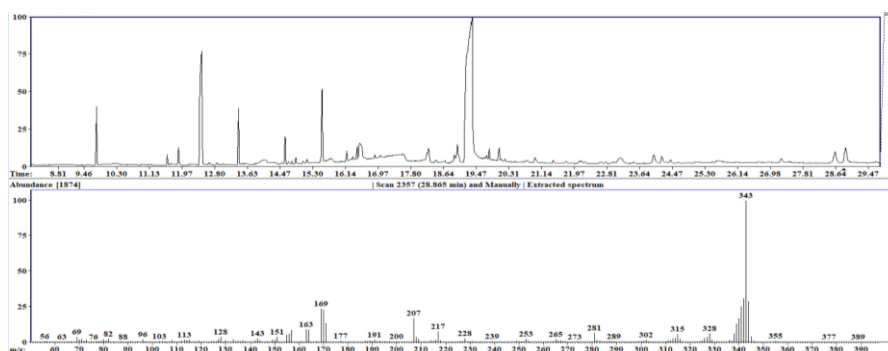
104
Exact Mass: 311,09



102
Exact Mass: 321,02



195
Exact Mass: 421,05



Appendix 1: GC traces of the photoredox catalytic reactions with observed product formation and the corresponding MS spectrum of the formed product.

9.2 Curriculum Vitae

The curriculum vitae is not included in the online version due to data protection reasons.

9.3 Eidesstattliche Erklärung

- (1) Ich erkläre hiermit an Eid statt, dass ich die vorliegende Arbeit ohne unzulässige Hilfe Dritter und ohne Benutzung anderer als der angegebenen Hilfsmittel angefertigt habe; die aus anderen Quellen direkt oder indirekt übernommenen Daten und Konzepte sind unter Angabe des Literaturzitats gekennzeichnet.

- (2) Bei der Auswahl und Auswertung folgenden Materials haben mir die nachstehend aufgeführten Personen in der jeweils beschriebenen Weise unentgeltlich geholfen:
 1. Kapitel 3: Verbindung **37** wurde hochskaliert von Christian Schreiber (Merck Electronics KGaA). DFT-Berechnungen zur Bildung von Verbindung **25** gegen **18** sowie der Verbindungen **5** und **6** wurden von Jens Pfalzgraf (Merck Electronics KGaA) durchgeführt. Die Charakterisierungsdaten aller synthetisierten Verbindungen wurden durch die Analytikabteilung von Merck KGaA gemessen.
 2. Kapitel 4: OLED-Bauteile wurden von der Physikabteilung von Merck KGaA gebaut und vermessen.
 3. Kapitel 5: Das Photoredoxkatalytische System wurde von Dr. Indrajit Ghosh (AK König, Universität Regensburg) entwickelt. GC-MS-Spektren wurden von Dr. Rudolf Vasold (Universität Regensburg) gemessen.

- (3) Weitere Personen waren an der inhaltlich-materiellen Herstellung der vorliegenden Arbeit nicht beteiligt. Insbesondere habe ich hierfür nicht die entgeltliche Hilfe eines Promotionsberaters oder anderer Personen in Anspruch genommen. Niemand hat von mir weder unmittelbar noch mittelbar geldwerte Leistungen für Arbeiten erhalten, die im Zusammenhang mit dem Inhalt der vorgelegten Dissertation stehen.

- (4) Die Arbeit wurde bisher weder im In- noch im Ausland in gleicher oder ähnlicher Form einer anderen Prüfungsbehörde vorgelegt.